

**BIOCHEMICAL ANALYSIS OF *ABCA4* MUTATIONS RESPONSIBLE FOR
STARGARDT DISEASE**

by

Fabian Garces

B.A., Simon Fraser University, 2011

A THESIS SUBMITTED IN PARTIAL FULFILLMENT OF
THE REQUIREMENTS FOR THE DEGREE OF

Doctor of Philosophy

in

THE FACULTY OF GRADUATE AND POSTDOCTORAL STUDIES
(Biochemistry and Molecular Biology)

THE UNIVERSITY OF BRITISH COLUMBIA
(Vancouver)

February 2021

© Fabian Garces, 2021

The following individuals certify that they have read, and recommend to the Faculty of Graduate and Postdoctoral Studies for acceptance, the dissertation entitled:

“Biochemical Analysis of *ABCA4* Mutations Responsible for Stargardt Disease”

submitted by Fabian Garces in partial fulfillment of the requirements for

the degree of Doctor of Philosophy

in Biochemistry and Molecular Biology

Examining Committee:

Dr. Robert Molday, Professor, Department of Biochemistry and Molecular Biology, UBC
Supervisor

Dr. Orson Moritz, Associate Professor, Department of Ophthalmology and Visual Science, UBC
Supervisory Committee Member

Dr. Frank Duong, Professor, Department of Biochemistry and Molecular Biology, UBC
Supervisory Committee Member

Dr. Hakima Moukhles, Associate Professor, Department of Cellular and Physiological Sciences, UBC
University Examiner

Dr. Joerg Gsponer, Associate Professor, Department of Biochemistry and Molecular Biology, UBC
University Examiner

Abstract

ABCA4 is an ABC transporter encoded by the ABCA4 gene. This transporter is predominantly expressed in the disc membranes of photoreceptor cells in the retina where it plays a crucial role. ABCA4 transports N-retinylidene-phosphatidylethanolamine (N-ret-PE), the Schiff-base adduct formed by all-trans-retinal or 11-cis-retinal with phosphatidylethanolamine, across the disc membranes of photoreceptors. In doing so, ABCA4 acts as an importer that helps to prevent the formation and accumulation of harmful bisretinoids in the disc membranes of photoreceptors. To date, more than 1000 point-mutations in the ABCA4 gene have been linked to the development of Stargardt disease (STGD1) and other retinopathies.

Although significant progress has been made in identifying disease-causing mutations in ABCA4, understanding genotype-phenotype relationships remains challenging because most patients are compound heterozygous for disease mutations in ABCA4 and phenotypic variations have been found in individuals with the same genotype. Furthermore, with some exceptions, analysis of STGD1 has relied on clinical and genetic data while lacking any biochemical characterization of disease-causing variants. As a result, it remains to be determined the extent to which the molecular properties of ABCA4 disease variants contribute to the etiology of STGD1 in relation to other factors, such as age, lifestyle, and environmental factors. To address this issue, a major aim of this thesis is to understand how the protein solubilization levels and residual activity of ABCA4 variants influence the disease outcome of STGD1 patients harboring these mutations.

Furthermore, to help us delineate the different molecular mechanisms that underpin STGD1, and to help us understand the transport mechanism of ABC transporters in general, this thesis will characterize disease variants found in the transmembrane and the nucleotide binding

domains of ABCA4. An in-depth functional analysis of the transmembrane domains (TMDs) will help us identify residues essential for the binding and translocation of N-ret-PE. Likewise, an investigation of common disease variants localized to the Walker-A motif of the nucleotide-binding-domains (NBDs) could help understand how ABCA4 couples binding and hydrolysis of ATP with N-ret-PE transport. Taken together, this information will be useful to develop a full understanding of the mechanism of transport of ABCA4 and similar transporters.

Lay Summary

Stargardt disease (STGD1) is a genetic eye disease that leads to macular dystrophy resulting in vision loss that can progress to blindness. STGD1 is caused by mutations in the *ABCA4* gene, which encodes the ABCA4 protein. ABCA4 is a membrane transporter found in the photoreceptors of the retina, where it prevents the accumulation of toxic bisretinoids that can damage the retina and lead to vision loss. In this thesis we biochemically characterized a large number of mutations in the *ABCA4* gene known to cause STGD1. Our results provide a thorough understanding of how these mutations affect the function of ABCA4 and result in STGD1. Furthermore, this work explains why some *ABCA4* mutations are more detrimental than others and cause more severe cases of STGD1. Likewise, this thesis provides new insights into the transport mechanism of ABCA4 and paves the way for the development of drugs for the treatment of STGD1.

Preface

All data chapters (chapter 2-4) have been or are planning to be published and the editing style of each chapter matches that of a publication. Hence all chapters include an introduction, materials and methods, results and a discussion section. While the materials and methods section is similar across each chapter, slight variations in the experimental procedures between chapters do occur underscoring the need to clearly delineate the materials and methods section of each data chapter.

A version of Chapter 2 has been published as:

Garces, F.A., Scortecci, J.F., Molday, R.S., (2021). Functional Characterization of ABCA4 Missense Variants Linked to Stargardt Macular Degeneration. *Int. J. Mol. Sci.* 22, 185. <https://dx.doi.org/10.3390/ijms22010185>

All experimental data and figures in Chapter 2 were done by me. The study design and experiments were conducted based on discussions with my supervisor, Dr. Robert Molday. Dr. Jessica Scortecci created the homology model of ABCA4 used in the published manuscript, whereas I generated the homology model used in Chapter 2. The chapter was written by me and edited by Dr. Molday.

Chapter 3 was a collaborative effort with several members of the Molday laboratory. The experimental design was developed through conversations between Dr. Molday and me. The cloning of the N965A, N965Q, N1974A, N1974Q, and N1974S mutants were done by Gilmar Gutierrez under my supervision, as part of an undergraduate thesis project. Gilmar gathered preliminary data on these constructs, which I repeated; only my data has been used in this thesis. I further cloned the N965D, N965K, N965Y, N1974D, N1974K, N1974Y mutants and gathered all biochemical data presented herein. Dr. Jessica Scortecci generated a homology model of

ABCA4 using I-Tasser, which I used to create figure 3.1 using pymol. The chapter was written by me and edited by Dr. Robert Molday.

A version of Chapter 4 has been published as:

Garces, F., Jiang, K., Molday, L.L., Stohr, H., Weber, B.H., Lyons, C.J., Maberley, D., Molday, R.S., (2018). Correlating the expression and functional activity of ABCA4 disease variants with the phenotype of patients with Stargardt disease. *Invest. Ophthalmol. Vis. Sci.* 59, 2305–2315.

Chapter 4 was a collaborative effort between the Molday laboratory, ophthalmologists in the Vancouver Eye Care Centre (ECC), and the Weber laboratory at the University of Regensburg, Germany. Clinical data and blood samples of the STGD patients recruited in the study was gathered by Dr. Jiang, a medical resident at the ECC under the supervision of Dr. Lyons and Dr. Maberley. DNA sequencing was carried out by Dr. Stohr and Dr. Weber. Confocal microscopy was done by Mrs. Laurie Molday. Cloning of G72R, M448K, V552I, G1091E, A1357T, A1794P, and R2077W were done by myself. Cloning of L541P, A1038V, G1961E, and L2027F were previously done over the years by several members of the Molday laboratory. Preparation of radioactive retinal substrate was done by me with the help of Mrs. Laurie Molday. All CHAPS and SDS solubilization assays, N-ret-PE binding assays, and ATPase assays were done by me. The manuscript was written and edited by me and Dr. Robert Molday.

Table of Contents

Abstract.....	iii
Lay Summary	v
Preface	vi
Table of Contents.....	viii
List of Tables	xiv
List of Figures.....	xv
Abbreviations.....	xvii
Acknowledgements	xx
Dedication.....	xxi
Chapter 1 : Introduction.....	1
1.1 ABC Transporter Superfamily.....	1
1.1.1 Transport Mechanisms	4
1.1.2 ABCA Subfamily	10
1.2 The Retina.....	19
1.2.1 Photoreceptors	20
1.2.2 Phototransduction	23
1.2.3 Visual Cycle	24
1.3 Retinal Degenerative Diseases	28

1.3.1	ABCA4 Associated Retinopathies.....	32
1.3.2	Stargardt Disease	33
1.3.3	Treatment Strategies	36
1.4	Genotype-Phenotype Correlations in ABCA4 Associated Retinopathies.....	41
1.5	Thesis Investigation.....	44
Chapter 2 : Biochemical Analysis of Transmembrane Mutations in ABCA4 Associated with		
Stargardt Disease		47
2.1	Introduction	47
2.2	Materials and Methods	49
2.2.1	Prediction of Transmembrane Helices	49
2.2.2	Cloning of ABCA4 Transmembrane Variants	49
2.2.3	Heterologous Expression of ABCA4 Variants in HEK293T Cells.....	49
2.2.4	Immunofluorescence Microscopy of ABCA4 Variants in COS7 Cells	51
2.2.5	ATPase Assay.....	51
2.2.6	N-ret-PE Binding Assay	53
2.3	Results	54
2.3.1	Sequence Prediction of the TMDs.....	54
2.3.2	Protein Solubilization and Cellular Localization of TMD Variants.....	57
2.3.3	Functional Analysis of TMD Variants: ATPase Assays	64
2.3.4	Functional Analysis of TMD Variants: N-ret-PE Binding Assays.....	68

2.3.5	Biochemical Characterization of R653 Variants	72
2.4	Discussion.....	74
Chapter 3 : Functional Characterization of p.N965 and p.N1974 Variants in the Walker A Motif Associated with Stargardt Disease		
		84
3.1	Introduction	84
3.2	Materials and Methods	88
3.2.1	Homology Model of ABCA4	88
3.2.2	Cloning of ABCA4 N965 and N1974 Variants.....	88
3.2.3	Heterologous Expression of ABCA4 N965 and N1974 Variants in HEK293T Cells	89
3.2.4	Cellular Localization of ABCA4 N965 and N1974 Variants in COS7 Cells.....	90
3.2.5	ATPase Assays	91
3.2.6	N-ret-PE Binding Assays.....	92
3.3	Results	93
3.3.1	Topological Organization of The ABCA4 Domains.....	93
3.3.2	Solubilization Levels and Cellular Localization of N965 and N1974 Variants	96
3.3.3	Functional Characterization of N965 and N1974 Variants	100
3.4	Discussion.....	104
Chapter 4 : Correlating the Expression and Functional Activity of ABCA4 Disease Variants with the Phenotype of Patients with Stargardt Disease		
		107

4.1	Introduction	107
4.2	Materials and Methods	109
4.2.1	Clinical Assessment and mutational Screening of STGD Patients	109
4.2.2	Generation of ABCA4 Mutant Constructs	110
4.2.3	Protein Solubilization Analysis of ABCA4 Variants	110
4.2.4	Immunofluorescence Microscopy of Transiently Transfected COS7 Cells.....	111
4.2.5	ATPase Assay.....	112
4.2.6	Retinoid Binding Assay.....	113
4.3	Results	115
4.3.1	Genetic Screening of STGD1 Patients	115
4.3.2	Clinical Assessment of STGD1 Patients	115
4.3.3	Protein Solubilization and Localization of ABCA4 Variants in Cultured Cells .	120
4.3.4	Functional Analysis of ABCA4 Variants	125
4.4	Discussion.....	130
Chapter 5 : Conclusions.....		136
5.1	Thesis Summary	136
5.1.1	Summary of Chapters	137
5.2	Significance	139
5.3	Future Prospects	140

Bibliography	143
Appendices	165
A1. TMD1 amino acid composition	165
A2. TMD2 amino acid composition	166
A3. Alignments of ABCA4 homology models using I-TASSER and SWISS-MODEL	167
A4. TMD1 variants statistical analysis of protein expression levels after solubilization with CHAPS or SDS.....	168
A5. TMD2 variants statistical analysis of protein expression levels after solubilization with CHAPS or SDS.....	169
A6. TMD1 variants statistical analysis of ATPase activity assays.....	170
A7. TMD2 variants statistical analysis of ATPase activity assays.....	171
A8. TMD1 variants statistical analysis of N-ret-PE binding assays.....	172
A9. TMD2 variants statistical analysis of N-ret-PE binding assays.....	173
A10. N965 and N1974 variants statistical analysis of protein expression levels after solubilization with CHAPS or SDS.....	174
A11. N965 and N1974 variants statistical analysis of ATPase activity assays.....	175
A12. N965 and N1974 variants statistical analysis of N-ret-PE binding assays.....	176
A13. Variants of B.C. cohort Stargardt patients statistical analysis of protein expression levels after solubilization with CHAPS or SDS	177

A14. Variants of B.C. cohort Stargardt patients statistical analysis of ATPase activity assays
.....178

A15. Variants of B.C. cohort Stargardt patients statistical analysis of N-ret-PE binding assays
.....179

List of Tables

Table 1.1 Lipid transporters of the ABCA subfamily	12
Table 2.1 Summary of Biochemical Analysis of TMD1 Variants	82
Table 2.2 Summary of Biochemical Analysis of TMD2 Variants	83
Table 4.1 Genotype and Phenotype Characteristics of STGD1 Patients harboring ABCA4 mutations	118
Table 4.2 Expression and Functional Activities of ABCA4 missense mutations identified in the STGD1 patients	129

List of Figures

Figure 1.1 Structures of prokaryotic ABC transporters.....	2
Figure 1.2 Eukaryotic ABC transporters.	6
Figure 1.3 Generalized transport model for ABC transporters.	9
Figure 1.4 Cladogram of the human ABCA subfamily.....	11
Figure 1.5 Cellular localization of ABCA4.....	15
Figure 1.6 Homology Model of ABCA4.....	18
Figure 1.7 Morphology of Photoreceptors Cells.	22
Figure 1.8 The Visual Cycle.....	27
Figure 1.9 Progression of retinal degenerative diseases.....	36
Figure 2.1 Homology model of ABCA4 showing TMD disease variants.....	55
Figure 2.2 Top View of the TMDs in the ABCA4 Homology Model.	56
Figure 2.3 Relative protein solubilization of TMD variants.	61
Figure 2.4 Solubilization levels of TMD Variants in SDS buffer.....	62
Figure 2.5 Cellular localization analysis of TMD and R653 variants in transfected COS7 Cells.....	63
Figure 2.6 ATPase Activity of TMD Variants.	66
Figure 2.7 Specific ATPase Activity Curves of TMD variants.....	67
Figure 2.8 N-ret-PE Binding of TMD Variants.....	70
Figure 2.9 N-ret-PE Binding Curves.....	71
Figure 2.10 Biochemical analysis of R653 Variants.	73
Figure 2.11 Biochemical classification of TMD Variants.....	81
Figure 3.1 Homology model of ABCA4.	95
Figure 3.2 CHAPS protein solubilization levels of N965 and N1974 variants.....	97

Figure 3.3 SDS protein solubilization levels of N965 and N1974 variants.	98
Figure 3.4 Cellular localization of N965 and N1974 variants in COS 7 cells.	99
Figure 3.5 Functional characterization of N965 and N1974 variants.....	102
Figure 3.6 The alternating access model for ABCA4.	103
Figure 4.1 Representative clinical features of STGD1 patients examined in this study.	119
Figure 4.2 Topological model of ABCA4 showing the location of missense mutations associated with Stargardt disease examined in this study.....	122
Figure 4.3 Relative solubility of ABCA4 variants in transiently transfected HEK293T cells....	123
Figure 4.4 Cellular localization of ABCA4 variants.	124
Figure 4.5 Purification and N-Ret-PE binding to ABCA4.....	127
Figure 4.6 ATPase activity of ABCA4 variants.	128

Abbreviations

A2E	N-retinylidene-N-retinylethanolamine
ABC	ATP-binding cassette
ADP	Adenosine diphosphate
AMD	Age related macular degeneration
ATP	Adenosine-5'-triphosphate
ATR	All- <i>trans</i> -retinal
BSA	Bovine serum albumin
cDNA	Complementary deoxyribonucleic acid
CRALBP	Cellular retinaldehyde binding protein
CFTR	Cystic Fibrosis Transmembrane Regulator
CHAPS	3-[(3-cholamidopropyl)dimethylammonio]-1-propanesulfonic acid
CHOL	Cholesterol
DAPI	4',6-diamidino-2-phenylindole
DMEM	Dulbecco's modified Eagle's medium
DOPC	1,2-dioleoyl-sn-glycero-3-phosphatidylcholine
DOPE	1,2-dioleoyl-sn-glycero-3-phosphatidylethanolamine
DOPS	1,2-dioleoyl-sn-glycero-3-phosphatidylserine
DTT	Dithiothreitol
ECD	Extracellular domain
EM	Electron microscopy
ER	Endoplasmic reticulum

GAP	GTPase activating protein
GPCR	G Protein-Coupled Receptor
GDP	Guanosine-5'-diphosphate
GTP	Guanosine-5'-triphosphate
HEK	Human embryonic kidney
HEPES	4-(2-Hydroxyethyl)-1-Piperazineethanesulfonic Acid
HPLC	High Pressure Liquid Chromatography
IF	Immunofluorescence
IRBP	Interphotoreceptor retinoid binding protein
kDa	Kilodalton
LCA	Leber congenital amaurosis
LRAT	Lecithin-retinol acyltransferase
MD	Macular dystrophy
NBD	Nucleotide binding domain
N-ret-PE	N-retinylidene PE
PAGE	Polyacrylamide gel electrophoresis
PB	Phosphate buffer
PBA	4-Phenyl butyrate
PBS	Phosphate buffered saline
PC	Phosphatidylcholine
PCR	Polymerase chain reaction
PE	Phosphatidylethanolamine

PVDF	Polyvinylidene fluoride
RDH	Retinol dehydrogenase
ROS	Rod outer segment
RP	Retinitis Pigmentosa
RPE	Retinal pigment epithelium
SDS	Sodium dodecyl sulfate
SM	Sphingomyelin
STGD	Stargardt disease
TMD	Transmembrane domain

Acknowledgements

I would like to start by thanking my supervisor, Dr. Robert Molday, for welcoming me into his laboratory and for his commitment and support to this PhD thesis. Throughout the years, Bob has been an invaluable source of guidance and knowledge, with his help, I have become a better scientist, a better biochemist. Thank you, Bob.

I would also like to thank my Committee members Dr. Orson Moritz and Dr. Franck Duong for overseeing my progress and providing thoughtful insights, guidance, and feedback that no doubt improved the quality of my scientific work.

Likewise, I would like to express my gratitude to Laurie Molday for her mentorship and patience when I first joined the lab and for her continuous support, both technical and beyond, and for ensuring the laboratory always ran smoothly. I also want to thank Laurie for helping me purify tritiated all-*trans*-retinal for my substrate binding assays, that was never an easy thing to do!

To my lab mates, thank you so much for your kindness, support and friendship. Thank you for being there during the highs and lows of grad school. This journey would have been that much harder without a great support group in the lab. A big thank you to Angela Liou, Dr. Jessica Scortessi, Hanbin Choi, Dr. Sue Curtis, Theresa Hii, Eli Matsell, Dr. Dan Ma, Dr. Madhavan Chalat, and Dr. Martin Bush.

Lastly, I want to thank my family. My parents Antonio and Elvira, and my sisters Alejandra and Angie. Without your love and support I would not be here today. You are and have always been my foundation, my rock. Mom, Dad, thank you for always being there for me, I know it has not always been easy, but all your worries, all your sacrifices, and all your efforts have been worth it. I hope I made you proud.

Dedication

To my parents Elvira and Antonio

Chapter 1 : Introduction

1.1 ABC Transporter Superfamily

ABC Transporters comprise a large superfamily of integral membrane proteins found in all domains of life (Dean and Allikmets, 1995; Rees, Johnson and Lewinson, 2009). These transporters bind and hydrolyze ATP or GTP to power the translocation of a wide variety of substrates including lipids, cholesterol, peptides, amino acids, sugars, vitamins, ions and small hydrophobic drugs across cellular membranes (Dean and Allikmets, 1995; Rees, Johnson and Lewinson, 2009). These transporters can be divided into importers or exporters depending on the direction of substrate transport relative to the cytosol. Importers translocate their substrate into the cytosol whereas exporters translocate their substrate out of the cytosol. The prototypical structure of an ABC transporter is composed of four main domains: two, well conserved, nucleotide binding domains (NBDs) that mediate the binding and hydrolysis of ATP, or in some cases, GTP; and two, non-conserved, transmembrane domains (TMDs) that anchor the protein to the membrane and regulate substrate binding and translocation (Linton, 2007; Rees, Johnson and Lewinson, 2009). The NBDs contain several well conserved motifs and loops that mediate ATP binding and hydrolysis including the Walker A motif, the Walker B motif, the LSGGQ signature motif, and the D, H and Q loops (Weng *et al.*, 1999; Linton, 2007; Ernest *et al.*, 2009; Rees, Johnson and Lewinson, 2009). In eukaryotes, the TMDs of most ABC transporters for which structural data is available, are composed of 6 hydrophobic alpha helices that form the substrate binding site and translocation pathway within the membrane (Ford and Beis, 2019). In prokaryotes, the structure of the TMDs is more diverse and ranges from 5 to 10 TM helices per TMD and 10 to 20 total TMs in the full transporter. For example, the MetI transporter has 5 TM

helices, ModAB and MsbA have 6 TM helices, and BtuC has 10 TM helices per TMD (Fig. 1.1) (Ward *et al.*, 2007; Gerber *et al.*, 2008; Kadaba *et al.*, 2008; Korkhov, Mireku and Locher, 2012). Additionally, prokaryotic ABC importers work in concert with ligand binding proteins that bind to their substrate in the periplasm of bacteria and deliver their ligand to specific ABC transporters (Fig. 1.1).

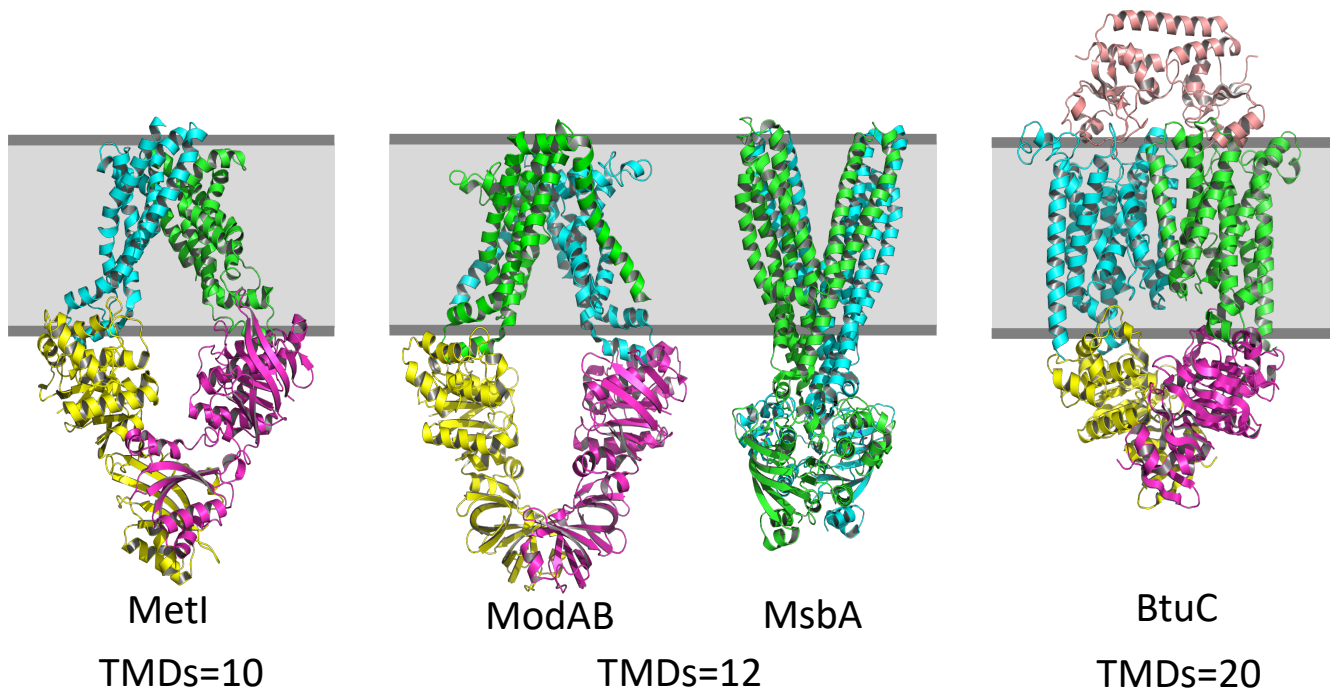


Figure 1.1 Structures of prokaryotic ABC transporters.

Several TMD folds composed of different numbers of transmembrane helices have been observed. The maltose transporter, Met1 (3DHW), has 5 TM helices per domain for a total of 10 TM helices. The molybdate transporter, ModAB (3D31), and the lipid A and multidrug transporter, MsbA (3B60), have 6 TM helices per domain and 12 total TM helices. The vitamin B12 transporter, BtuC (4FI3), has 10 TM helices per domain and 20 TM helices total. Additionally, a ligand binding protein can be seen on the periplasmic side of the membrane in the BtuC complex. Each polypeptide chain that makes up the subunits of these complexes has been assigned a different color.

In eukaryotes, ABC transporters can be either half or full transporters. Half transporters form homodimers or heterodimers with other half transporters in order to form a functional protein, whereas full transporters already contain the two TMDs and NBDs required for transport

activity and may not need to oligomerize (Fig. 1.2) (Dean, 2002). Plants generally have a particularly large number of ABC transporters, exceeding more than 100 ABC transporters in most plant genomes. For example, *Arabidopsis thaliana* has 129 known ABC transporters which are subdivided into 8 subfamilies (Linton, 2007). Part of this large number of ABC transporters in plants has to do with steep concentrations gradients that need to be maintained across cellular membranes, the transport of hormones, lipids, metabolites, and metal ions, and vacuolar deposition of toxic compounds (Kang *et al.*, 2011; Lane *et al.*, 2016). In humans, 48 ABC transporters have been identified so far. These transporters have been grouped into 7 subfamilies (ABCA – ABCG) based on sequence homology and protein topology (Vasiliou, Vasiliou and Nebert, 2009).

The ABCA subfamily is composed of 12 members. It contains some of the largest ABC transporters, with the majority of them being more than 2100 amino acids in length, with the ABCA13 transporter predicted to be 5058 amino acids long, making it the largest ABC transporter known. Members of this subfamily are full transporters organized into two tandem halves, with each half containing one TMD, one NBD and a large extra-cytosolic domain (ECD) (Bungert, Molday and Molday, 2001; Dean, 2002; Vasiliou, Vasiliou and Nebert, 2009; Molday, 2015). Some ABCA transporters have been implicated in the transport of lipids and cholesterol based on knockout-mice studies, cell-based studies, and biochemical studies (Weng *et al.*, 1999; McNeish *et al.*, 2000; Orsó *et al.*, 2000; Wang *et al.*, 2003; Tanaka *et al.*, 2003, 2011; Fitzgerald *et al.*, 2004; Kim *et al.*, 2005; Macé *et al.*, 2005; Brunham *et al.*, 2006; Cuchel *et al.*, 2010; Tarling, Vallim and Edwards, 2013; Quazi and Molday, 2013).

Several ABC transporters are clinically relevant. In bacteria, some ABC transporters export antibiotics and are a contributing factor to antibiotic resistance (Davidson *et al.*, 2008). Genetic

diseases caused by mutations in human ABC transporters include cystic fibrosis, diabetes, Stargardt disease, Tangier disease, pseudoxanthoma elasticum, adrenoleukodystrophy, and sitosterolemia (Linton, 2007; Tarling, Vallim and Edwards, 2013; Molday, 2015). Furthermore, several gene variants in some ABC transporters have also been associated as risk factors for Alzheimer disease (Abuznait and Kaddoumi, 2012; De Roeck, Van Broeckhoven and Slegers, 2019; Jia *et al.*, 2020), and over-expression of the P-glycoprotein (ABCB1) in cancer cells is known to lead to chemotherapy-drug resistance (Dean, 2002; Linton, 2007; Montanari and Ecker, 2015).

1.1.1 Transport Mechanisms

The molecular mechanism of transport of substrates across cellular membranes by ABC transporters has been extensively studied. Crystal structures from prokaryotic and eukaryotic transporters, from importers and exporters, and in the apo or nucleotide or substrate bound state have been resolved over the years (Rees, Johnson and Lewinson, 2009; Montanari and Ecker, 2015; Wilkens, 2015; Ford and Beis, 2019). Furthermore, biophysical and biochemical studies using non-hydrolysable ATP analogues, cross-linking agents, radio-labelled substrates and nucleotides, substrate transport assays, electron paramagnetic resonance (EPR), single molecule Förster resonance energy transfer (smFRET), and more, have also provided key insights into the kinetic details of substrate translocation (Senior, Al-Shawi and Urbatsch, 1995; Loo, Bartlett and Clarke, 2003; Borbat *et al.*, 2007; Ward *et al.*, 2007; Siarheyeva, Liu and Sharom, 2010; Verhalen and Wilkens, 2011; Husada *et al.*, 2018). Based on these structural and biochemical studies, three major models for substrate transport have been proposed: The alternating access model, the switch model, and the constant contact model (Higgins and Linton, 2004; Dawson, Hollenstein and Locher, 2007; Sauna *et al.*, 2007; Oldham, Davidson and Chen, 2008; Rees,

Johnson and Lewinson, 2009; Siarheyeva, Liu and Sharom, 2010; Wilkens, 2015). While these models share some fundamental steps such as the dimerization of the NBDs upon ATP binding, key differences exist in the translocation mechanism.

The alternating access model for substrate transport has been the predominant substrate translocation mechanism proposed for ABC transporters (Fig. 1.3) (Dawson, Hollenstein and Locher, 2007; Oldham, Davidson and Chen, 2008; Rees, Johnson and Lewinson, 2009; Wilkens, 2015). This model was suggested as a result of different crystal structures from ModABC, MalFGK₂, MsbA, and Sav1866 (Dawson and Locher, 2006; Hollenstein, Frei and Locher, 2007; Oldham *et al.*, 2007; Ward *et al.*, 2007; Khare *et al.*, 2009). A main premise of this model is that the substrate binding site and translocation pathway in the TMDs can alternate between an inward facing conformation, where the substrate binding site is open towards the cytosolic side of the membrane, and an outward facing conformation, where the substrate binding site is open towards the extracytosolic side of the membrane. In this model, the substrate binding site of ABC transporters has access to both sides of the membrane depending on whether the NBDs are in an apo state (or ADP bound state) or bound to ATP (Dawson, Hollenstein and Locher, 2007). Binding of ATP leads to the dimerization of the NBDs leading to a conformational change in the TMDs that switches the inward and outward facing states (Fig. 1.3). The changes in the NBDs and TMDs are mediated via the coupling helices in the TMDs and the Q-loop and α -helical domain, where the LSGGQ motif resides, in the NBDs (Khare *et al.*, 2009; Orelle *et al.*, 2010). For importers, the affinity for the substrate is higher in an outward facing conformation, allowing for tight substrate binding, and lower in an inward facing conformation, leading to substrate release into the cytosol, the opposite is true for exporters.

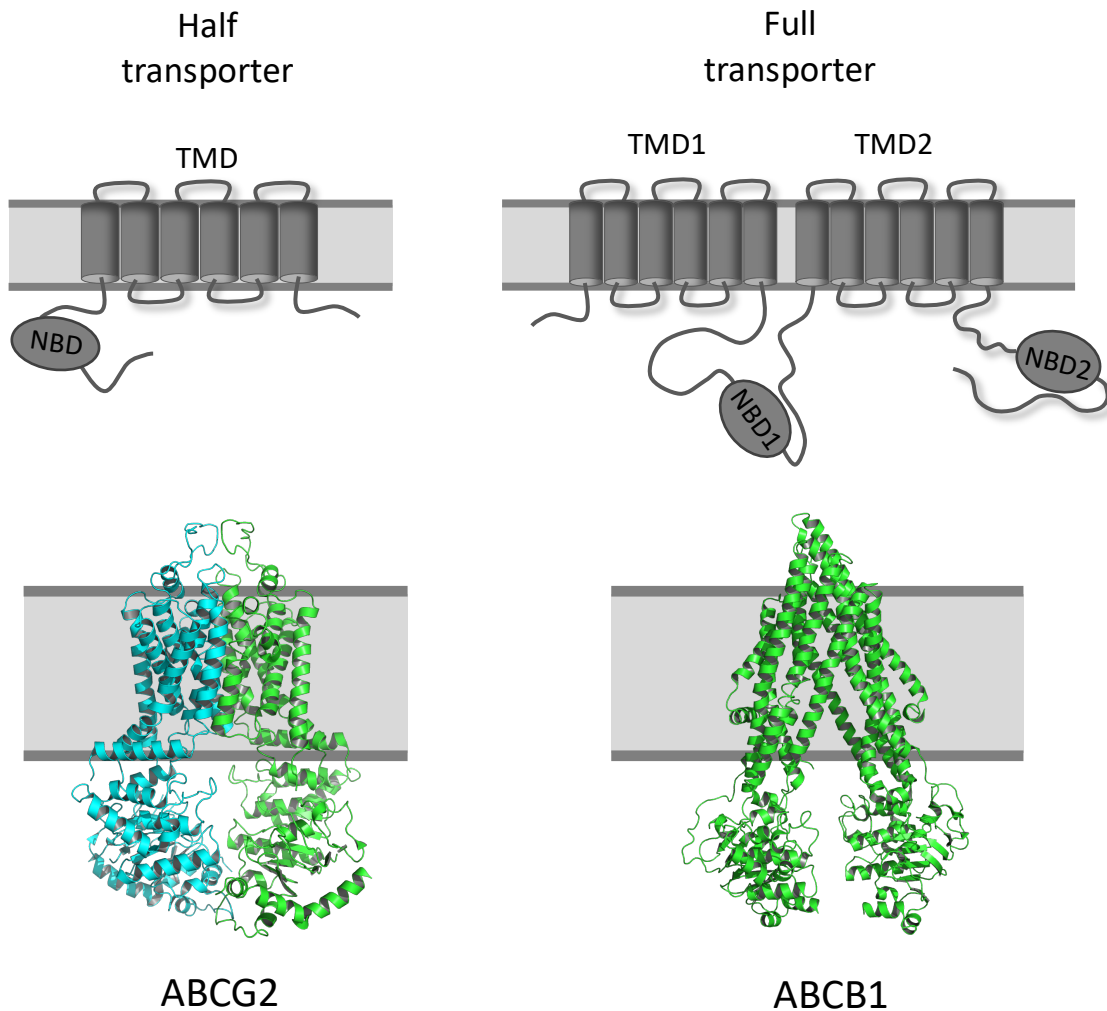


Figure 1.2 Eukaryotic ABC transporters.

In eukaryotes, ABC transporters, the majority of which are exporters, can be subdivided into half transporters or full transporters. Half transporters form homo or heterodimers to form a full working protein. The ABCG2 transporter (6VXF) is a half transporter that forms a homodimer and is involved in multiple drug resistance. The ABCB1 protein (6C0V), more commonly known as the P-glycoprotein, is a full transporter also involved in multiple drug resistance.

The switch model focuses on the kinetic steps that happen in the NBDs during ATP binding and hydrolysis which allow for substrate transport (Higgins and Linton, 2004; Wilkens, 2015). A fundamental characteristic of this model is that binding of ATP in the NBDs leads to

their dimerization (closing), and this dimerization provides the key power stroke that drives the conformational changes in the TMDs resulting in substrate translocation (Linton, 2007).

Hydrolysis of ATP to ADP and sequential ADP release restores the TMDs to their original resting conformation to allow for another transport cycle (Fig. 1.3) (Higgins and Linton, 2004).

The closing and opening of the NBDs as a result of ATP binding or hydrolysis acts as a switch that can regulate the conformational changes in the TMD necessary for substrate transport. In turn, it is postulated that substrate binding is necessary to increase the affinity of the NBDs for ATP to allow for dimerization of the NBDs (Fig. 1.3). This model assumes that binding and hydrolysis of two ATP molecules occurs sequentially rather than simultaneously (Higgins and Linton, 2004). Furthermore, this model suggest that ADP also dissociates sequentially from the NBDs after ATP hydrolysis and that the nucleotide free (apo) form of the transporter is likely necessary for substrate binding.

The constant contact model has been described in detail in biochemical studies with the P-glycoprotein using non-hydrolyzable ATP analogues (Sauna *et al.*, 2007; Siarheyeva, Liu and Sharom, 2010; Verhalen and Wilkens, 2011; Wilkens, 2015). This model, like the switch model, also focuses more on what is happening in the NBDs during the ATP binding and hydrolysis steps rather than whether the substrate has an alternating access to either side of the membrane based on ATP binding and hydrolysis; like the switch model and the alternating access model, this model assumes the TMDs have access to both sides of the membrane. In this model, the two ATP molecules that bind to each of the ATP binding pockets formed at the interface of the two NBDs, between the LSGGQ motif of one NBD and the Walker-A motif of the adjacent NBD, do not bind equally. Rather, each ATP has different affinity to the NBDs (Siarheyeva, Liu and Sharom, 2010). One ATP molecule remains “occluded” and has 120 fold higher affinity to the

NBDs than the other ATP molecule (Sauna *et al.*, 2007; Siarheyeva, Liu and Sharom, 2010).

This differential affinities of the ATP molecules switch back and forth between each ATP binding site, leading to assymetrical hydrolysis of ATP. As a result, there is always at least one nucleotide binding site occouped by either ATP or ADP during each transport cycle (Siarheyeva, Liu and Sharom, 2010).

Overall, while there are parallels between each of these models, the detailed kinetic steps that occur during substrate binding, ATP binding, NBD dimerization, and ATP hydrolysis, remained to be fully elucidated. It is still not well understood how tightly coupled substrate translocation and ATP hydrolysis are in terms of the stoichiometric ratio of substrate transport to ATP molecules hydrolyzed. Likewise, whether substrate binding is necessary to facilitate binding of ATP in the NBDs, and, whether ATP binding and hydrolysis occurs in sequential steps or simultaneously are important questions that remain to be resolved. Similarly, key steps in the catalytic cycle of ATP hydrolysis remain uncharacterized, such as which amino acid acts as the catalytic base during ATP hydrolysis. Of course, given the diversity of ABC transporters, the fact that some transporters can transport more than one substrate, whereas other transporters are substrate specific; or the fact that different folds are found within the TMDs domains of different transporters; or that ABC transporters can act as importers or exporters, it is likely that there may be more than a single transport mechanism across all ABC transporters. To get to the bottom of these issues, more structures of ABC transporters in different states (apo, substrate bound, ATP bound, ADP bound) need to be resolved and this structural data needs to be complemented with an in-depth biochemical assessment of the kinetics of substrate translocation and ATP binding and hydrolysis.

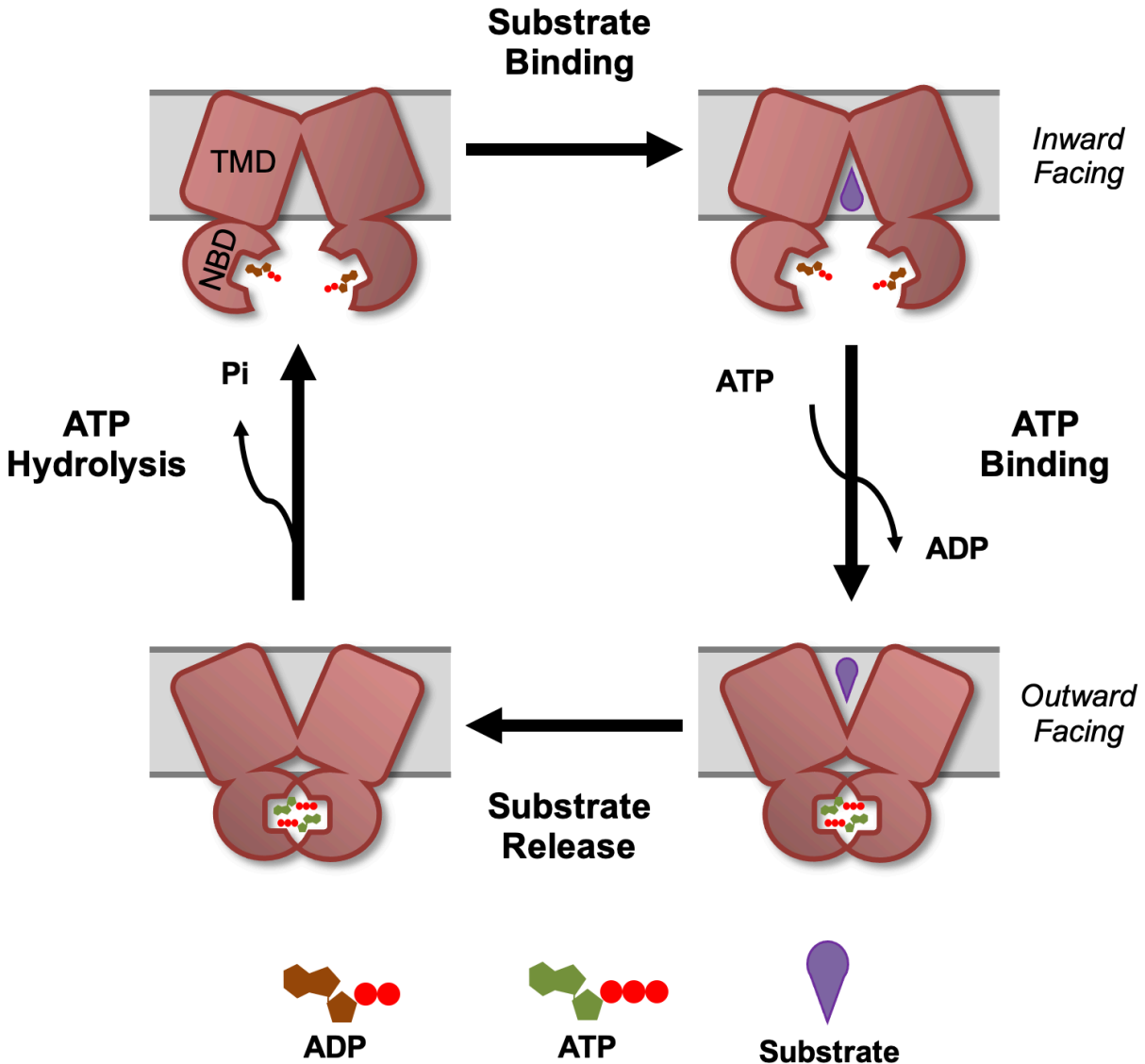


Figure 1.3 Generalized transport model for ABC transporters.

Although several key details in the transport mechanism of ABC transporter remain to be fully elucidated, a generalized model of transport can be conceptualized based on crystal structures from prokaryotic and eukaryotic ABC transporters. In this model, the translocation pathway, where the substrate binding site is, has access to both sides of the membrane depending on whether it is bound to substrate or ATP (or both) or it is in an Apo (or ADP bound) state. For an exporter, as depicted here, substrate binding would occur in an inward facing conformation. This would be followed by ATP binding, leading to dimerization of the NBDs and a switch from an inward to an outward facing conformation. In this conformation, the exporter is in a low affinity state for its substrate and substrate release occurs. ATP hydrolysis would soon follow, which would revert back the transporter to its original inward facing conformation.

1.1.2 ABCA Subfamily

The ABCA subfamily is characterized by the presence of two ECDs, which are not found in any other ABC transporter. These ECDs have several N-glycosylation sites and form disulfide bonds with each other (Bungert, Molday and Molday, 2001). Although the function of these ECDs is not well understood, mutations in these domains of several ABCA members are known cause genetic diseases. This subfamily is composed of 12 genes and 5 pseudogenes (Dean, 2002; Vasiliou, Vasiliou and Nebert, 2009; Molday, 2015). The 12 genes that make up the ABCA subfamily can be subdivided into two distinct evolutionary branches based on phylogenetic analysis (Fig. 1.4). One branch gives rise to the ABCA5, ABCA6, ABCA8, ABCA9, and ABCA10 transporters. All these transporters localize to the same chromosomal position, 17q24, and likely arose as a result of a gene duplication event (Fig. 1.4) (Molday, 2015). The other evolutionary branch contains the ABCA1, ABCA2, ABCA3, ABCA4, ABCA7, ABCA12, and ABCA13 transporters. These genes are not clustered to a single chromosomal region and are found in six different chromosomes (Fig. 1.4).

The substrates of some members of the ABCA subfamily have been characterized through genetic studies, animal models, and biochemical and cell-based assays. Several studies have investigated the role of ABCA1, ABCA2, ABCA3, ABCA4, ABCA7 and ABCA12 in lipid transport (Table 1.1). ABCA1 and ABCA7 are lipid floppases, or exporters, that transport phosphatidylcholine (PC) and phosphatidylserine (PS) from the luminal side to the extracytosolic side of the membrane (Oram and Lawn, 2001; Quazi and Molday, 2013). ABCA2 has two protein isoforms with similar expression and localization patterns and is thought to transport PS, phosphatidylethanolamine (PE), and sphingomyelin (SM) and other sterols (Ile *et al.*, 2004; Davis and Tew, 2018). ABCA3 is an exporter that has been shown to transport PC and indirect

biochemical evidence suggest that it is also involved in SM transport (Cheong *et al.*, 2006; Li *et al.*, 2019). ABCA4 is a flippase, or importer, that transports PE and N-retinylidene phosphatidylethanolamine (N-ret-PE) from the luminal side to the cytosolic side of the disc membranes of photoreceptor cells (Quazi, Lenevich and Molday, 2012; Quazi and Molday, 2013). ABCA7 transports PS and SM, and ABCA12 transports ceramide (Wang *et al.*, 2003; Quazi and Molday, 2013; Haller *et al.*, 2014). Furthermore, ABCA1, ABCA2 and ABCA7 have also been implicated in the transportation of cholesterol and have been linked to cholesterolemias.

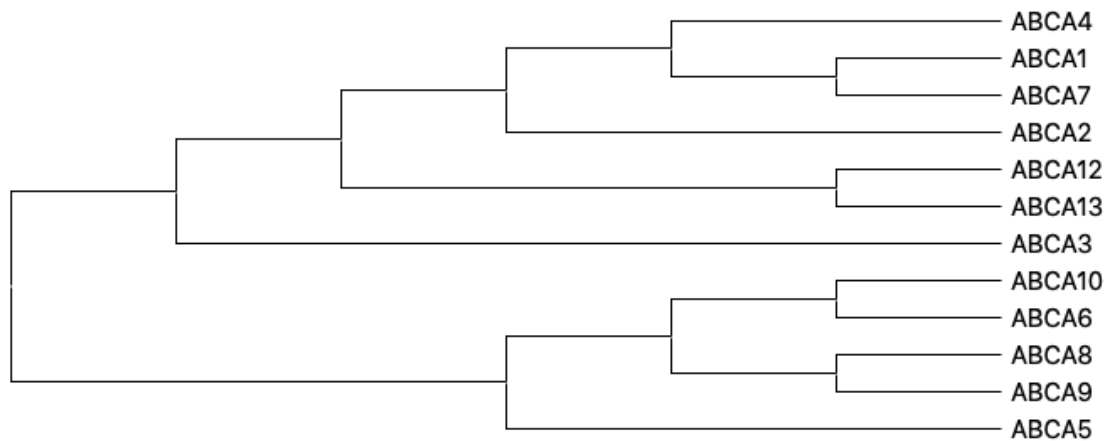


Figure 1.4 Cladogram of the human ABCA subfamily.

The human ABCA subfamily contains 12 genes that are split into two different evolutionary branches. ABCA5, 6, 8, 9, and 10 cluster together to chromosomal position 17q24 and likely arose as a result of a gene duplication event. The other branch gave rise to ABCA1, 2, 3, 4, 7, 12 and 13, with ABCA1, 4 and 7 sharing around 50% sequence identity.

Several genetic diseases have been associated with members of the ABCA subfamily including Tangier disease (ABCA1); Surfactant metabolism dysfunction (ABCA3); Stargardt disease, retinitis pigmentosa and cone-rod dystrophy (ABCA4); werewolf syndrome (Inherited hypertrichoses) (ABCA5); and harlequin type ichthyosis and lamellar ichthyosis type 2

(ABCA12) (Allikmets, 1997; Rust *et al.*, 1999; DeStefano *et al.*, 2014; Sheth *et al.*, 2018; Oltvai *et al.*, 2020). Moreover, Alzheimer disease has been associated with ABCA2 and ABCA7 (Macé *et al.*, 2005; De Roeck, Van Broeckhoven and Slegers, 2019; Jia *et al.*, 2020). Table 1.1 summarizes the different substrates and diseases associated with several members of the ABCA subfamily.

Table 1.1 Lipid transporters of the ABCA subfamily

Gene	Chromosomal location	Expression	Lipid Substrates	Clinical implications
ABCA1	9q31	Ubiquitous	PC, PS, Chol, SM	Tangier disease
ABCA2	9q34	Brain	PS, PE, SM	Alzheimer disease and chemotherapy drug resistance
ABCA3	16p13	Lung, heart, brain, pancreas	PC, SM	Surfactant metabolism dysfunction and chemotherapy drug resistance
ABCA4	1p22	Photoreceptors and RPE cells	PE, N-ret-PE	Stargardt disease, cone-rod dystrophy, retinitis pigmentosa
ABCA7	19p13	Lymphatic systems, brain, kidney and skin	PC, SM, Chol	Alzheimer disease
ABCA12	2q35	Skin	Ceramide	Harlequin type ichthyosis and lamellar ichthyosis type 2

1.1.2.1 ABCA4

ABCA4 is a 250kDa ABC transporter encoded by the *ABCA4* gene. Historically, ABCA4 was known as the Rim protein due to its localization to the rim regions of the outer segment disc membranes of rod photoreceptors, based on early immunocytochemical microscopy studies on frog ABCA4 (Fig. 1.5) (Papermaster *et al.*, 1978). In 1997, the bovine ortholog of the Rim protein was identified as a member of the ABC transporter superfamily (Illing, Molday and Molday, 1997). That same year, the human gene encoding for the Retinal ABC transporter, or ABCR, in humans was cloned and was identified as the gene responsible for Stargardt macular

degeneration (Allikmets, 1997). ABCR turned out to be the human ortholog of the Rim protein (Weng *et al.*, 1999). Over the years, as more ABC transporters were cloned and classified into their respective subgroups, ABCA4 became the preferred name for the ABCR transporter and Rim protein.

Initial immunocytochemical microscopy studies in frog retinas showed that ABCA4 localized to the outer segments of rod and cone photoreceptors (Papermaster *et al.*, 1978; Papermaster, Reilly and Schneider, 1982). Follow-up studies, however, only found strong labelling of human and bovine ABCA4 in the outer segments of rod photoreceptors, but not cone photoreceptors (Hui Sun and Jeremy Nathans, 1997; Illing, Molday and Molday, 1997). Yet, in 2000, confocal microscopy studies of human retina cryosections confirmed the original findings of Papermaster *et al.* and showed that ABCA4 was also found in the cone photoreceptors of the fovea as well as the peripheral regions in the retina (Molday, Rabin and Molday, 2000). More recently, ABCA4 was shown to be expressed in the RPE cells, though the predominant localization of ABCA4 is the outer segment disc membrane of photoreceptors cells (Lenis *et al.*, 2018).

Structure of ABCA4:

Like all members of the ABCA subfamily, ABCA4 is a full transporter organized in two tandem halves with each half containing one TMD, NBD and ECD. The structure of ABCA4 in the apo state has been resolved by single particle electron microscopy to a resolution of 18 Å (Tsybovsky *et al.*, 2013). Although at this resolution major structural details are missing, the overall shape of ABCA4 can be discerned. Further structural insights have been attained with homology models that use the ABCA1 cryo-EM structure as the template, since ABCA1 shares 50% sequence homology with ABCA4 (Fig. 1.6). Additionally, hidden Markov algorithms have

been used to predict the amino acid sequences that make up the transmembrane segments of the TMDs (Garces *et al.*, 2021). Based on these algorithms and the homology model of ABCA4, each TMD of ABCA4 is predicted to have 6 transmembrane helices. The TMDs form the substrate binding site and translocation pathway in ABCA4. Each TMD has two coupling helices on the cytosolic side of the membrane. For TMD1, the coupling helices are located before T1 and between T2 and T3; similarly, for TMD2 the coupling helices are before T7 and between T8 and T9 (Fig. 1.6). These coupling helices are likely important for coordinating the conformational changes that occur in the NBDs in response to ATP binding and hydrolysis with the conformational changes in the TMDs that result in the translocation of the substrate across the disc membrane in the photoreceptor outer segments. On the luminal side of the TMDs, the ECDs extend between T1 and T2 for ECD1, and between T7 and T8 for ECD2. Additionally, two V-shaped alpha-helical hairpins that protrude slightly into the membrane connect T5 and T6 in TMD1 and T11 and T12 in TMD2 (Fig. 1.6). The two ECDs vary considerably in size, ECD1 is approximately 600 amino acids and ECD2 is approximately 280 amino acids in length. These ECDs have several N-glycosylation sites and form disulfide bridges with each other which likely helps to stabilize their folds (Illing, Molday and Molday, 1997; Bungert, Molday and Molday, 2001; Tsybovsky *et al.*, 2011).

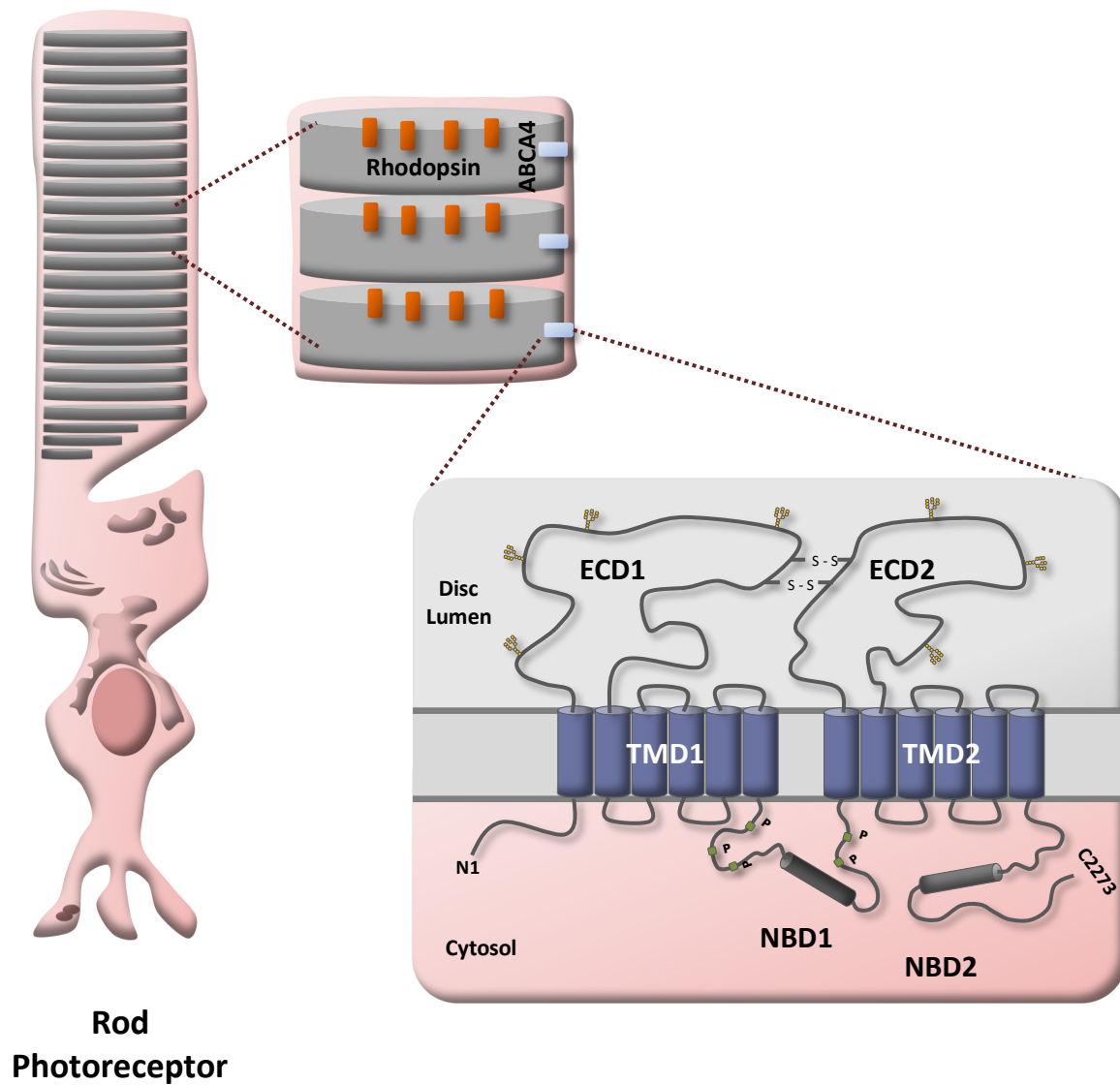


Figure 1.5 Cellular localization of ABCA4.

ABCA4 is predominantly found in the disc membranes of rod and cone photoreceptors, although expression in the RPE cells has been documented as well. Within the disc membranes, ABCA4 resides in the rim region of these discs. ABCA4 is a full transporter containing 2 ECDs, TMDs and NBDs. The ECDs have intra and inter disulfide bridges, likely involved in stabilizing the tertiary structure of these domains. The TMDs form the N-ret-PE and PE translocation pathway. The NBDs mediate binding and hydrolysis of ATP with N-ret-PE or PE transport.

Function of ABCA4:

Biochemical studies with immunopurified ABCA4 and *Abca4*^{-/-} knockout mice provided the first evidence of its involvement in the transport of retinoid compounds (Weng *et al.*, 1999; Mata, Weng and Travis, 2000). Early studies showed that when ABCA4 was purified and reconstituted into proteoliposomes the ATPase activity of ABCA4 increased about twofold in the presence of all-*trans* and 11-*cis* retinal but not retinol or retinyl esters (Illing, Molday and Molday, 1997; Sun, Molday and Nathans, 1999; Ahn, Wong and Molday, 2000). Furthermore, it was shown that this increase in ATPase activity required the presence of PE (Ahn, Wong and Molday, 2000). Substrate-induced ATPase activity has been documented in other ABC transporters, such as the multiple-drug resistance P-glycoprotein (ABCB1) (Shapiro and Ling, 1994; Senior, Al-Shawi and Urbatsch, 1995; Verhalen and Wilkens, 2011). Additionally, solid-phase N-ret-PE binding assays showed that ABCA4 bound tightly to N-ret-PE and that addition of ATP would lead to release of N-ret-PE from ABCA4 (Beharry, Zhong and Molday, 2004). Based on these observations, it seemed likely that N-ret-PE, the Schiff base formed between PE and all-*trans* or 11-*cis* retinal, could be the substrate of ABCA4.

Mouse models have also been used to gain functional insights into ABCA4. The first *Abca4*^{-/-} knockout mice studies were done by the Travis research group (Weng *et al.*, 1999; Mata, Weng and Travis, 2000). *Abca4*^{-/-} knockout mice had delayed dark adaptation, and increased concentration of all-*trans*-retinal, protonated N-ret-PE, and PE, and decreased levels of retinol and all-*trans*-RE (retinyl esters) when subjected to light (Weng *et al.*, 1999). Furthermore, N-retinylidene-N-retinylethanolamine (A2E) and lipofuscin deposits accumulated in the retinas of these *Abca4*^{-/-} mice upon photobleaching (Weng *et al.*, 1999; Mata, Weng and Travis, 2000). Later work done by the Crouch's laboratory, showed that *Abca4*^{-/-} mice accumulated N-ret-PE,

A2E and lipofuscin at much higher levels than age-matched WT mice. However, in contrast to the findings of the Travis laboratory, this increase in bisretinoid species and lipofuscin was not dependent on light exposure (Boyer *et al.*, 2012). Taken together, these results suggest that ABCA4 plays an important role in the clearance of excess all-*trans*-retinal as well as 11-*cis*-retinal from photoreceptor discs thereby preventing the formation and accumulation of bisretinoids such as A2E and of lipofuscin in RPE cells. Patients with STGD1 and other ABCA4 related retinopathies, exhibit high concentrations of retinoid, bisretinoids and lipofuscin, suggesting that the long-term accumulation of these compounds have a detrimental role in the photoreceptors and RPE cells likely leading to their death.

Although the previous biochemical and animal studies provided strong evidence on the role of ABCA4 in the clearance of all-*trans*-retinal and 11-*cis*-retinal via the transport of their Schiff base with PE, N-ret-PE, it was not until 2012 that a biochemical assay was developed by the Molday research group to directly measure the transport of N-ret-PE across disc membranes (Quazi, Lenevich and Molday, 2012). This assay used tritiated all-*trans*-retinal to measure the direct transport and transfer of N-ret-PE from a donor proteoliposome (or native photoreceptor disc membranes) to an empty liposome in the presence of ATP. The results from this transport assay provided direct evidence that ABCA4 was an importer of N-ret-PE (Quazi, Lenevich and Molday, 2012).

ABCA4 MODEL

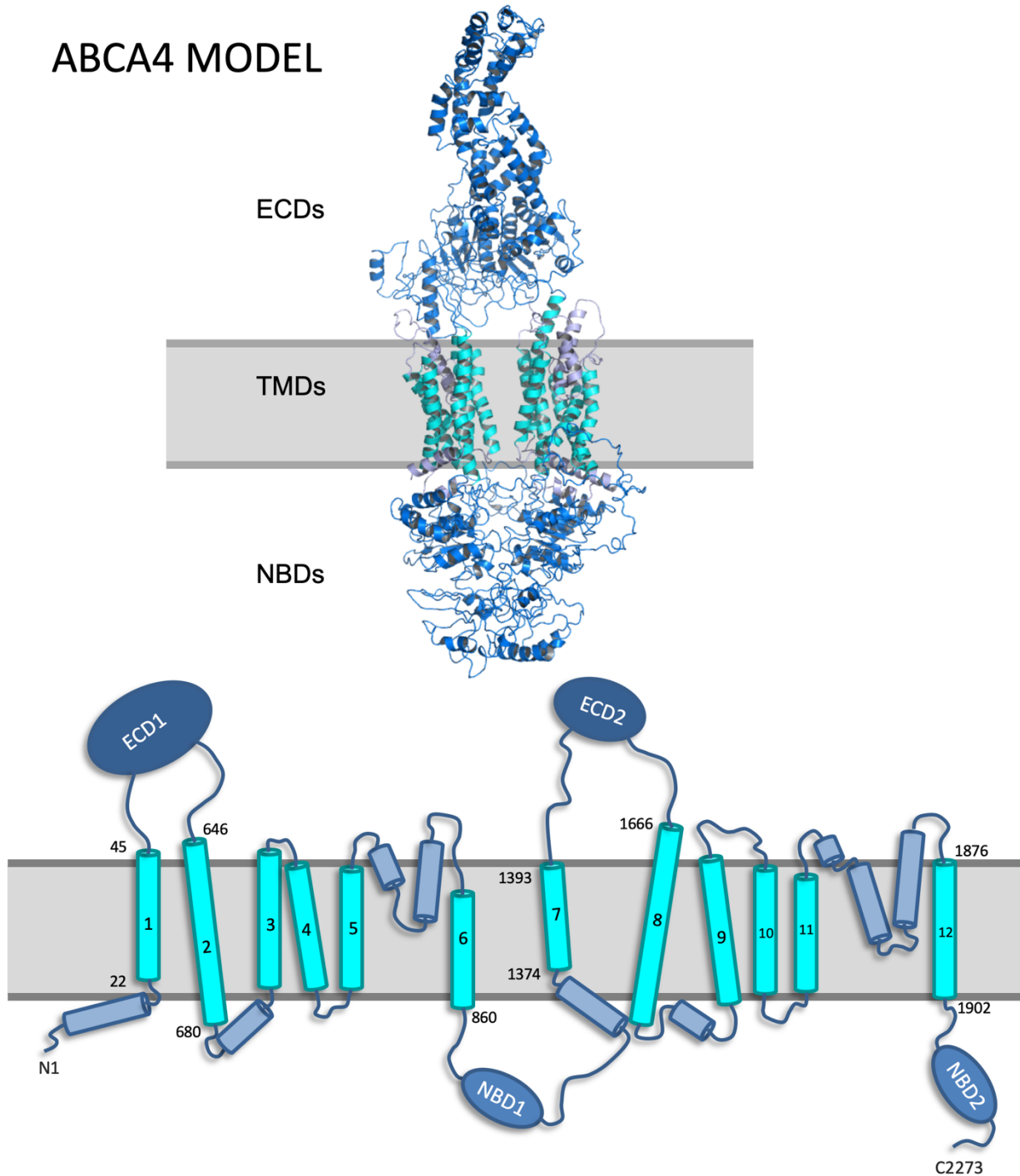


Figure 1.6 Homology Model of ABCA4

SWISS-MODEL was used for modeling ABCA4 using the ABCA1 Cryo-EM structure (5XYJ) as template, which bears 50% sequence identity with ABCA4. The homology model highlights the ECDs (dark blue), TMDs (Cyan for TM helices, and light blue for interconnecting loops/helices), and NBDs (dark blue).

1.2 The Retina

The retina is a light sensing tissue localized to the back of the eye. It is composed of different types of neurons and synapses that form defined layers and work together to sense and transmit light signals. The photoreceptor layer contains the rod and cone photoreceptor neurons. Rod photoreceptors are responsible for sensing dim light and black and white vision. Cone photoreceptors, found in high density within the fovea of the retina, are responsible for color vision and high acuity vision. The retinal pigment epithelium (RPE) forms a layer on the basal side of the photoreceptors, where the outer segments of photoreceptors are found. The RPE cells are closest to the choroid and provide nourishment and support to the photoreceptors of the retina. These cells are also important for the renewal of the outer segments of photoreceptors as they are continuously phagocytosing the ends of the photoreceptors. Anterior to the outer segment layer of the photoreceptors, is the inner segment and the outer nuclear layer, which contains the cell bodies of the photoreceptors. Next, is the outer plexiform layer, which forms synapses between the rod and cone photoreceptors and the dendrites of bipolar cells and horizontal cells. The inner nuclear layer contains the cell bodies of the amacrine cells, bipolar cells and horizontal cells. This is followed by the inner plexiform layer where synapses form between the axons of bipolar cells, horizontal cells, and amacrine cells and the dendrites of ganglion cells. The ganglion cell layer contains the cell bodies of the ganglion cells, the axons of these ganglion cells become part of the optic nerve. Molday and Moritz provide a good summary of the morphology and function of the retina, RPE cells, photoreceptors, phototransduction and the visual cycle (Molday and Moritz, 2015).

1.2.1 Photoreceptors

The photoreceptor cells of the retina are highly differentiated neurons responsible for light perception via the phototransduction pathway. There are two types of photoreceptors, the rod photoreceptors and the cone photoreceptors. The rod photoreceptors are spread throughout the retina and are involved in peripheral vision and in vision under dim light due to their high sensitivity to photons. The structure of the rod photoreceptor can be subdivided into distinct regions: The outer segment, the connecting cilium, the inner segment, the cell body and the synaptic region (Fig. 1.7). The outer segment is an extension of the connecting cilium, it is composed of approximately 1000 stacked discs that are enclosed by a separate membrane (Reviewed in Molday and Moritz, 2015). Outer segment renewal is a continuous process where the distal ends of the outer segments of both rod and cone photoreceptors are continuously phagocytosed by the RPE cells (Kevany and Palczewski, 2010), while new discs are formed at the base of the outer segments (Young and Droz, 1968), just above the connecting cilium (Reviewed in Molday and Moritz, 2015). These discs are enriched with the protein machinery necessary for phototransduction, with 85% of the total membrane protein in the outer segments composed of the G-protein coupled receptor rhodopsin for rod photoreceptors, or cone opsin for cone photoreceptors (Fotiadis *et al.*, 2003; Gunkel *et al.*, 2015; Liebman and Entine, 1974). The connecting cilium of rod and cone photoreceptors is non-motile and has a 9+0 microtubule arrangement in the axoneme (Gilliam *et al.*, 2012; reviewed Molday and Moritz, 2015). At the base of the connecting cilium, the basal body and axoneme meet. The basal body, in turn, is anchored to the ciliary rosette, which extends proximally into the inner segment of the photoreceptors (Gilliam *et al.*, 2012; reviewed Molday and Moritz, 2015). The main purpose of the connecting cilium is to connect the outer and inner segments of the photoreceptors and

regulate protein trafficking between these two segments (Jin *et al.*, 2010; Molday and Moritz, 2015; Nachury *et al.*, 2007; Wang and Deretic, 2015). The inner segment of the photoreceptors is where the majority of the organelles reside, and it is particularly enriched with mitochondria (Reviewed in Molday and Moritz, 2015). The cell body contains the nucleus and ER and the synaptic region contains the synaptic vesicles (Fig. 1.7). The synaptic vesicles are filled with glutamate, which acts as a neurotransmitter (Reviewed in Waldner *et al.*, 2018). The release of glutamate at the synapse of the photoreceptors is inhibited as a result of hyperpolarization that ensues during phototransduction (Reviewed in Waldner *et al.*, 2018).

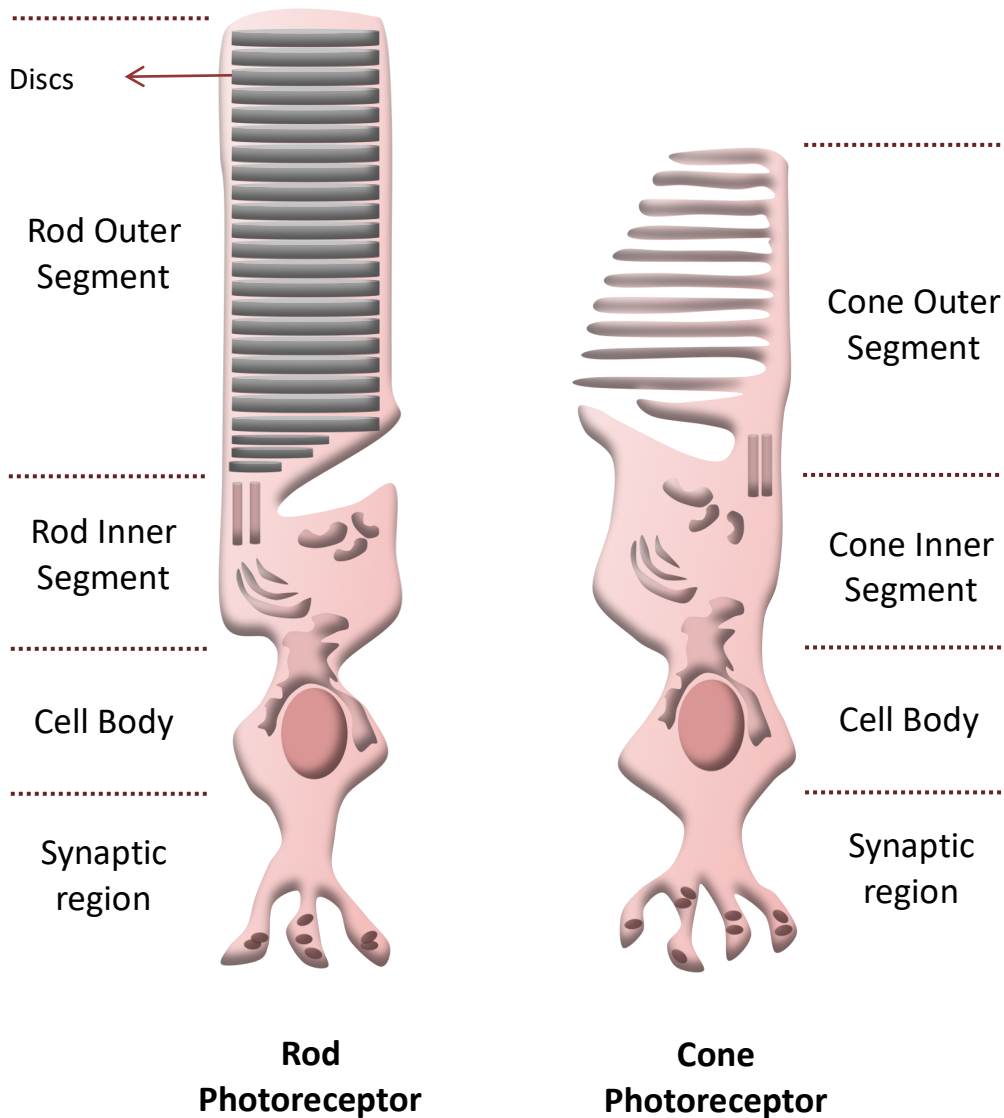


Figure 1.7 Morphology of Photoreceptors Cells.

The light sensing rod and cone photoreceptor cells of the retina are highly differentiated neurons responsible for the phototransduction pathway. Both photoreceptors can be divided into distinct functional and morphological regions: The outer segment, the inner segment, the cell body and the synaptic region. The rod photoreceptors, which are evenly distributed throughout the retina and are responsible for vision under low light intensity, have longer outer segments and their discs are circumscribed by their own membrane. The cone photoreceptors, which concentrate in the macula of primate retina, have shorter outer segments and their discs are continuous with the plasma membrane. Additionally, there are three types of cone cells responsible for sensing three distinct wavelengths of light, necessary for color vision.

1.2.2 Phototransduction

The first step in the phototransduction pathway involves the light-sensitive retinoid chromophore 11-*cis*-retinal and the G-protein coupled receptor (GPCR), opsin. In the rod photoreceptors, rhodopsin refers to opsin containing a bound 11-*cis*-retinal. Phototransduction is initiated when a photon of light photoisomerizes 11-*cis*-retinal to all-*trans*-retinal within the context of rhodopsin (Kukura *et al.*, 2005; Lamb and Pugh, 2006; Arshavsky and Burns, 2012). This activated form of rhodopsin, referred to as metarhodopsin II, activates the heterotrimeric G-protein transducin by catalyzing the exchange of GDP for GTP in the α subunit of transducin (Fung and Stryer, 1980; Fung *et al.*, 1981; Lamb and Pugh, 2006; Arshavsky and Burns, 2012). This leads to the dissociation of the α subunit from the β and γ subunits of transducin. The dissociated α -transducin stimulates the enzyme phosphodiesterase 6 (PDE6), which then catalyzes the hydrolysis of cGMP to 5'-GMP (Catty, *et al.*, 1992; Clerc and Bennett, 1992; Clerc, *et al.*, 1992; D'Amours and Cote, 1999; Fung *et al.*, 1981; Mou, *et al.*, 1999). This leads to a reduction of the intracellular concentration of cGMP resulting in the dissociation of cGMP from the CNG channels, causing their closure. The closing of the cGMP-gated channels interrupts the influx of Ca^{2+} and Na^{+} into the cytosol of the outer segments, leading to the hyperpolarization of the plasma membrane and inhibition of glutamate release at the synapse of the photoreceptors. At the same time, the continuous efflux of Ca^{2+} from the NCKX1 channel leads to a decrease in intracellular Ca^{2+} concentration.

To return to a dark state after photobleaching of the photoreceptors, several steps occur (Lamb and Pugh, 2006). First, the decrease in Ca^{2+} concentration promotes the phosphorylation of rhodopsin by the GPCR kinase (GRK1), thereby allowing arrestin to bind to and inhibit phosphorylated rhodopsin (Lamb and Pugh, 2006; C. K. Chen *et al.*, 2012). At the same time, the

GTPase activating protein (GAP), RGS9, accelerates the hydrolysis of GTP bound to α -transducin to GDP thereby inactivating α -transducin and causing it to reform the heterotrimeric structure with its β and γ counterparts (Arshavsky and Wensel, 2013). This prevents PDE6 from further hydrolyzing cGMP. Similarly, the guanylate cyclase activating protein (GCAP) activates guanylate cyclase 1 (GC1) which catalyses the synthesis of cGMP from GTP, restoring the concentration of intracellular cGMP. The increased concentration of cGMP leads to the binding of cGMP to the CNG channel and the opening of the channels (Baehr and Palczewski, 2007). The opening of the CNG channels, in turn, re-establishes the influx of Ca^{2+} and Na^{+} ions into the cells thereby restoring the cell to its partially depolarized state, and original voltage differentials across the plasma membrane of the photoreceptors. This restores the release of the glutamate neurotransmitter in the synaptic region of the photoreceptors (Molday and Moritz, 2015).

1.2.3 Visual Cycle

After 11-*cis*-retinal has been photoisomerized to all-*trans*-retinal within the context of rhodopsin (metarhodopsin II), as part of the initial step of the phototransduction pathway, it is imperative that all-*trans*-retinal be recycled back to 11-*cis*-retinal for phototransduction to continue. The process of recycling all-*trans*-retinal to 11-*cis*-retinal is called the visual cycle, and it involves several key enzymes and two cell layers: the outer segment of the photoreceptors and the RPE cells. The visual cycle begins as all-*trans*-retinal, formed by the photoisomerization of 11-*cis*-retinal, dissociates from rhodopsin. Free all-*trans*-retinal is then reduced to all-*trans*-retinol by the enzyme retinol dehydrogenase 8 (RDH8) (Ishiguro *et al.*, 1991). Additionally, any all-*trans*-retinal that is trapped in the luminal side of the disc membranes can react reversibly with PE to form the Schiff base condensation product, N-ret-PE (Molday, 2015; Molday and Moritz, 2015). ABCA4 can then bind to N-ret-PE and flip it towards the cytosolic leaflet of the

disc membranes where N-ret-PE then dissociates from ABCA4 so that all-*trans*-retinal can be reduced to all-*trans*-retinol by RDH8. All-*trans*-retinol is more soluble and less reactive than all-*trans*-retinal and more easily diffuses through the cytosol of the photoreceptors until it reaches the interphotoreceptor matrix. All-*trans*-retinol is then transported to the adjacent RPE cells by the interphotoreceptor retinoid binding protein (IRBP) (Saari *et al.*, 1985; Saari, 2012). Once inside the cytosol of the RPE cells, all-*trans*-retinol is esterified to all-*trans*-retinyl ester by the lecithin-retinol acyltransferase (LRAT) enzyme (Ruiz and Bok, 2010). The retinylesters formed by LRAT can be stored in specialized compartments in the RPE cells called retinosomes (Saari, 2012). Alternatively, all-*trans*-retinyl ester can be hydrolyzed and isomerized to 11-*cis*-retinol by the isomerohydrolase enzyme RPE65 (Jin *et al.*, 2005). This is followed by the oxidation of 11-*cis*-retinol to 11-*cis*-retinal by the 11-*cis*-retinol dehydrogenase enzyme 5 (RDH5), which restores the light sensing chromophore pigment used in phototransduction (McBee *et al.*, 2001). Subsequently, 11-*cis*-retinal likely bound to cellular retinaldehyde binding protein (CRALBP) diffuses through the RPE cytosol and into the interphotoreceptor matrix, where it is shuttled back to the photoreceptors by IRBP, for the regeneration of rhodopsin, thus allowing the continuation of the light-sensing phototransduction pathway (Fig. 1.8).

The accumulation of retinaldehydes after photobleaching can be detrimental to the photoreceptors and the RPE cells. Any retinaldehyde (all-*trans* or 11-*cis* retinal) that makes it to the inner segment of the photoreceptor can be reduced to retinol by the RDH12 enzyme, thereby preventing the accumulation of these toxic species in the photoreceptors (Maeda, Golczak, *et al.*, 2009). Retinaldehydes are toxic to the photoreceptors both indirectly and directly. The aldehyde group of these retinoids is highly reactive and can cause direct oxidative damage in the photoreceptors (Maeda, Maeda, *et al.*, 2009; Masutomi *et al.*, 2012; Y. Chen *et al.*, 2012;

Fujinami *et al.*, 2015; Cubizolle *et al.*, 2020). At the same time, the Schiff base conjugate N-ret-PE can react with a free retinal molecule and form bisretinoid mixtures within the photoreceptors such as phosphatidylpyridinium bisretinoid (A2PE), or phosphatidyl-dihydropyridine bisretinoid, (A2-DHP-PE) among others (Liu *et al.*, 2000; Ueda *et al.*, 2016). Subsequently, as the RPE cells phagocytose the distal end of the outer segments of photoreceptors as part of the renewal process, these bisretinoid mixtures accumulate in the RPE cells where they undergo hydrolysis and formation of the major components of lipofuscin (eg: A2E), which are likely toxic to the RPE cells (Radu *et al.*, 2014; Sawada *et al.*, 2014; Li *et al.*, 2015; Zhu *et al.*, 2016; Cubizolle *et al.*, 2020). Overall, the different retinoid species in the retina are tightly controlled through the visual cycle in order to prevent the formation of toxic retinoid and bisretinoid byproducts. For this reason, mutations in several enzymes associated with the visual cycle have been linked to one or more retinal degenerative diseases, collectively known as retinopathies (Fig. 1.8).

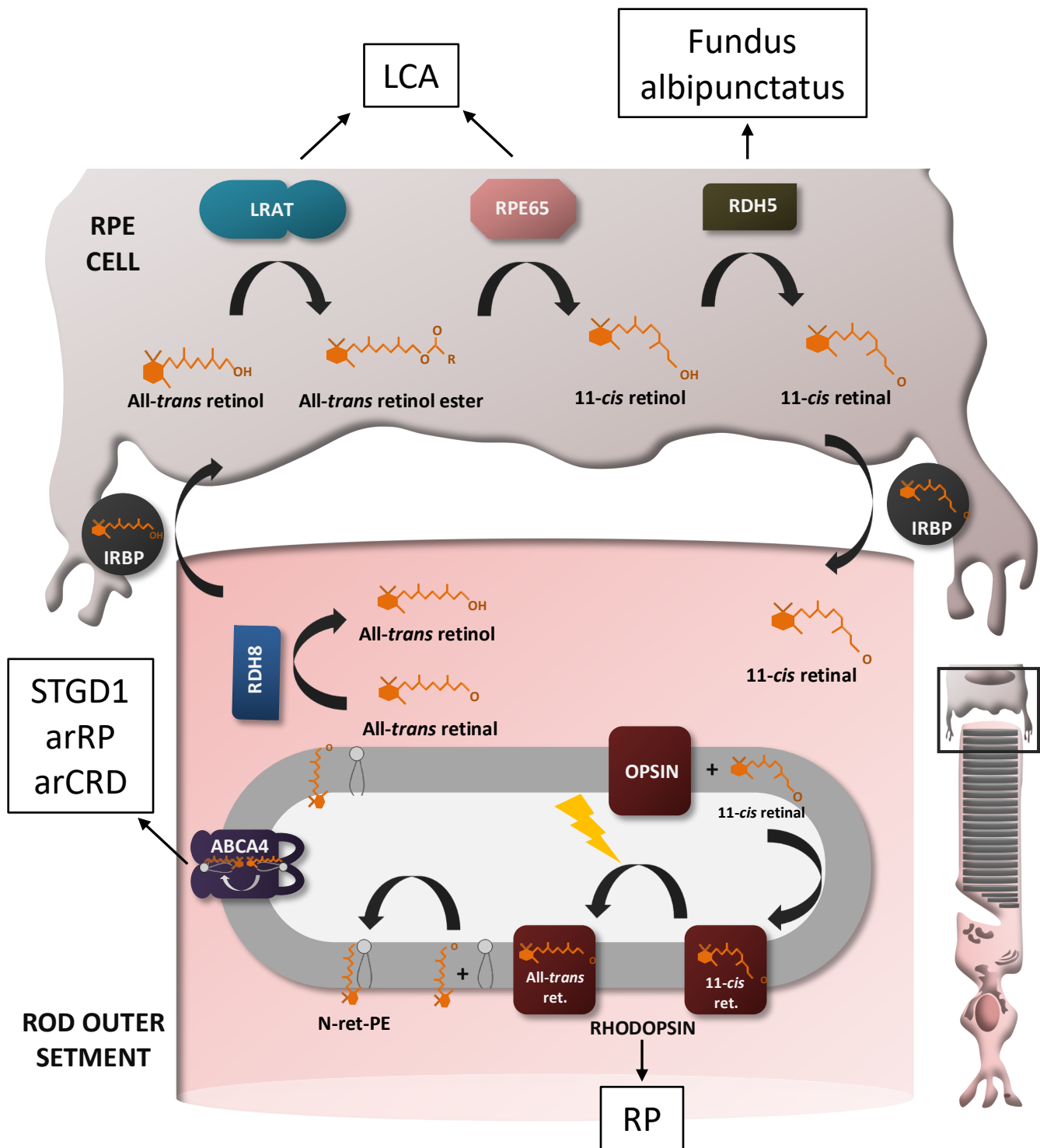


Figure 1.8 The Visual Cycle.

The retinoid cycle or the visual cycle describes the enzymatic recycling of the light-sensing chromophore 11-cis-retinal from photobleached all-trans-retinal. Two types of cell layers are involved in this cycle: The photoreceptors and the RPE cells. Several enzymes involved in this process are known to cause retinal degenerative diseases when mutated. RP = Retinitis pigmentosa, arRP = autosomal recessive RP, arCRD = autosomal recessive Cone-Rod dystrophy, STGD1 = Stargardt disease, LCA = Leber congenital amaurosis.

1.3 Retinal Degenerative Diseases

Retinal degenerative diseases can be caused by genetic mutations important for the structure and function of the retina, by environmental factors such as prolonged over exposure to UV light or smoking, by complications from other diseases such as diabetes, or as a result of the aging process such as in age related macular degeneration (AMD) or glaucoma. Furthermore, a combination of aging, environmental, and genetic risk factors can contribute to the development and severity of certain retinopathies (Heesterbeek *et al.*, 2020). Diabetic retinopathy can be non-proliferative or proliferative. In non-proliferative diabetic retinopathy, the blood vessels of the retina deteriorate and get blocked, leading to leakage of fluids and fats from the blood vessels that accumulate in the retina and result in vision loss. In proliferative retinopathy new blood vessels grow into the surface of the retina, which can lead to bleeding and scarring overtime (Fong *et al.*, 2004; Lee, Wong and Sabanayagam, 2015).

AMD is a progressive retinal degenerative disease that generally starts to develop around age 60-65. This retinopathy leads to the deterioration of the macula over time resulting in loss of central vision which can vary in severity. The different stages of AMD include early, intermediate and late, with the late stages further subdivided into dry or wet AMD (Fritsche *et al.*, 2014; Stahl, 2020). In dry AMD, granular yellow deposits called drusen build up between the choroid and the retina. These granules gradually and progressively damage the macula and lead to scarring and atrophy of the retina, which results in central vision loss. Wet AMD (or exudative AMD) is the more severe form of advanced AMD; 10-20% of individuals with dry AMD will progress to develop wet AMD (Heesterbeek *et al.*, 2020). Wet AMD is characterized by the abnormal proliferation of blood vessels (neovascularization) in the choriocapillaris as a result of vascular endothelial growth factor (VEGF) stimulation (Campochiaro *et al.*, 1999).

Neovascularization in the choriocapillaris can lead to bleeding, leakage, and scarring in the macula, resulting in vision loss. For this reason, VEGF inhibitors such as the RNA aptamer pegaptanib, the partial and full-length antibodies ranibizumab and bevacizumab, and tyrosine kinase inhibitors such as vatalanib and pazopanib, are common treatment strategies for individuals with wet AMD (Barakat and Kaiser, 2009). Several genetic markers have been associated with AMD, including *ARMS2*, *TIMP3*, and *CFH* among others (Fritsche *et al.*, 2014; Heesterbeek *et al.*, 2020). Similarly, several lifestyle and environmental factors such as smoking, obesity, high cholesterol and UV light exposure along with age have been identified as risk factors for AMD (Chalam *et al.*, 2011; Heesterbeek *et al.*, 2020).

Another common retinopathy is glaucoma, which refers to several forms that all result in permanent damage to the optic nerve, leading to vision loss. There are three distinct types of glaucoma: open-angle, closed-angle and normal-tension glaucoma. Open-angle glaucoma, so called because the drainage angle formed between the iris and cornea remains open, but the trabecular meshwork is partially blocked, results in an increase in intraocular pressure that damages the optic nerve (Weinreb *et al.*, 2016). This form of glaucoma does not cause any pain and individuals may not notice any loss in vision until the condition progresses to a more advanced state. Closed-angle glaucoma occurs when the cornea extends forward and blocks the drainage angle between the cornea and the iris resulting in pressure increase and optic nerve damage (Flores-Sánchez and Tatham, 2019). This form of glaucoma can cause intense eye pain, blurred vision, headache and nausea. Finally, normal-tension glaucoma occurs when the optic nerve is damaged without there being an increase in intraocular pressure (Killer and Pircher, 2018). The cause of normal-tension glaucoma is not fully understood though underlying

problems with poor circulation, arterial hypotension and ethnicity may be risk factors for this type of glaucoma.

Inherited retinal diseases constitute a large number of retinopathies caused by mutations in more than 240 genes (<http://www.sph.uth.tmc.edu/Retnet/>). These genes are involved in all aspects of retina health, including photoreceptor structure, disc morphogenesis, protein trafficking, phototransduction, and the visual cycle. The main types of inherited retinal degenerative diseases lead to different forms of retinitis pigmentosa (RP) or macular degeneration (MD) (Fig. 1.9) (Molday and Moritz, 2015). Retinitis pigmentosa affects about 1 in 4000 individuals and more than 60 genes are known to cause some form of RP. RP is characterized by initial loss of night vision (night blindness), and the development of peripheral blind spots that over time extend and merge with each other causing significant loss of peripheral vision, termed “tunnel vision” (Fig. 1.9) (Megaw and Hurd, 2018). Eventually, patients with RP can become legally blind. RP can be classified based on its inheritance pattern: Autosomal dominant, autosomal recessive, or X-linked (Hartong, Berson and Dryja, 2006; Ferrari *et al.*, 2011). The majority of RP cases are caused by mutations in rhodopsin, which predominantly causes an autosomal dominant form of RP (adRP) (Ferrari *et al.*, 2011). Over 150 mutations in rhodopsin are known to cause RP, most of which cause adRP, though some mutations in rhodopsin do cause autosomal recessive RP (arRP) (Ferrari *et al.*, 2011). Dominant RP is associated with gain of function mutations or dominant negative activity, whereas recessive RP is caused by loss of function mutations. Another major gene involved in adRP is peripherin-2, which, along with Rom1, is important for maintaining the structural integrity of the rod outer segments (Ferrari *et al.*, 2011). Less frequently, RP is caused as part of a genetic disorder that

affects other tissues and organs in the body as in the case of Usher syndrome, Bardet-Biedl syndrome and Refsum disease (Megaw and Hurd, 2018; Tsang and Sharma, 2018).

Inherited forms of macular degeneration, also known as macular dystrophies, constitute the other major type of genetic retinopathies. To date 38 genes have been associated with some form of monogenic maculopathies (Molday and Moritz, 2015). Generally, MD leads to loss of both rod and cone photoreceptors and the RPE cells of the retina particularly in the macula and fovea region. As a result, MD often leads to severe loss in central vision, and, depending on the severity, the extent of peripheral vision left intact may vary (Fig. 1.9). Inherited MDs can be subdivided into distinct diseases based on concrete clinical features, often as a result of mutations in different genes. The age of onset of inherited MDs can vary between patients and between different disorders, though symptoms often arise within the first two decades of life. One of the most common monogenic MDs is Stargardt disease (STGD). This is an autosomal recessive retinopathy predominantly caused by mutations in the *ABCA4* gene (Allikmets, 1997), though rare autosomal-dominant forms of STGD can occur due to mutations in *ELOVL4* (Maugeri *et al.*, 2004) and *PROM1* (Kim *et al.*, 2017). Other monogenic MDs include Best MD, caused by mutations in the *VMD2* gene and adult vitelliform dystrophy, caused by mutations in *Peripherin-2* gene; both of these MDs are inherited as autosomal dominant monogenic diseases (Krämer *et al.*, 2003; Boon *et al.*, 2009; Coco-Martin *et al.*, 2020). Juvenile retinoschisis, another maculopathy, is caused by mutations in *RS1* and is inherited in an X-linked inheritance pattern (Vijayasarathy, Ziccardi and Sieving, 2012).

The enzymes of the visual cycle have been linked to several retinal degenerative diseases. Mutations in the lecithin retinol acyltransferase gene (*LRAT*), involved in the esterification of all-*trans*-retinol to retinylesters, is known to cause Leber congenital amaurosis (LCA), an early

onset retinopathy that leads to extreme farsightedness, photophobia, and nystagmus. Mutations in other genes that also lead to LCA include *RPE65*, involved in the hydrolysis and isomerization of retinylesters to 11-*cis*-retinol, and *RDH12*, which reduces retinal isomers to retinol in the inner segments of photoreceptors (Baehr *et al.*, 2003; Sarkar and Moosajee, 2019). Fundus albipunctatus, is a rare retinal degenerative disease that leads to night blindness and is caused by mutations in *RDH5* (Baehr *et al.*, 2003).

1.3.1 ABCA4 Associated Retinopathies

To date, over 1000 mutations are known to cause ABCA4 retinopathies, with the majority of these mutations causing Stargardt disease 1 (STGD1), a juvenile form of macular dystrophy that, in its more severe form, can lead to drastic vision loss that can progress to blindness within the first decade of life (Cornelis *et al.*, 2017; Cremers *et al.*, 2020; Khan *et al.*, 2020). Other retinopathies associated with ABCA4 mutations include autosomal recessive RP (RP19), and autosomal recessive cone-rod dystrophy (CRD) (CRD3) (Valverde *et al.*, 2007; Sharon *et al.*, 2019a; Cremers *et al.*, 2020; Whelan *et al.*, 2020).

The most common type of pathogenic mutations in ABCA4 are missense mutations, accounting for 50 to 60% of the known disease-causing mutations (Jiang *et al.*, 2016; Cornelis *et al.*, 2017; Khan *et al.*, 2020). Other pathogenic mutations in ABCA4 include nonsense mutations, frameshift mutations, insertion and deletions, splicing variants, and deep intronic mutations (Cremers *et al.*, 2020). These disease variants are found throughout the entire gene with no apparent clusters or hotspots. However, some variants are enriched in various geographical locations and ethnic groups as a result of founder effects. For example, the variant N965S was first shown to be enriched in the Danish population (Rosenberg *et al.*, 2007). Other studies have also shown that this variant is found in high frequency in China (Jiang *et al.*, 2016). A common

variant found through Germany and Eastern Europe is the complex mutation L541P;A1038V, whereas the G863A/G863del variant is common in Western and Northern Europe (Maugeri *et al.*, 1999, 2002; Rivera *et al.*, 2000; Ścieżyńska *et al.*, 2016; Tracewska *et al.*, 2019). Other variants with founder effects in Europe include the R1129L variant commonly found in Spain, and the c.768G>T mutant commonly found in the Dutch population (Maugeri *et al.*, 1999; Valverde *et al.*, 2006). Outside of Europe, the A1773V variant has a founder effect in Mexico, and several disease variants have been identified in the Ashkenazi Jewish population including the c.4254-15del23, and P1380L mutants (Chacón-Camacho *et al.*, 2013; Sharon *et al.*, 2019a). Similarly, in Brazil, R602W is a common disease variant (Salles *et al.*, 2017, 2018). Certain racial groups also have a high frequency of some pathogenic variants. African Americans have high frequencies for the V989A, G991R, and R2107H variants (Zernant *et al.*, 2014). Likewise, in China, the Y808* and F2188S variants are among the most common (Jiang *et al.*, 2016; Hu *et al.*, 2019). By far one of the most prevalent variants across the world is the G1961E variant (Burke *et al.*, 2012). This variant has been traced back to Eastern Africa, where it has spread around the world through population migration dynamics. Interestingly, this variant is very rare in African Americans (Burke *et al.*, 2012; Cremers *et al.*, 2020).

1.3.2 Stargardt Disease

Stargardt disease (STGD1) (STGD1:MIM 248200) is the most common monogenic macular dystrophy with a prevalence of 1 in 8,000 to 10,000 individuals (Molday, 2015; Cremers *et al.*, 2020). STGD leads to central vision loss that can progress to blindness, delayed dark adaptation, atrophy of the macula and choriocapillaris, accumulation of flecks in the retina and lipofuscin deposits in the RPE cells, and death of the photoreceptors and RPE cells (Fishman *et*

al., 1999; Scholl *et al.*, 2002; Kang-Derwent *et al.*, 2004). Other symptoms may include color vision deficiency and photophobia (Klevering *et al.*, 2002).

STGD1 is caused by mutations in the *ABCA4* gene, accounting for approximately 95% of all STGD cases, but other genes such as *ELOVL4* (STGD3) and *PROM1* (STGD4) are also known to cause rare forms of STGD (Stone *et al.*, 1994; Kniazeva *et al.*, 1999; Cremers *et al.*, 2020). STGD1 was first described in detail by the German ophthalmologist Karl Stargardt in a 1909 seminal paper (Stargardt, 1909). Therein, he included detailed clinical features of 7 STGD1 patients and described STGD1 as a neuroepithelial disease that affected cone photoreceptors first, followed by the RPE cells and finally leading to deterioration of the choroid (Stargardt, 1909). A similar disorder was independently described in a cohort of patients in 1962 by the Swiss ophthalmologist Adolph Franceschetti which he called Fundus Flavimaculatus (FF) (Franceschetti, 1965). It was later shown that FF and STGD1 were describing the same underlying retinal dystrophy (Deutman, 1972; François *et al.*, 1975; Cremers *et al.*, 2020).

Although the severity and rate of progression of STGD1 can vary significantly among patients, distinct clinical and electrophysiological features can be used to describe the progression of STGD1. In 1976, Gerald Fishman devised a classification system that is still widely used today by ophthalmologists to determine the stage of STGD1 in patients. This system subdivides STGD1 progression into 4 stages with stage 1 being the mildest form of STGD1 and stage 4 being the most severe (Fishman, 1976). In the Fishman classification, stage 1 patients have yellow flecks in the foveal region, pigmentary changes in the macula and normal ERGs and mild loss in visual acuity and central vision; stage 2 patients have more yellow fundus flecks, now expanding the posterior lobe, and normal ERGs but prolonged dark adaptation with mild to moderate loss in visual acuity and central vision; stage 3 patients have extensive flecks and

pigmentary changes, deterioration to the choriocapillaris in the macula and reduced cone or cone and rod ERGs, and significant central, and in some cases peripheral, vision loss; stage 4 patients display extensive atrophy of the choroid and RPE throughout the fundus, drastically decreased ERG cone and rod amplitudes and severe loss in central vision with moderate to severe loss in peripheral vision (Fishman, 1976).

The age of onset in STGD1 can vary widely between patients, and correlates well with the rate of progression and severity outcome of STGD1 patients. Severe forms of STGD1 tend to manifest within the 1st decade of life and progress rapidly to an advanced stage (Fujinami *et al.*, 2015; Zernant *et al.*, 2017; Tanaka *et al.*, 2018). The youngest documented case of STGD1 has been 5 years old (Burke *et al.*, 2013). Moderate forms of STGD1 become apparent around the 2nd and 3rd decade of life, whereas mild forms of STGD1 will not manifest until the 4th to 7th decade of life and generally progress much slower than moderate forms of STGD1 (Yatsenko *et al.*, 2001; Zernant *et al.*, 2017, 2018; Runhart *et al.*, 2019). The exact age of onset can be difficult to determine since, at the early stages of STGD1, many patients may not notice any significant loss in vision. This is particularly true in children since central vision can be preserved in the initial stages of STGD1 due to foveal sparing (Nakao *et al.*, 2012; Fujinami, Sergouniotis, *et al.*, 2013; Lambertus *et al.*, 2016; Runhart *et al.*, 2019). Late onset STGD1 is common in patients carrying hypomorphic or modifier variants such as the common N1868I hypomorphic mutation, which often spares the function and structure of the fovea until much later in life (Zernant *et al.*, 2017; Runhart *et al.*, 2018).

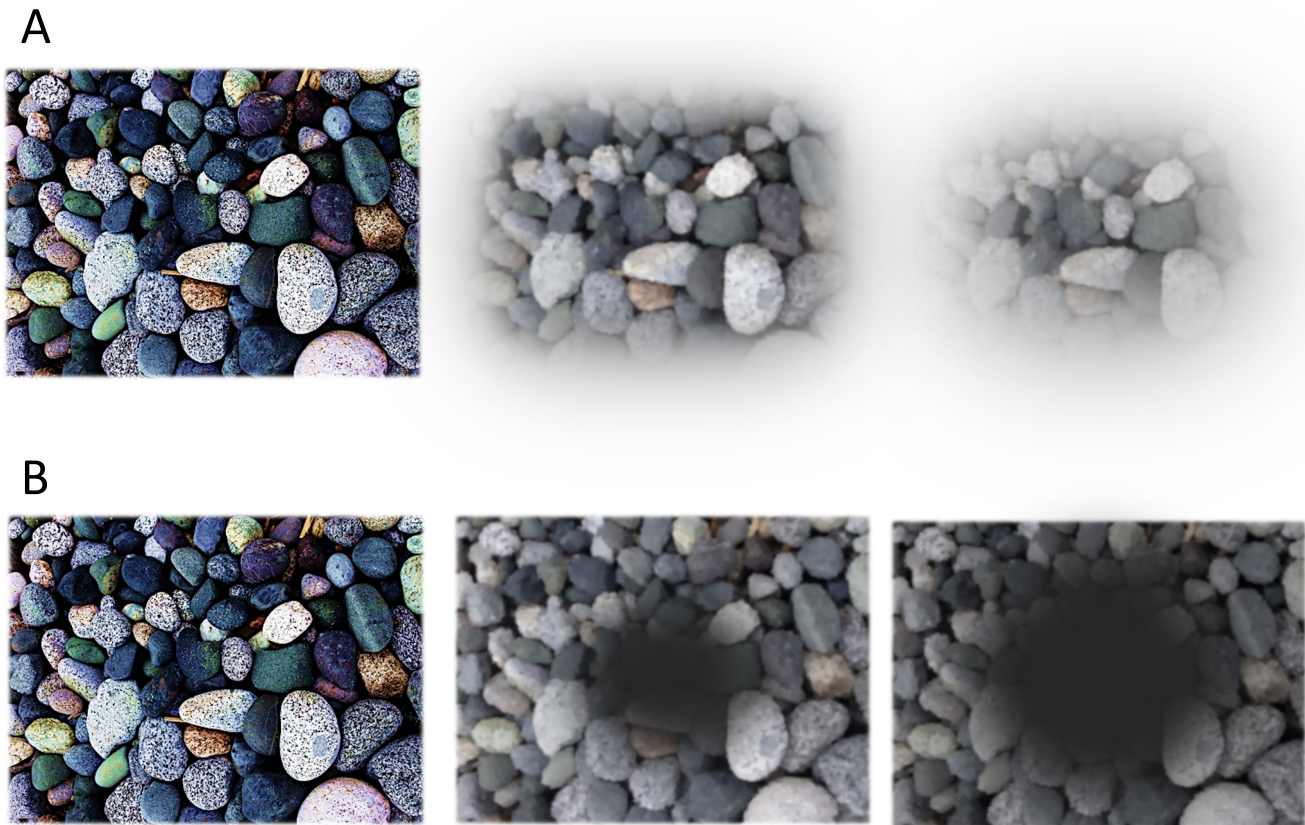


Figure 1.9 Progression of retinal degenerative diseases.

The two most common forms of retinal degenerative diseases are those that lead to forms of Retinitis Pigmentosa (RP), or Macular Dystrophies (MDs). A. RP is characterized by the loss of peripheral vision and night vision leading to extreme “tunnel vision” that can progress to blindness. B. MD is characterized by the loss in central vision and visual acuity, which may or may not spare peripheral vision and can also progress to blindness.

1.3.3 Treatment Strategies

To date there is no cure or approved therapy for the treatment of STGD1 and other ABCA4 associated retinopathies. However, there are several treatment strategies under development, in pre-clinical trials, and in clinical trials at the moment. Currently, there are 16 ongoing registered clinical trials. The therapeutic interventions for the treatment or possible cure

of ABCA4 associated retinopathies can be divided into three types: Drug therapy, cell-based therapy, and gene therapy (Cremers *et al.*, 2020).

Drug therapy:

The safety and efficacy of several drugs has been investigated as part of clinical and pre-clinical trials. The results for two compounds that used oral based supplements has already been published (Cremers *et al.*, 2020). One study investigated the effect of Saffron in 31 patients with ABCA4 associated retinopathies (Piccardi *et al.*, 2019). The reasoning behind this is that Saffron contains carotenoids that can act as anti-oxidants and reduce oxidative stress. Their results showed that while oral uptake of Saffron was well tolerated no improvement in clinical outcomes was seen in the treated vs. the placebo cohorts (Piccardi *et al.*, 2019). Another study investigated the use of oral docosahexaenoic acid (DHA) for the treatment of ABCA4 retinopathies. In this study 11 patients were recruited and while DHA was generally well tolerated no improvement in vision was seen in these patients (MacDonald and Sieving, 2018).

Other studies have been done using different compounds and administration methods. For example, the use the use of 4-methylpyrazole (4-MP), an alcohol dehydrogenase inhibitor, for improvements in delayed dark adaptation was assessed after positive results in mice models (Raskin, Sligar and Steinberg, 1976; Duester, 2000). The idea behind 4-MP treatment is that it would slow down the formation of lipofuscin thereby preventing the downstream physiological damage in the RPE cells that is thought to be caused my lipofuscin accumulation overtime. This study intravenously administered 4-MP into the eyes of the patients and initial results suggest that 4-MP does not have an effect on the rate of lipofuscin deposition in patients with ABCA4 variants (Jurgensmeier, Bhosale and Bernstein, 2007). Another compound that also aims to reduce lipofuscin formation and accumulation is ALK-001, a deuterated form of vitamin A that

should prevent the formation of A2PE and other bisretinoids, major components of lipofuscin. Positive animal studies using ALK-001 showed reduced formation of A2E in treated mice (Charbel Issa *et al.*, 2015). Phase I clinical trials using ALK-001 is now completed and a phase II clinical trial is currently ongoing; no results from the phase I trial have been published. Other compounds in clinical trials include Emixustat hydrochloride, an RPE65 inhibitor, Zimura, a modulator of the complement pathway, and Soraprazan, an inhibitor of H⁺,K⁺-ATPase (Simon *et al.*, 2007; Kubota *et al.*, 2014; Drolet *et al.*, 2016). While there is limited published data on the safety and efficacy of these compounds for the treatment of AMD for Emixustat and Zimura, or gastroesophageal reflux disease for Soraprazan, no results have been published for their treatment in ABCA4 associated retinopathies.

Finally, several compounds are currently being investigated at the biochemical level which have been successfully used for the treatment of cystic fibrosis due to mutations in the *CFTR* gene. For example, the corrector VX-809 (Lumacaftor), has been shown to rescue the trafficking of mistrafficked ABCA4 variants that cause misfolding. These studies would make Lumacaftor a good candidate for follow up pre-clinical animal studies and clinical studies as well (Sabirzhanova *et al.*, 2015; Liu *et al.*, 2019). The drugs ivacaftor and genistein, belong to a different set of drug therapies called potentiators or activators, which have been used to treat *CFTR* variants that do not cause mistrafficking but affect the residual activity of *CFTR* (Sohma, Yu and Hwang, 2013). Previous studies have shown that ivacaftor and genistein can increase the functional activity of ABCA3 disease variants but these compounds have not been tried on ABCA4 variants yet (Kinting *et al.*, 2019).

Overall, while most compounds that have made it to clinical trials have shown high safety profiles, they have fallen short on their efficacy to improve the outcomes of ABCA4 associated

retinopathies. More research with larger cohorts, different doses and administration of the drugs are needed to prove whether or not some of these compounds have any true therapeutic potential. At the same time, there are several drugs that have been successful at rescuing the trafficking or the functional activity of CFTR variants and have shown promising results in disease variants in the *ABCA4* and *ABCA3* genes. Their therapeutic potential needs to be further explored in animal models and clinical studies.

Cell-based therapy:

Unlike drug therapy strategies, the use of stem cells for the replacement of dead RPE and photoreceptor cells in the retina has seen better efficacy results. However, these therapies are still at an infancy stage and this is an area of active pre-clinical and clinical research (Morizur *et al.*, 2020). Two approaches used in cell-based therapies is the direct transplantation of undifferentiated stem cells into the retina and the *in vitro* differentiation of stem cells into RPE cells prior to transplantation (Cremers *et al.*, 2020). Furthermore, three different methodologies have been used to administer stem cells or differentiated RPE cells into the retina. These include subretinal, intravitreal and intravenous injections of cells in the eye (Cremers *et al.*, 2020). Likewise, the safety and efficacy of the transplantation of individual cells or cell sheets as well as the source of stem cells (bone-marrow derived or human embryonic) are areas of active research (Schwartz *et al.*, 2012, 2015; Song *et al.*, 2015; Mehat *et al.*, 2018; Oner *et al.*, 2019; Cremers *et al.*, 2020). Modest improvements in visual outcomes and ERG responses in preliminary studies have been documented (Schwartz *et al.*, 2012, 2015; Song *et al.*, 2015; Mehat *et al.*, 2018; Oner *et al.*, 2019). However, these studies have used small cohort of patients, as little as just one patient, and therefore large clinical trials are needed in order to fully understand the benefits of cell replacement therapies over other treatment strategies for *ABCA4*

associated retinopathies. So far, these clinical studies have focused on the generation and transplantation of RPE cells while largely ignoring the photoreceptor cells. However, while there are no current clinical trials, some pre-clinical studies have been able to form photoreceptors from stem cells and retinal precursor cells (Khalili, *et al.*, 2018; reviewed in Han and Xu, 2020). One important consideration for future studies is the transplantation of photoreceptor cells, since a major component of the pathology of ABCA4 retinopathies is due to the effects of ABCA4 variants on the photoreceptor cells. Cell replacement therapy has had some promising initial results, though much more research at the pre-clinical and clinical level is required to develop comprehensive protocols for transplantation, source of stem cells, and other factors. This technology holds a lot of promise in development a long-term treatment and possible cure for ABCA4 associated retinopathies.

Gene therapy:

The application of gene therapy or gene augmentation therapy for the treatment or cure of ABCA4 associated retinopathies has been a challenging endeavour given the large size of the cDNA of ABCA4 (7 kb). This is an issue since most gene therapies for diseases have used delivery vectors based on the adeno associated virus (AAV). However, the payload capacity of AAVs is around 4.5 kb, much smaller than the cDNA of ABCA4. To get around this problem, the dual AAV system has been used to split the cDNA of ABCA4 roughly in half with each half being loaded onto one component of the AAV dual system (Dyka *et al.*, 2019). Different strategies using dual AAVs have been tried including hybrid, trans splicing, and overlapping AAVs dual systems (Dyka *et al.*, 2019). Studies using dual AAVs are currently at the pre-clinical stage, though some positive results from animal models are encouraging (Dyka *et al.*, 2019; McClements *et al.*, 2019). Other studies have used lentivirus to deliver the cDNA of ABCA4

(Parker *et al.*, 2016). An advantage of lentiviral vectors in gene therapy is their capacity to carry much larger payloads so that the entire cDNA of ABCA4 can fit in a single viral particle.

However, concerns over safety for the treatment of other monogenic disease have overshadowed the potential benefits of lentiviral systems for gene therapy, though new generations of lentiviral vectors are thought to be safe and better at long term expression of the target genes due to DNA integration into the host genome. A phase 1-2 clinical trial for ABCA4 retinopathies using lentiviral vectors has been done though no results have been published. Lastly, a non-viral option being explored for gene therapy is the use of lipid nanoparticles for DNA delivery. Pre-clinical animal studies using lipid nanoparticles have shown positive results, which could open the way for the next generation of gene therapies (Sun *et al.*, 2019).

1.4 Genotype-Phenotype Correlations in ABCA4 Associated Retinopathies

Concrete genotype-phenotype correlations in patients with ABCA4 associated retinopathies has been hindered as a result of the significant heterogeneity in the clinical features of patients, the large number of pathogenic mutations, and the incomplete penetrance of hypomorphic mutations and genetic modifiers. It is also not well understood the extent to which lifestyle and environmental factors may play in the progression of ABCA4 retinopathies. At the same time, it is difficult to discern the extent to which specific variants contribute to the severity of ABCA4 retinopathies in most patients since the vast majority are compound heterozygous (Lewis *et al.*, 1999; Rozet *et al.*, 1999; Klevering *et al.*, 2002). Furthermore, for the majority of mutants, not enough clinical data from a large pool of patients is available to make reliable observations regarding the clinical severity of most mutations. This lack of patient data is exacerbated by the fact that the number of disease variants continues to increase as better sequencing technologies are developed and non-coding regions of the *ABCA4* gene are more

carefully examined for intronic mutations and splicing variants (Runhart *et al.*, 2019; Sharon *et al.*, 2019a; Cremers *et al.*, 2020; Khan *et al.*, 2020; Whelan *et al.*, 2020).

Some exceptions do exist for several pathogenic mutations that are enriched in certain geographical locations and ethnic backgrounds for which clinical data from a large number of patients with identical compound-heterozygous genotypes is available (eg: G863A, N965S, P1380L, N1868I, G1961E) (Lewis *et al.*, 1999; Maugeri *et al.*, 1999; Rosenberg *et al.*, 2007; Cideciyan *et al.*, 2009; Hwang *et al.*, 2009; Burke *et al.*, 2010, 2012, 2014; Downes, S. M., 2012; Riveiro-Alvarez *et al.*, 2013; Fujinami, Lois, *et al.*, 2013; Bauwens *et al.*, 2015; Jiang *et al.*, 2016; Lee *et al.*, 2017; Cornelis *et al.*, 2017; Nassisi *et al.*, 2018; Runhart *et al.*, 2018). Furthermore, homozygous patients with detailed clinical data for several mutations have been documented (Paloma *et al.*, 2001; Rosenberg *et al.*, 2007; Cideciyan *et al.*, 2009; Genead *et al.*, 2009; Hwang *et al.*, 2009; Burke *et al.*, 2010, 2012, 2014; Garces *et al.*, 2018). Patients carrying homozygous mutations present a unique opportunity to better understand genotype-phenotype correlations by isolating the effects that specific mutations have on the age of onset and progression of ABCA4 retinopathies associated with these variants. However, since most data available from homozygous patients comes from a single patient or small sample size, this makes it hard to validate the reliability of the clinical data, such as the age of onset and the rate of disease progression, associated with homozygous variants. Despite this limitation, clinical data from homozygous patients remain an important tool for delineating genotype-phenotype correlations in ABCA4 associated retinopathies.

Over the past 20 years the majority of studies on ABCA4 associated retinopathies have focused on understanding the genetics and clinical features of patients in cohorts of varying in size, nationality and ethnic background. These studies have been successful at identifying the

large number of disease-causing mutations that we know today and the variants that have founder effects. Additionally, these cohort studies have also identified specific *ABCA4* variants associated with STGD1, CRD and RP (Allikmets, 1997; Cremers *et al.*, 1998, 2020; Martinez-Mir *et al.*, 1998; Rivera *et al.*, 2000; Klevering *et al.*, 2002; Fishman *et al.*, 2003; Cideciyan *et al.*, 2009; Cornelis *et al.*, 2017). Likewise, insights into the complex genetics of autosomal recessive *ABCA4* retinopathies, the incomplete penetrance of hypomorphic variants, and the role of complex mutations in the etiology of these retinopathies, have also been well established by the numerous genetic and clinical analyses done to date (Rivera *et al.*, 2000; Cideciyan *et al.*, 2009; Zhang *et al.*, 2014; Ścieżyńska *et al.*, 2016; Zernant *et al.*, 2017, 2018; Runhart *et al.*, 2018; Cremers *et al.*, 2020; Khan *et al.*, 2020). Thanks to all this work, it is becoming apparent that *ABCA4* variants can, generally speaking, be categorized into ‘mild’, ‘moderate’, or ‘severe’ based on the clinical phenotype in patients harboring these mutations. Furthermore, it has been proposed that disease outcomes are predominantly influenced by the amount of residual functional activity of the *ABCA4* variants based on a patient’s genotype (Cremers *et al.*, 1998; Martinez-Mir *et al.*, 1998; Maugeri *et al.*, 1999; Garces *et al.*, 2018). However, although some studies have measured the residual activity of a number of disease variants at the biochemical level and have found a general correlation between the amount of residual activity and the severity of a particular mutation, most biochemical studies have relied on looking at basal and retinal induced ATPase activity as the gold standard defining the severity of a specific variant, while ignoring other aspects of *ABCA4* function such as substrate affinity and transport activity (Sun, Molday and Nathans, 1999; Sun, Smallwood and Nathans, 2000; Wiszniewski *et al.*, 2005; Quazi, Lenevich and Molday, 2012; Zhang *et al.*, 2014; Garces *et al.*, 2018; Molday *et al.*, 2018). In order to fully comprehend the pathological mechanism of *ABCA4* associated

retinopathies at the molecular level, and to fully discern phenotype-genotype correlations, a biochemical analysis of a large number of disease variants localized to different areas of the ABCA4 protein needs to be done. Furthermore, while measuring changes in ATPase activity in these variants remains paramount, it is also as important to understand how other aspects in the overall function of ABCA4 are affected by disease variants. Are these variants getting misfolded or mistrafficked? Is the substrate affinity being affected? Is the substrate binding affinity and ATPase activity tightly coupled? To what extent is the function of hypomorphic variants affected? How do changes in trafficking and functional activity in different variants relate to disease outcomes in patients with these mutations? These are but some of the questions that need to be answered if we want to truly understand the molecular mechanisms of ABCA4 associated retinopathies and to firmly establish genotype-phenotype correlations.

1.5 Thesis Investigation

An underlying theme throughout this thesis is the biochemical characterization of a large number of pathogenic *ABCA4* variants in order to delineate genotype-phenotype correlations. Chapters 2 and 3 offer valuable insights into the molecular mechanism of N-ret-PE transport by ABCA4. Chapter 2 focuses on the characterization of ABCA4 variants localized to the TMDs and chapter 3 focuses on the characterization of variants found in conserved asparagine residues in the Walker A motifs of the NBDs. Our results identified key residues important for N-ret-PE binding and for ATP binding and hydrolysis. We also determined genotype-phenotype correlations based on published clinical data of patients carrying the mutations we characterized. In chapter 4, we further delineated genotype-phenotype correlations by studying a cohort of Canadian patients diagnosed with STGD1. Notably, we identified two novel pathogenic mutations in *ABCA4*, one of which was a missense mutation that belonged to a homozygous

patient. This allowed us to properly investigate the extent of which protein solubilization levels and residual activity have on disease outcomes such as age of onset and disease severity.

Chapter 2 focuses on the functional characterization of pathogenic variants localized to the TMDs of ABCA4. Based on protein solubilization levels and residual functional activity, we subdivided the effects of these STGD1 variants into severe, serious, moderate and mild. Furthermore, our data found a strong correlation between the amount of residual functional activity and the clinical severity of patients with STGD1 mutations. Moreover, we identified a residue that seems to be directly involved in binding to N-ret-PE. We believe this residue could form part of the substrate binding site.

In chapter 3, we switched our attention to the conserved Walker A motifs of the NBDs. In particular we biochemically characterized disease and non-disease associated variants localized to the conserved asparagines N965, found in NBD1, and N1974, found in NBD2. The biochemical analysis of these variants indicates that the N965 and N1974 residues play an important role in ATP hydrolysis. Likewise, based on the N-ret-PE binding and ATPase functional studies, we observed that ATP binding and ATP hydrolysis are two kinetically distinct steps that do not necessarily occur sequentially.

In chapter 4, a clinical study on a cohort of 11 STGD1 patients from British Columbia was done to further assess genotype-phenotype correlations. This study was part of a collaboration with a clinician that provided the clinical data of the STGD1 patients, and a laboratory team lead by Dr. Bernhard Weber that carried out the sequencing of the exons and flanking regions of the *ABCA4*, *ELOVL4*, and *CNGB3* genes. Our laboratory biochemically characterized the missense mutations identified in these patients. Two novel STGD-causing mutations in the *ABCA4* gene were identified, with one of these novel mutants, A1794P,

belonging to a homozygous patient. The homozygous patient had a severe form of STGD1, characterized by an early age of onset, and by age 11 the patient had stage 3 STGD1 and was legally blind. Our analysis showed that A1794P leads to protein misfolding though some limited functional activity is retained. Overall, the biochemical assessment of the variants found in this cohort, and those studied in the TMDs and NBDs as part of this thesis, provide strong support for genotype-phenotype relationships in terms of the amount of soluble protein available and the residual functional activity of these disease variants. These biochemical markers are good determinants of the severity of specific pathogenic ABCA4 variants in STGD1 and other ABCA4 associated retinopathies.

Taken together, the biochemical characterization of all the disease variants analyzed as part of this thesis will help determine the role that these residues play in protein solubilization, substrate binding, and ATPase activity. Ultimately, this information will help us understand how specific mutations in ABCA4 contribute to the development of retinal degenerative diseases, and will also provide key biochemical insights into the transport mechanism of ABCA4 and similar ABC transporters.

Chapter 2 : Biochemical Analysis of Transmembrane Mutations in ABCA4 Associated with Stargardt Disease

2.1 Introduction

ABCA4 is a large 250 kDa ABC-transporter encoded by the *ABCA4* gene (Allikmets, 1997; Illing, Molday and Molday, 1997). This transporter is predominantly expressed in the outer segment disc membranes of the rod and cone photoreceptor cells in the retina, as well as RPE cells, where it plays a crucial role in the visual cycle (Papermaster *et al.*, 1979; Hui Sun and Jeremy Nathans, 1997; Illing, Molday and Molday, 1997; Molday, Rabin and Molday, 2000; Lenis *et al.*, 2018). Previous research has shown that ABCA4 transports N-retinylidene phosphatidylethanolamine (N-ret-PE), the Schiff-base adduct formed by all-*trans*-retinal or 11-*cis*-retinal with phosphatidylethanolamine (PE), across the disc membranes of rod and cone photoreceptors (Quazi, Lenevich and Molday, 2012; Quazi and Molday, 2014). In doing so, ABCA4 acts as an importer that helps to prevent the formation and accumulation of harmful bisretinoids in the outer segments of photoreceptors (Weng *et al.*, 1999; Mata, Weng and Travis, 2000; Zhong and Molday, 2010; Boyer *et al.*, 2012; Quazi, Lenevich and Molday, 2012; Quazi and Molday, 2014). To date, more than 1000 point-mutations in the *ABCA4* gene (<https://databases.lovd.nl/shared/genes/ABCA4>) have been directly linked to the development of Stargardt macular degeneration (STGD) (STGD1:MIM 248200) and other related retinopathies, including, autosomal recessive cone-rod dystrophy (CRD3: MIM 604116) and retinitis-pigmentosa (RP19, MIM #601718) (Cremers *et al.*, 1998, 2020; Martinez-Mir *et al.*, 1998; Stone *et al.*, 1998; Rozet *et al.*, 1999; Rivera *et al.*, 2000; Webster *et al.*, 2001; Jaakson *et al.*, 2003; Zernant *et al.*, 2011; Cornelis *et al.*, 2017).

Disease-causing mutations in *ABCA4* include missense mutations, frameshifts, truncations, small deletions, insertions, splicing mutations and deep intronic mutations. However, the majority of these disease-causing mutations are missense mutations, accounting for 50 to 60% of all STGD1 cases (Jiang *et al.*, 2016; Cornelis *et al.*, 2017; Khan *et al.*, 2020). These STGD1 associated missense mutations are found throughout the gene with no apparent clusters or hotspots. Several missense mutations in the extracytosolic domains (ECDs) and the nucleotide-binding domains (NBDs) of *ABCA4* have been biochemically characterized in previous studies (Sun, Smallwood and Nathans, 2000; Wiszniewski *et al.*, 2005; Quazi, Lenevich and Molday, 2012; Garces *et al.*, 2018; Molday *et al.*, 2018). Disease mutations in these domains have shown that protein misfolding, attenuated basal and N-ret-PE induced ATPase activity, and decreased transport activity result in the accumulation of bisretinoids in the photoreceptors and RPE cells. However, little is known about how disease-causing mutations within the transmembrane domains (TMDs) of *ABCA4* affect its activity and contribute to the development of STGD1 and related retinopathies.

In this study we present a comprehensive biochemical analysis of STGD1 mutations localized to the transmembrane domains (TMDs) of *ABCA4*. We show that solubilization levels, ATPase activity, and substrate binding affinity play a complementary role in determining their contribution to the severity of STGD1. At the same time, our data helps to explain how the functional activity of the common hypomorphic mutation N1868I is affected and likely contributes to the development of STGD1. Furthermore, we identified a key residue, arginine 653, known to cause STGD1 when mutated to cysteine (R653C) or histidine (R653H), that plays a direct role in binding to N-ret-PE and likely forms part of the substrate binding site. These

results provide new insights to our current understanding of STGD1 and the transport mechanism of N-ret-PE by ABCA4.

2.2 Materials and Methods

2.2.1 Prediction of Transmembrane Helices

The amino acid sequence of the transmembrane (TM) helices that form the TMDs of ABCA4 were predicted using algorithms based on hidden Markov models (DAS-TMfilter, ExPASy TMpred, HMMTOP, MP Toppred, PredictProtein, and TMHMM). The TM predictions from each program were pooled together and the overlapping predictions common to all programs were used as the most probable TM sequences in the TMDs. To validate the quality of these predictions, we used the same approach to predict the TMD sequences of integral membrane proteins for which structures has been resolved (ABCA1 and ABCB1). Furthermore, a homology model of ABCA4 was used to see how well these predictions matched the TM helices of the model.

2.2.2 Cloning of ABCA4 Transmembrane Variants

The cDNA of human ABCA4 containing a 1D4 tag (TETSQVAPA) at the C-terminus was cloned into a pCEP4 vector using the Nhe-I and Not-I restriction sites (Molday and Molday 2014). Missense mutations were generated by PCR based site-directed mutagenesis. All DNA constructs were verified by Sanger sequencing. Primer sequences used for site-directed mutagenesis are available upon request.

2.2.3 Heterologous Expression of ABCA4 Variants in HEK293T Cells

Ten micrograms of pCEP4-ABCA4-1D4 construct were transfected into one 10 cm plate containing HEK293T cells at 80% confluency using 1 mg/mL PolyJet™ (SignaGen, Rockville, MD) at a 3:1 PolyJet™ to DNA ratio for 6 to 8 hours before replacing with fresh media. At 48

hours post-transfection, the cells were harvested and centrifuged at 2800 g for 10 minutes. The pellet was resuspended in 200 μ L of resuspension buffer (50 mM HEPES, 100 mM NaCl, 6 mM MgCl₂, 10% glycerol, pH 7.4). A 40 μ L aliquot of the resuspended pellet was solubilized at 4°C for 40 minutes in 500 μ L of either 3-[(3-Cholamidopropyl) dimethylammonio]-1-propanesulfonate hydrate (CHAPS) solubilization buffer (20 mM CHAPS, 50 mM HEPES, 100 mM NaCl, 6 mM MgCl₂, 1 mM dithiothreitol [DTT], 1X ProteaseArrest, 10% glycerol, 0.19 mg/mL brain-polar-lipid [BPL], and 0.033 mg/mL 1,2-dioleoyl-sn-glycero-3-phospho-L-ethanolamine [DOPE] [Avanti Polar Lipids, Alabaster, AL], pH 7.4) or at room temperature in SDS solubilization buffer (3% SDS, 50 mM HEPES, 100 mM NaCl, 6 mM MgCl₂, 1 mM DTT, 1X ProteaseArrest, 10% glycerol, 0.19 mg/mL BPL, and 0.033 mg/mL DOPE, pH 7.4). The samples were then centrifuged at 100,000 g for 10 minutes (TLA110.4 rotor Beckman Optima TL centrifuge [Brea, CA]) and the supernatant was collected. The absorbance of the supernatant at 280 nm was taken to determine protein concentration and 7-8 μ g of total protein was loaded and resolved on an 8% polyacrylamide gel and transferred onto a polyvinylidene difluoride membrane for Western blotting. The blots were blocked in 1% milk for 1 hour and labelled for 2 hours with the Rho1D4 mouse monoclonal antibody (Molday and Mackenzie, 1983; Mackenzie *et al.* 1984; Hodges *et al.* 1988; Molday and Molday 2014) (1:100 dilution in phosphate-buffered saline (PBS; 137mM NaCl, 10mM Phosphate, 2.6mM KCl, pH 7.4) and rabbit-anti- β -tubulin (1:1000 dilution in PBS) was used for the loading control. The blots were washed 3 times for 10 minutes with PBS-T followed by incubation for 1 hour with donkey anti-mouse IgG or donkey anti-rabbit IgG conjugated to IR dye 680 (1:20,000 dilution in PBS-T (PBS containing 0.05% Tween 20)). The blots were washed 3 times with PBS-T and imaged on an Odyssey Li-Cor imager (Li-Cor, Lincoln, NE). Protein expression levels were quantified based on the intensity of

the ABCA4 bands as measured by Western blotting and normalized from the intensity of the bands of the β -tubulin loading control.

2.2.4 Immunofluorescence Microscopy of ABCA4 Variants in COS7 Cells

COS-7 cells were seeded 24 hours before transfection on six-well plates containing coverslips coated with poly-L-lysine to promote cell adhesion to coverslips. The cells were transfected with 1 μ g of DNA and 3 μ L of 1mg/mL PolyJet™ for 6 to 8 hours before replacing with fresh media. At 48 hours post-transfection, the cells were fixed with 4% paraformaldehyde in 0.1M phosphate buffer (PB; 75.4 mM Na₂HPO₄-7H₂O, 24.6 mM NaH₂PO₄H₂O, pH 7.4), for 25 minutes and washed 3 times with PBS. The cells were then blocked with 10% goat serum in 0.2% Triton X-100 and PB for 30 minutes. Primary antibody labeling was carried out for 2 hours (2.5% goat serum, 0.1% Triton X-100 and PB) using the Rho1D4 antibody to detect ABCA4 containing a 1D4-tag and the calnexin rabbit-polyclonal antibody as an endoplasmic reticulum (ER) marker. The coverslips were washed 3 times with PB, followed by secondary labeling using Alexa-488 goat-anti-mouse (for ABCA4), Alexa-594 goat-antirabbit (for calnexin), and DAPI for 1 hour. Excess antibody was washed off 3 times with PB and the coverslips were mounted onto microscope slides in Mowiol mounting medium and kept in the dark at 4°C. The microscope slides were visualized under a Zeiss (Oberkochen, Germany) LSM700 confocal microscope using a 40X objective (aperture of 1.3). Images were analyzed using Zeiss Zen software and ImageJ.

2.2.5 ATPase Assay

Depending on the ABCA4 variant, 1 to 3 cm plates of HEK293T at 80% confluency were transfected as described above. At 24 hours post-transfection, the cells were harvested and centrifuged at 2800 g for 10 minutes. Depending on the number of plates transfected, the pellet

was resuspended in 1-2 mL of CHAPS solubilization buffer for 60 minutes at 4°C followed by a 100,000 g centrifugation for 10 minutes. The supernatant was incubated with 70 μ L of packed Rho1D4-Sepharose affinity matrix for 60 minutes at 4°C. The beads were washed twice with 500 μ L of column buffer (10 mM CHAPS, 50 mM HEPES, 100 mM NaCl, 6 mM MgCl₂, 1 mM DTT, 1X ProteaseArrest, 10% glycerol, 0.19 mg/mL BPL, and 0.033 mg/ml DOPE, pH 7.4) and transferred to an Ultrafree-MC spin column and washed another five times with 500 μ L of column buffer. Bound ABCA4 was eluted from the Rho1D4 matrix twice with 75 μ L of 0.5 mg/mL 1D4 peptide in column buffer at 18°C. When necessary, the absorbance at 280 nm was taken to calculate the protein concentration and dilute samples with column buffer to have equal protein concentration across all variants tested. Thirty microliters of purified ABCA4 was loaded onto an 8% acrylamide gel along with BSA standards to calculate the amount of ABCA4 protein in each sample.

ATPase assays were carried out using the ADP-GLO™ Max Assay kit (Promega, Madison, WI) according to the manufacturer's guidelines. For each ABCA4 variant tested, 15 μ L aliquots of purified ABCA4 (~100 ng of protein per tube) was added to six microcentrifuge tubes. One microliter of 0.8 mM all-*trans* retinal in column buffer (or column buffer alone) was added to half of the samples (done in triplicate) to obtain a final concentration of 0 or 40 μ M all-*trans* retinal. Each tube was incubated for 15 minutes at room temperature in the dark to allow all-*trans* retinal to react with PE and form the Schiff base adduct N-ret-PE; the substrate of ABCA4. Subsequently, 4 μ L of a 1 mM ATP solution (in column buffer) was added and the samples were incubated at 37°C for 40 minutes. The final concentrations of all-*trans* retinal and ATP in each sample were 40 μ M (or 0 μ M) and 200 μ M, respectively. For all ATPase assays, the ATPase deficient mutant ABCA4-MM, in which a lysine residue in the Walker A motif of

nucleotide binding domain 1 (NBD1) and nucleotide binding domain 2 (NBD2) was substituted for methionine, was used to subtract non-specific ATPase activity.

2.2.6 N-ret-PE Binding Assay

Tritiated all-*trans* retinal was prepared by the method of Garwin and Saari with minor modifications (Garwin and Saari, 2000; Zhong and Molday, 2010). [³H] all-*trans* retinal was mixed with unlabeled all-*trans* retinal to obtain a final concentration of 1 mM and a specific activity of 500 dpm/pmol. For a typical binding assay, depending on the ABCA4 variant, 2-5 10 cm plates of transfected HEK293T cells were harvested 48 hours post-transfection and centrifuged for 10 minutes at 2800 g. The pellet was resuspended and solubilized in 3 mL of CHAPS solubilization buffer for 40 to 60 minutes at 4°C and centrifuged at 100,000 g for 10 minutes to remove unsolubilized material. The supernatant was collected and divided in half. Each half was incubated with 80 µL of packed Rho1D4-Sepharose affinity matrix equilibrated in column buffer and mixed by rotation for 60 minutes at 4°C. The affinity matrix was washed twice with 500 µL of column buffer and mixed with 250 µL of 10 µM [³H] all-*trans* retinal (500 dpm/pmol) in column buffer for 30 minutes at 4°C. The matrix was then washed 6 times with 500 µL of column buffer. One sample was incubated with 1 mM ATP and the other half was incubated in the absence of ATP for 15 minutes at 4°C. The affinity matrices were washed 5 times with 500 µL of column buffer and transferred to an Ultrafree-MC (0.45 µm filter) spin column followed by another 5 washes of 500 µL of column buffer. Bound [³H] all-*trans* retinal was extracted with 500 µL of ice-cold ethanol with shaking at 500 rpm for 20 minutes at room temperature and counted in a liquid scintillation counter. Bound ABCA4 was eluted from the Rho1D4-bead matrix with 3% SDS in column buffer and resolved in an 8% SDS-polyacrylamide

gel for analysis of protein levels by Western blotting. All washes and incubations with [³H] all-*trans* retinal were done in the dark.

2.3 Results

2.3.1 Sequence Prediction of the TMDs

Our initial assessment to predict the amino acid sequence of the TMDs of ABCA4 was done using DAS-TMfilter, ExPASy Tmpred, HMMTOP, MP Toppred, PredictProtein, and TMHMM. The results from these algorithms were pooled together to identify the TM helices that were predicted across all of the algorithms. The accuracy of these programs was assessed by comparing their pooled predictions to the structures of ABCA1 and ABCB1. Pooling the results from these programs correctly predicted the location of the TM helices in the structures. Furthermore, we used SWISS-MODEL to create a homology model of ABCA4 using the ABCA1 Cryo-EM structure (5XYJ), which bears 50% sequence identity with ABCA4, as a template (Fig. 2.1). The homology model of ABCA4 was used to refine our initial predictions of the TMDs and to estimate the topological localization of the STGD1 mutations analyzed in this study (Fig. 2.1 and 2.2).

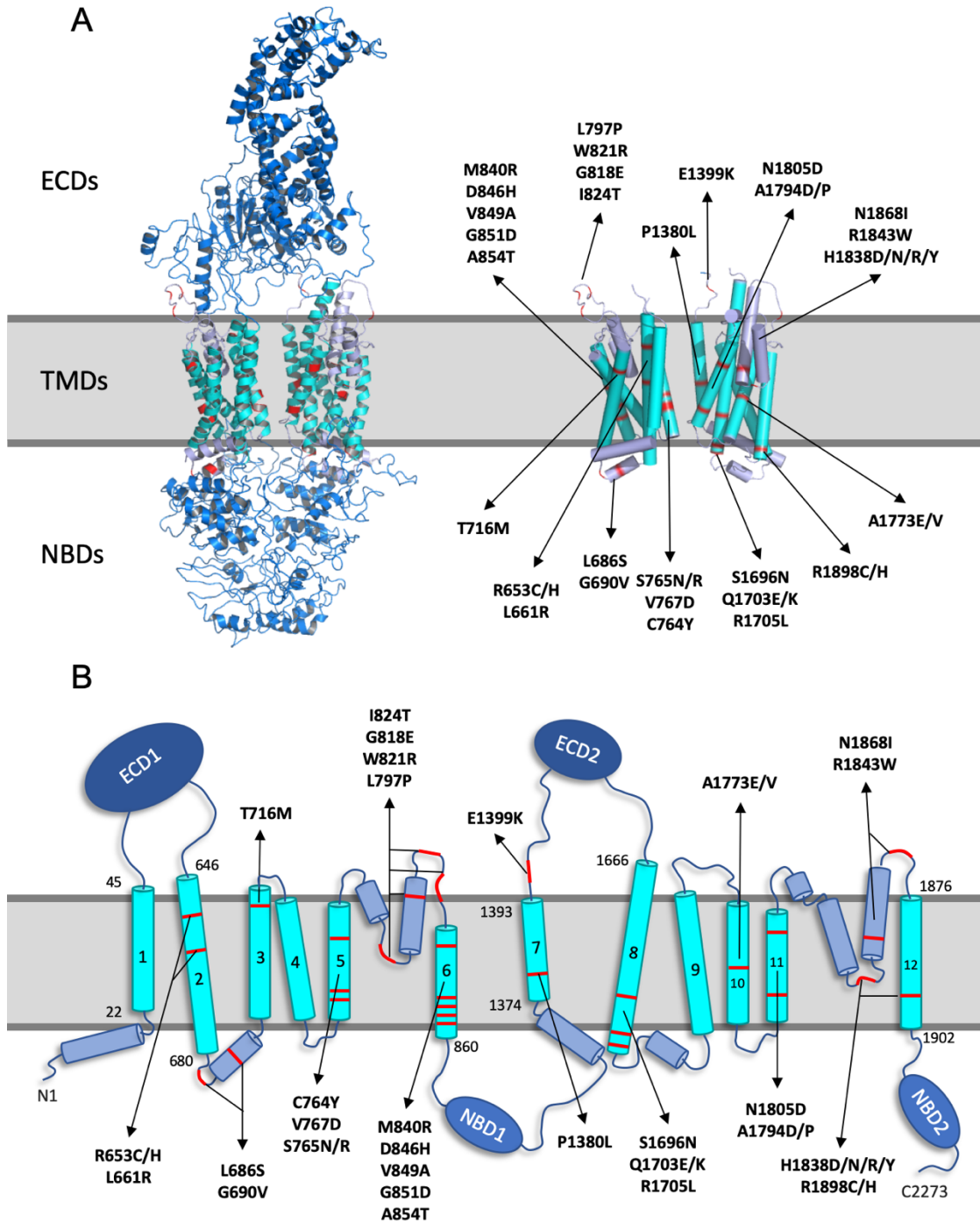


Figure 2.1 Homology model of ABCA4 showing TMD disease variants.

SWISS-MODEL was used for modeling ABCA4 using the ABCA1 Cryo-EM structure (5XYJ) as template, which bears 50% sequence identity with ABCA4. A. The homology model highlights the ECDs (dark blue), TMDs (Cyan for TM helices, and light blue for interconnecting loops/helices), and NBDs (dark blue) as well as the TMD disease variants analyzed in this study (Red). B. Topological model of ABCA4 (ECD = Extracytosolic Domain), (TMD = Transmembrane Domain), (NBD = Nucleotide Binding Domain).

TMDs top view

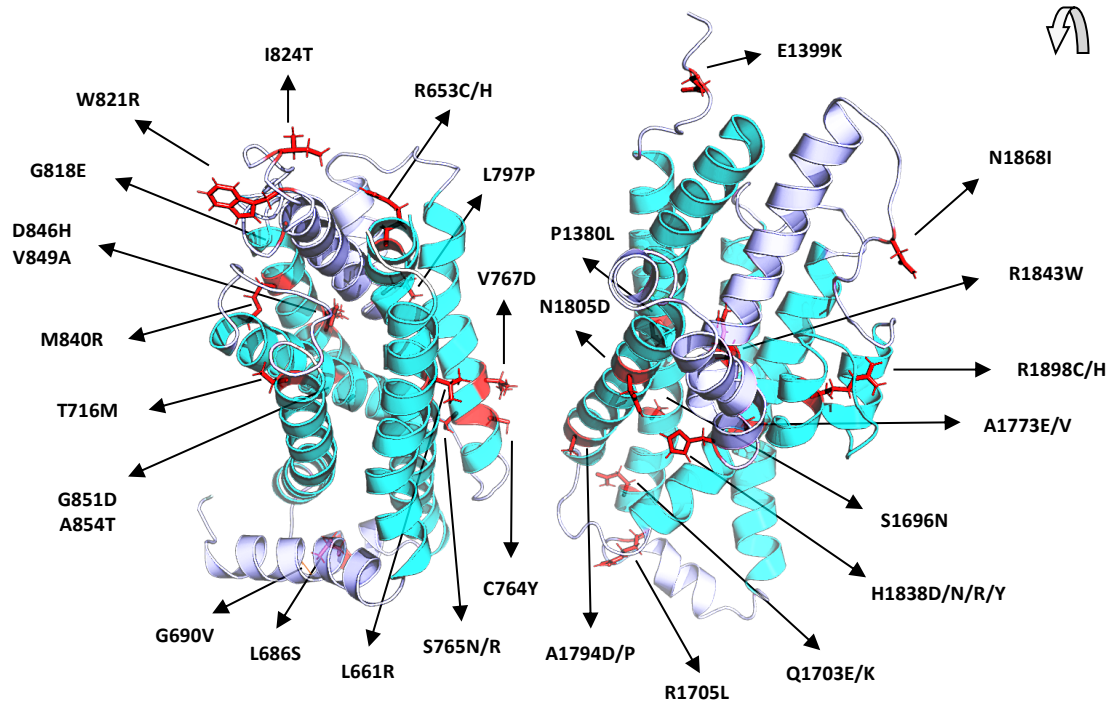


Figure 2.2 Top View of the TMDs in the ABCA4 Homology Model.

The top view of the TMDs in the ABCA4 homology model. This view shows a clear perspective of the translocation pathway of ABCA4 and the localization of the STGD mutants analyzed in this study.

2.3.2 Protein Solubilization and Cellular Localization of TMD Variants

To determine the effect that the TMD disease mutants have on *in vitro* protein solubilization and cellular trafficking, we transiently transfected HEK293T and COS-7 cells, respectively. For the solubilization and functional studies, we used the mild zwitterionic detergent CHAPS to solubilize and purify the ABCA4 TM variants, as this detergent has been shown to purify membrane proteins in a native-like state (Fig. 2.3) (Ahn, Wong and Molday, 2000; Sun, Smallwood and Nathans, 2000). To determine total protein expression in WT and the TMD mutants, the strong ionic detergent SDS was used for solubilization (Fig. 2.4).

For TMD1 and TMD2, all variants had similar expression levels in SDS solubilization buffer (Fig. 2.4). However, for TMD1, 13 TM mutants (L661R, L686S, G690V, S765N, S765R, V767D, L797P, G818E, W821R, I824T, M840R, D846H, G851D) solubilized at or below 50% WT levels in CHAPS solubilization buffer, and the remaining 6 TMD1 mutants (R653C, R653H, T716M, C764Y, V849A, A854T) solubilized at levels comparable to WT (Fig 2.3, Table 2.1). For TMD2 mutants, 5 TM mutants had expression levels below 50% of WT (R1705L, A1773E, A1773V, H1838R, H1838Y), 5 mutants expressed between 50-80% of WT (P1380L, Q1703K, A1794D, A1794P, H1838D) and 9 mutants expressed at similar levels as WT (E1399K, S1696N, Q1703E, H1838N, N1805D, R1843W, N1868I, R1898C, R1898H) (Fig 2.3, Table 2.2). The CHAPS solubilization levels of these mutants relative to WT suggest the extent to which some of these mutants may be aggregating due to protein misfolding.

Cellular Localization of TMD Variants and Co-translational Translocation

Co-translational translocation is the most common translation and targeting pathway used by secreted proteins, proteins localized to the ER, Golgi, or endosomes, as well as membrane proteins during protein synthesis (Braakman and Hebert, 2013; Nyathi *et al.* 2013). In this

pathway, a signal peptide localized at the N-terminus of the nascent polypeptide is recognized by the signal recognition particle (SRP) while the protein is being synthesized (Saraogi and Shan, 2011; Nyathi *et al.* 2013). Binding of the SRP to the signal peptide temporarily pauses protein synthesis and targets the entire complex to the ER membrane where it binds to the SRP receptor; this interaction guides the ribosome and nascent polypeptide to the translocon (also known as the Sec61 complex in eukaryotes or SecYEG complex in prokaryotes) (Kurzchalia *et al.*, 1986; Krieg *et al.*, 1986; Mary *et al.*, 2010; Nyathi *et al.* 2013). Once in the translocon, the signal sequence can be removed by a signal peptidase complex if the protein is destined to be secreted, or if the protein is a type I single-pass transmembrane protein; however, this signal sequence is not removed in type II single-pass transmembrane proteins (Braakman and Hebert, 2013). Likewise, for multipass transmembrane proteins, such as ABC transporters, the signal peptide acts as the first stop-transfer sequence which forms the first transmembrane segment of the protein. At the end of this signal, the transmembrane segment is transferred laterally and protein synthesis across the membrane continues until the next stop-transfer sequence is encountered by the translocon, which halts protein translocation until the end of the stop-transfer sequence, thereby forming the next transmembrane segment. While this process occurs, the growing polypeptide can begin N-linked glycosylation (with the help of oligosaccharyltransferase (OST)) and disulfide bond formation (Nilsson and von Heijne, 1993; Braakman and Hebert, 2013). Furthermore, premature protein folding and protein aggregation is prevented by the early binding of the BiP and PDI chaperones, and later on by interactions with calnexin (CNX) and calreticulin (CRT) (Braakman and Hebert, 2013; Leach and Williams, 2013; Nyathi *et al.* 2013). In general, molecular chaperones facilitate the proper folding of proteins by preventing premature folding

and aggregation, and by providing an optimal and protected folding micro-environment for the nascent polypeptide.

Chaperones belonging to the Hsp70 and Hsp90 families can bind directly to a protein. They recognize aggregation-prone areas by binding to exposed hydrophobic regions that normally would be found in the core of a protein. CNX and CRT, on the other hand, do not bind directly to a polypeptide, but rather to the N-linked carbohydrate groups attached to the growing polypeptide (Leach and Williams, 2013; Kozlov and Gehring, 2020). These carbohydrate-binding chaperones help to stabilize folding events and slowdown the folding process in a protein-domain specific manner (Leach and Williams, 2013; Kozlov and Gehring, 2020). CNX and CRT also prevent protein aggregation, retain unfolded or misfolded proteins in the ER, and facilitate the formation of disulfide bond formation via their interaction with the oxidoreductase ERp57 (Leach and Williams, 2013; Kozlov and Gehring, 2020).

The calnexin-binding cycle is regulated by two types of enzymes: Glucosidases and glucotransferases which, together, control the glucose composition of the glycan during N-linked glycosylation in the ER (Kozlov and Gehring, 2020). CNX or CRT binding to a glycan in a protein occurs when glucosidase II removes a glucose moiety and generates a monoglucosylated glycan in the polypeptide (Kozlov and Gehring, 2020). When glucosidase II removes the last glucose, to generate an unglucosylated proteoglycan, CNX and CRT unbind from the protein to allow it to fold onto its native conformation. If misfolding occurs, the quality-control sensor protein UGT1 (a glucotransferase) will transfer back a glucose molecule to the protein to allow CNX or CRT to bind to the protein once again and re-attempt the protein folding cycle (Kozlov and Gehring, 2020). This process results in the prolonged retention of misfolded proteins in the ER (Kozlov and Gehring, 2020).

Previously, we showed that ABCA4 variants with low solubilization levels in CHAPS buffer relative to WT tend to be retained in the ER of transfected COS-7 cells, whereas variants that express near WT levels are able to leave the ER and accumulate in vesicle-like structures (Garces *et al.*, 2018). The reason for reticular over vesicular expression patterns is indicative of protein misfolding due to ER-retention by the quality control system of the cell. For TMD1, the 13 TM mutants with low solubilization levels also showed reticular expression, whereas those that solubilized at WT levels predominantly had vesicular expression (Fig. 2.5). Likewise, for TMD2, the 10 mutants with solubilization levels at 75% or below WT also showed reticular expression, whereas the 9 mutants expressing at or near WT levels had vesicular expression (Fig. 2.5). Taken together, our solubilization and microscopy studies identified the TMD mutants that are likely misfolded.

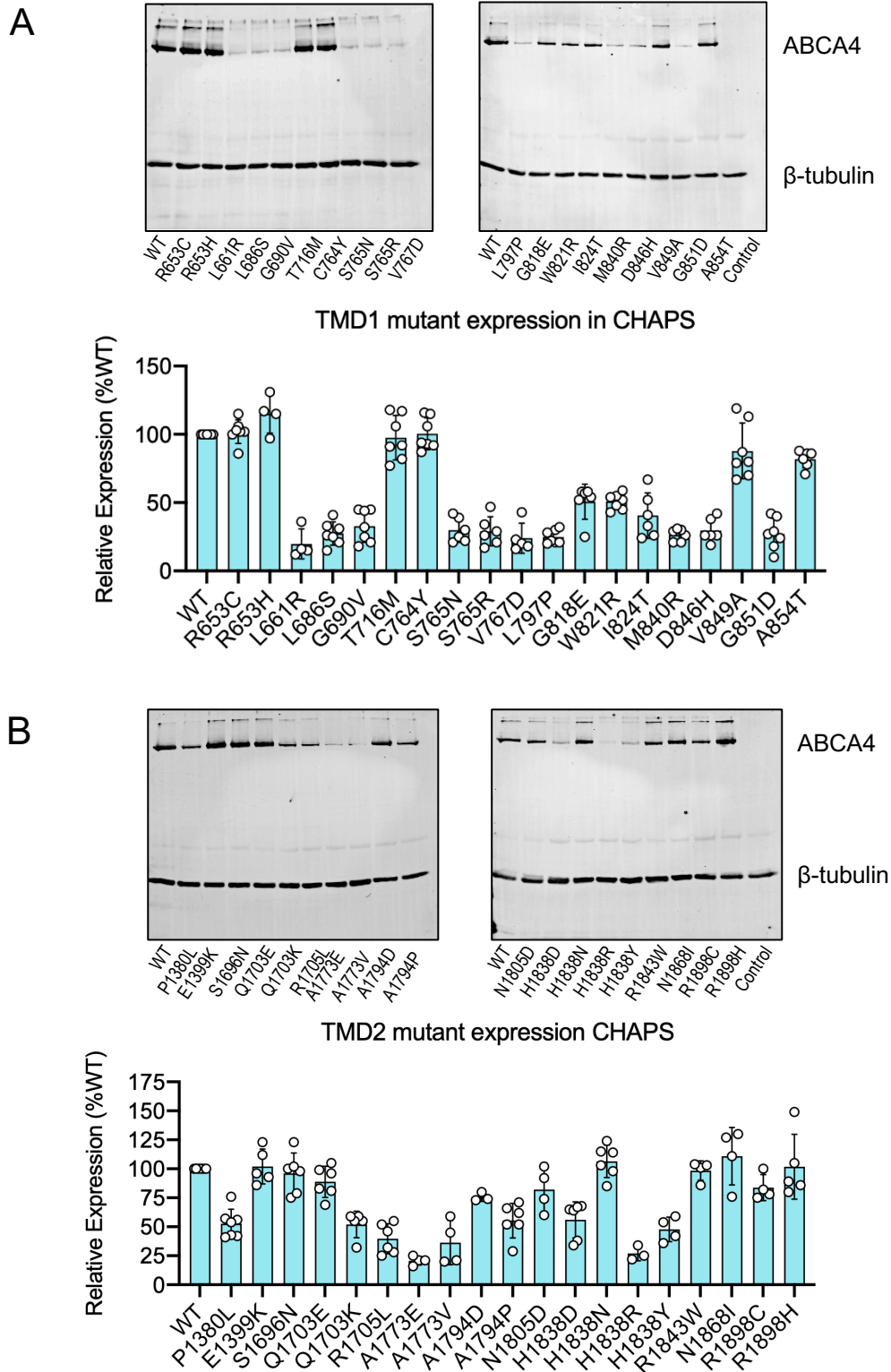


Figure 2.3 Relative protein solubilization of TMD variants.

A. Representative western blots of TMD1 variants solubilized in CHAPS, labelled for ABCA4. B. Representative western blots of TMD2 variants. Bar plots for A and B show the mean of relative expression levels \pm SD for $n \geq 3$ independent experiments. Adapted from Garces *et al.* 2021.

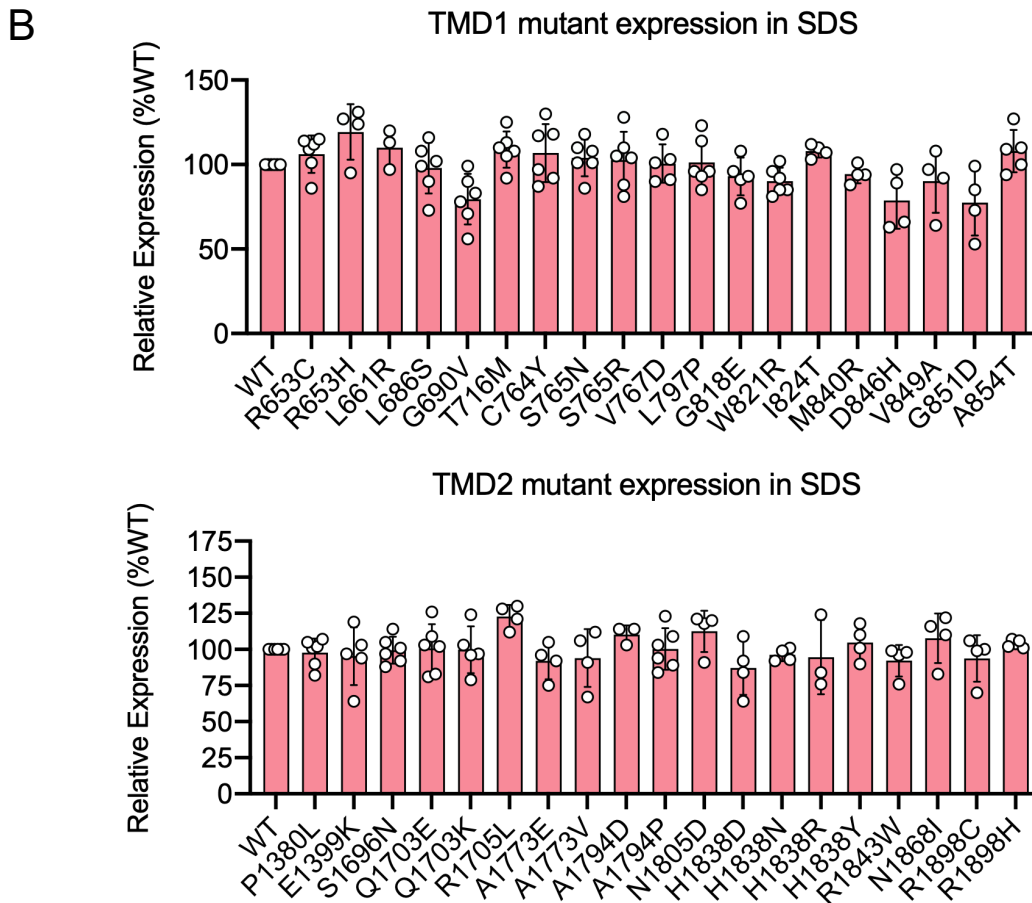
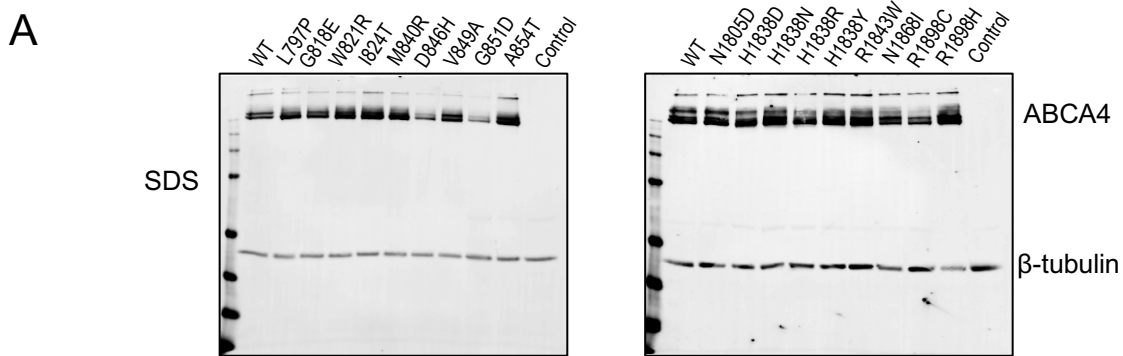


Figure 2.4 Solubilization levels of TMD Variants in SDS buffer.

The solubilization levels of the TMD variants in SDS buffer were done to have a representative idea of how the total amount of protein may change in each variant. A. Representative western blots of SDS solubilized lysate. B. Apart from G690V, D846H and G851D, for the majority of the variants in TMD1 or TMD2, the SDS solubilization levels are comparable to WT (within 80% of WT solubilization levels). This suggests that the amount of heterologous gene expression across these variants in transfected HEK293T cells is occurring at similar levels and further highlights that any difference in the relative solubilization levels in CHAPS buffer is likely a result of protein misfolding, as opposed to changes in availability of the mRNA transcript (i.e. gene expression levels) or as a result of transfection variability or undetected mutations within the pCEP4-plasmid carrying the TMD variants. Adapted from Garces *et al.* 2021.

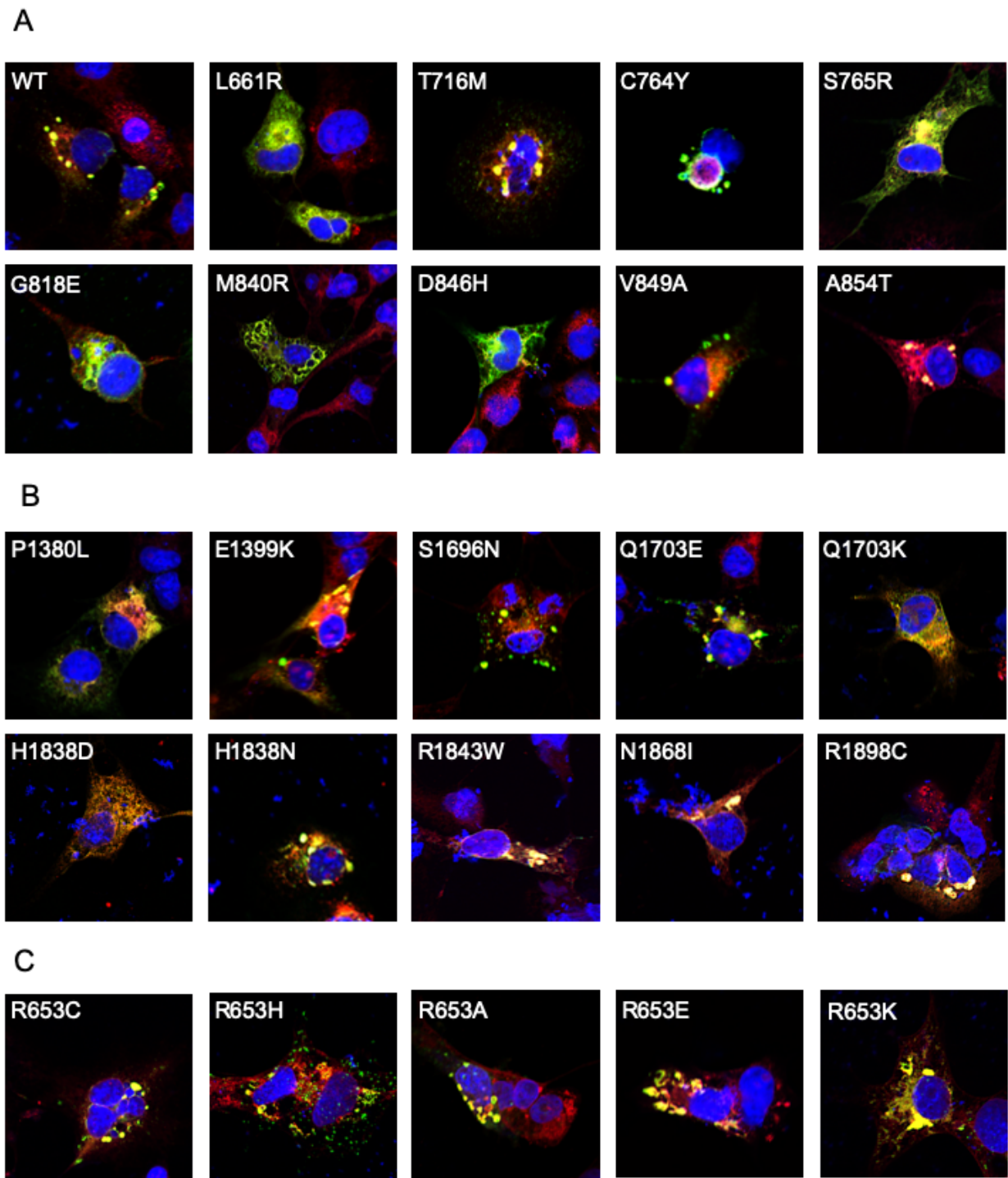


Figure 2.5 Cellular localization analysis of TMD and R653 variants in transfected COS7 Cells.

Representative pictures of ABCA4 variants transfected in COS7 cells. Their cellular localization was analyzed by confocal microscopy. The prevalence of vesicles over reticular localization suggest correct protein folding. Likewise, predominant reticular localization suggests protein misfolding. A. Representative TMD1 variants B. Representative TMD2 Variants. C. R653 Variants. GREEN = anti-ID4 tag (ABCA4), RED = anti-calnexin (ER marker), BLUE = DAPI (nucleus). Adapted from Garces *et al.* 2021.

2.3.3 Functional Analysis of TMD Variants: ATPase Assays

To understand how these disease-associated mutants may be affecting the function of ABCA4, we examined the ATPase activity and N-ret-PE binding properties of these mutants. For the ATPase assays, all the ABCA4 variants were solubilized with CHAPS and immunopurified with a Rho1D4 column. The quality and quantity of the purified variants was measured in protein-stained gels to ensure the assays were done at a similar protein concentration across all samples (Fig. 2.6). The ATPase activity was measured in the absence or presence of N-ret-PE, which is formed when the aldehyde group of all-*trans* retinal reacts reversibly with the primary amine group of PE to form the Schiff base N-ret-PE. In the absence of N-ret-PE, ABCA4 retained some basal ATPase activity, as PE also functions as a secondary substrate of ABCA4 (Ahn, Wong and Molday, 2000; Quazi and Molday, 2013). Addition of N-ret-PE increased the ATPase activity of ABCA4 by approximately twofold, in accordance with previous findings (Fig. 2.6) (Ahn, Wong and Molday, 2000; Quazi, Lenevich and Molday, 2012; Garces *et al.*, 2018; Molday *et al.*, 2018).

The ATPase activity of the TMD mutants can be divided into three distinct groups. Group one: mutants with basal ATPase activity below 50% of WT levels that have minimal N-ret-PE induced ATPase activity; group two: mutants with basal ATPase activity between 50-80% of WT levels that retain N-ret-PE induced ATPase activity; and group three: mutants that have both basal and N-ret-PE induced ATPase activity similar to WT. For TMD1, 10 mutants had severe loss of ATPase activity and belonged to group one (L661R, L686S, G690V, S765N, S765R, V767D, L797P, M840R, D846H, G851D), 4 mutants belonged to group two and had a moderate loss in ATPase activity (G818E, W821R, I824T, A854T), and 4 mutants belong to group three and had mild effects on ATPase activity (R653H, T716M, C764Y, V849A) (Fig. 2.6,

Table 2.1). Similarly, for TMD2 mutants, 8 mutants belonged to group one (Q1703E, Q1703K, A1773E, A1773V, A1794D, H1838D, H1838R, H1838Y), 6 mutants belonged to group 2 (P1380L, R1705L, A1794P, N1805D, H1838N, R1843W), and 5 mutants belonged to group 3 (E1399K, S1696N, N1868I, R1898C, R1898H) (Fig. 2.6, Table 2.2). Interestingly, the R653C variant retains basal ATPase activity at levels similar to WT and does not have a significant increase in ATPase activity when stimulated by N-ret-PE (Fig. 2.6, Table 2.1).

To further define how various disease-associated mutations affect the ATPase activity of ABCA4, we measured the changes in specific ATPase activity (nmol of ATP hydrolyzed per minute per mg of ABCA4) as a function of all-*trans* retinal concentration for variants that solubilize near WT levels and retained N-ret-PE induced ATPase activity. For TMD1, Group 3 variants, T716M and V849A, showed specific ATPase activity profiles similar to WT ABCA4, while C764Y variants had higher activity (Fig. 2.7). The A854T variant in Group 2 which solubilizes in CHAPS at WT levels, had a lower specific ATPase activity than WT (Fig. 2.7). For the Group 3 variants in TMD2, four variants (E1399K, N1868I, R1898C and R1898H) had similar specific ATPase activities as WT while the S1696N mutant had higher specific activity (Fig. 2.7). Also shown is the baseline activity measurements of the ATP-deficient MM double mutant (K969M/K1978M) (Ahn, J. *et al*, 2003) used to correct for any nonspecific luminescence signal generated in the ATPase assay.

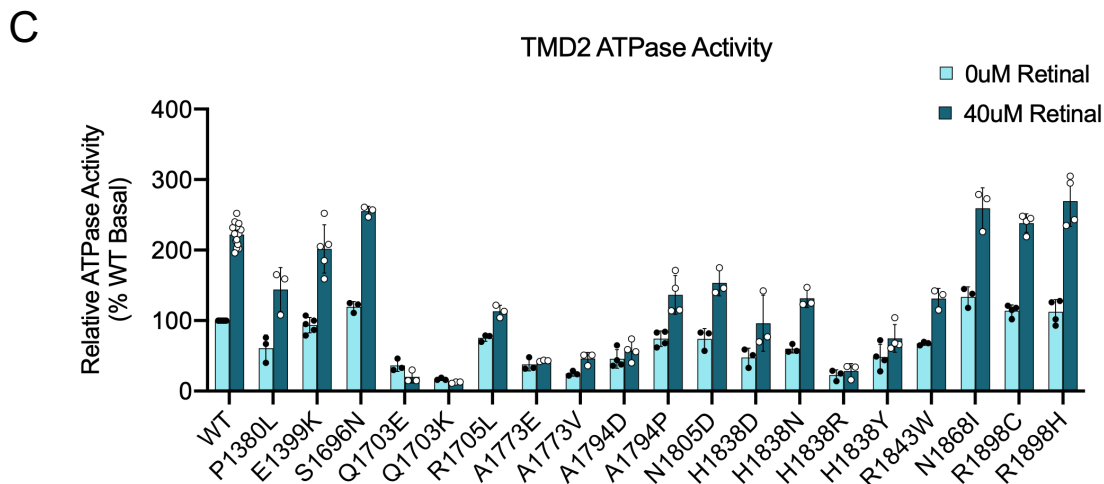
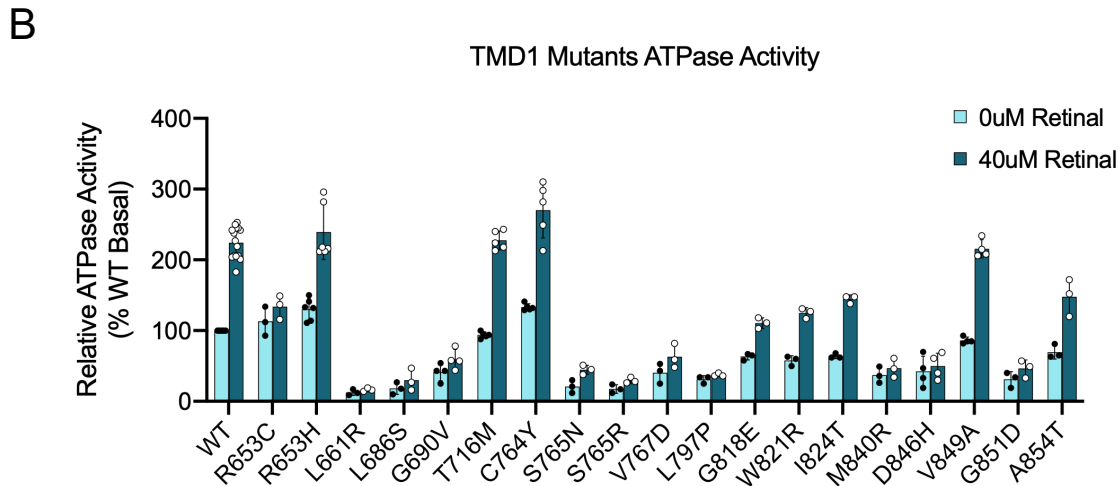
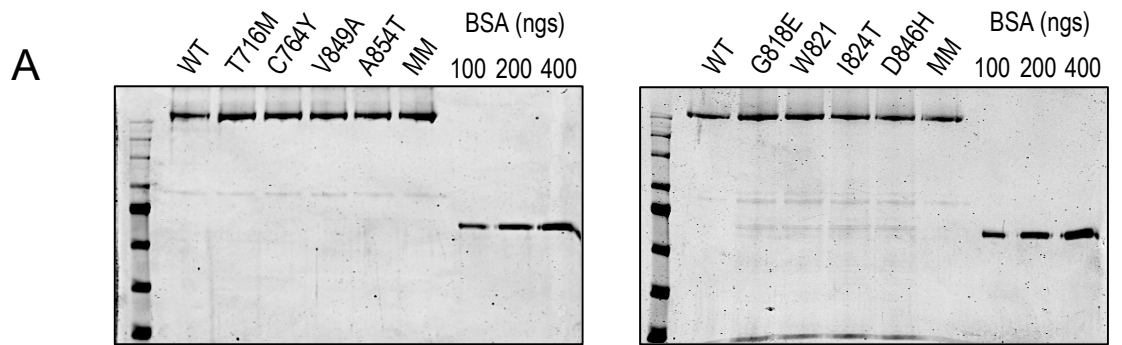


Figure 2.6 ATPase Activity of TMD Variants.

A. TMD variants were purified, and the protein concentration and quality of the purification was analyzed by SDS-PAGE and Coomassie blue protein staining. The MM mutant, which has two Lysine residues in the NBDs mutated to Methionine and has minimal, non-specific ATPase activity, was used as a negative control. BSA standards were used to generate a standard curve to calculate specific ATPase activity. ATPase assays were done with purified ABCA4 variants in the presence (dark cyan) or absence (cyan) of all-trans-retinal and ATP hydrolysis was measured by luminescence using the ADP-Glo Kinase Assay Kit. B. ATPase activity profile TMD1 variants ($n \geq 3$). C. ATPase activity profile for TMD2 variants ($n \geq 2$). Adapted from Garces *et al.* 2021.

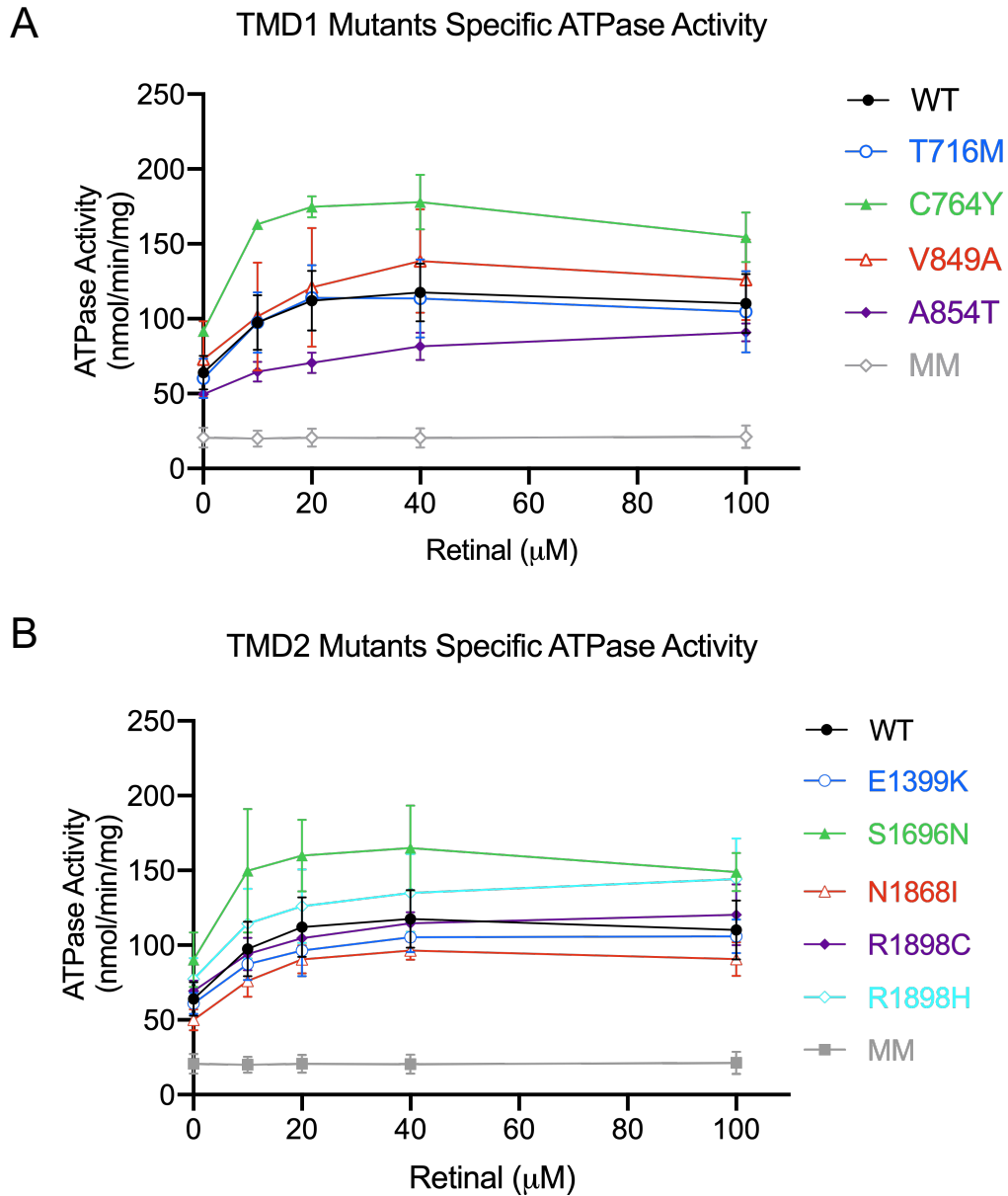


Figure 2.7 Specific ATPase Activity Curves of TMD variants.

Specific ATPase activity (nmol of ATP hydrolyzed per minute per milligram of ABCA4) was calculated for TMD variants that solubilized at similar levels of WT ABCA4 for A. TMD1 and B. TMD2. ($n \geq 2$). Adapted from Garces *et al.* 2021.

2.3.4 Functional Analysis of TMD Variants: N-ret-PE Binding Assays

Next, we performed substrate binding assays to investigate if N-ret-PE binding was affected in the TMD variants. To do this, we immobilized ABCA4 on a Rho1D4 immunoaffinity column and we measured the binding to N-ret-PE in the absence or presence of 1 mM ATP. In the absence of ATP, ABCA4 is in a high-affinity state that binds tightly to N-ret-PE (Beharry *et al.*, 2004). Addition of ATP to the ABCA4-Rho1D4 immunoaffinity column leads to a conformational change in ABCA4 resulting in N-ret-PE release from the column (Beharry *et al.*, 2004; Zhong and Molday, 2010).

The N-ret-PE binding profile for the TMD mutants followed a similar pattern as the ATPase activity profile. Generally, the TMD mutants could fall into three distinct groups. Group A: mutants that bind at or below 50% of WT levels; group B: mutants that binding between 50 to 80% of WT levels; group C: mutants that bind 80% or above WT levels. For TMD1, 15 mutants belonged to group A and had a moderate to drastic loss in N-ret-PE binding (R653C, R653H, L661R, L686S, G690V, S765N, S765R, V767D, L797P, G818E, W821R, I824T, M840R, D846H, G851D); 4 mutants belonged to group B and displayed a mild to moderate loss in N-ret-PE binding (T716M, C764Y, V849A, A854T) (Fig. 2.8, Table 2.1.); but no mutants belonged to group C. For TMD2, 9 mutants belonged to group A (Q1703E, Q1703K, A1773E, A1773V, A1794D, A1794P, N1805D, H1838N, H1838Y); 5 mutants belonged to group B (P1380L, R1705L, H1838D, H1838R, R1898C); and 5 mutants belonged to group C (E1399K, S1696N, R1843W, N1868I, R1898H) (Fig. 2.8, Table 2.2).

Substrate binding curves were done to further investigate how the affinity of the group B TMD1 mutants and the group C TMD2 mutants for N-ret-PE compared to WT. For the group B TMD1 mutants (T716M, C764Y, V849A, A854T), the apparent K_d was 4 to 7 times higher than

WT, indicating that these variants had lower affinity for N-ret-PE than WT (Fig. 2.9). For the TMD2 mutants, there was a wide range in the apparent K_d across these mutants. For E1399K and S1696N the K_d that was roughly 2 and 3 times higher than WT. However, the K_d for N1868I and R1898C was 12 to 14 times higher than WT, respectively (Fig. 2.9). For this analysis, we also included the group B R1843W mutant, this mutant solubilized at WT levels but had an apparent K_d 26 times higher than WT, much higher than those in group C in TMD2 (Fig. 2.9). These results indicate that the affinity for N-ret-PE was slightly decreased in T716M, C764Y, V849A, E1399K and S1696N (K_d 2.8-6.3 μ M), whereas the other TMD mutants had a more considerable decrease in N-ret-PE affinity (K_d 8.6-31.1 μ M).

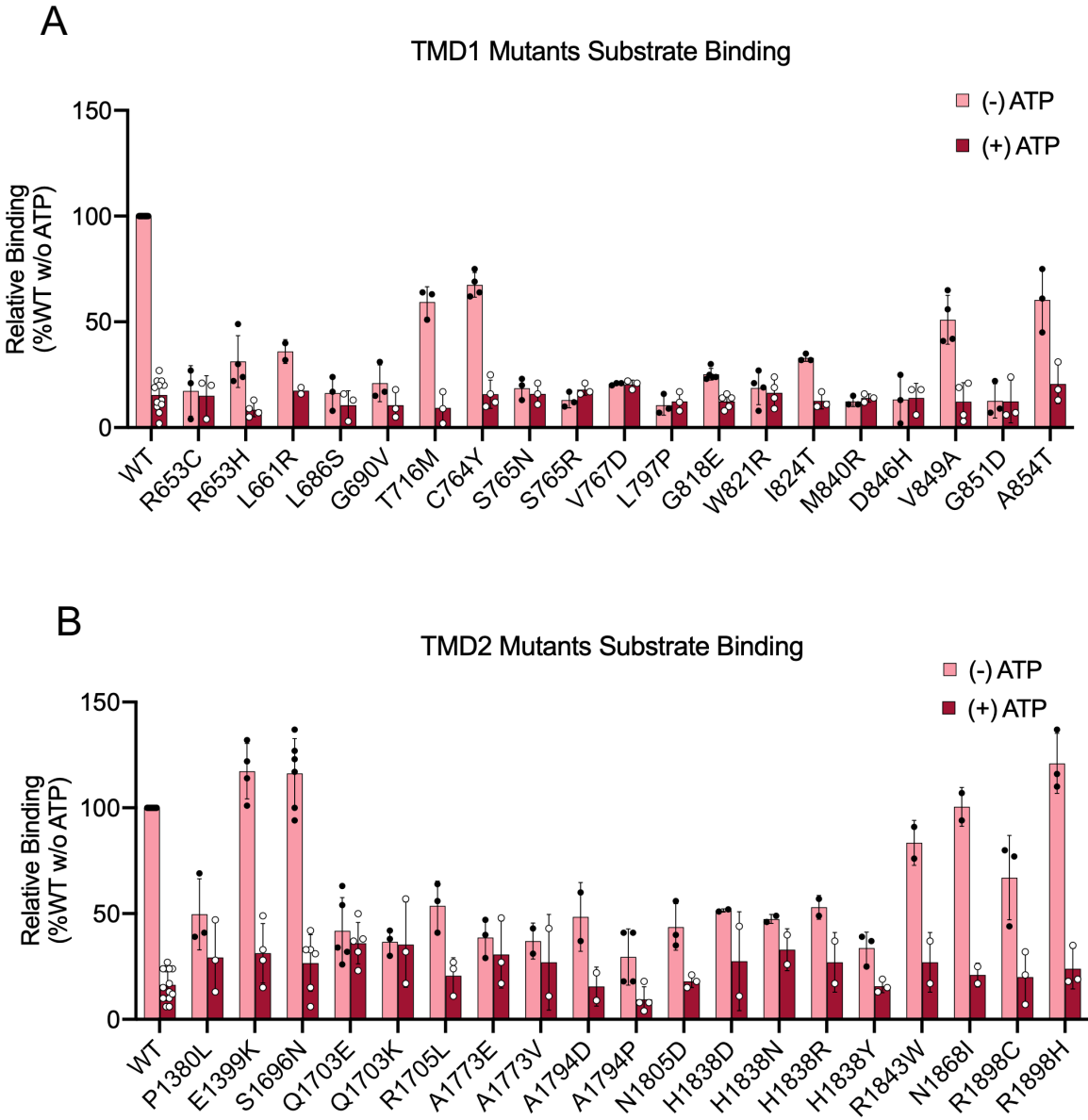


Figure 2.8 N-ret-PE Binding of TMD Variants.

Tritiated all-trans-retinal was used to measure the relative binding to N-ret-PE in the absence (pale red) or presence (red) of ATP for the TMD variants. A. N-ret-PE binding profile for TMD1 variants ($n \geq 3$) and B. TMD2 variants ($n \geq 2$). Adapted from Garces *et al.* 2021.

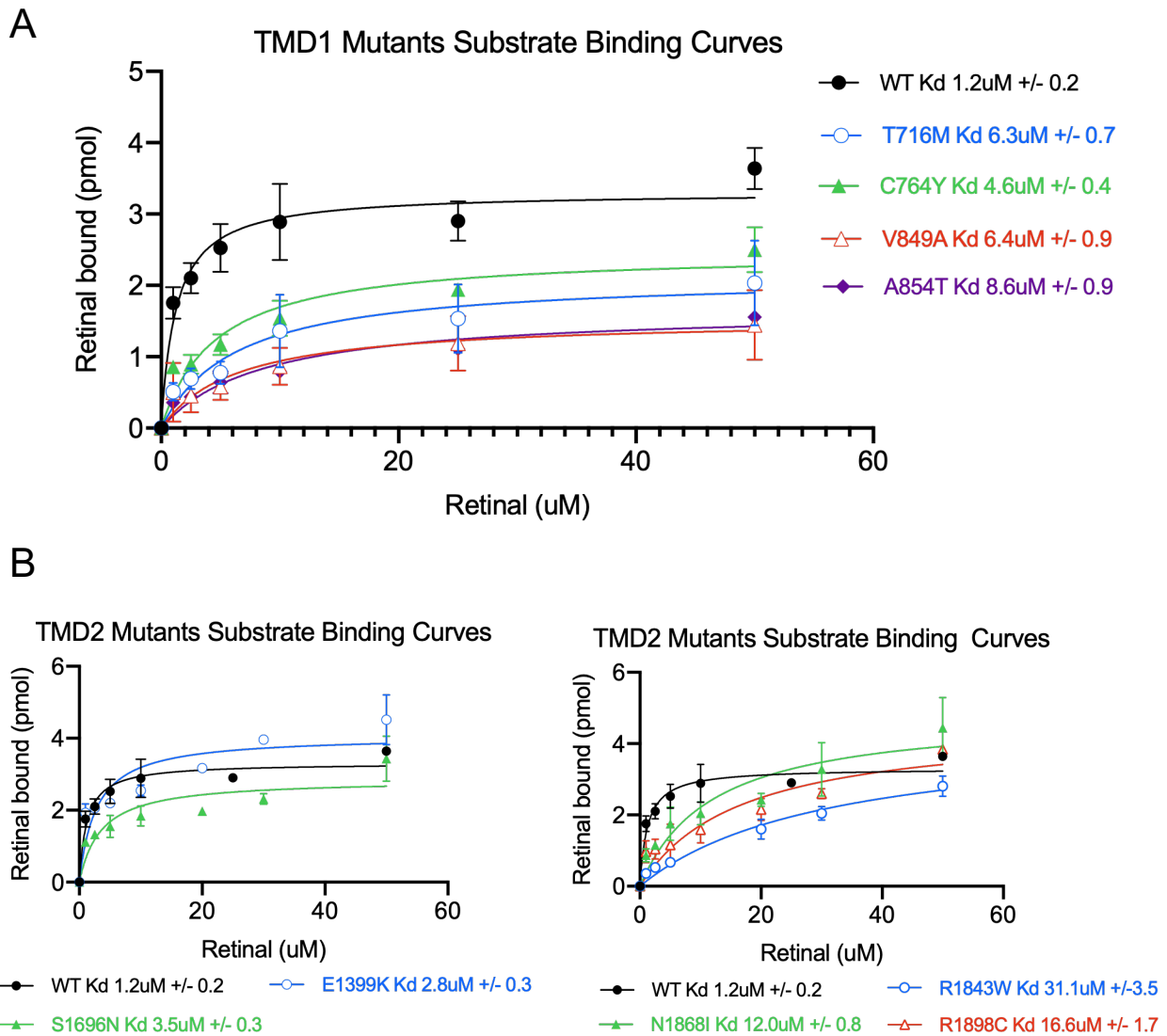


Figure 2.9 N-ret-PE Binding Curves.

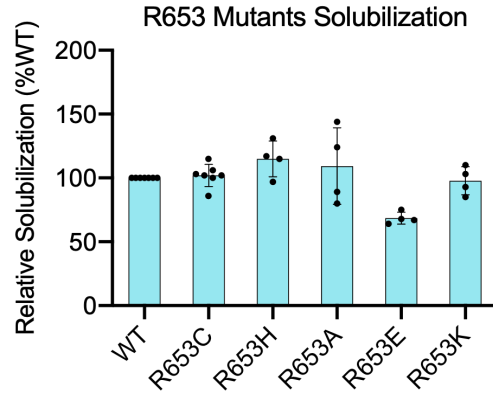
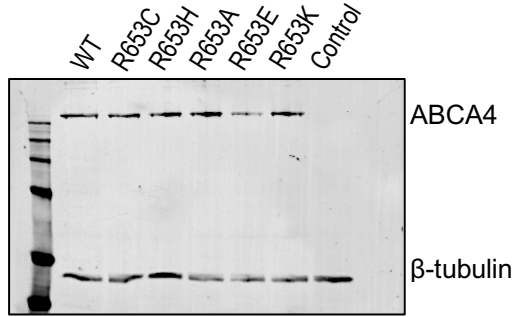
Substrate binding curves were done to calculate the K_d to N-ret-PE for all the variants that solubilized near WT levels and had similar levels of relative N-ret-PE binding as WT. A. TMD1 substrate binding curves, these higher apparent K_d to N-ret-PE than WT ($n \geq 2$). B. TMD2 substrate binding curves, E1399K and S1696N had an apparent K_d to N-ret-PE slightly higher than WT. The R1843W, N1868I and R1898C, however, had noticeably higher K_d to N-ret-PE than WT. Adapted from Garces *et al.* 2021.

2.3.5 Biochemical Characterization of R653 Variants

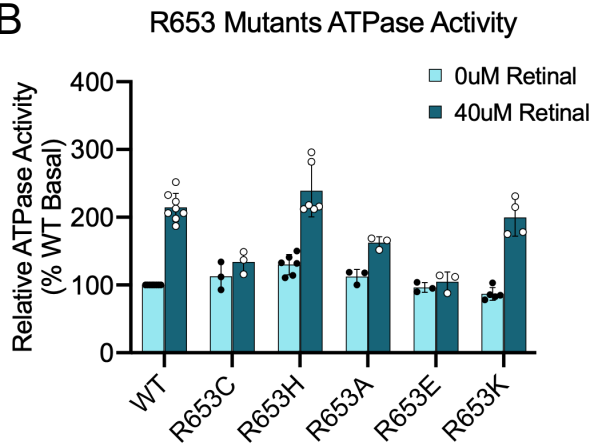
The biochemical properties of the R653C and R653H mutants prompted us to investigate whether the R653 residue could be directly involved in binding to N-ret-PE. These disease variants solubilized near WT levels and displayed a vesicular expression pattern in transfected COS-7 cells, indicating that they are not getting misfolded (Fig. 2.5 and 2.10). Furthermore, both the R653C and R653H variants retain WT levels of basal ATPase activity (Fig. 2.10). However, R653C does not have any N-ret-PE induced ATPase activity whereas R653H does have N-ret-PE induced ATPase activity (Fig. 2.10). Likewise, while the N-ret-PE binding is drastically reduced in both variants, only R653H can still release N-ret-PE in the presence of ATP (Fig. 2.10).

Given these observations, we decided to explore the implications of having a positively charged arginine at this location by characterizing other variants at this position with different biochemical properties (R653A, R653E, R653K). All these R653 variants solubilized near WT levels and formed vesicle-like structures in COS-7 cells, indicative of proper protein folding (Fig. 2.5 and 2.10). Similarly, all variants retained basal ATPase activity closed to WT levels, however, only the positively charged variants (R653H and R653K) had significantly higher N-ret-PE induced ATPase activity (Fig. 2.10). Interestingly, the specific ATPase activity of R653H was higher than WT whereas that of R653K was comparable to WT (Fig. 2.10). The N-ret-PE binding properties of these variants was drastically reduced for R653C, R653H, R653A, and R653E but only mildly reduced for R653K (Fig. 2.10). Moreover, only R653H and R653K had noticeable levels of N-ret-PE release in the presence of ATP, with R653K behaving similarly to WT. Indeed, the K_d of R653K for N-ret-PE is 2.5 μM which is close to the K_d of WT for N-ret-PE of 1.2 μM (Fig. 2.10). However, R653H had a much lower affinity for N-ret-PE with a K_d of 13.3 μM (Fig 2.10).

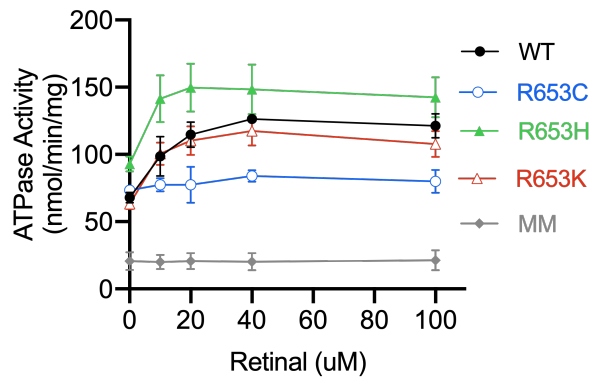
A



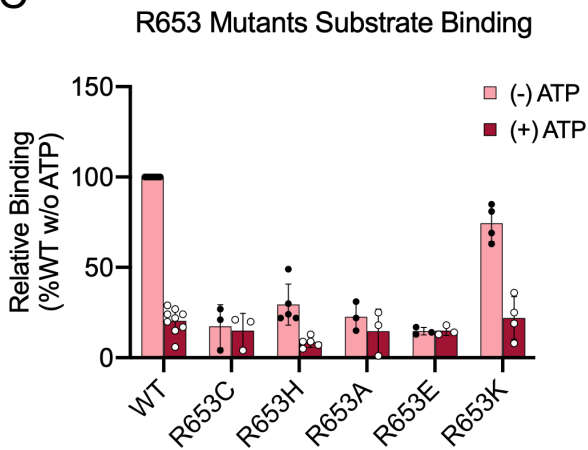
B



R653 Mutants Specific ATPase Activity



C



R653 Mutants Substrate Binding Curves

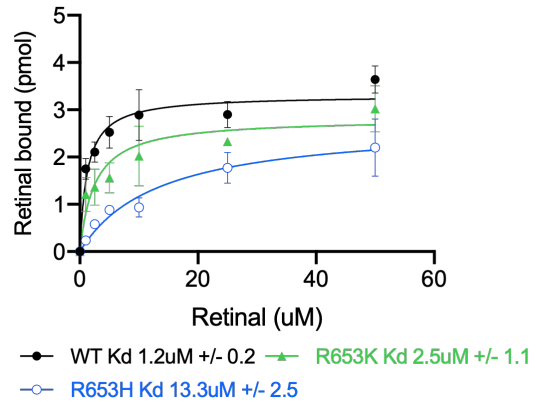


Figure 2.10 Biochemical analysis of R653 Variants.

A. Representative western blots showing the solubilization levels of the R653 mutants. Bar plot indicates the average relative expression of these variants +/- SD ($n \geq 3$). B. Relative ATPase activity of R653 variants in the absence (cyan) or presence (dark cyan) of all-trans-retinal ($n \geq 3$). R653K has similar levels of ATPase activity than WT and R653H has higher levels of ATPase activity. R653C/A/E retain only basal ATPase activity. The specific ATPase activity was measured for R653C/H/K as a function of retinal concentration ($n \geq 2$). C. Relative binding to N-ret-PE in the absence (pale red) or presence (dark red) of ATP ($n \geq 3$). R653K partially restores N-ret-PE binding to WT levels. Substrate binding curves of WT, R653K and R653H were done to calculate their apparent K_d to N-ret-PE ($n \geq 2$). Adapted from Garces *et al.* 2021.

2.4 Discussion

The biochemical characterization of disease variants is essential to help us understand the molecular mechanisms underpinning Stargardt disease. For this study, we targeted our analysis to pathogenic mutations localized to the TMDs of ABCA4. Our results indicate that mutations within the TMDs of ABCA4 contribute to a loss in ABCA4 function likely as a result of protein misfolding, decreased basal or N-ret-PE induced ATPase activity, decreased N-ret-PE binding affinity, or a combination of these phenotypes.

Our structural and functional studies of the TMD variants demonstrate a strong correlation between the relative levels of protein solubilization and the extent to which functional activity is affected. For example, in our ATPase functional studies, with the exception of Q1703E, all TMD mutants in group one expressed at 50% or below WT levels, suggesting that protein misfolding affects ATPase activity (Fig. 2.3 and 2.6). Moreover, with the exception of 4 mutants that solubilized near WT levels (A854T, N1805D, H1838N, R1843W) all TMD mutants in group two had higher solubilization levels than those in group one, but lower than those in group three (Fig. 2.3 and 2.6). In a similar manner, all TMD mutants in group three solubilized near WT levels (Fig. 2.3 and 2.6).

In accordance with the ATPase assays and the CHAPS solubilization levels, similar observations can be made with our substrate binding studies. For example, the group A TMD mutants tended to solubilize below ~50% of WT levels with the exception of R653C, R653H, and Q1703E, which solubilized near WT levels (Fig. 2.3 and 2.8). Additionally, with the exception of H1838R, the TMD group B and group C mutants solubilized above 50% of WT levels (Fig. 2.3 and 2.8). At the same time, all the TMD mutants that retained N-ret-PE induced ATPase activity (i.e. mutants in group two or three in the ATPase assays) were also able to

release N-ret-PE in the presence of ATP (Fig. 2.6 and 2.8). These results support the alternating access model for substrate transport, wherein the access of the substrate binding site in the TMDs can alternate between outward and inward facing conformations depending on the state of ATP binding and hydrolysis (Rees, Johnson and Lewinson, 2009; Molday, 2015). Based on this model, N-ret-PE release occurs upon binding of ATP to the NBDs, which is then followed by ATP hydrolysis. As a result, the TMD mutants that cannot bind to ATP will not be able to release N-ret-PE.

The grouping system from our functional data can be used to predict the severity of each mutation in STGD. For example, group 1A mutants (i.e. ATPase activity group one and substrate-binding group A) have no residual function and are, in biochemical terms, the most severe; whereas those in group 3C retain both ATPase and substrate-binding levels close to WT, thereby contributing only mildly to STGD in patients harboring these mutations. In less extreme cases, some TMD variants fall between a moderate to serious phenotype. Mutants classified as 3B and 2C retain more functional activity than those classified as 1B or 2A and are therefore predicted to be mild to moderate, whereas 1B and 2A are classified as moderate to severe depending on their solubilization levels in CHAPS (Fig. 2.11, Table 2.1 and 2.2).

Two disease variants at the same amino acid position, R653C and R653H, had unique functional groupings. For instance, the ATPase activity of R653C did not fit within the ATPase grouping system, as this mutant had normal levels of basal ATPase activity, similar to group three variants, but had no N-ret-PE induced ATPase activity at all (Fig. 2.6). On the other hand, the basal and N-ret-PE induced ATPase activity for R653H was not affected and was placed in group 3 (Fig. 2.6). Furthermore, like all group A variants, the N-ret-PE binding affinity was severely reduced for R653C and R653H, though R653H could still release N-ret-PE in the

presence of ATP (Fig. 2.8). These results suggested that while these mutants solubilized near WT levels, and were likely still able to transport PE, their ability to bind to and transport N-ret-PE was hindered. Indeed, substituting this R653 residue for R653A, R653E, or R653K provided additional insights into the role this amino acid is playing in the transport cycle of N-ret-PE. For example, regardless of the hydrophobicity, net charge, and size of the side group, all these R653 variants expressed near WT levels, and their basal ATPase activity was not affected (Fig. 2.10). Interestingly, however, only the positively charged variants, R653H and R653K, retained significant N-ret-PE induced ATPase activity (Fig. 2.10). Binding to N-ret-PE was severely reduced in all the R653 variants with the exception of R653K, which was able to bind and release N-ret-PE at similar levels to WT, depending on the presence of ATP (Fig. 2.10). The preference of a lysine residue over a histidine was highlighted by looking at the dissociation constants of these variants. For example, the K_d of R653H for N-ret-PE is 13.3 μM , whereas for R653K it is 2.5 μM , which is similar to the 1.2 μM K_d of WT for N-ret-PE. Taken together, these results indicate that the R653 residue is important for binding to N-ret-PE, and may form part of the substrate binding site (Fig. 2.10). This may be because a positively charged side group may be required at this position for N-ret-PE binding.

The majority of the serious to severe mutations analyzed here occurred in variants that cause some level of protein misfolding as assessed by ER retention in transfected cells in our confocal microscopy experiments, and low expression levels after solubilization with the mild detergent CHAPS (Tables 2.1 and 2.2). The low basal and substrate stimulated ATPase activity, as well as the low levels of N-ret-PE binding in these severe to serious mutations coincides well with protein misfolding (Table 2.1 and 2.2). Of the 38 disease variants analyzed, 23 are considered serious to severe, and 21 of those are thought to cause protein misfolding (Tables 2.1

and 2.2), this highlights the profound effect that protein misfolding has in the overall function of ABCA4 and in determining the severity of STGD1. Indeed, most of these severe and serious missense mutations involve amino acid substitutions altering the charge, polarity, or size of the side chain (eg: L661R, L686S, G690V, V767D, L797P, G818E, W821R, I824T, M840R, G851D, Q1703K, R1705L, A1773E, A1794D, A1794P, H1838Y). As a result, these changes may affect the folding and packing of the transmembrane helices, the coupling helices, the V-shaped alpha-helical hairpins, or the conformation of the connecting loops. For example, L661R, L686S, V767D, W821R, I824T, M840R, Q1703K, R1705L, A1773E, A1794D, and H1838Y are all example of amino acid substitutions affecting the polarity or charge of these amino acids at different locations within the transmembrane domain. Additionally, G690V, L797P, G818E, G851D, and A1794P are examples of substitutions likely affecting the packing of transmembrane helices (L797P, A1794P), or causing major steric changes or changes in polarity within the transmembrane domains (G690V, G818E, G851D). It is likely for these reasons that these amino acid substitutions affect the structural integrity of the transmembrane domains of ABCA and lead to protein misfolding thereby severely impacting the function of ABCA4.

Genotype-Phenotype Correlations:

From a clinical perspective, detailed data for some mutations is available for patients in a homozygous state, in *trans* with a severe nonsense or frameshift mutation, or in *trans* with mutations for which we have biochemical data (e.g. R653C, V767D, P1380L, N1868I) (Lewis *et al.*, 1999; Simonelli *et al.*, 2000, 2005; Shroyer, 2001; Fumagalli *et al.*, 2001; Hwang *et al.*, 2009; Maia-Lopes *et al.*, 2009; Cideciyan *et al.*, 2009; Genead *et al.*, 2009; Burke *et al.*, 2010, 2014; Zernant *et al.*, 2011; Oldani *et al.*, 2012; Downes, S. M., 2012; Riveiro-Alvarez *et al.*, 2013; Fujinami, Lois, *et al.*, 2013; Huang *et al.*, 2013; Nõupuu *et al.*, 2014; Utz *et al.*, 2014;

Lambertus *et al.*, 2015; Duncker *et al.*, 2015; Fujinami *et al.*, 2015; Ścieżyńska *et al.*, 2016; Lee *et al.*, 2017; Nassisi *et al.*, 2018; Runhart *et al.*, 2018). However, for several mutations, sufficient metadata such as age of onset or visual acuity, was not collected or not enough patients have been reported to make reliable phenotype-genotype correlations (e.g. L797P, M840R, Q1703K, R1898C) (Papaioannou *et al.*, 2000; Briggs *et al.*, 2001; Passerini *et al.*, 2010). Furthermore, for some mutations the only genetic and clinical data available is from unresolved cases of monoallelic patients, or from patients whose genotype was not provided (eg: S765N, I824T, H1838R, R1843W) (Shroyer *et al.*, 2001; Webster *et al.*, 2001; Jaakson *et al.*, 2003). Nonetheless, for each of the severity phenotypes, there is at least one TMD mutation for which detailed clinical data is available from more than one patient that can be used to make correlations between our biochemical results and STGD severity.

For the severe mutants L686S and V767D, the age of onset varied depending on the genotype of the patient. For instance, the age of onset of patients carrying the L686S mutation varied from 11 to 18 in two patients with the same genotype (L686S/R1108C) (Paloma *et al.*, 2001). When L686S was in *trans* with the moderate A1357T variant, for which functional data is available, the age of onset was 14 years (Riveiro-Alvarez *et al.*, 2013; Garces *et al.*, 2018). For the V767D mutant, all patients carrying this mutation had an early onset (5-10 years) (Simonelli *et al.*, 2000; Shroyer, 2001; Burke *et al.*, 2010; Zernant *et al.*, 2011; Oldani *et al.*, 2012; Utz *et al.*, 2014) with the exception of one patient (V767D/R2030X) that had a late age of onset (27 years) (Simonelli *et al.*, 2005). Looking at the serious to moderate mutations, a relatively large amount of clinical data is available for P1380L. For R653C, a severe to serious mutation, the average age of onset for patients carrying this mutation is 14 years, though this can vary depending on the nature of the second mutation. When R653C is in *trans* with a presumed severe

mutation (e.g. c.4604dup or R2030*) it leads to an early age of onset in the range of 6 – 10 years of age (Huang *et al.*, 2013; Fujinami *et al.*, 2015). When R653C is in *trans* with a serious or moderate mutation (e.g. P1380L) it leads to an onset between 12 – 16 years (Fujinami *et al.*, 2015), and in combination with a mild mutation (e.g. G1961E) it has a late onset of 25 years or older (Lee *et al.*, 2017). Similar observations can be made for the P1380L variant. Patients carrying this variant had an average age of onset of 19 years, with the youngest patients being 4 years of age and the oldest being 53 (Cideciyan *et al.*, 2009). When P1380L is in *trans* with known or presumed severe mutations (e.g. [L541P;A1038V], p.S1071Cfs*1084, c.2005delAT) it leads to an early age of onset (4 – 10 years) (Lewis *et al.*, 1999; Cideciyan *et al.*, 2009; Fujinami, Lois, *et al.*, 2013). Alternatively, when this mutation is in combination with a serious to moderate mutation such as W821R, or when it is in a homozygous state, the age of onset ranges between 10 – 27 years (Lewis *et al.*, 1999; Fujinami *et al.*, 2015). When this mutation is combined with a mild mutation such as G1961E or S1696N, patients tend to have a late onset ranging from 20 – 50 years of age (Hwang *et al.*, 2009; Burke *et al.*, 2014; Nõupuu *et al.*, 2014). Finally, for mild mutations, clinical data from a large number of patients is available for the N1868I variant. The age of onset in patients carrying this mutation varies quite widely between the first and eight decade of life, though the majority are late onset (Jiang *et al.*, 2016; Nassisi *et al.*, 2018; Runhart *et al.*, 2018). For the 43 patients for which the age of onset has been provided, the average onset occurred at 37 years, with most cases (70%) having a late onset above 25 years. The majority of the cases occurred as frameshift mutations in *trans* with N1868I (60% of patients), and their age of onset varied significantly between 18 to 72 even in patients with the same genotype (e.g. N1868I/L257Vfs*17) (Runhart *et al.*, 2018), perhaps due to gene-modifiers, environmental factors, epigenetic changes among other reasons. The most severe cases occurred

in patients harboring N1868I as a complex allele with another disease variant, and in *trans* with a frameshift mutation (e.g. [A2064V;N1868I]/Q1513Pfs*42 or A1324Rfs*65/[R1640W;N1868I]), the age of onset in these cases varied from 8 to 15 years (Nassisi *et al.*, 2018). The penetrance of mild variants such as N1868I has brought forward fruitful discussions highlighting the complexities of STGD1 (Zernant *et al.*, 2017; Allikmets, Zernant and Lee, 2018; Cremers *et al.*, 2018; Runhart *et al.*, 2018). Our results indicate that while N1868I and other mild TMD mutations behave very close to WT in terms of solubilization levels and ATPase activity, generally, their pathogenicity may be attributed to lower affinity for the N-ret-PE substrate.

Based on these observations, it is evident that the presence of a severe mutation is not necessarily enough to cause a severe clinical phenotype with an early age of onset in patients harboring these mutations as compound heterozygotes. The severity of the second mutation plays a critical role in determining the onset and progression of STGD. As expected, when known severe mutations are paired in *trans* with other severe mutations, early onset of disease is the most common result. On the other hand, patients carrying mild mutations such as N1868I, or R1898H, generally have a mid to late age of onset even when they were in *trans* with severe mutations, though exceptions to this rule have been observed (Jiang *et al.*, 2016). Moreover, patients carrying serious to moderate mutations such as P1380L could lead to early, mid, or late onset of STGD1 depending on the nature of the second mutation, though some exceptions have also been observed (Burke *et al.*, 2014). Taken together, our results indicate that the amount of functional activity and protein solubilization levels play a fundamental role in delineating the age of onset in STGD1; though other elements such genetic modifiers, ethnicity, lifestyle, and environmental factors may also contribute to the onset and progression of STGD.

Biochemical Classification of TMD Mutants

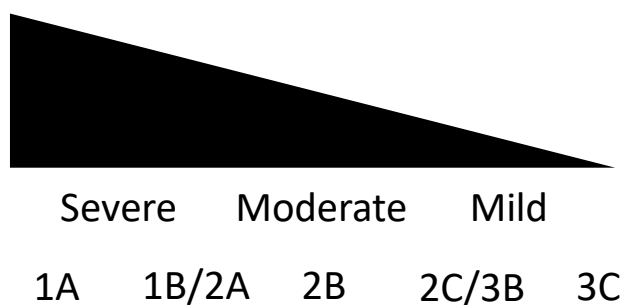


Figure 2.11 Biochemical classification of TMD Variants.

The TMD variants were classified based on their ATPase and N-ret-PE activity levels relative to WT. ATPase activity variants were divided into three groups. Group 1: mutants with basal ATPase activity below 50% of WT levels that have minimal N-ret-PE induced ATPase activity. Group 2: mutants with basal ATPase activity between 50-80% of WT levels that retain N-ret-PE induced ATPase activity. Group 3: mutants that have both basal and N-ret-PE induced ATPase activity similar to WT. Similarly, the TMD variants could be divided into three distinct groups based on N-ret-PE binding levels. Group A: mutants that bind at or below 50% of WT levels. Group B: mutants that binding between 50 to 80% of WT levels. Group C: mutants that bind 80% or above WT levels. The combination of both levels of functional data was used to predict the severity of these STGD variants. Comparison of these severity-predictions with published clinical data correlated strongly.

Table 2.1 Summary of Biochemical Analysis of TMD1 Variants

Variant	Localization	Relative Solubilization +/- SD	Relative Basal ATPase Activity +/- SD	Relative N-ret-PE induced ATPase Activity +/- SD	Relative N-ret-PE Binding +/- SD no ATP	Relative N-ret-PE Binding +/- SD with ATP	Class	Predicted Severity
WT	Vesicles/ER	100	100	224 +/- 22	100	15 +/- 7	--	Normal
R653C	Vesicles/ER	102 +/- 9	113 +/- 21	134 +/- 17	17 +/- 12	15 +/- 10	-A	Severe/Serious
R653H	Vesicles/ER	115 +/- 14	130 +/- 15	239 +/- 39	31 +/- 12	9 +/- 3	3A	Moderate
L661R	ER	20 +/- 11	13 +/- 4	16 +/- 3	36 +/- 6	18 +/- 2	1A	Severe
L686S	ER	27 +/- 8	18 +/- 9	30 +/- 16	16 +/- 8	11 +/- 7	1A	Severe
G690V	ER	33 +/- 12	41 +/- 12	59 +/- 14	21 +/- 9	11 +/- 7	1A	Severe
T716M	Vesicles/ER	98 +/- 16	94 +/- 4	228 +/- 13	59 +/- 7	9 +/- 8	3B	Mild
C764Y	Vesicles/ER	100 +/- 12	133 +/- 5	270 +/- 39	68 +/- 6	16 +/- 7	3B	Mild
S765N	ER	30 +/- 9	21 +/- 9	45 +/- 7	19 +/- 5	16 +/- 5	1A	Severe
S765R	ER	29 +/- 11	18 +/- 6	29 +/- 4	13 +/- 4	18 +/- 3	1A	Severe
V767D	ER	24 +/- 11	40 +/- 14	63 +/- 17	21 +/- 1	20 +/- 2	1A	Severe
L797P	ER	25 +/- 5	31 +/- 5	37 +/- 2	11 +/- 5	12 +/- 5	1A	Severe
G818E	ER	51 +/- 13	63 +/- 5	111 +/- 8	25 +/- 3	12 +/- 3	2A	Serious
W821R	ER	51 +/- 6	58 +/- 7	125 +/- 7	19 +/- 8	17 +/- 6	2A	Serious
I824T	ER	41 +/- 17	64 +/- 3	145 +/- 6	33 +/- 2	13 +/- 4	2A	Serious
M840R	ER	26 +/- 4	37 +/- 12	47 +/- 14	12 +/- 2	14 +/- 2	1A	Severe
D846H	ER	30 +/- 9	42 +/- 22	50 +/- 18	13 +/- 12	14 +/- 7	1A	Severe
V849A	Vesicles/ER	88 +/- 20	86 +/- 5	216 +/- 13	51 +/- 12	12 +/- 9	3B	Mild
G851D	ER	27 +/- 11	31 +/- 11	46 +/- 12	13 +/- 8	12 +/- 10	1A	Severe
A854T	Vesicles/ER	82 +/- 6	70 +/- 10	148 +/- 26	60 +/- 5	21 +/- 9	2B	Moderate/Mild

Table Adapted from Garces *et al.* 2021.

Table 2.2 Summary of Biochemical Analysis of TMD2 Variants

Variant	Localization	Relative Solubilization +/- SD	Relative Basal ATPase Activity +/- SD	Relative N-ret-PE induced ATPase Activity +/- SD	Relative N-ret-PE Binding +/- SD no ATP	Relative N-ret-PE Binding +/- SD with ATP	Class	Predicted Severity
WT	Vesicles/ER	100	100	222 +/- 16	100	16 +/- 7	--	Normal
P1380L	ER	53 +/- 12	61 +/- 19	144 +/- 31	55 +/- 20	21 +/- 11	2B	Moderate
E1399K	Vesicles/ER	102 +/- 15	94 +/- 11	202 +/- 34	117 +/- 13	31 +/- 14	3C	Mild
S1696N	Vesicles/ER	96 +/- 17	120 +/- 8	255 +/- 7	116 +/- 16	27 +/- 13	3C	Mild
Q1703E	Vesicles/ER	89 +/- 13	36 +/- 9	20 +/- 9	42 +/- 16	36 +/- 10	1A	Severe
Q1703K	ER	52 +/- 11	17 +/- 2	12 +/- 1	37 +/- 6	35 +/- 20	1A	Severe
R1705L	ER	40 +/- 13	76 +/- 5	113 +/- 9	54 +/- 12	21 +/- 9	2B	Moderate
A1773E	ER	21 +/- 4	38 +/- 9	43 +/- 1	39 +/- 9	31 +/- 16	1A	Severe
A1773V	ER	36 +/- 20	25 +/- 4	46 +/- 9	37 +/- 8	27 +/- 23	1A	Severe
A1794D	ER	76 +/- 4	46 +/- 13	57 +/- 14	49 +/- 16	16 +/- 9	1A	Severe
A1794P	ER	55 +/- 15	74 +/- 11	137 +/- 27	30 +/- 13	10 +/- 6	2A	Serious
N1805D	Vesicles/ER	82 +/- 18	74 +/- 15	154 +/- 19	44 +/- 11	18 +/- 3	2A	Moderate
H1838D	ER	56 +/- 16	48 +/- 13	96 +/- 40	52 +/- 1	28 +/- 23	1B	Serious
H1838N	Vesicles/ER	107 +/- 14	60 +/- 6	132 +/- 13	48 +/- 2	33 +/- 10	2A	Moderate
H1838R	ER	27 +/- 6	23 +/- 8	28 +/- 11	53 +/- 6	27 +/- 14	1B	Severe/Serious
H1838Y	ER	48 +/- 11	48 +/- 18	75 +/- 20	34 +/- 8	16 +/- 3	1A	Severe
R1843W	Vesicles/ER	99 +/- 8	68 +/- 3	131 +/- 14	84 +/- 11	27 +/- 14	2C	Moderate/Mild
N1868I	Vesicles/ER	111 +/- 25	134 +/- 14	259 +/- 29	101 +/- 9	21 +/- 6	3C	Mild
R1898C	Vesicles/ER	84 +/- 11	114 +/- 8	238 +/- 13	67 +/- 20	20 +/- 13	3B	Mild
R1898H	Vesicles/ER	102 +/- 28	112 +/- 17	270 +/- 35	121 +/- 14	24 +/- 10	3C	Mild

Table Adapted from Garces *et al.* 2021.

Chapter 3 : Functional Characterization of p.N965 and p.N1974 Variants in the Walker A Motif Associated with Stargardt Disease

3.1 Introduction

ABCA4 is an ABC importer predominantly expressed the outer disc membranes of the rod and cone photoreceptors in the retina (Papermaster *et al.*, 1979; Illing, Molday and Molday, 1997; Quazi, Lenevich and Molday, 2012). ABCA4 transports phosphatidylethanolamine (PE) as well as the Schiff base N-retinylidene-phosphatidylethanolamine (N-ret-PE), formed between PE and all-*trans*-retinal or 11-*cis*-retinal (Quazi, Lenevich and Molday, 2012; Quazi and Molday, 2014). The transport of N-ret-PE across the disc membranes of photoreceptors helps prevent the formation of harmful bisretinoids in the retina, while at the same time recycles all-*trans*-retinal back to the light sensitive pigment 11-*cis*-retinal as part of the visual cycle. To date, more than 1000 point-mutations in *ABCA4* have been associated with autosomal recessive Stargardt disease (STGD1:MIM 248200) and other retinal degenerative diseases (Allikmets *et al.*, 1997; Cornelis *et al.*, 2017; Sharon *et al.*, 2019b; Cremers *et al.*, 2020; Khan *et al.*, 2020; Whelan *et al.*, 2020). These pathogenic mutations have been found in all domains of ABCA4 with 50-60% of the mutations being missense mutations (Jiang *et al.*, 2016; Cornelis *et al.*, 2017; Khan *et al.*, 2020). The other 50-40% of pathogenic mutations are divided into frameshifts, truncations, small deletions, insertions, splicing mutations and deep intronic mutations (Jiang *et al.*, 2016; Cornelis *et al.*, 2017; Khan *et al.*, 2020).

ABCA4 is a large 250 kDa protein composed of two fused tandem halves that are structurally similar, each containing one extracytosolic domain (ECD), one transmembrane domain (TMD) and one nucleotide binding domain (NBD). The ECDs are unique to the ABCA

subfamily of eukaryotic ABC transporters (Fig. 1.1). These domains are highly glycosylated and their function is not known, however, some STGD1 mutations localized to these domains have been shown to affect the ATPase activity and N-ret-PE binding of ABCA4, suggesting that the ECDs are important for the function of ABCA4 (Garces *et al.*, 2018). The TMDs of ABC transporters are generally composed of 6 transmembrane helices per transmembrane domain so that a full transporter has a total 12 transmembrane helices, though exceptions to this have been found (Rees, Johnson and Lewinson, 2009; Ford and Beis, 2019). The TMDs form a substrate specific translocation pathway which can interact with the NBDs, via coupling helices, to couple the binding and hydrolysis of ATP with the transport of substrates across cellular membranes (Wen and Tajkhorshid, 2011). The NBDs are highly conserved across all ABC transporters and contain several functionally and structurally relevant motifs and loops that mediate binding and hydrolysis of ATP in response to substrate binding to the TMDs.

Exactly how substrate transport is coupled to ATP binding and hydrolysis is not fully understood. Though major insights regarding the transport mechanism(s) of ABC transporters has been gained from high resolution crystallography and, more recently, cryo-EM structures of ABC transporters (Wilkens, 2015; Ford and Beis, 2019). Even though several mechanisms for substrate transport have been proposed, the alternating access model, and renditions of it, fit the biochemical and structural data currently available (Higgins and Linton, 2004; Dawson and Locher, 2006; Dawson, Hollenstein and Locher, 2007; Sauna *et al.*, 2007; Oldham, Davidson and Chen, 2008; Khare *et al.*, 2009; Rees, Johnson and Lewinson, 2009; Siarheyeva, Liu and Sharom, 2010; Verhalen and Wilkens, 2011; Wilkens, 2015; Ford and Beis, 2019). In this model, the substrate binding site in the TMDs can alter between an outward facing and inward facing conformation depending on cycles of ATP binding and hydrolysis (Fig. 3.6). For an importer,

like ABCA4, the resting and apo state of this transporter is in an outward facing conformation with the substrate binding site open towards to the lumen side of the outer discs (Fig. 3.6). In this conformation, ABCA4 binds tightly to its substrates PE and N-ret-PE. Binding of ATP to the NBDs leads to the dimerization (closing) of the NBDs, which drives the switch from an outward to an inward facing conformation with the substrate binding site now facing to the cytosol side of the membrane. For ABCA4, this inward facing conformation results in a low affinity state to PE or N-ret-PE resulting in substrate dissociation from ABCA4. This is then followed by ATP hydrolysis which reverts ABCA4 back to its original outward facing conformation so that another transport cycle can begin (Molday, 2015).

Several key steps of the transport cycle are still not known, including how tightly coupled ATP hydrolysis and substrate transport are, the ratio between ATP molecules hydrolyzed per substrate translocated, whether both ATPs occupying the two ATP-binding sites are hydrolyzed in a sequential manner or in unison, and whether ADP remains bound to the NBDs upon ATP hydrolysis and is only displaced by ATP after substrate binding occurs in the TMDs. These questions require detailed biochemical, biophysical and structural data in different states of the cycle from a diverse number of ABC transporters. While it is not known that in fact a common model of transport is universal across all ABC transporters, the presence of well conserved motifs involved in binding and hydrolysis of ATP suggest that at least key elementary steps of the transport cycle are likely conserved. For example, the head-to-tail alignment of the two NBDs forms the ATP binding interface between the Walker-A motif of one NBD and the LSGGQ signature motif of the adjacent NBD so that each ABC transporter contains two ATP binding sites (Rees, Johnson and Lewinson, 2009). Furthermore, several structures in different transport conformations of the maltose transporter suggest that ATP hydrolysis is likely driven

by a catalytic glutamate found in the Walker-B motif and stabilized by the conserved D, H and Q loops (Wilkens, 2015; Ford and Beis, 2019). The Q loop is thought to interact with the coupling helices in the TMDs to drive the conformational changes caused by ATP binding and hydrolysis (Wen and Tajkhorshid, 2011; Ford and Beis, 2019).

Mutations associated with STGD1 in the Walker-A (e.g. N965S, N1974S), Walker-B (e.g. D2095V), and LSGGQ (e.g. S1063P) motifs have been documented in several patients, with the Walker-A motif having the largest diversity in STGD1 mutations within the motifs of the NBDs. The N965S mutation in the Walker-A motif of NBD1 is a common mutation in STGD1 patients and has a founder effect in the Danish population (Rosenberg *et al.*, 2007). This mutation has been biochemically characterized before and mouse models suggest that it affects the function and the trafficking of ABCA4 (Quazi, Lenevich and Molday, 2012; Molday *et al.*, 2018). The analogous N1974S mutation in the Walker-A motif of NBD2, has also been shown to cause STGD1, though its effects in the folding properties and function on ABCA4 has not been studied (Stenirri *et al.*, 2008). Furthermore, the N965D/K/Y variants are also known to cause STGD1, underscoring the importance of this residue, however their effects on the function of ABCA4 also remain to be analyzed (Allikmets, 1997; Zernant *et al.*, 2011; Duno *et al.*, 2012; Duncker *et al.*, 2015).

In this study, we biochemically characterized the N965D/K/S/Y STGD1 variants as well as the analogous N1974D/K/S/Y mutations. We also included the non-pathogenic N965A/Q and N1974A/Q mutations in our analysis in order to get a full understanding of the importance of these conserved asparagines in the Walker-A motif. Our functional studies suggest that, depending on the type of mutation, the ability of these mutants to hydrolyze ATP varies, with N965D/K/Y and N1974D/K/Y having the worse functional outcomes. Interestingly, our results

suggest the changes in ATPase activity in these N965 and N1974 Walker-A variants, is not due to changes in ATP binding, as would be expected for mutations in the Walker-A motif, but rather due to the inability to hydrolyze ATP.

3.2 Materials and Methods

3.2.1 Homology Model of ABCA4

The homology model of ABCA4 was made with I-TASSER using the ABCA1 Cryo-EM structure (5XYJ) as template, which bears 50% sequence identity with ABCA4 (Qian *et al.*, 2017). To do this, ABCA4 was split into two tandem halves and each half was modeled individually in I-TASSER. The two halves had a 9 amino acid region of overlap just after the NBD1 (GDRIAlIAQ), and the two models were aligned and fused at this region of overlap using PyMol to construct the full homology model of ABCA4. Furthermore, a second homology of ABCA4 was made using SWISS-MODEL and the ABCA1 Cryo-EM structure (5XYJ). Both models were used to compare the potential effects of pathogenic mutations in the structure of ABCA4. An alignment between these two models did not show any major differences in the overall structure of ABCA4 (Appendix 3).

3.2.2 Cloning of ABCA4 N965 and N1974 Variants

To clone the N965 and N1974 variants, the cDNA of human ABCA4 containing a 1D4 tag (TETSQVAPA) at the C-terminus was cloned into a pCEP4 vector using the Nhe-I and Not-I restriction sites. Missense mutations were generated by PCR based site-directed mutagenesis. All DNA constructs were verified by Sanger sequencing. Primer sequences used for site-directed mutagenesis are available upon request.

3.2.3 Heterologous Expression of ABCA4 N965 and N1974 Variants in HEK293T Cells

A 10 cm plate of HEK293T cells at 80-90% confluency was transfected with 10 µg of pCE4-ABCA4-1D4 DNA. PolyJet™ (1 mg/mL) (SignaGen, Rockville, MD), was used as a transfection reagent at a 3:1 PolyJet™ to DNA ratio for 6 to 8 hours before replacing the media. The transfection was done according to the manufacturer's instructions. Forty-eight hours post transfection, the cells were harvested and centrifuged at 2800 g for 10 minutes. The supernatant was discarded and the cell pellet was resuspended in 200 µL of detergent-free resuspension buffer (50 mM HEPES, 100 mM NaCl, 6 mM MgCl₂, 10% glycerol, pH 7.4). A 40 µL aliquot of resuspended pellet was added to 500 µL of either CHAPS buffer (20 mM 3-[(3-Cholamidopropyl) dimethylammonio]-1-propanesulfonate hydrate (CHAPS), 50 mM HEPES, 100 mM NaCl, 6 mM MgCl₂, 1 mM dithiothreitol [DTT], 1X ProteaseArrest, 10% glycerol, 0.19 mg/mL brain-polar-lipid [BPL], and 0.033 mg/mL 1,2-dioleoyl-sn-glycero-3-phospho-L-ethanolamine [DOPE] [Avanti Polar Lipids, Alabaster, AL], pH 7.4) or SDS buffer (3% SDS, 50 mM HEPES, 100 mM NaCl, 6 mM MgCl₂, 1 mM DTT, 1X ProteaseArrest, 10% glycerol, 0.19 mg/mL BPL, and 0.033 mg/mL DOPE, pH 7.4) and the pellet was solubilized for 40-60 minutes at either 4°C or room temperature respectively. Following solubilization, the samples were centrifuged at 100,000 g for 10 minutes (TLA110.4 rotor Beckman Optima TL centrifuge [Brea, CA]) and the supernatant was collected. The absorbance at 280 nm of the supernatant was taken to determine protein concentration and 7-8 µg of protein was loaded and resolved on an 8% polyacrylamide SDS gel and transferred to a polyvinylidene difluoride membrane for western blotting. The blots were hydrated with methanol for 3-5 minutes before blocking with 1% milk in PBS (137mM NaCl, 10mM Phosphate, 2.6mM KCl, pH 7.4) for 60 minutes. The blots were incubated with primary antibodies against the 1D4 tag (1:100 in PBS) and the loading control b-

tubulin (1:2000 in PBS) for 2 hours, followed by three washes with PBS-T (PBS containing 0.05% Tween 20) for 10 minutes. Secondary antibody incubation was done at a 1:20,000 dilution in PBS-T against the 1D4 antibody (donkey anti-mouse IgG) or actin (donkey anti-rabbit IgG) conjugated to IR dye 680 for 60 minutes, followed by three washes with PBS-T. The blot was imaged on an Odyssey Li-Cor imager (Li-Cor, Lincoln, NE), and the intensity of the bands was quantified to determine the solubilization levels of the ABCA4 variants in CHAPS and SDS relative to WT ABCA4.

3.2.4 Cellular Localization of ABCA4 N965 and N1974 Variants in COS7 Cells

Immunofluorescence microscopy was done on six-well plates containing coverslips coated with poly-L-lysine to promote cell adhesion. COS7 cells were seeded on top of these coverslips 24 hours before transfection. For transfection, 1-3 μg of pCEP4-ABCA4-1D4 construct and 3-9 μL of PolyJetTM (1 mg/mL) were mixed at a 3:1 ratio of PolyJetTM (1 mg/mL) to DNA for 6 to 8 hours before changing media, in accordance to the manufacturer's instructions. Forty-eight hours post transfection, the cells were fixed with 1 mL of 4% paraformaldehyde in 0.1M phosphate buffer (PB; 75.4 mM $\text{Na}_2\text{HPO}_4\cdot 7\text{H}_2\text{O}$, 24.6 mM $\text{NaH}_2\text{PO}_4\cdot \text{H}_2\text{O}$, pH 7.4), for 25 minutes, followed by 3 five-minute washes with PBS. Next, the cells were blocked with 10% goat serum in 0.2% Triton X-100 and PB for 30 minutes. Labelling with the primary antibody was done using the Rho1D4 antibody (1:100 dilution) against the 1D4-tag of the ABCA4 variants and the calnexin rabbit-polyclonal antibody (1:1000) was used as endoplasmic reticulum (ER) marker. Labelling was done for 2 hours in 2.5% goat serum, 0.1% Triton X-100, and PB. The coverslips were washed 3 times with PB for 10 minutes, followed by secondary labeling using Alexa-488 goat-anti-mouse (for ABCA4), Alexa-594 goat-antirabbit (for calnexin), and DAPI for 1 hour at a 1:20,000 dilution. The coverslips were washed 3 more times with PB for 15 minutes and

mounted onto microscope slides in Mowiol mounting medium and kept in the dark at 4°C. The microscope slides were visualized with a Zeiss (Oberkochen, Germany) LSM700 confocal microscope using a 40X objective (aperture of 1.3). Images were analyzed using Zeiss Zen software and ImageJ.

3.2.5 ATPase Assays

A 10 cm plate of HEK293T cells at 80% confluency was transfected as described above. Twenty-four hours post transfection, the cells were harvested and centrifuged at 2800 g for 10 minutes. The supernatant was discarded and the cell pellet was resuspended and solubilized in 1 mL of CHAPS solubilization buffer for 60 minutes at 4°C. Next, the samples were centrifuged at 100,000 g for 10 minutes and the supernatant was incubated with 70 µL of packed Rho1D4-Sepharose affinity matrix for 60 minutes at 4°C in a 1.5 mL tube. The beads were washed twice with 500 µL of column buffer (10 mM CHAPS, 50 mM HEPES, 100 mM NaCl, 6 mM MgCl₂, 1 mM DTT, 1X ProteaseArrest, 10% glycerol, 0.19 mg/mL BPL, and 0.033 mg/ml DOPE, pH 7.4) and transferred to an Ultrafree-MC spin column and washed another five times with 500 µL of column buffer. Bound ABCA4 was eluted from the Rho1D4 matrix twice with 80 µL of 0.5 mg/mL 1D4 peptide in column buffer at 18°C. Thirty microliters of purified ABCA4 were loaded onto an 8% acrylamide gel along with BSA standards to calculate the amount of ABCA4 protein in each sample.

ATPase assays were done using the ADP-GLO™ Max Assay kit (Promega, Madison, WI) according to the manufacturer's guidelines. For each ABCA4 variant tested, six 15 µL aliquots of purified ABCA4 (~100 ng of protein per tube) were added to six 600 µL tubes. One microliter of 0.8 mM all-*trans* retinal in column buffer (or 1 µL of column buffer without all-*trans* retinal) was added to half of the samples (three 600 µL tubes) to obtain a final

concentration of 0 or 40 μM all-*trans* retinal. The tubes were incubated at room temperature for 15 minutes to allow the formation of the Schiff base adduct, N-ret-PE, to occur between all-*trans* retinal and PE. Then, 4 μL of a 1 mM ATP solution (in column buffer) was added to start the ATPase reaction. The ATPase reaction occurred at 37°C for 40 minutes. The final concentrations of all-*trans* retinal and ATP in each sample were 40 μM (or 0 μM) and 200 μM , respectively. For all ATPase assays, the ATPase deficient mutant ABCA4-MM, in which the lysine residues in the Walker A motif of nucleotide binding domain 1 (NBD1) and nucleotide binding domain 2 (NBD2) was substituted for methionine, was used as a negative control to subtract non-specific ATPase activity.

3.2.6 N-ret-PE Binding Assays

Tritiated all-*trans* retinal was prepared as previously described by the Garwin and Saari method, with minor modifications. [^3H] all-*trans* retinal was mixed with unlabeled all-*trans* retinal to obtain a final concentration of 1 mM and a specific activity of 500 dpm/pmol. For a typical binding assay, two 10 cm plates of transfected HEK293T cells were harvested 48 hours post transfection and centrifuged for 10 minutes at 2800 g. The pellet was resuspended and solubilized in 3 mL of CHAPS buffer for 40 to 60 minutes at 4°C and centrifuged at 100,000 g for 10 minutes. The supernatant was collected and divided in half into two 1.5 mL tubes. Each tube was incubated with 80 μL of packed Rho1D4-Sepharose affinity matrix equilibrated in column buffer and mixed by rotation for 60 minutes at 4°C. The affinity matrix (beads) was washed twice with 500 μL of column buffer and transferred to a 500 μL tube. The matrix was then incubated with 250 μL of 10 μM [^3H] all-*trans* retinal in column buffer for 30 to 60 minutes at 4°C. Next, the matrix was washed 6 times with 500 μL of column buffer to remove unbound [^3H] all-*trans* retinal from the column. Then, one sample was incubated with 1 mM ATP and the

other half was incubated with column buffer without ATP for 15 minutes at 4°C. The beads were washed 5 times with 500 µL of column buffer and transferred to an Ultrafree-MC (0.45 µm filter) spin column followed by another 5 washes of 500 µL of column buffer. Bound [³H] all-*trans* retinal was extracted with 500 µL of ice-cold ethanol by rigorous shaking for 20 minutes at room temperature. The extracted [³H] all-*trans* retinal was mixed with 2 mL of scintillation fluid and the radioactivity level was determined using a Beckman scintillation counter. Bound ABCA4 was eluted from the Rho1D4-bead matrix by shaking the beads with 80 µL of 3% SDS in column buffer for 25 minutes at room temperature. The samples were resolved in an 8% SDS-polyacrylamide gel and transferred to a polyvinylidene difluoride membrane for western blotting. All washes and incubations with [³H] all-*trans* retinal were done in the dark.

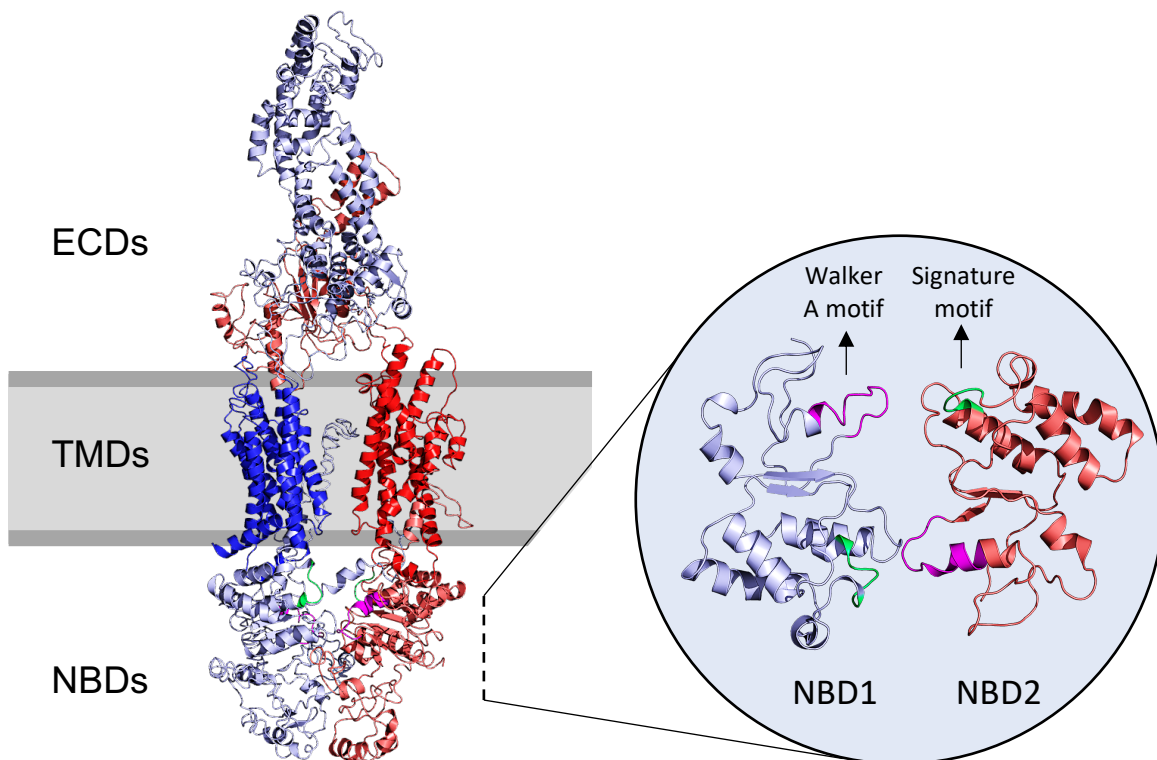
3.3 Results

3.3.1 Topological Organization of The ABCA4 Domains

We created homology models of ABCA4 with I-TASSER using the Cryo-EM structure of ABCA1 (5XYJ), which bears 50% sequence identity with ABCA4, as a template (Qian *et al.*, 2017). The model highlights the topological organization of the extracytosolic domains (ECDs), transmembrane domains (TMDs), and the nucleotide binding domains (NBDs) of ABCA4 (Fig. 3.1). The NBDs of ABC transporters are highly conserved and contain several motifs that play important roles in mediating the binding and hydrolysis of ATP. This is indicated by the high structural similarity of the NBDs in the ABCA4 model with the ABCA1 Cryo-EM structure and the high sequence identity of different motifs in the NBDs such as the Walker-A motifs (Fig. 3.1). Several mutations in the Walker-A motifs of ABCA4 are known to cause STGD1. For example, the residues N965 and N1974 are highly conserved and several variants at these positions (N965D/K/S/Y and N1974S) have been shown to cause STGD1 (Fig. 3.1). To improve

our understanding of the molecular mechanism of STGD1 and the transport cycle of ABCA4, we decided to explore how these STGD1 variants at the N965 and N1974 positions may affect the functional properties of ABCA4. Moreover, we also characterized other non-disease associated variants (N965A/Q and N1974D/K/Y/A/Q) at these positions to explore the implications that these conserved residues have in the overall function of ABCA4.

A



B

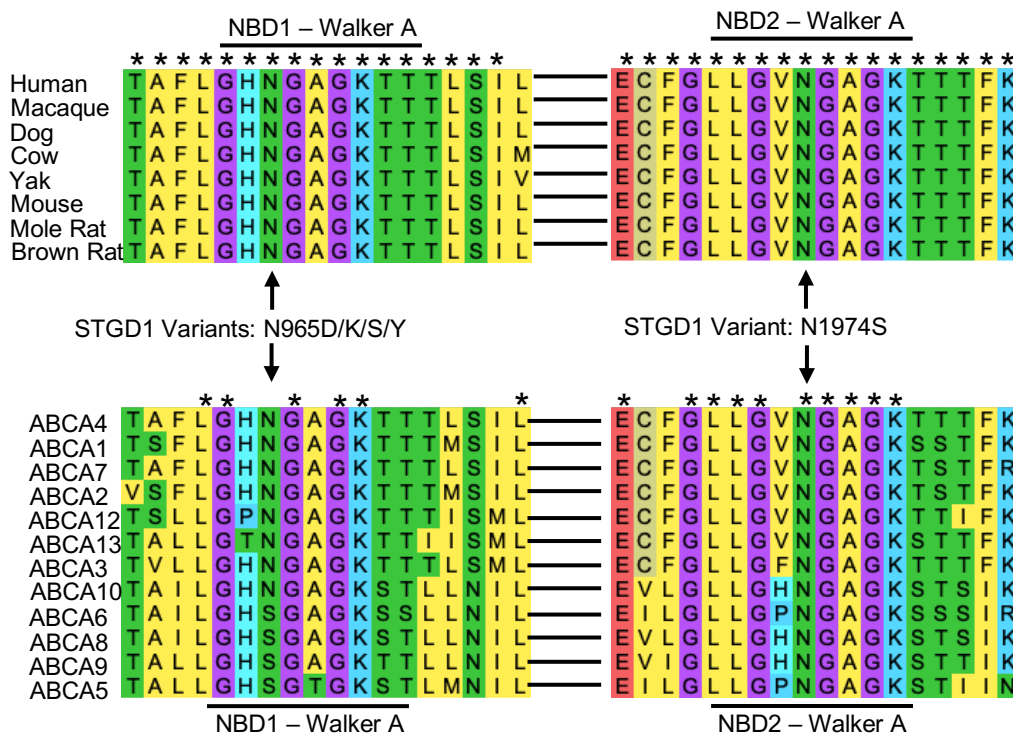


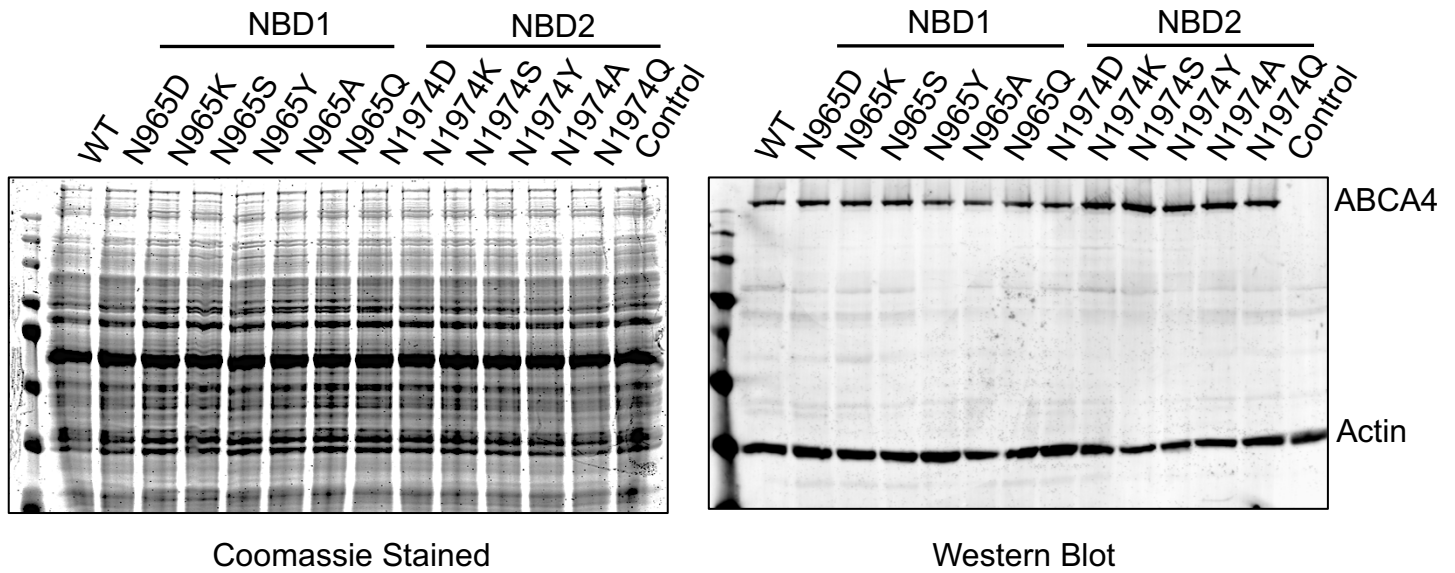
Figure 3.1 Homology model of ABCA4.

A. I-TASSER was used for modeling ABCA4 using the ABCA1 Cryo-EM structure (5XYJ) as template, which bears 50% sequence identity with ABCA4. (ECD = Exocytosomal Domain), (TMD = Transmembrane Domain), (NBD = Nucleotide Binding Domain). (Purple = Walker A motif), (Green = LSGGQ motif). B. Multiple sequence alignment of the Walker A motif of ABCA4 across different species and of the ABCA4 subfamily. The N965 and N1974 ABCA4 variants known to cause STGD1 are highlighted.

3.3.2 Solubilization Levels and Cellular Localization of N965 and N1974 Variants

Our first assessment of the N965 and N1974 variants focused on understanding how mutations at these positions would affect protein folding of ABCA4. To do this, we measured changes in solubility of these variants relative to WT with the non-denaturing detergent CHAPS and with the denaturing detergent SDS (Fig. 3.2 and 3.3). Additionally, we used confocal microscopy to look at the cellular localization of these variants in transfected COS7 cells. Previous research has shown that misfolded mutants have low solubilization levels in CHAPS buffer, and are retained in the ER of COS7 cells (Garces *et al.*, 2018). As shown by western blots of cell lysate solubilized with CHAPS buffer, the solubilization levels of the N965 and N1974 variants were comparable to WT ABCA4 (Fig. 3.2). We observed similar results in the SDS solubilized SDS lysate (Fig. 3.3). This suggests that the relative amount of soluble ABCA4 is similar in WT and the N965 and N1974 variants. Likewise, our microscopy results showed that WT ABCA4 as well as the N965 and N1974 variants were able to leave the ER and localize to vesicles (Fig. 3.4). Taken together, these analyses indicate that the N965 and N1974 variants do not lead to major misfolding of ABCA4.

A



B

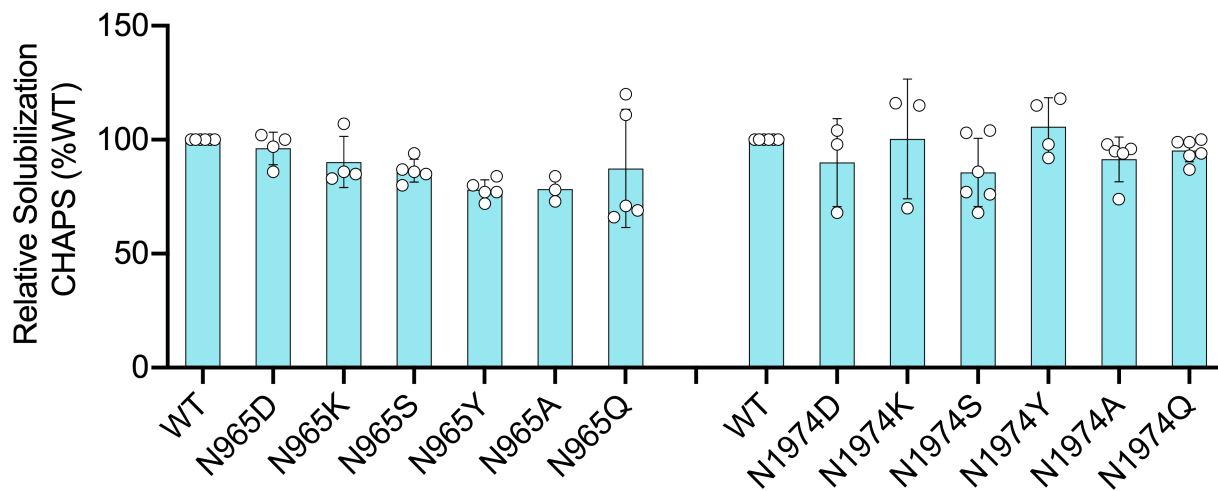


Figure 3.2 CHAPS protein solubilization levels of N965 and N1974 variants.

Transfected HEK293T cells were solubilized using a non-denaturing detergent (CHAPS) to compare the solubility of the Walker A variants. Cell lysates were centrifuged to remove unsolubilized material and the supernatant was loaded and resolved by SDS electrophoresis and analyzed by western blots to compare the expression levels of the N965 and N1974 variants relative to WT in each detergent. A. Representative western blots of lysates solubilized in CHAPS labelled for ABCA4. Actin was used as a loading control. All variants solubilize at similar levels to WT. B. Bar plots showing the mean relative solubilization \pm SD for $n \geq 3$ independent experiments.

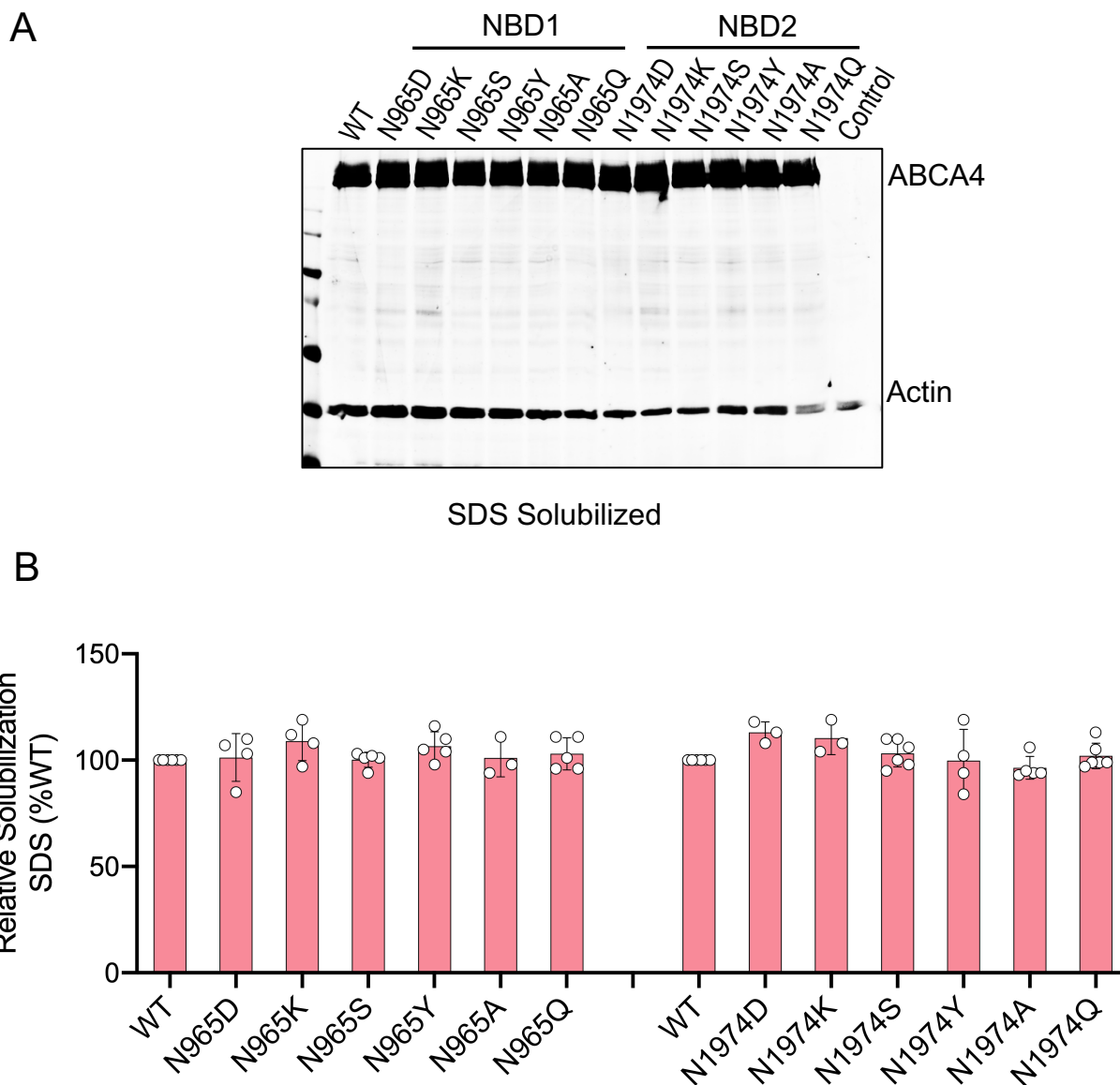


Figure 3.3 SDS protein solubilization levels of N965 and N1974 variants.

Transfected HEK293T cells were solubilized using with SDS to compare protein expression levels of the Walker A variants A. Representative western blot of lysates solubilized in SDS labelled for ABCA4. Actin was used as a loading control. All variants solubilize at similar levels to WT. B. Bar plots showing the mean relative solubilization +/- SD for n≥4 independent experiments.

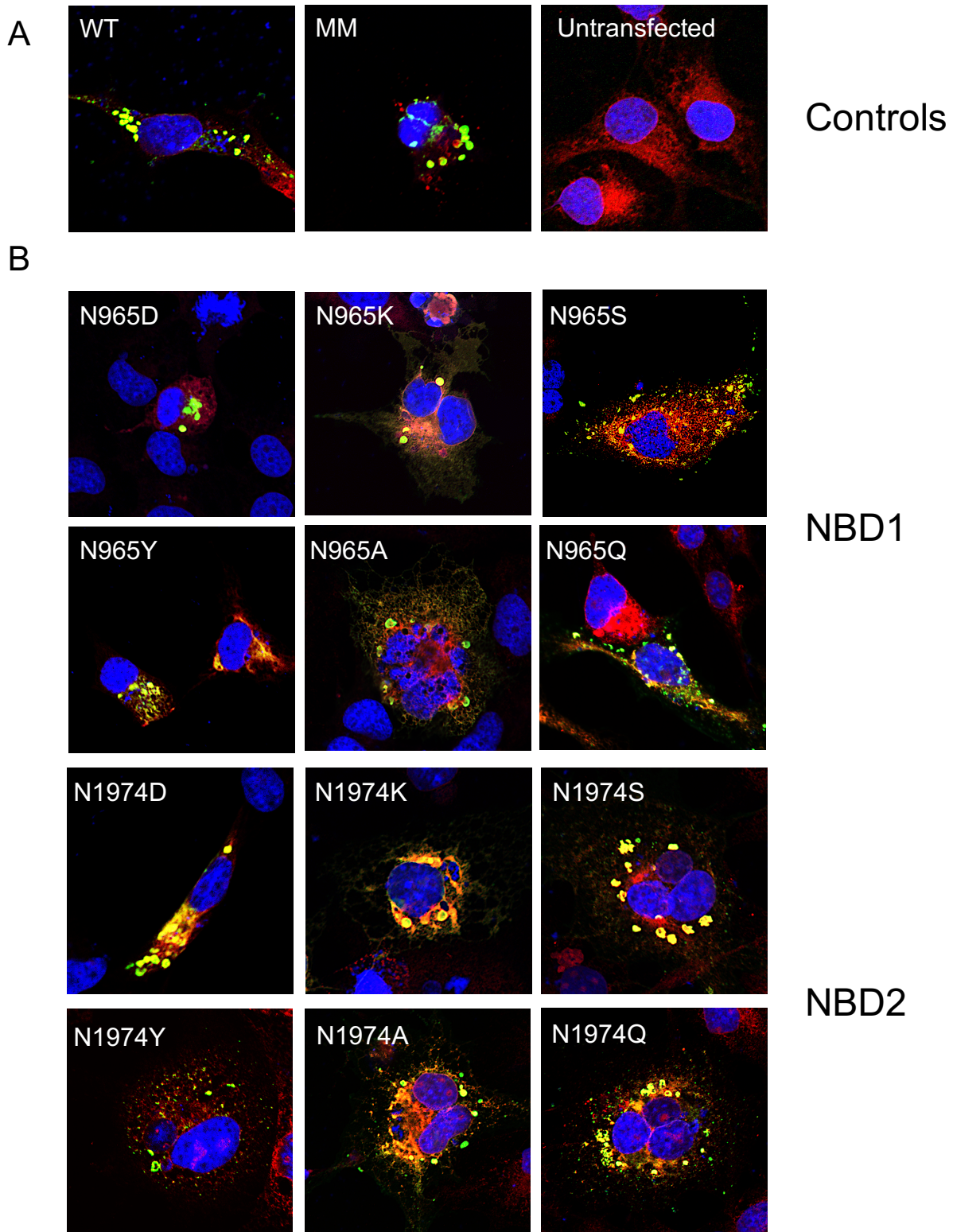


Figure 3.4 Cellular localization of N965 and N1974 variants in COS 7 cells.

Representative micrographs of ABCA4 variants transfected in COS7 cells. Their cellular localization was analyzed by confocal microscopy. The prevalence of vesicles over reticular localization suggest correct protein folding. Likewise, predominant reticular localization suggest protein misfolding. A. WT, MM and untransfected controls. B. N965 and N1974 variants. GREEN = anti-ID4 tag (ABCA4), RED = anti-calnexin (ER marker), BLUE = DAPI (nucleus).

3.3.3 Functional Characterization of N965 and N1974 Variants

Next, we wanted to understand how mutations at amino acid position N965 and N1974 would affect the ATPase activity and N-ret-PE binding levels of these variants relative to WT ABCA4. To measure the ATPase activity of these variants, we first purified ABCA4 using a Rho1D4 affinity column to bind to and pull down ABCA4 using the 1D4-tag placed at the C-terminus. The quality of the purification and quantity of ABCA4 protein was assessed using Coomassie blue protein-stained gels and BSA protein standards (Fig. 3.5). Purified ABCA4 was used to measure the ATPase activity of WT and the N965 and N1974 ABCA4 variants in the absence or presence of all-*trans* retinal (Fig. 3.5). In the absence of all-*trans* retinal, WT ABCA4 retains a basal level of ATPase activity due to the presence of PE (Ahn, Wong and Molday, 2000). PE is a substrate of ABCA4 that can be transported (flipped) across membranes with the help of ATP hydrolysis (Beharry, Zhong and Molday, 2004; Quazi, Lenevich and Molday, 2012). Addition of all-*trans* retinal leads to the formation of N-ret-PE, the Schiff base of all-*trans* retinal and PE, which increases the ATPase activity of WT ABCA4 about twofold from basal levels (Fig. 3.5) (Illing, Molday and Molday, 1997; Sun, Molday and Nathans, 1999; Ahn, Wong and Molday, 2000). In general, the ATPase activity of the Walker-A variants varied depending on the mutations. The N965D/K/Y and N1974D/K/Y variants were the most severely affected, with a drastic reduction on basal ATPase activity that was not stimulated further by N-ret-PE. The N965Q mutant was moderately affected, with lower levels of basal ATPase activity, that was higher than the severe mutants, but retained no N-ret-PE induced ATPase activity. The variants N965S/A and N1974S/A/Q had WT levels of basal ATPase activity and their N-ret-PE induced ATPase activity was mildly to moderately affected. For these experiments, the MM mutant, which has two lysine residues in the NBDs mutated to methionine and has minimal, non-

specific ATPase activity, was used as a negative control (Quazi, Lenevich and Molday, 2012)(Fig. 3.5).

To measure N-ret-PE binding, the ABCA4 variants and WT ABCA4 were immobilized in a Rho 1D4-affinity-column and incubated with 250 μ L of 10 μ M [3 H] all-*trans* retinal to allow the formation and binding of [3 H] N-ret-PE to ABCA4. Binding of [3 H] N-ret-PE was measured in the absence or presence of ATP. In the absence of ATP, ABCA4 is in an outward facing conformation, with the substrate binding site open towards to lumen side of the outer segment disc. In this outward facing conformation ABCA4 binds tightly to its substrate N-ret-PE. Binding of ATP to the NBDs leads to their dimerization and a switch to an inward facing conformation with the substrate binding site now open towards the cytosol side of the membrane (Fig. 3.6). This inward facing conformation has a low affinity for N-ret-PE, which leads to substrate release from ABCA4 (Fig. 3.6). The two conformational states, driven by binding and hydrolysis of ATP, can be observed in the N-ret-PE binding profile of WT ABCA4 (Fig. 3.5). The substrate binding levels of the Walker-A mutants varied depending on the variant, but, for all variants, addition of ATP led to substrate release. The N965D/K and N1974D/K variants bound to N-ret-PE at ~50% or below WT levels, with the N1974D being the most affected. The N965S/Y/A/Q and N1974S/Y/A/Q had relatively mild effects on N-ret-PE binding and behaved similarly to WT. Interestingly, the MM mutant, which is devoid of ATPase activity but has been shown to bind to ATP (Ahn, J. *et al.*, 2003), bound to N-ret-PE at about 50% of WT levels and could not release N-ret-PE in the presence of ATP, suggesting that this mutant does not undergo the conformational changes to allow for substrate dissociation in the presence of ATP (Fig. 3.5).

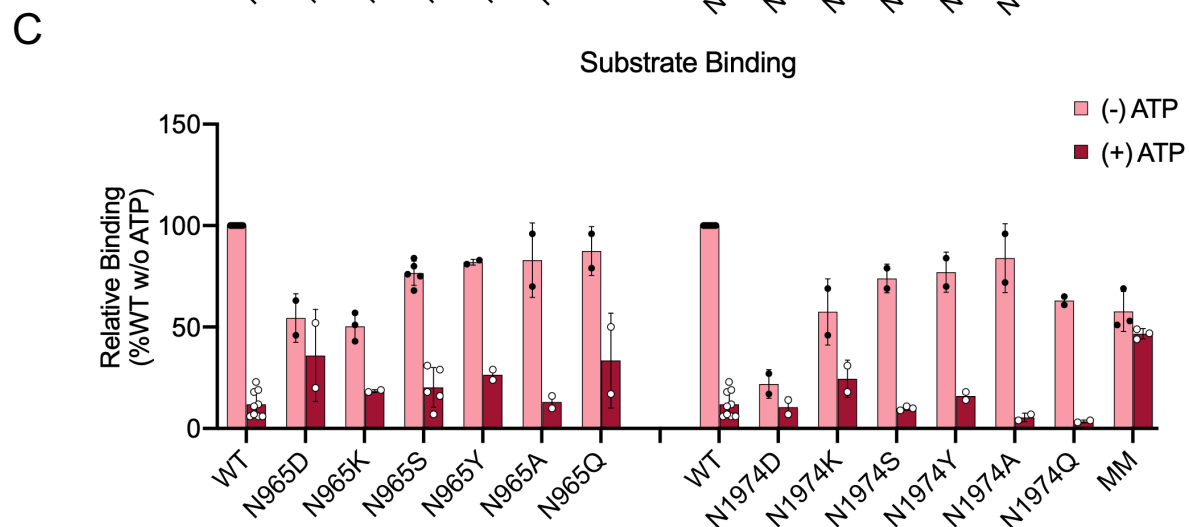
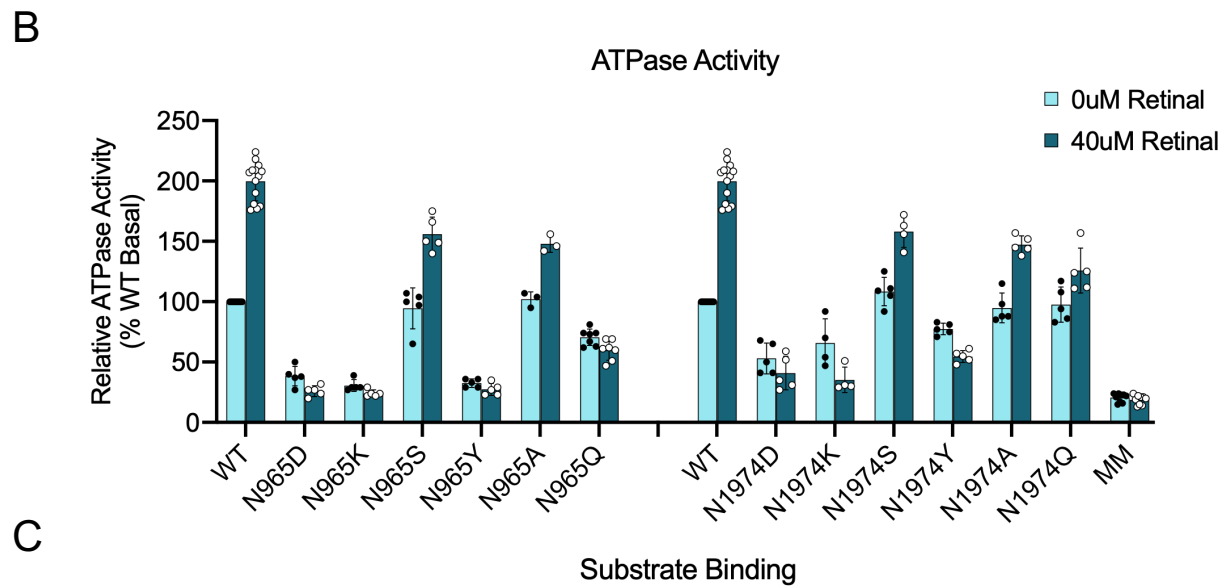
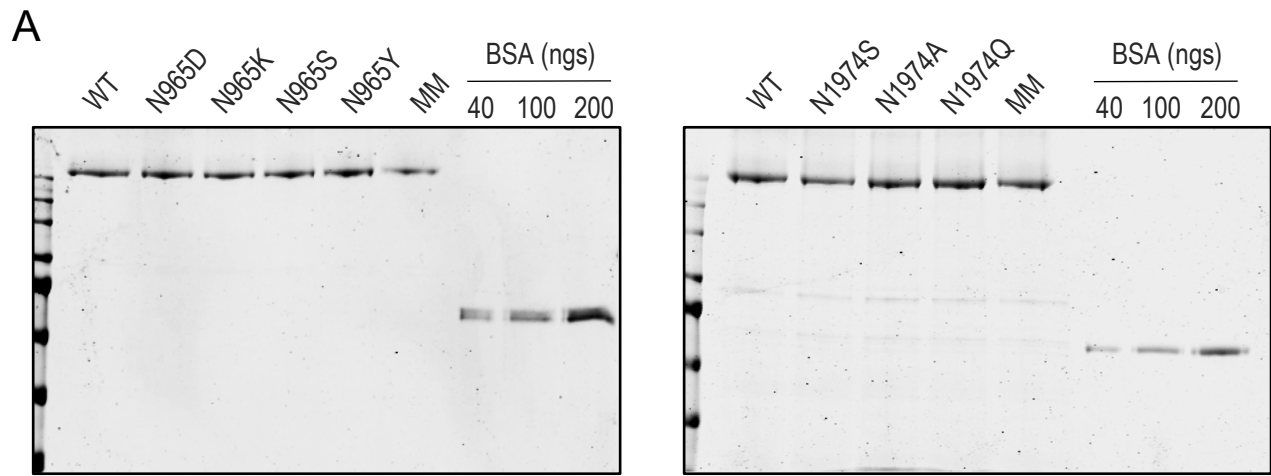


Figure 3.5 Functional characterization of N965 and N1974 variants.

A. N965 and N1974 variants were purified and the protein concentration and quality of the purification was analyzed by SDS-PAGE and Coomassie blue protein staining. BSA standards were used to generate a standard curve. B. ATPase assays were done with purified ABCA4 variants in the absence (cyan) or presence (dark cyan) of all-*trans*-retinal and ATP hydrolysis was measured by luminescence using the ADP-Glo Kinase Assay Kit. C. Tritiated all-*trans*-retinal was used to measure the binding properties of the N965 and N1974 variants to N-ret-PE in the absence (pale red) or presence (red) of ATP. Binding of ATP to the NBDs leads to the dimerization of the NBDs and dissociation of the substrate N-ret-PE. All variants showed some levels of N-ret-PE dissociation in the presence of ATP suggesting that they can still bind to ATP. The MM mutant, which cannot hydrolyze ATP, however, does not display any major dissociation of N-ret-PE in the presence of ATP.

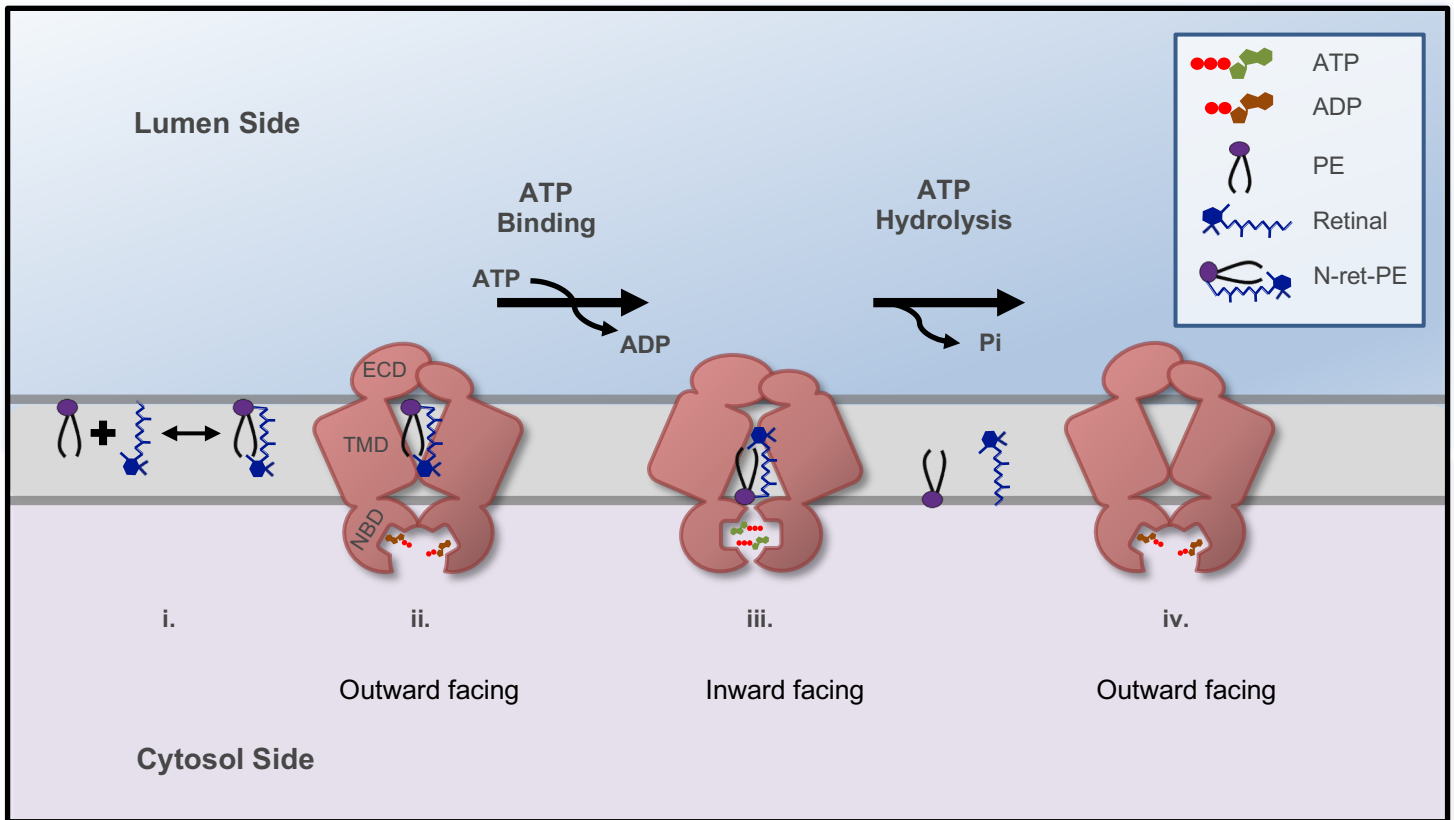


Figure 3.6 The alternating access model for ABCA4.

i. On the luminal side of an outer segment disc membrane, phosphatidylethanolamine (PE) and all-*trans*-retinal (or 11-*cis*-retinal) exist in equilibrium with their Schiff base N-retinylidene-phosphatidylethanolamine (N-ret-PE). ii. At its resting state, the importer ABCA4, is in an outward facing conformation with its substrate binding site open towards the lumen side of the outer-disk membrane. In this conformation, ABCA4 has a high affinity for PE or N-ret-PE and association of the substrate with the substrate binding site of ABCA4 occurs. At this point, the NBDs of ABCA4 are not dimerize and are (possibly) bound to ADP. iii. ATP binding leads to the dimerization of the NBDs (and displacement of ADP). This causes ABCA4 to go from an outward facing to an inward facing conformation with the substrate binding site now open towards the cytosol side of the outer-disk membrane. In this conformation ABCA4 has a lower affinity to PE or N-ret-PE, leading to their dissociation from ABCA4. iv. ATP hydrolysis soon follows, this reverts ABCA4 back to its original outward facing conformation with its substrate binding site open towards the lumen side of the outer-disk membrane and the NBDs apart from each other.

3.4 Discussion

The NBDs of ABC transporters contain several motifs and loops that are highly conserved, these include the Walker-A and Walker-B motifs, the LSGGQ signature motif, as well as the D, H, and Q loops. These structural moieties work together to mediate the coupling of ATP binding and hydrolysis with the translocation of various substrates across cellular membranes. Mutations in several of these motifs have been associated with STGD1. In this study we aimed to understand how mutations in the conserved N965 and N1974 residues, found in the Walker-A motifs, affect the function of ABCA4.

We have shown the correlation between the relative solubility of ABCA4 and cellular trafficking, and that these are good indicators to assess the extent of protein misfolding caused by specific mutations (Garces *et al.*, 2018). To investigate the solubility of the N965 and N1974 variants we used the CHAPS detergent. CHAPS is a mild zwitterionic detergent that does not cause protein denaturation and has been used to solubilize and purify membrane proteins in a native-like functional state (Ahn, Wong and Molday, 2000; Sun, Smallwood and Nathans, 2000; Garces *et al.*, 2018). For the Walker-A variants analyzed in this study, their solubility in CHAPS buffer was similar to WT, ranging from ~80-100% of WT levels. Furthermore, the *in vitro* trafficking of these mutants was assessed by immunofluorescence microscopy of transfected COS7 cells. When ABCA4 is processed and correctly folded, it is able to leave the ER of these cells and localize to vesicles in the cytosol. This vesicular localization pattern is another indicator that ABCA4 is not getting misfolded. All the Walker-A variants analyzed here showed vesicular localization in transfected COS7 cells, providing further evidence that protein misfolding is not happening. Taken together, the solubilization levels and cellular trafficking of

the N965 and N1974 mutants indicate that these mutations are not causing major changes in the protein folding of ABCA4 and are able to retain their structural integrity.

Our functional studies highlight the importance that the residues N965 and N1974 have in mediating ATP hydrolysis. Looking at the ATPase assays, the N965D/K/Y mutants had drastically reduced levels of basal ATPase activity, between 30-40% of WT. In a similar manner, the N1974D/K/Y mutants had a moderate reduction in basal ATPase activity, between 50-75% of WT. The addition of all-*trans*-retinal did not lead to an increase in ATPase activity in N965D/K/Y, and in fact, seemed to lower the ATPase activity of the N1975D/K/Y variants. For the N965S/A and N1974S/A mutants, the basal ATPase activity was not affected at all but these variants had lower levels of N-ret-PE induced ATPase activity relative to WT. Interestingly, while both N965Q and N1974Q mutants had slightly lower levels of basal ATPase activity than WT, around 70-90% of WT, N965Q did not have any N-ret-PE induced ATPase activity, while N1974Q did, albeit at lower levels than the N1974S/A variants.

The N-ret-PE binding profile generally showed a similar trend across the N965 and N1974 variants. For example, all the N965 and N1974 variants had lower levels of N-ret-PE binding. With the exception of N1974D, which bound N-ret-PE at around 20% of WT levels, all the other N965 and N1974 variants were able to bind N-ret-PE at levels ranging from 50-88% of WT. Moreover, all variants, including N1974D, were able to release N-ret-PE in the presence of ATP. The ability for these variants to release N-ret-PE in the presence of ATP suggest that they can still undergo the conformational change necessary for substrate release as a result of ATP binding. A possible explanation for this, rooted in the alternating access model, is that ATP binding to the NBDs leads to dimerization of the NBDs and a switch from an outward facing to an inward facing conformation that leads to N-ret-PE dissociation from ABCA4 (Fig. 3.6). Of

course, follow up structural studies are needed to explore if these asparagine residues are indeed playing a crucial role in binding to ATP. This is in contrast to the MM mutant, which cannot release N-ret-PE in the presence of ATP. The implications of these functional studies support the idea that ATP binding and ATP hydrolysis are two kinetically distinct steps during the transport cycle of ABCA4.

Chapter 4 : Correlating the Expression and Functional Activity of ABCA4 Disease Variants with the Phenotype of Patients with Stargardt Disease

4.1 Introduction

Stargardt disease (STGD1:MIM 248200) is the most common inherited macular dystrophy affecting 1 in 10,000 people (Stargardt, 1909; Gelisken and De Laey, 1985; Weleber, 1994). Affected individuals typically show bilateral loss of central vision, impaired color vision, delayed dark adaptation, atrophy of the macula, and accumulation of yellow-white flecks at the level of the retinal pigment epithelium (RPE) (Fishman, Farbman and Alexander, 1991; Mäntyjärvi and Tuppurainen, 1992; Weleber, 1994; Rotenstreich, Fishman and Anderson, 2003; Kang-Derwent *et al.*, 2004; Tanna *et al.*, 2017). The age of onset and disease severity vary widely, but in most cases, STGD1 patients experience a significant reduction in visual acuity in their first or second decade of life and progressive loss in vision during their lifetime (Fishman *et al.*, 1987; Rotenstreich, Fishman and Anderson, 2003).

STGD1 is caused by mutations in the gene encoding the ATP-binding cassette (ABC) transporter ABCA4, originally known as ABCR and the Rim protein (Allikmets, 1997; Illing, Molday and Molday, 1997). To date, over 1000 mutations are known to cause STGD1 and the related ABCA4-associated diseases including a subset of autosomal recessive cone-rod dystrophies and retinitis pigmentosa (Allikmets, 1997; Cremers *et al.*, 1998; Rivera *et al.*, 2000; Klevering *et al.*, 2002; Fishman *et al.*, 2003; Jaakson *et al.*, 2003; Cornelis *et al.*, 2017; Lee *et al.*, 2017; Schulz *et al.*, 2017; Zernant *et al.*, 2017). Disease-causing mutations include missense mutations, frameshifts, truncations, small deletions, insertions, and splicing mutations with most

being missense mutations encoding amino acid substitutions throughout the protein (Cremers *et al.*, 2020).

ABCA4 is expressed in rod and cone photoreceptors where it predominantly localizes to the rim region of outer segment disc membranes, though more recent studies have also indicated that it is also expressed in the RPE cells (Hui Sun and Jeremy Nathans, 1997; Illing, Molday and Molday, 1997; Molday, Rabin and Molday, 2000; Lenis *et al.*, 2018). Biochemical studies have shown that ABCA4 actively transports *N*-retinylidene-phosphatidylethanolamine (*N*-Ret-PE), the Schiff-base adduct of retinal and phosphatidylethanolamine (PE), from the lumen to the cytoplasmic leaflet of disc membranes (Sun, Molday and Nathans, 1999; Beharry, Zhong and Molday, 2004; Quazi, Lenevich and Molday, 2012; Quazi and Molday, 2014). This enables the reduction of all-*trans* retinal and excess 11-*cis* retinal to retinol by retinol dehydrogenase 8 (RDH8) thereby preventing side reactions that produce toxic bisretinoid compounds (Weng *et al.*, 1999; Sparrow and Boulton, 2005; Molday, Zhong and Quazi, 2009; Boyer *et al.*, 2012; Quazi and Molday, 2014).

Although significant progress has been made in identifying disease-causing mutations in *ABCA4*, deciphering genotype-phenotype relationships remain challenging since most patients are compound heterozygous for disease mutations in *ABCA4* and phenotypic variations are found in individuals with the same mutations and in the same family (Lewis *et al.*, 1999; Rozet *et al.*, 1999; Valkenburg *et al.*, 2019). Furthermore, with some exceptions (Sun, Smallwood and Nathans, 2000; Wiszniewski *et al.*, 2005; Quazi, Lenevich and Molday, 2012; Zhang *et al.*, 2014), analysis of STGD1 has relied on clinical and genetic data while lacking molecular characterization of disease-causing variants. As a result, it remains to be determined the extent to which the properties of ABCA4 disease variants contribute to the etiology of STGD1 in relation

to other factors such as age, life-style, environmental factors, and genetic modifiers. Nonetheless, clinical and genetic studies have provided a thorough assessment of disease-associated mutations in *ABCA4* with respect to population frequency, ethnic groups, age of onset, and severity (Rivera *et al.*, 2000; Kim and Fishman, 2006; Rosenberg *et al.*, 2007; Cideciyan *et al.*, 2009; Jiang *et al.*, 2016; Cornelis *et al.*, 2017; Schulz *et al.*, 2017; Salles *et al.*, 2018; Sharon *et al.*, 2019a; Khan *et al.*, 2020).

In this study, we combine clinical and genetic data with protein expression and functional analysis of disease-associated variants of *ABCA4* found in 10 patients in Western Canada diagnosed with STGD1. We also report, for the first time, a novel c.5380G>C/p.Ala1794Pro missense mutation located within the second transmembrane domain of *ABCA4*, which causes an early onset and severe form of STGD1 in an individual homozygous for this mutation.

4.2 Materials and Methods

4.2.1 Clinical Assessment and mutational Screening of STGD Patients

Individuals in this study were clinically assessed by measuring visual acuity (VA), retina autofluorescence (AF), full-field electroretinography (ERG), spectral domain optical coherence tomography (SD-OCT), intravenous fluorescein angiography (IVFA), slit-lamp biomicroscopy, and tonometry and their disease stage was categorized according to the Fishman classification (FC) for Stargardt disease (Fishman, 1976; Kim and Fishman, 2006; Cremers *et al.*, 2020). In this clinical classification, Stage 1 patients typically show parafoveal or perifoveal flecks, pigmentary changes in the macula, and normal ERGs; Stage 2 patients exhibit flecks throughout the posterior pole, anterior to the vascular arcades and nasal to the optic disc and relatively normal ERGs but with prolonged dark adaptation; Stage 3 patients display diffusely resorbed flecks, choriocapillaris atrophy in the macula, reduced cone or cone and rod ERGs, and central

and peripheral field impairment; and Stage 4 patients show extensive choroid and retinal pigment epithelium (RPE) atrophy throughout the fundus, decreased ERG cone and rod amplitudes, and moderate to severe peripheral field restriction.

For genotyping, DNA was isolated from 3-5 ml of peripheral blood using the Qiagen QIAamp DNA blood Maxi-kit. Mutation testing of all coding exons and the flanking intronic sequences of the *ABCA4*, *CNGB3* and *ELOVL4* genes was performed by Next Generation Sequencing (NGS) as described previously (Schulz *et al.*, 2017). Informed consent was obtained from all individuals and all procedures were approved by the Institutional Ethics Review Board at the University of British Columbia and followed the tenets of the Declaration of Helsinki.

4.2.2 Generation of ABCA4 Mutant Constructs

The cDNA of human *ABCA4* engineered to contain a 1D4 tag (TETSQVAPA) at the C-terminus of the protein has been described previously (Zhong, Molday and Molday, 2009). Missense mutations were generated by PCR based site-directed mutagenesis. All DNA constructs were verified by Sanger DNA sequencing. Primer sequences used for site-directed mutagenesis are available upon request.

4.2.3 Protein Solubilization Analysis of ABCA4 Variants

Ten cm dishes containing HEK293T cells at 80-90% confluency were transiently transfected with 10 µg of pCEP4-ABCA4-1D4 mutant constructs using 1 mg/ml linear polyethyleneimine (PEI) average MW-25,000 daltons at a 1:3 DNA:PEI ratio for 6-8 h before replacing with fresh media. Forty-eight h post-transfection cells were harvested and centrifuged at 2800 x g for 15 min. The pellet was resuspended in 100 µl of resuspension buffer (50 mM HEPES, 100 mM NaCl, 5 mM MgCl₂, 10% glycerol, pH 7.4). The solution was divided in half and solubilized for 40 min in 500 µl of either 3-[(3-Cholamidopropyl)dimethylammonio]-1-

propanesulfonate hydrate (CHAPS) solubilization buffer (20 mM CHAPS, 50 mM HEPES, 100 mM NaCl, 5 mM MgCl₂, 1 mM dithiotreitol (DTT), 1X ProteinArrest, 10% glycerol, 0.15 mg/ml brain-polar-lipid (BPL), and 0.15 mg/ml 1,2-dioleoyl-sn-glycero-3-phospho-L-ethanolamine (DOPE) (Avanti Polar Lipids), pH 7.4) or SDS solubilization buffer (3% SDS, 50 mM HEPES, 100 mM NaCl, 5 mM MgCl₂, 1 mM DTT, 1X ProteinArrest, 10% glycerol, 0.15 mg/ml BPL, and 0.15 mg/ml DOPE, pH 7.4). The samples were then centrifuged at 100,000 x g (TLA110.4 rotor Beckman Optima TL centrifuge) and the supernatant was collected. Protein concentration of the supernatant was determined from the absorbance at 280 nm. The samples (7-8 µg of total protein per lane) were resolved on an 8% polyacrylamide gel and transferred onto a polyvinylidene difluoride (PVDF) membrane for western blotting. Blots were blocked in 1% milk for 60 min and subsequently labeled with Rho1D4 mouse monoclonal antibody (1:100 dilution) and rabbit-anti-β-tubulin (1:1000 dilution) as a loading control followed by donkey anti-mouse IgG or donkey anti-rabbit IgG conjugated to IRdye 680 for imaging on an Odyssey Licor imager. Protein expression levels were quantified based on the intensity of the ABCA4 bands as measured by western blotting and normalized from the intensity of the bands of the β-tubulin loading control.

4.2.4 Immunofluorescence Microscopy of Transiently Transfected COS7 Cells

COS-7 cells were transfected with PolyJet™ (SignaGen) reagent according to the manufacturer's guidelines. In brief, COS-7 cells were seeded 24 h prior to transfection on 6-well plates containing coverslips coated with poly-L-lysine to promote cell adhesion to coverslips. The cells were transfected at 70-80% confluency with 1 µg of DNA and 3 µl of PolyJet™ for 6-8 h prior to replacing with fresh media. At 48 h post-transfection, the cells were fixed with 4% paraformaldehyde (PFA) in 0.1M phosphate buffer (PB), pH 7.4, and blocked with normal goat

serum in 0.2% Triton X-100 and PB for 30 min. Primary antibody labeling was carried out for 3 h using the Rho1D4 antibody against the 1D4-tag and the calnexin rabbit-polyclonal antibody as an endoplasmic reticulum (ER) marker. Secondary labeling was carried out using Alexa-488 goat-anti-mouse (for ABCA4) and Alexa-594 goat-anti-rabbit (for calnexin) for 1 h. The cells were visualized under a Zeiss LSM700 confocal microscope using a 40X objective (aperture of 1.3). Images were analyzed using Zeiss Zen software.

4.2.5 ATPase Assay

Transfected HEK293T cells (1-2 150mm X 25 mm dishes of HEK293T cells at 80-90% confluency) were solubilized in 3 ml of CHAPS solubilization buffer for 40-60 min at 4°C followed by a 100,000 x g centrifugation for 10 min. The supernatant was incubated with 100 µl of packed Rho1D4-Sepharose matrix 60 min at 4°C. The beads were washed twice with 500 µl column buffer and transferred to an Ultrafree-MC spin column and washed another six times with 500 µl of column buffer. Bound ABCA4 was eluted from the Rho1D4 matrix twice with 100 µl of 0.5 mg/ml 1D4 peptide in column buffer. The eluates were pooled and the ABCA4 protein concentration was estimated from the absorbance 280 nm readings. Liposomes consisting of 9.6 mg/ml brain polar-lipid, 2.4 mg/ml DOPE, 0.001% cholesteryl hemisuccinate, 50 mM HEPES, 150 mM NaCl, 5 mM MgCl₂, 10% glycerol, 1 mM DTT, 0.5% octyl β-D-glucopyranoside were prepared by bath sonication for 3-5 h at 4°C until turbidity of solution was minimal. ABCA4 eluates were then dialyzed for 24 h with three 1 liter changes of dialysis buffer (50 mM HEPES, 100 mM NaCl, 5 mM MgCl₂, 1 mM DTT, 10% sucrose) to remove the detergent.

ATPase assays were carried out using the ADP-Glo™ Kinase Assay kit (Promega) according to the manufacturer's instructions. Reconstituted ABCA4 proteoliposomes were

divided into six microcentrifuge tubes containing 15 μ l of reconstituted protein (\sim 200 ng of ABCA4). One μ l of 0.8 mM all-*trans* retinal (or ATPase buffer alone) was added to half of the reconstituted samples (done in triplicate) to obtain a final concentration of 40 μ M all-*trans* retinal and incubated for 15 min at room temperature in the dark. After initial incubation period, 4 μ l of a 1 mM ATP solution (in ATPase buffer) was added and the samples were incubated at 37°C for 40 min. Five μ l of each sample was placed into a well of a 384-well white bottom plate and incubated with 5 μ l of ADP-Glo™ reagent for 60 min to stop the ATPase reaction and deplete remaining ATP. Ten μ l of ADP-Glo™ detection reagent was added and samples were incubated for 60 min at room temperature prior to luminescence readings. Standard ADP:ATP solutions were used to generate a standard curve and calculate the amount of ATP hydrolyzed. Luminescence was measured with a microtiter plate reader. Reconstituted ABCA4 samples were loaded onto an 8% acrylamide gel along with bovine-serum-albumin (BSA) standards to calculate the amount of ABCA4 in each sample. The ATPase-deficient mutant ABCA4-MM, in which the lysine residues in the Walker A motif of NBD1 and NBD2 were substituted for methionine, was used to subtract background luminescence (Ahn *et al.*, 2003; Quazi, Lenevich and Molday, 2012).

4.2.6 Retinoid Binding Assay

Tritiated all-*trans* retinal was prepared by the method of Garwin and Saari (Garwin and Saari, 2000) with minor modifications (Zhong and Molday, 2010). [³H] all-*trans* retinal was mixed with unlabeled all-*trans* retinal to obtain a final concentration of 1 mM and a specific activity of 500-1000 dpm/pmol. The binding of [³H] all-*trans* retinal was carried out as previously described (Zhong, Molday and Molday, 2009). For a typical binding assay, two 150 mm diameter X 25 mm tissue culture dishes of transfected HEK293T cells at 80-90% confluency

were harvested in 10 ml of DMEM and centrifuged for 15 min at 2800 x g for 15 min. The pellet was resuspended in 100 µl of resuspension buffer (50 mM HEPES, 100 mM NaCl, 5 mM MgCl₂, 10% glycerol, pH 7.4) and solubilized in 3 ml of CHAPS solubilization buffer for 40-60 min at 4°C as described above. After centrifugation at 100,000 x g for 10 min to remove unsolubilized material, the supernatant was divided in half. Each half was incubated with 80 µl of packed Rho1D4-Sepharose-2B affinity matrix equilibrated in column buffer (10 mM CHAPS, 50 mM HEPES, 100 mM NaCl, 5 mM MgCl₂, 1 mM DTT, 1X ProteinArrest, 10% glycerol, 0.15 mg/mL BPL, and 0.15 mg/ml DOPE, pH 7.4) and mixed by rotation for 60 min at 4°C. The affinity matrix was washed twice with 500 µl of column buffer and mixed with 250 µl of 10 µM [³H] all-*trans* retinal (500 dpm/pmol) in column buffer for 30 min at 4°C. The matrix was washed six more times with 500 µl of column buffer. One sample was incubated with 1 mM ATP and the other half was incubated in the absence of ATP for 15 min at 4°C. The affinity matrices were washed twice with 500 µl of column buffer and subsequently transferred to an Ultrafree-MC (0.45 µm filter) spin column (Millipore) followed by another five washes of 500 µl of column buffer. Bound [³H] all-*trans* retinal was extracted with 500 µl of ice-cold ethanol with shaking at 500 rpm for 20 min at room temperature and counted in a liquid scintillation counter. Bound ABCA4 was eluted from the Rho1D4-bead matrix with 3% SDS in column buffer and applied to an 8% SDS-polyacrylamide gel for analysis of protein levels by western blotting. ABCA1, which does not bind retinal (Zhong, Molday and Molday, 2009), was used as a control to subtract out nonspecific [³H] all-*trans* retinal binding to the affinity matrix.

4.3 Results

4.3.1 Genetic Screening of STGD1 Patients

Eleven individuals from British Columbia, Canada with impaired vision and clinical features characteristic of STGD1 were recruited for this study. The patients were screened for mutations in the *ABCA4*, *CNGB3* and *ELOVL4* genes. Sequence variations in the *ABCA4* were identified in ten patients, two of which (c.213dupG and c.5380G>C) have not been previously reported (Table 1). Seven patients had two mutations including one patient who was homozygous for the novel c.5380G>C, p.Ala1794Pro mutation. A mutation in only one *ABCA4* allele was found in two patients. One other individual had two mutations, p.Leu541Pro and p.Ala1038Val. These two mutations are commonly found together as a complex mutation c.[1622T>C;3113C>T]/p.[Leu541Pro;Ala1038Val] in the German population (Rivera *et al.*, 2000; Cideciyan *et al.*, 2009; Zhang *et al.*, 2014). One patient (patient 7) with a STGD1 phenotype had no detectable mutations in the *ABCA4* gene and therefore was excluded from our study. No disease-associated mutations were found in *CNGB3* encoding the cone cyclic nucleotide-gated channel B3 subunit or *ELOVL4* encoding the elongation of very long chain fatty acids protein 4 in any of the patients examined in this study.

4.3.2 Clinical Assessment of STGD1 Patients

Patient 3, 28 years old, carrying the c.214G>A/p.Gly72Arg and c.5882G>A/p.Gly1961Glu mutations is legally blind with VA of 20/200 and stage 3 FC. This patient displayed considerable foveal retinal pigment epithelium (RPE) atrophy accounting for poor VA (Fig. 4.1). The 22-years old younger sibling (patient 2; Table 1) also carried these mutations, but showed a VA of 20/30 and stage 1 FC. The difference in VA between the two siblings with identical genotype may be due to the progressive nature of the disease and/or

familial variation. The mother (Patient 1) with normal 20/20 VA and no signs of STGD1 was a carrier of the p.Gly1961Glu mutation consistent with the recessive nature of STGD1 (Fig. 4.1). At a genetic level, both the p.Gly1961Glu and p.Gly72Arg are classified as pathogenic and likely pathogenic, respectively, consistent with the STGD1 disease assessment (see Table 4.1).

Patient 4, a 30 year old individual with the deleterious c.213dupG/p.Ile73Asnfs*26 frameshift mutation and the c.1654G>A/p.Val552Ile missense mutation, displayed mild STGD1 with stage 2 FC and 20/30 VA. The p.Ile73Asnfs*26 mutation is classified as a pathogenic mutation whereas the p.Val552Ile mutation is classified as likely neutral. Biochemical analysis of the p.Val552Val, however, suggests that this is a mild mutation at a functional level consistent with the clinical assessment of patient 4 (see Discussion section for additional information).

Patient 8, a 13 year old individual carrying two mutations, the p.Leu541Pro and p.Ala1038Val, most likely as a complex allele, had an early disease onset with 20/200 VA and stage 4 FC (Table 4.1). Previous reports have documented the severity and early age of onset associated with the p.[Leu541Pro;Ala1038Val] complex variant (Cideciyan, et al., 2009; Zhang, et al., 2015). Our screening studies failed to detect an additional mutation in *ABCA4* in patients 6, 8 and 12.

Patients 9, 10, and 11, all carrying one deleterious splice site mutation and a missense mutation (c.5714+5G>A/p.Gly1091Glu; c.5461-10T>C/p.Leu2027Phe; c.1099+1G>C/p.Met448Lys), had advanced STGD1 with stage 4 FC, and poor VA (Table 1). The missense variants were classified as pathogenic or likely pathogenic by genetic analysis (Table 1).

Patient 5, an 11-year-old child, had severe STGD1 with VA of 20/200, bilateral bull's eye maculopathy with dull fovea reflex, peripheral flecks, bilateral dark choroid with central RPE disruption, paracentral pisciform lesions on fluorescence angiography, and central outer retinal disruption as visualized by SD-OCT (Fig. 4.1). The FC of this patient is stage 3 despite poor VA and advanced RPE atrophy since the ERG measurements displayed severely reduced cone response but near normal rod response. Sequence analysis indicated that this patient was homozygous for a novel p.Ala1794Pro missense mutation classified genetically as likely pathogenic (Fig. 4.1, Table 4.1).

Table 4.1 Genotype and Phenotype Characteristics of STGD1 Patients harboring ABCA4 mutations

Patient [#]	Age	Mutation 1	Category*	Mutation 2	Category*	Visual Acuity	FC [†]
2	22	Exon 3: c.214G>A, p.(Gly72Arg)	UV4	Exon 42: c.5882G>A, p.(Gly1961Glu)	UV5	20/30	Stage 1
3	28	Exon 3: c.214G>A, p.(Gly72Arg)	UV4	Exon 42: c.5882G>A, p.(Gly1961Glu)	UV5	20/200	Stage 3
4	30	Exon 3: c.213dupG, p.(Ile73Aspfs*26) [‡]	UV5	Exon 12: c.1654G>A, p.(Val552Ile)	UV2	20/30	Stage 2
5	11	Exon 38: c.5380G>C, p.(Ala1794Pro) [‡]	UV4	Exon 38: c.5380G>C, p.(Ala1794Pro) [‡]	UV4	20/200	Stage 3
6	55	Exon 45: c.6229C>T, p.(Arg2077Trp)	UV4	--		20/40	Stage 3
8	13	c. [1622T>C; 3113C>T], p. [Leu541Pro; Ala1038Val]	UV5	--		20/200	Stage 4
9	30	Intron 40: c.5714+5G>A, p.[=,Glu1863Leufs*33]	UV4	Exon 22: c.3272G>A, p.(Gly1091Glu)	UV5	20/160	Stage 4
10	36	Intron 38: c.5461-10T>C, p.(Thr1821Aspfs*6)	UV5	Exon 44: c.6079C>T, p.(Leu2027Phe)	UV5	20/200	Stage 4
11	45	Intron 8: c.1099+1G>C, p.(?)	UV5	Exon 10: c.1343T>A, p.(Met448Lys)	UV4	20/400	Stage 4
12	63	Exon 27: c.4069G>A, p.(Ala1357Thr)	UV4	--		20/400	Stage 3

Patient 1, a carrier of the c.5882G>A, p.(Gly1961Glu) mutation, is the parent of patient 2 and 3 and does not have STGD1. Patient 7, a patient with STGD1 and FC 3, did not have any detectable mutations in the *ABCA4* gene and was not included in this table. *UV1 – neutral; UV2 – likely neutral; UV3 – unknown pathogenicity; UV4 – likely pathogenic; UV5 – pathogenic (Schulz, et al. 2017; Cornelis, et al. 2017). † Fishman Classification (FC) as described in Material and Methods (Fishman, 1976; Kim and Fishman, 2006). ‡ This study. (--) Wild type.

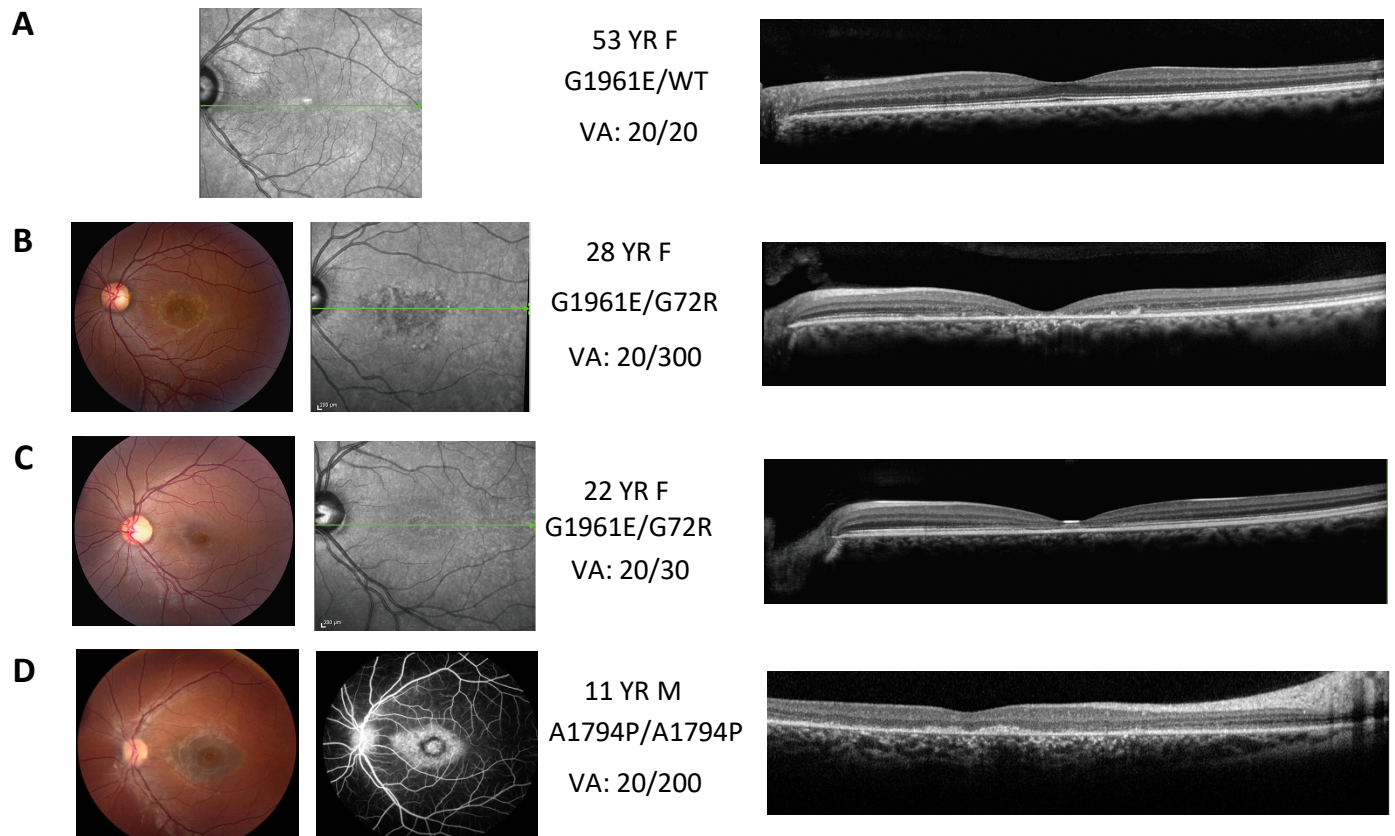


Figure 4.1 Representative clinical features of STGD1 patients examined in this study.

Left: Color fundus (CF) images and retinal autofluorescence (AF) and Right: optical coherence tomography (OCT) images. (A) Patient 1, a carrier of the p.Gly1961Glu mutation (WT/G1961E), showing normal CF, AF and OCT images. (B) and (C) Patients 2 and 3, two-siblings with identical genotype p.Gly1961Glu/p.Gly72Arg (G1961E/G72R); and (D) Patient 5, an individual homozygous for the p.Ala1794Pro (A1794P) mutation. AF illustrates lipofuscin accumulation in all STGD1 patients but not the carrier individual. OCT of patients shows atrophy of the RPE cells around the fovea of STGD1 with the most severe degeneration for patient 5. Panel D (left) shows a fluorescein angiogram alongside of a fundus photograph of a dark choroid. Adapted from Garces et al. 2018.

4.3.3 Protein Solubilization and Localization of ABCA4 Variants in Cultured Cells

The distribution of the 11 missense mutations found in our STGD1 patient cohort within the current topological model for ABCA4 (Bungert, Molday and Molday, 2001; Molday, Zhong and Quazi, 2009) is presented in Figure 4.2. Four missense mutations were found within the exocyttoplasmic domain 1 (ECD1), three in or near nucleotide binding domain 1 (NBD1), three in nucleotide binding domain 2 (NBD2), and 1 mutation within transmembrane segment 11 of transmembrane domain 2 (TMD2).

To determine the effect of disease-causing mutations on ABCA4, we first investigated the level of expression and cellular distribution of the 11 variants and wild-type (WT) ABCA4 transiently expressed in mammalian culture cells. This was carried out by comparing the solubility of the proteins in CHAPS relative to SDS and visualizing the subcellular localization of these mutants in transfected cells by immunofluorescence microscopy.

CHAPS is a mild detergent widely used to solubilize and purify membrane proteins in a native-like state for functional characterization (Hui Sun and Jeremy Nathans, 1997; Zhong, Molday and Molday, 2009). Denatured proteins typically aggregate in CHAPS and can be effectively removed by high speed centrifugation. In contrast, SDS is a strong detergent that solubilizes both native and denatured proteins. It can be used to determine total expression of proteins e.g. both native and denatured protein. The degree of detergent solubilization of the ABCA4 mutants by CHAPS and SDS is shown in western blots in Figure 4.3A and quantified in Figure 4.3B and C. All variants expressed at similar levels as determined by solubilization with SDS. In CHAPS detergent, however, five variants (p.Gly72Arg, p.Met448Lys, p.Leu541Pro, p.Val552Ile, and p.Gly1961Glu) solubilized at levels broadly similar to WT ABCA4; two mutants (p.Ala1038Val and p.Gly1091Glu) solubilized at 70% WT level, and the remaining 4

mutants (p.Ala1357Thr, p.Ala1794Pro, p.Leu2027Phe, and p.Arg2077Trp) solubilized at or below 50% of the WT level as shown in Figure 4.3B and C.

The distribution of ABCA4 variants in transiently transfected COS-7 cells was visualized by immunofluorescence microscopy (Fig. 4.4). As previously reported (Ahn *et al.*, 2003; Zhong, Molday and Molday, 2009), WT ABCA4 showed a punctate staining pattern characteristic of intracellular vesicle-like structures containing calnexin with some evidence of ER reticular staining. Seven disease-variants (p.Gly72Arg, p.Met448Lys, p.Leu541Pro, p.Val552Ile, p.Ala1038Val, p.Gly1091Glu, and p.Gly1961Glu) showed similar calnexin-associated vesicle structures and reticular ER staining (Fig. 4.4). A distinctive reticular expression pattern was most evident for p.Ala1357Thr, p.Ala1794Pro, p.Leu2027Phe, and p.Arg2077Trp disease variants with little or no vesicular structures. In general, disease variants that expressed at or near WT ABCA4 levels as determined by CHAPS solubilization exhibited vesicular staining, whereas lower expressing mutants exhibited primarily a reticular staining pattern (Table 2) indicative of protein misfolding and ER retention by the quality control system of the cell.

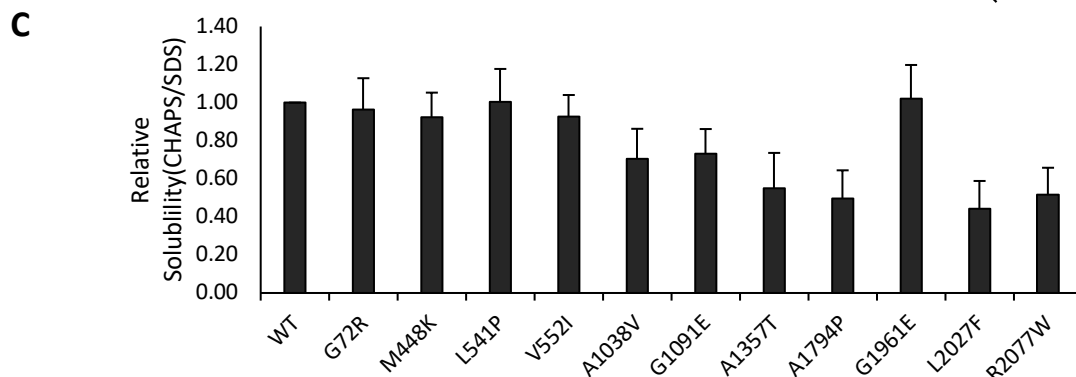
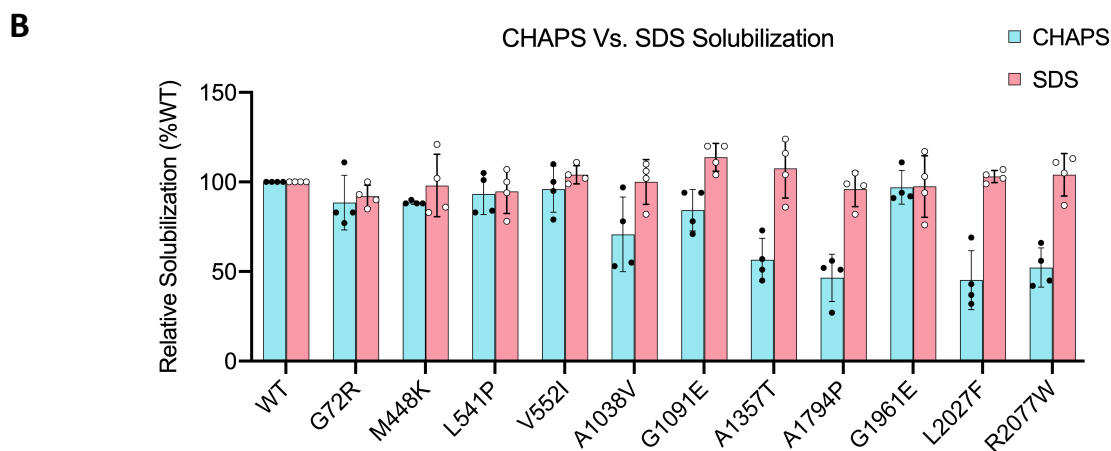
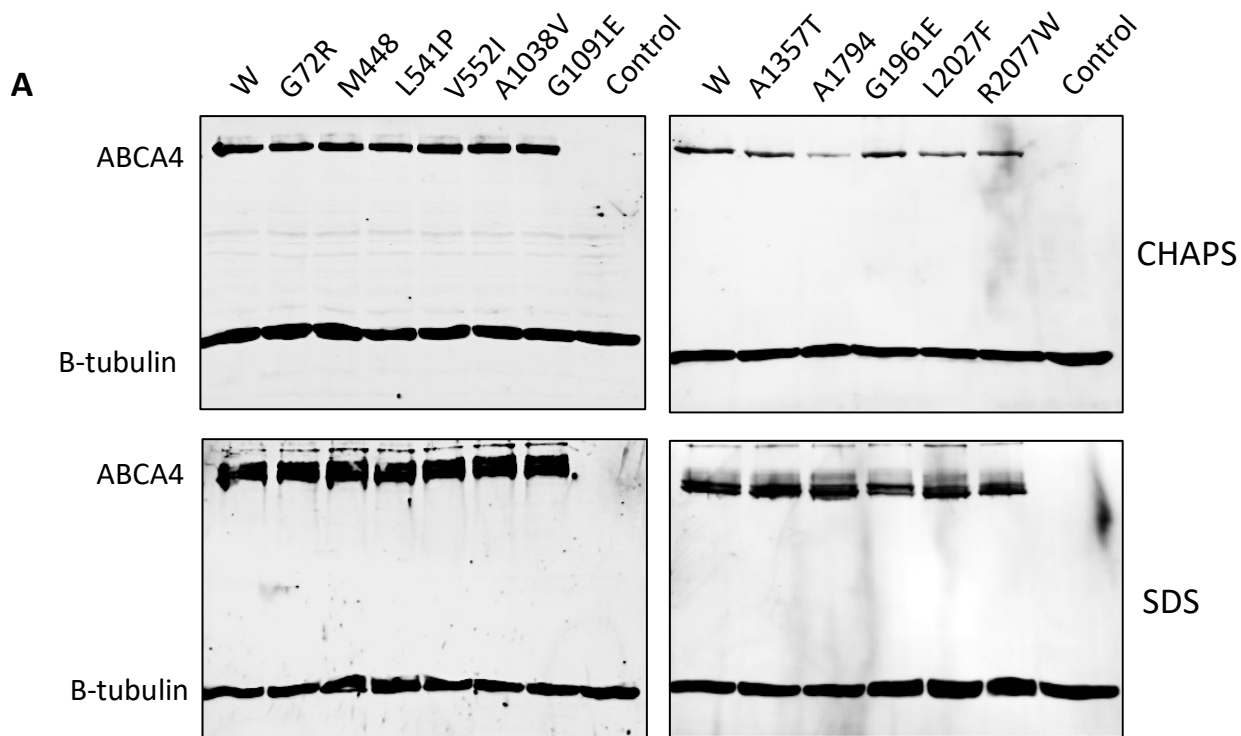


Figure 4.3 Relative solubility of ABCA4 variants in transiently transfected HEK293T cells.

Transfected HEK293T cells were solubilized using either the mild detergent CHAPS or the strong denaturing detergent SDS. The cell lysates were subjected to high speed centrifugation to remove unsolubilized material and the supernatants (7-8 μ g protein per lane) were resolved by SDS gel electrophoresis and subsequently analyzed on western blots labeled for ABCA4. (A) Western blots labeled with the rho 1D4 antibody to epitope-tagged ABCA4; β -tubulin was used as a loading control to normalize the amount of protein loaded across all samples. (B) Quantification of the western blots of CHAPS solubilized ABCA4 relative to SDS solubilized ABCA4. Graph showing the ratio of ABCA4 variants in CHAPS vs. SDS relative to WT levels as determined from western blots. Data is the average \pm SD for $n = 4$ independent experiments. Adapted from Garces *et al.* 2018.

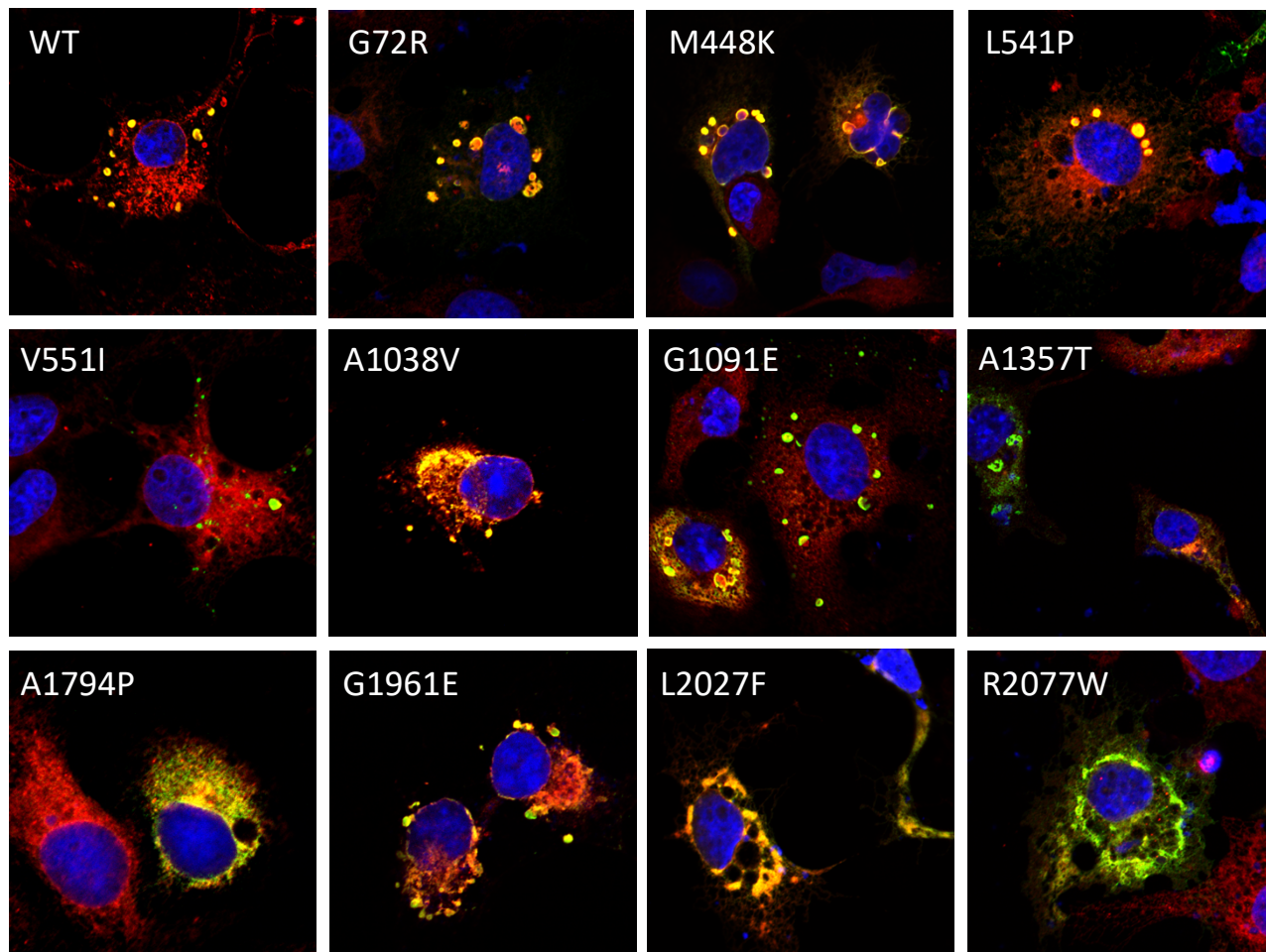


Figure 4.4 Cellular localization of ABCA4 variants.

COS7 cells were transfected with mutant constructs and double labeled for ABCA4 (green) and the ER marker calnexin (red) for visualization by confocal scanning microscopy. The prevalence of punctate staining characteristic of a vesicular structure is evident for WT ABCA4. The variants showed either punctate staining together with reticulum staining or primarily reticulum staining as in A1794P, L2027F and R2077W. The cells were counterstained with DAPI nuclear stain (blue). Adapted from Garces *et al.* 2018.

4.3.4 Functional Analysis of ABCA4 Variants

The functional properties of the ABCA4 variants were determined by 1) measuring *N*-Ret-PE substrate binding in the absence of ATP and loss in binding upon addition of ATP (Beharry, Zhong and Molday, 2004; Zhong, Molday and Molday, 2009) and 2) determining the basal and *N*-Ret-PE stimulated ATPase activity (Sun, Molday and Nathans, 1999; Quazi, Lenevich and Molday, 2012). All-*trans* retinal was used in these assays since in the presence of PE the aldehyde group of all-*trans* retinal reacts reversibly with the primary amine group of PE to form the substrate *N*-Ret-PE (Ahn, Wong and Molday, 2000; Beharry, Zhong and Molday, 2004). For these studies, WT and ABCA4 variants were solubilized in CHAPS and immobilized on an immunoaffinity column. Figure 4.5A shows the ABCA4 variants after elution from the column confirming the purity of the proteins.

The binding profile of *N*-Ret-PE to ABCA4 variants immobilized on an immunoaffinity matrix is shown in Figure 4.5B. In the absence of ATP, *N*-Ret-PE binds strongly to WT ABCA4 (Beharry, Zhong and Molday, 2004). More than 95% of *N*-Ret-PE binding is abolished by the addition of 1 mM ATP. ABCA4 mutants showed variable substrate binding in the absence and presence of ATP. Generally, they could be divided into 3 groups: Group 1 (p.Val552Ile, p.Gly1091Glu, p.Ala1357Thr) showed similar substrate binding properties as WT ABCA4; Group 2 (p.Met448Lys, p.Ala1038Val, p.Ala1794Pro, and p.Leu2027Phe) showed a significant reduction in substrate binding in the absence of ATP (35% or lower compared to WT ABCA4) with a further reduction in substrate binding in the presence of ATP; and Group 3 (p.Gly72Arg, p.Leu541Pro, p.Gly1961Glu, p.Arg2077Trp) showed significantly reduced substrate binding that was insensitive to ATP.

Next, we measured the effect of disease-associated mutations on the ATPase activity of ABCA4. WT and ABCA4 variants were solubilized in CHAPS, purified by immunoaffinity chromatography, and subsequently reconstituted into PE-containing liposomes at similar protein concentrations. The ATPase activity of the mutants in the presence and absence of *N*-Ret-PE substrate is shown in Figure 4.6A, B. As previously reported (Sun, Molday and Nathans, 1999; Ahn, Wong and Molday, 2000), addition of 40 μ M all-*trans* retinal to WT ABCA4 resulted in a 1.8-2.5 fold increase in ATPase activity (Fig. 4.6). The ATPase activity of the mutants was measured at the same protein concentration as WT ABCA4 in order to determine the effect of the mutation on the functional activity of ABCA4. Five mutants (p.Val552Ile, p.Ala1038Val, p.Ala1357Thr, p.Ala1794Pro, and p.Leu2027Phe) showed reduced basal ATPase activity relative to WT ABCA4 (~ 40-85%), but this activity was stimulated 1.6-3.0 fold by the addition of all-*trans* retinal. On the other hand, the p.Gly72Arg, p.Met448Lys, p. Leu541Pro, p.Gly1091Glu, pGly1961Glu and p.Arg2077Trp variants showed drastically reduced basal activity with no significant substrate stimulation.

To more directly evaluate the expression and function of the p.Ala1794Pro variant, we transfected HEK293T cells separately with WT *ABCA4* and the p.Ala1794Pro mutant cDNAs at similar levels. After solubilization in CHAPS buffer, the samples were subjected to high-speed centrifugation and the supernatant was reconstituted into liposomes for analysis of its basal and substrate activated ATPase activity. As shown in Fig. 4.6C, the p.Ala1794Pro had a significantly reduced activity due largely to the low solubilization of this variant. These studies indicate that only a small fraction of the p.Ala1794Pro mutant folds into a functionally active protein and correlates well with the phenotype of patient 5.

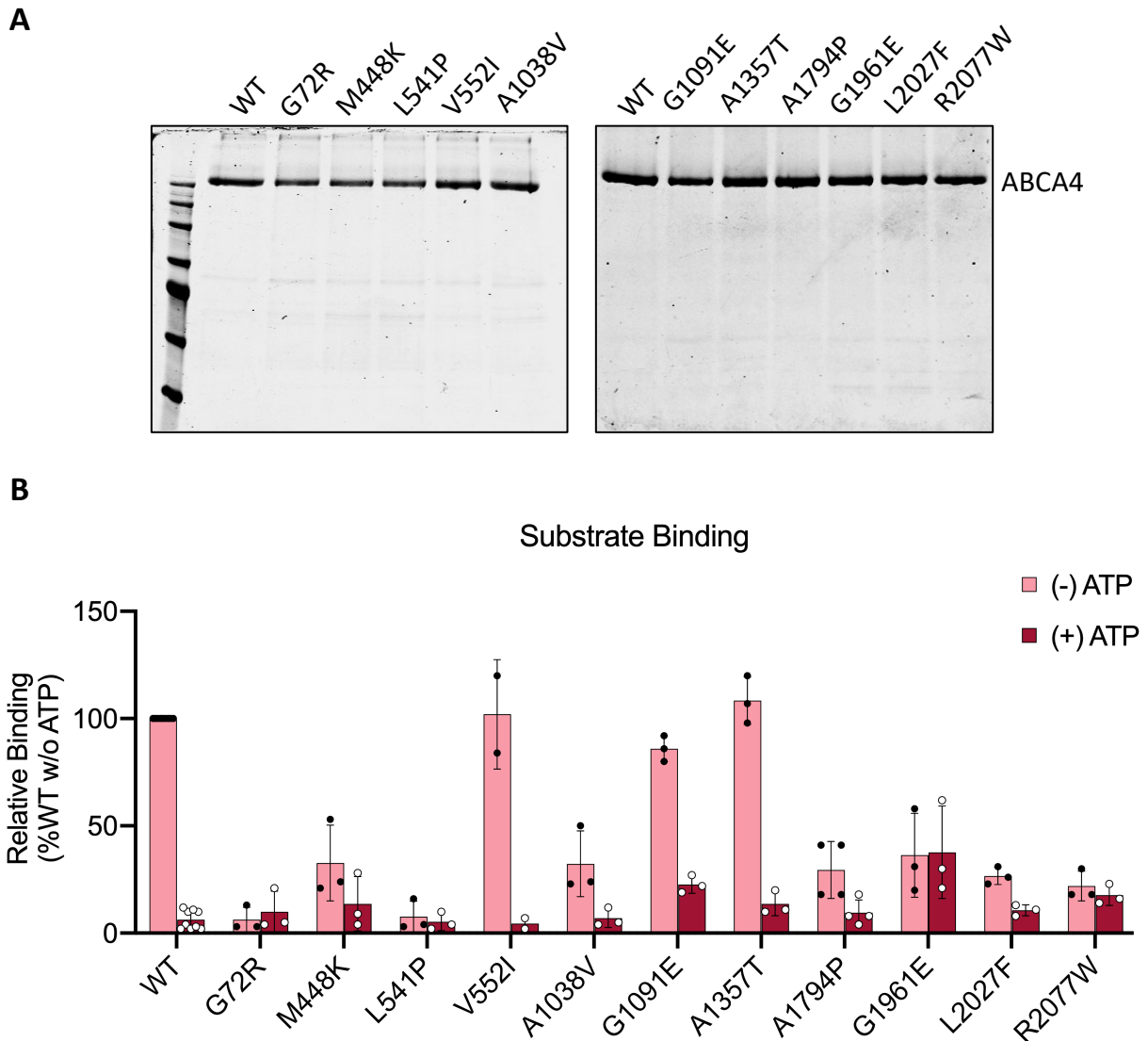


Figure 4.5 Purification and N-Ret-PE binding to ABCA4.

ABCA4 variants from transfected HEK293T cells were purified on a rho 1D4-immunoaffinity column. (A) Coomassie blue stained SDS gels of WT and ABCA4 variants purified by immunoaffinity chromatography. (B) Binding of *N*-Ret-PE to ABCA4 variants in the absence and presence of ATP. *N*-Ret-PE binding was normalized to WT ABCA in the absence of ATP. Data is the average \pm SD for $n \geq 3$ independent experiments. Adapted from Garces *et al.* 2018.

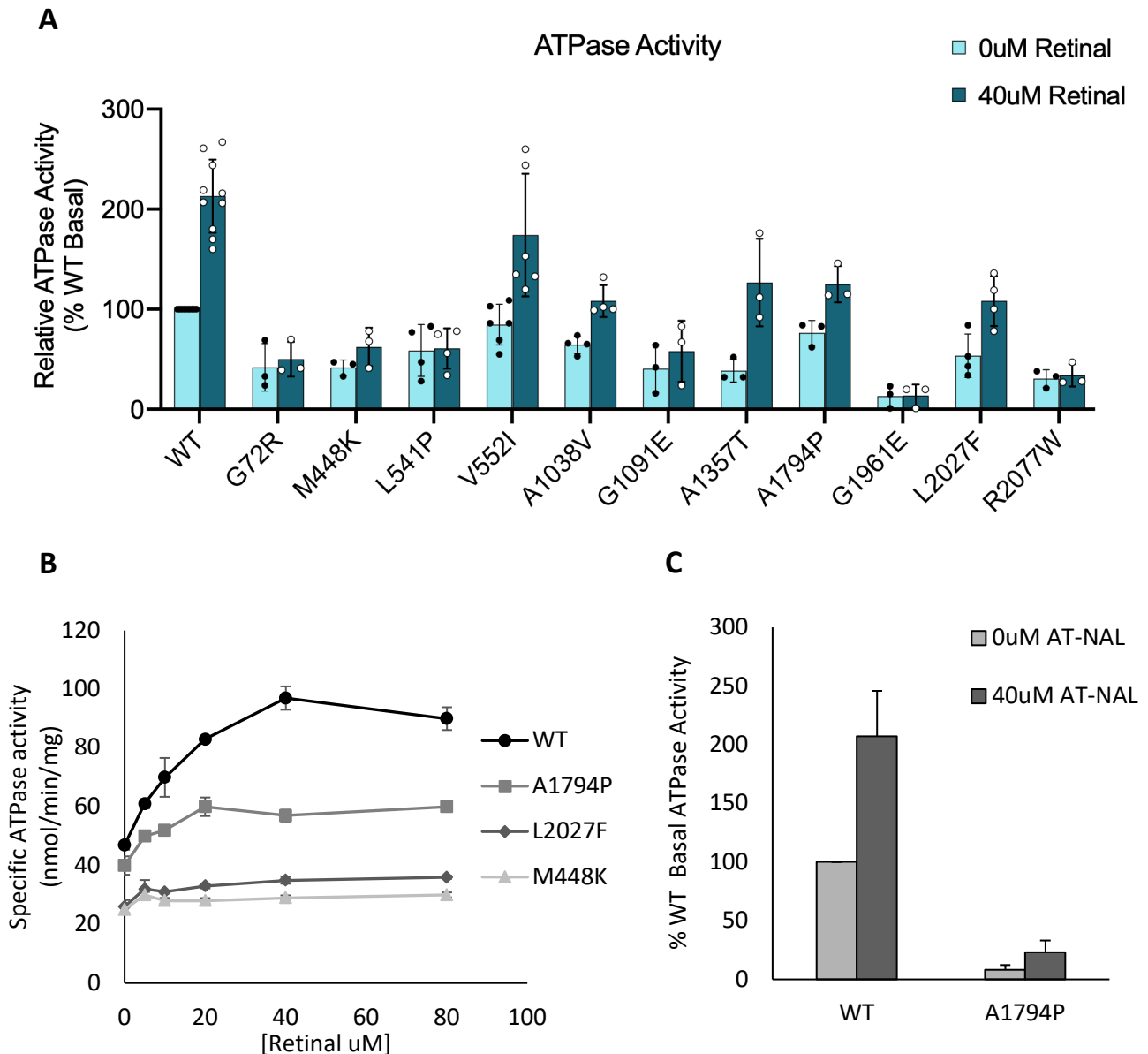


Figure 4.6 ATPase activity of ABCA4 variants.

The ATPase activity of immunopurified and reconstituted ABCA4 variants was measured in the presence or absence of all-*trans*-retinal. (A) Quantification of the basal and retinal stimulated ATPase activity of ABCA4 variants normalized to WT basal ATPase activity. ATPase assays were carried out using similar concentrations of purified ABCA4. Data expressed as an average \pm SD for $n \geq 3$ independent experiments. (B) Representative curves of specific ATPase activity as a function of all-*trans* retinal concentration for WT and ABCA4 variants. (C) Relative basal ATPase activity of WT and A1794P using equal amounts of transfected HEK293T cells. Data expressed as an average \pm SD. Measurements were done in triplicate. Adapted from Garces *et al.* 2018. All-*trans* retinal (AT-NAL).

Table 4.2 Expression and Functional Activities of ABCA4 missense mutations identified in the STGD1 patients

Variant	Cellular Localization	Relative solubility +/- SD	Relative N-Ret-PE binding +/- SD w/o ATP	Relative N-Ret-PE binding +/- SD w/ ATP	Relative ATPase basal activity +/- SD	Relative Retinal stimulated ATPase activity +/- SD	Predicted Effect of the Mutation
WT	Vesicles	100	100	6±5	100	209±40	Normal
G72R	Vesicles	97±16	6±7	8±11	42±19	50±14	Severe
M448K	Vesicles	92±13	33±18	14±12	46±1	62±5	Severe
L541P	Vesicles	100±17	7±7	5±4	59±23	61±18	Severe
V552I	Vesicles	93±11	102±26	4±4	85±13	174±13	Mild
A1038V	Vesicles	71±16	33±15	7±4	65±8	108±14	Moderate
G1091E	Vesicles	73±13	86±6	23±4	41±20	58±25	Moderate
A1357T	E.R.	55±19	108±11	14±6	39±9	127±36	Moderate
A1794P	E.R.	50±0.15	29±13	9±6	76±10	125±15	Severe
G1961E	Vesicles	102±18	36±19	38±22	12±10	13±10	(Mild)*
L2027F	E.R.	44±15	26±4	11±3	54±19	108±22	Severe
R2077W	E.R.	52±14	22±7	18±5	31±7	34±9	Severe

*G1961E mutation appears mild when this variant is retained in the membrane based on expression studies and consistent with the relatively mild phenotype of individuals homozygous for this mutation. However, after detergent solubilization the variant is devoid of functional activity including N-Ret-PE binding and ATPase activity. Detergent solubilization may adversely affect the functional activities of this mutant.

4.4 Discussion

STGD1, like most other inherited retinal degenerative diseases, is a highly heterogeneous disorder at both a clinical and genetic level. This is evident in our cohort of patients who show wide variation in phenotypes and genotypes. Phenotypic variation extended from early disease onset with poor VA and evidence of macular atrophy to patients that develop STGD1 well into their adulthood and whose symptoms, including VA, remain relatively mild. Genetic variations included splice site, frameshift, and missense mutations resulting in amino acid substitutions in various domains of ABCA4 (Fig. 4.2). In agreement with previous large genetic screens, we identified two mutations in ~65% of our patients, one mutation in ~25% of the patients, and no mutations in 1 patient (10%). As discussed elsewhere (Cornelis *et al.*, 2017; Zernant *et al.*, 2018; Runhart *et al.*, 2019; Khan *et al.*, 2020), the missing disease-causing mutations in patients diagnosed with STGD1 may be due to mutations in noncoding regions of ABCA4 not sequenced in this study, mutations in other genes that can result in phenotypes similar to STGD1, or hypomorphic alleles overlooked in most genetic screens (Zernant *et al.*, 2017, 2018; Runhart *et al.*, 2018).

In addition to variation in clinical and genetic traits, our studies showed considerable variation in the extent of expression and functional activity of the missense variants as summarized in Table 2. Some mutants expressed at or near WT ABCA4 levels when assayed after mild detergent solubilization including p.Gly72Arg, p.Met448Lys, p.Leu541Pro, p.Gly1961Glu, and p.Val552Ile, whereas others showed significant reduction in expression including p.Ala1357Thr, p.Ala1794Pro, p.Leu2027Phe, and p.Arg2077Trp. Variation in *N*-Ret-PE binding and ATPase activity was also observed. Two mutants p.Val552Ile and p.Ala1357Thr showed *N*-Ret-PE binding and release by ATP at levels similar to WT ABCA4, whereas other

mutants such as p.Gly72Arg, p.Met448Lys, p.Leu541Pro, and p.Arg2077Trp showed diminished substrate binding in the presence and absence of ATP. Likewise, basal and retinal activated ATPase activity varied widely with p.Val552Ile showing almost WT-like activity and other mutants including p.Gly72Arg, p.Leu541Pro, p.Gly1961Glu, and p.Arg2077Trp showing significantly reduced basal activity and little, if any substrate stimulated activity.

A main focus of this study was to correlate the expression and functional activity of missense mutations identified in our cohort of STGD1 patients with the clinical phenotypes. Patient 5, homozygous for the p.Ala1794Pro mutation, offers a unique opportunity to directly compare the biochemical properties of this ABCA4 variant with the disease severity. Half of the p.Ala1794Pro mutant expressed in HEK293T cells failed to solubilize in CHAPS. Immunofluorescence studies further indicated that most of the p.Ala1794Pro mutant was retained in the ER. These results suggest that a large fraction of p.Ala1794Pro is present in a highly misfolded, aggregated state. Interestingly, the fraction that does solubilize in CHAPS displays *N*-Ret-PE binding and ATPase activity, but at a significantly lower level than WT ABCA4 (Table 2). Combination of low expression and reduced functional activity as shown in Figure 4.6C indicates that only a small fraction of this mutant protein is potentially capable of transporting *N*-Ret-PE across membranes consistent with the severe phenotype of this patient. The inability to clear *N*-Ret-PE and retinal from disc membranes gives rise to the production of bisretinoids that accumulate in RPE cells as evident in the fundus photographs and dark choroid observed for patient 5 (Fig. 4.2). This in turn leads to degeneration of central RPE and photoreceptor cells, and the early onset and severe phenotype displayed by this patient. The alanine 1794 residue is predicted to reside within transmembrane segment 11 of ABCA4 (Fig. 4.2) based on the topological model of ABCA4 (Fig. 2.1 and 3.1) (Bungert, Molday and Molday,

2001) and supported by the structure of ABCA1 (Qian *et al.*, 2017), an ABC lipid transporter which is over 50% identical in sequence to ABCA4. Substitution of an alanine with a proline likely disrupts the α -helical conformation of transmembrane segment 11 resulting in significant misfolding of ABCA4 and retention in the ER of photoreceptor cells. In another study, substitution of alanine 1794 with aspartic acid (p.Ala1794Asp) has been reported to be a STGD1 disease-causing mutation (Maugeri *et al.*, 1999). In this case the negatively charged aspartic acid residue within transmembrane segment 11 also likely affects the protein folding leading to reduced expression and functional activity of ABCA4 and a STGD1 phenotype.

Patient 4 with an early frameshift mutation in one allele and a downstream p.Val552Ile mutation in the second allele has a mild form of STGD1. Since the frameshift mutation is likely to result in a null allele, any residual functional activity of ABCA4 would arise from ABCA4 harboring the p.Val552Ile missense mutation. Our *in vitro* studies showing that the p.Val552Ile variant expresses at close to WT levels, exhibits normal *N*-Ret-PE binding properties, and has only a modest reduction in ATPase activity (Table 2) are consistent with the mild disease phenotype of patient 4. Another study has also reported that the p.Val552Ile mutation is associated with a STGD1 disease phenotype (Michaelides *et al.*, 2007). However, *in silico* predictions on the pathological relevance of this mutation have been variable (Cornelis *et al.*, 2017; Schulz *et al.*, 2017). On the basis of allele frequencies in controls vs. patients, it has been argued that the p.Val552Ile is most likely benign (Cornelis *et al.*, 2017). At a protein level a hydrophobic amino acid residue valine is replaced with another hydrophobic residue isoleucine. Accordingly, this substitution would be predicted to have only a marginal impact on ABCA4 protein structure and function. However, valine at position 552 of ABCA4 is invariable among vertebrate species including other mammals, chicken, *Xenopus* and Japanese puffer fish

(*Takifugu rubripes*) attesting to the likely importance of valine at this position. Collectively, these studies suggest that the p.Val552Ile is a mild mutation in which the pathogenicity may only be displayed in selected cases. More specifically, the p.Val522Ile would display a mild STGD1 phenotype when combined with a null allele as in the case of patient 4 or a missense mutation with little or no functional activity, but would not display a disease phenotype in a patient homozygous for this mutation or patients in which this mutation is combined with a mutation that shows significant ABCA4 function, since under these circumstances sufficient ABCA4 activity would be realized to prevent the accumulation of toxic retinoids.

The ATPase activity of two disease-associated variants (p.Leu541Pro and p.Ala1038Val) expressed in culture cells have been described previously (Sun, Smallwood and Nathans, 2000; Zhang *et al.*, 2014). In our study, the p.Leu541Pro expressed at WT levels in HEK293T cells, but was largely devoid of *N*-Ret-PE binding activity and displays low basal ATPase activity that is not activated by retinoid substrate. These results are in line with previous ATPase activity studies (Sun, Smallwood and Nathans, 2000; Zhang *et al.*, 2014). In contrast, the p.Ala1038Val variant has reduced expression (~70% WT), but displays retinal stimulated ATPase activity and retinal binding activity although at a lower level than WT. Two previous studies differed in the functional assessment of the p.Ala1038Val variant with one study reporting little if any activity (Sun, Smallwood and Nathans, 2000), and another study demonstrating a relatively high level of activity (Zhang *et al.*, 2014). Our data is consistent with the latter showing significant activity. These mutants are most commonly present as a complex allele (Cornelis *et al.*, 2017; Salles *et al.*, 2017). Biochemical studies indicate that both mutations contribute to the loss in function of p.[Leu541Pro;Ala1038Val] ABCA4, but the p.Leu541Pro mutation is the major contributor to the severe pathogenicity associated with this complex mutation. A similar conclusion was

derived from the knock-in mouse studies of Zhang et al. (Zhang *et al.*, 2014) and an *in silico* analysis of Cornelis et al. (Cornelis *et al.*, 2017).

The p.Gly1961Glu variant is another well-studied mutation found in our cohort of STGD1 patients. It is the most common mutation found in STGD1 patients although its frequency varies between ethnic populations and geographical origins. Previous studies of homozygous and compound heterozygous patients with the p.Gly1961Glu mutation indicate that it is most often associated with a milder, late onset retinal disease phenotype with individuals typically displaying central macula atrophy, the absence of a dark choroid, and normal full-field ERGs (Burke *et al.*, 2012). Two siblings in our cohort had the p.Gly1961Glu mutation in association with the p.Gly72Arg mutation with one sibling exhibiting a mild-moderate phenotype. The p.Gly72Arg variant expressed at WT levels, but was deficient in *N*-Ret-PE binding and substrate dependent ATPase activity indicating that this mutation severely affects ABCA4 function. The p.Gly1961Glu mutation also expressed at WT levels, but displayed a loss in *N*-Ret-PE binding and ATPase activity. The discrepancy between the mild phenotype generally displayed by individuals with p.Gly1961Glu and the severe loss in function observed in the *in vitro* studies described here and in a previous report (Sun, Smallwood and Nathans, 2000) requires further study. However, it is possible that the loss in function exhibited by the p.Gly1961Glu mutant arises from the effect of detergent solubilization on the functional activity of this variant. In this instance, CHAPS detergent may irreversibly denature the p.Gly1961Glu ABCA4 variant resulting in the loss in activity. If this is the case, the p.Gly1961Glu variant would be predicted to show significant activity in an *in vitro* or *in vivo* assay that does not require detergent solubilization. Such activity assays have yet to be developed. The late onset

relatively mild phenotype of our patients with p.Gly1961Glu may result from residual functional activity of membrane bound ABCA4 harboring this mutation.

Lastly, patients 9 to 11 were found to have a splice site mutation in one allele and a missense mutation in the other allele. The effect of the splice mutations on residual expression of full-length *ABCA4* has been recently studied for two of these mutations (c.5461-10T>C and c.5714+5G>A) (Sangermano *et al.*, 2016, 2018). The c.5461-10T>C mutation causes the skipping of exon 39 or 39/40 resulting in no full-length transcript (Sangermano *et al.*, 2018). On the other hand, the c.5714+5G>A resulted in about 40% normally spliced *ABCA4* mRNA. The missense mutations in the other allele (p.Gly1091Glu, p.Leu2027Phe, or p.Met448Lys) which significantly reduces the expression and/or functional activity of ABCA4 as measured in our *in vitro* assays, is consistent with the relatively severe phenotype found in these patients.

In conclusion, biochemical analyses of ABCA4 variants harboring missense mutations correlate well with the disease phenotype of our STGD1 patients. Although many factors contribute to the phenotype of STGD1 patients, the expression of ABCA4 mutants and the existence of at least some functional activity play an important role in determining the severity of STGD1.

Chapter 5 : Conclusions

5.1 Thesis Summary

This thesis presents a detailed biochemical analysis of a large number of ABCA4 variants known to cause STGD1 and other ABCA4 associated retinopathies. Although the majority of the pathogenic variants analyzed here were located in the TMDs of ABCA4, a significant portion were also found in the NBDs and the ECDs. Our findings revealed that not all missense mutations affect ABCA4 in the same way, and that STGD1 disease can progress through different pathological mechanisms that correlate with the severity of STGD1 patients harboring these mutations. For example, some mutations affect the protein solubilization levels of ABCA4 when the mild detergent CHAPS is used to solubilize the cellular membranes. The reason for this is likely due to the inability of these variants to leave the ER of transfected COS7 or HEK293T cells because of protein misfolding. As a result, these mutants are probably targeted for degradation by the quality control system of the ER and would not be trafficked to the outer segment of photoreceptors. On the other hand, the protein solubilization levels of other variants is only moderately to mildly affected, if at all, suggesting that these mutants fold properly. Indeed, this subset of mutations are able to leave the ER of transfected cells and would likely be trafficked to the outer segments of photoreceptors.

In terms of residual activity, it may not be a surprise that those mutations that lead to protein misfolding have low levels of basal and retinal induced ATPase activity and N-ret-PE binding and are associated with more severe STGD1 outcomes with an early age of onset. Exceptions to this have been observed in some of these variants where some functional activity is preserved, suggesting that at least a portion of these partially-misfolded mutants can still fold

and retain some functionality (eg: W821R); STGD1 patients harboring these mutations tend to be associated with a serious to moderate phenotype. In a similar manner, the majority of the variants that do not cause misfolding retain much higher levels of functional activity and are generally associated with mild forms of STGD1. In particular, while the ATPase activity for most mild variants is relatively similar to WT, the affinity for N-ret-PE tends to be affected in these variants. Exceptions to this include the A854T and H1838N variants, which have moderately to seriously affected ATPase activity and/or N-ret-PE affinity and tend to be associated with patients with a moderate to serious STGD1 phenotype.

Notably, within the variants that do not cause protein misfolding, we identified important residues that played key functional roles such as binding to N-ret-PE in the TMDs (chapter 2), or hydrolyzing ATP in the NBDs (chapter 3). We further characterized these residues by making non-disease-causing mutations in order to elucidate the functional role that specific amino acids played at these locations within the protein and to further understand the transport mechanism of ABCA4.

5.1.1 Summary of Chapters

In chapter 2 we biochemically characterized 38 disease variants localized to the TMDs of ABCA4. Our data suggested that there is a clear correlation between the amount of residual functional activity and the clinical severity of patients with STGD1 mutations. As mentioned previously, we subdivided the TMD variants into those that cause protein misfolding and those that fold properly based on protein solubility levels and *in vitro* cellular trafficking. Overall, 60% of the TMD variants analyzed caused some degree of protein misfolding. At the same time, the functional properties of these variants were assessed using ATPase assays and N-ret-PE substrate binding assays. Based on the residual activity of these variants, we subdivided them into severe,

serious, moderate or mild mutations. Importantly, this biochemical classification strongly correlated with the severity of STGD1 patients carrying these mutations. Additionally, we characterized the common hypomorphic mutation, N1868I, and discovered that while its trafficking, protein solubilization levels and ATPase activity were similar to WT, the affinity to the N-ret-PE substrate was much lower than WT, which highlights a possible pathological mechanism for this mutation and variants with a similar functional profile. Lastly, we identified a residue that seemed to be directly involved in binding to N-ret-PE. Based on the functional data of the STGD1 mutant R653C, we believed this residue could form part of the substrate binding site. Our results indicate that an amino acid with a positively charged side chain plays an important role in mediating binding to N-ret-PE.

Chapter 3 focused on studying two conserved asparagine residues that are found in each of the Walker A motifs of the NBDs, namely, N965 for NBD1 and N1974 for NBD2. These asparagines are known to cause STGD1 when mutated to other residues. Our biochemical data for these conserved asparagines suggested that the N965 and N1974 residues play an important role in ATP hydrolysis. All the mutants analyzed at amino acid position 965 (N965D/K/S/Y/A/Q) and 1974 (N1975D/K/S/Y/A/Q) solubilized near WT levels and co-localize like WT in transfected cells, suggesting that little or no protein misfolding is occurring. At the functional level, however, the ATPase activity was severely hindered for N965D/K/Y disease mutants and the analogous N1974D/K/Y mutations. Intriguingly, the N-ret-PE binding properties of most of these variants was generally similar to WT, indicating that they can still bind to ATP, thereby allowing for substrate release. Based on these observations, we concluded that the N965 and N1974 residues play a more prominent role in hydrolysis of ATP rather than binding to ATP. These revelations are particularly surprising since the Walker A motif has been generally

thought to be involved in binding to ATP rather than hydrolysis of ATP (Rees, Johnson and Lewinson, 2009).

In chapter 4, we examined genotype-phenotype correlations in a cohort of patients from British Columbia diagnosed with STGD. To do this, we collaborated with a clinician at the Vancouver Eye Care Centre who examined the STGD patients and determined their STGD stage based on the Fishman classification system. Likewise, we worked with the laboratory of Dr. Bernhard Weber to sequence the exons and flanking regions of the *ABCA4*, *ELOVL4*, and *CNGB3* genes to identify the pathogenic mutations in these patients. Overall, we identified and biochemically characterized 11 missense mutations associated with STGD1. Notably, we were able to identify two novel STGD1-causing mutations in the *ABCA4* gene. Furthermore, the novel A1794P mutation belonged to a homozygous patient, which gave us a unique opportunity to understand genotype-phenotype relationships in STGD1. The homozygous patient had a severe form of STGD1 with an early age of onset and stage 3 STGD1. Biochemical analysis of the A1794P variant showed that this mutant had low protein solubilization levels and was retained in the ER of transfected cells, suggesting this mutation primarily caused protein misfolding. Interestingly, some residual activity could still be detected in this variant, though at much lower levels than WT *ABCA4*. Taken together, this is one of the first studies to contain both clinical and biochemical data for STGD1 mutations in *ABCA4* identified in a cohort of patients, making these findings especially significant in the field.

5.2 Significance

While genetic modifiers and environmental and lifestyle factors may contribute to the severity of *ABCA4* associated retinopathies, it is becoming clear that effects on gene expression, splicing, protein folding, trafficking, and/or residual activity of pathogenic *ABCA4* mutations are

the major driving factors contributing to the severity of patients with STGD1 and other ABCA4 associated retinopathies. This thesis provides a large body of biochemical evidence delineating the molecular mechanisms by which pathogenic missense mutations contribute to the development of ABCA4 associated retinopathies. Herein, we showed that the severity of STGD1 and related ABCA4 retinopathies correlates with the the amount of soluble protein available and residual functional activity of these disease variants. These results highlight the importance that ABCA4 has in maintaining the overall health of the photoreceptors and the adjacent RPE cells by preventing the accumulation of toxic bisretinoid species that contribute to the formation of lipofuscin. Furthermore, this thesis has identified a residue within the TMDs, namely R653, that seems to be involved in N-ret-PE binding and therefore likely forms part of the substrate binding site. At the same time, we have shown that the conserved asparagine residue found in the Walker A motifs of NBD1 (N965) and NBD2 (N1974) is important for ATP hydrolysis. These results provide important insights into the transport mechanism of N-ret-PE by ABCA4.

5.3 Future Prospects

Now that we know how ABCA4 disease variants can affect the folding and functional properties of ABCA4, it is important to shift research efforts to develop therapeutic treatments that can target protein misfolding or increase the functional activity of ABCA4 variants. For example, a family of drugs known as chemical chaperones has been successfully used to rescue mistrafficked mutants. Members of this family of drugs contain the corrector VX-809 (Lumacaftor), which has been used to treat mutations in the *CFTR* gene known to cause cystic fibrosis (Wainwright *et al.*, 2015), or the compound 4-phenylbutyrate (PBA) which our laboratory has shown to increase the amount of soluble protein in variants that cause protein misfolding (unpublished data). Though a possible explanation for this increased expression of

ABCA4 misfolded variants by PBA could be attributed to its ability to inhibit HDAC, a histone deacetylase, which may have downstream effects in the gene expression of ABCA4, or other genes involved in the ER quality control system, that would indirectly result in increased protein expression levels. Therefore, the effects of this compound as a possible chemical chaperone for misfolded proteins need to be further assessed. Similarly, another family of drugs known as activators or potentiators is known to increase functional activity in ABC transporters. These drugs include ivacaftor and genistein, which have been used to treat CFTR variants that have attenuated levels of functional activity (Sohma, Yu and Hwang, 2013) and are being tested to treat ABCA3 variants known to cause surfactant deficiency (Kinting *et al.*, 2019). Additionally, preliminary work in our laboratory has shown that the anti-arrhythmia drug dronedarone has been used to increase residual activity in functional mutants (data not published). It is important to try both correctors and potentiators not only *in vitro* biochemical assays, but also in mouse models to see if these drugs can 1. Rescue misfolded mutants, 2. Decrease the rate of accumulation of bisretinoids (eg: A2E) in mouse models and 3. Slowdown the progression of STGD. What is promising is that these compounds have already gone through clinical trials for the treatment of other illnesses and therefore their safety has been well established.

Another area of future research should focus on resolving the structure of ABCA4 in order to fully understand the transport mechanism of N-ret-PE. While we have identified the prominent role that the residue R653 plays in binding to N-ret-PE within the TMDs, or the role that the N965 and N1974 residues have in hydrolyzing ATP, a detailed transport mechanism cannot be elucidated without a set of structures showing the conformational changes that ABCA4 goes through during a single transport cycle. For this reason, it is imperative to resolve the structures of ABCA4 in the apo, N-ret-PE bound, ATP-bound, and ADP-bound states to help

provide detailed account of the transport mechanism of ABCA4. Ultimately, this structural information will provide further evidence to help us understand whether all ABC transporters use a similar and universal mechanism of transport, or, if there are key structural and functional differences in the transport mechanism across ABC transporters.

Bibliography

Abuznait, A. H. and Kaddoumi, A. (2012) 'Role of ABC transporters in the pathogenesis of Alzheimers disease', *ACS Chemical Neuroscience*, 3(11), pp. 820–831. doi: 10.1021/cn300077c.

Ahn, J. *et al.* (2003) 'Functional interaction between the two halves of the photoreceptor-specific ATP binding cassette protein ABCR (ABCA4). Evidence for a non-exchangeable ADP in the first nucleotide binding domain', *Journal of Biological Chemistry*, 278(41), pp. 39600–39608. doi: 10.1074/jbc.M304236200.

Ahn, J., Wong, J. T. and Molday, R. S. (2000) 'The effect of lipid environment and retinoids on the ATPase activity of ABCR, the photoreceptor ABC transporter responsible for Stargardt macular dystrophy', *Journal of Biological Chemistry*, 275(27), pp. 20399–20405. doi: 10.1074/jbc.M000555200.

Allikmets, R. *et al.* (1997) 'Mutation of the Stargardt disease gene (ABCR) in age-related macular degeneration', *Science*, 277(5333), pp. 1805–1807. doi: 10.1126/science.277.5333.1805.

Allikmets, R. *et al.* (1997) 'A photoreceptor cell-specific ATP-binding transporter gene (ABCR) is mutated in recessive Stargardt macular dystrophy', *Nature*, 15, pp. 236–246.

Allikmets, R., Zernant, J. and Lee, W. (2018) 'Penetrance of the ABCA4 p.Asn1868Ile allele in stargardt disease', *Investigative Ophthalmology and Visual Science*, 59, pp. 5564–5565. doi: 10.1167/iovs.18-25944.

Arshavsky, V. Y. and Burns, M. E. (2012) 'Photoreceptor signaling: Supporting vision across a wide range of light intensities', *Journal of Biological Chemistry*, 287(3), pp. 1620–1626. doi: 10.1074/jbc.R111.305243.

Arshavsky, V. Y. and Wensel, T. G. (2013) 'Timing is everything: GTPase regulation in phototransduction', *Investigative Ophthalmology and Visual Science*, 54(12), pp. 7725–7733. doi: 10.1167/iovs.13-13281.

Baehr, W. *et al.* (2003) 'The retinoid cycle and retina disease', *Vision Research*, 43(28), pp. 2957–2958. doi: 10.1016/j.visres.2003.10.001.

BAEHR, W. and PALCZEWSKI, K. (2007) 'Guanylate Cyclase-Activating Proteins and Retina Disease', in Carafoli, E. and Brini, M. (eds) *Calcium Signalling and Disease: Molecular Pathology of Calcium*. Dordrecht: Springer Netherlands, pp. 71–91. doi: 10.1007/978-1-4020-6191-2_4.

Barakat, M. R. and Kaiser, P. K. (2009) 'VEGF inhibitors for the treatment of neovascular age-related macular degeneration', *Expert Opinion on Investigational Drugs*, 18(5), pp. 637–646. doi: 10.1517/13543780902855316.

Bauwens, M. *et al.* (2015) 'An augmented abca4 screen targeting noncoding regions reveals a deep intronic founder variant in Belgian stargardt patients', *Human Mutation*, 36(1), pp. 39–42. doi: 10.1002/humu.22716.

Beharry, S., Zhong, M. and Molday, R. S. (2004) 'N-retinylidene-phosphatidylethanolamine is the

preferred retinoid substrate for the photoreceptor-specific ABC transporter ABCA4 (ABCR)', *Journal of Biological Chemistry*, 279(52), pp. 53972–53979. doi: 10.1074/jbc.M405216200.

Boon, C. J. F. *et al.* (2009) 'The spectrum of ocular phenotypes caused by mutations in the BEST1 gene', *Progress in Retinal and Eye Research*, 28(3), pp. 187–205. doi: 10.1016/j.preteyeres.2009.04.002.

Borbat, P. P. *et al.* (2007) 'Conformational motion of the ABC transporter MsbA induced by ATP hydrolysis', *PLoS Biology*, 5(10), pp. 2211–2219. doi: 10.1371/journal.pbio.0050271.

Boyer, N. P. *et al.* (2012) 'Lipofuscin and N-retinylidene-N-retinylethanolamine (A2E) accumulate in retinal pigment epithelium in absence of light exposure: Their origin is 11-cis-RETINAL', *Journal of Biological Chemistry*, 287(26), pp. 22276–22286. doi: 10.1074/jbc.M111.329235.

Braakman, I. and Hebert, D. N. (2013) 'Protein Folding in the Endoplasmic Reticulum', *Comprehensive Biotechnology, Second Edition*, 5. doi: 10.1016/B978-0-08-088504-9.00029-5.

Briggs, C. E. *et al.* (2001) 'Mutations in ABCR (ABCA4) in patients with Stargardt macular degeneration or cone-rod degeneration', *Investigative Ophthalmology and Visual Science*, 42(10), pp. 2229–2236.

Brunham, L. R. *et al.* (2006) 'Tissue-specific induction of intestinal ABCA1 expression with a liver X receptor agonist raises plasma HDL cholesterol levels', *Circulation Research*, 99(7), pp. 672–674. doi: 10.1161/01.RES.0000244014.19589.8e.

Bungert, S., Molday, L. L. and Molday, R. S. (2001) 'Membrane topology of the ATP binding cassette transporter ABCR and its relationship to ABC1 and related ABCA transporters: Identification of N-linked glycosylation sites', *Journal of Biological Chemistry*, 276(26), pp. 23539–23546. doi: 10.1074/jbc.M101902200.

Burke, T. R. *et al.* (2010) 'Loss of peripapillary sparing in non-group I Stargardt disease', *Experimental Eye Research*, 91(5), pp. 592–600. doi: 10.1016/j.exer.2010.07.018.

Burke, T. R. *et al.* (2012) 'Retinal Phenotypes in Patients Homozygous for the G1961E Mutation in the ABCA4 Gene', *Investigative Ophthalmology and Visual Science*, 53(8), pp. 4458–4467. doi: 10.1167/iovs.11-9166.

Burke, T. R. *et al.* (2013) 'Abnormality in the external limiting membrane in early Stargardt disease', *Ophthalmic Genetics*, 34(1–2), pp. 75–77. doi: 10.3109/13816810.2012.707271.

Burke, T. R. *et al.* (2014) 'Quantitative fundus autofluorescence in recessive stargardt disease', *Investigative Ophthalmology and Visual Science*, 55(5), pp. 2841–2852. doi: 10.1167/iovs.13-13624.

Campochiaro, P. A. *et al.* (1999) 'The pathogenesis of choroidal neovascularization in patients with age-related macular degeneration.', *Molecular vision*, 5(May), p. 34.

Catty, P., Pfister, C., Bruckert, F., Deterre, P. (1992) 'The cGMP phosphodiesterase-transducin complex of retinal rods. Membrane binding and subunits interactions' *J. Biol. Chem*, 1992 Sep 25;267(27):19489-93.

Chacón-Camacho, O. F. *et al.* (2013) 'ABCA4 mutational spectrum in Mexican patients with Stargardt

disease: Identification of 12 novel mutations and evidence of a founder effect for the common p.A1773V mutation', *Experimental Eye Research*, 109, pp. 77–82. doi: 10.1016/j.exer.2013.02.006.

Chalam, K. V. *et al.* (2011) 'A review: Role of ultraviolet radiation in age-related macular degeneration', *Eye and Contact Lens*, 37(4), pp. 225–232. doi: 10.1097/ICL.0b013e31821fbd3e.

Charbel Issa, P. *et al.* (2015) 'Rescue of the Stargardt phenotype in Abca4 knockout mice through inhibition of vitamin A dimerization', *Proceedings of the National Academy of Sciences of the United States of America*, 112(27), pp. 8415–8420. doi: 10.1073/pnas.1506960112.

Chen, C. K. *et al.* (2012) 'Modulation of mouse rod response decay by rhodopsin kinase and recoverin', *Journal of Neuroscience*, 32(45), pp. 15998–16006. doi: 10.1523/JNEUROSCI.1639-12.2012.

Chen, Y. *et al.* (2012) 'Mechanism of all-trans-retinal toxicity with implications for stargardt disease and age-related macular degeneration', *Journal of Biological Chemistry*, 287(7), pp. 5059–5069. doi: 10.1074/jbc.M111.315432.

Cheong, N. *et al.* (2006) 'Functional and trafficking defects in ATP binding cassette A3 mutants associated with respiratory distress syndrome', *Journal of Biological Chemistry*, 281(14), pp. 9791–9800. doi: 10.1074/jbc.M507515200.

Cideciyan, A. V. *et al.* (2009) 'ABCA4 disease progression and a proposed strategy for gene therapy', *Human Molecular Genetics*, 18(5), pp. 931–941. doi: 10.1093/hmg/ddn421.

Clerc, A. and Bennett, N. (1992) 'Activated cGMP phosphodiesterase of retinal rods. A complex with transducin alpha subunit', *Journal of Biological Chemistry*, Apr 5;267(10):6620-7.

Clerc, A., Catty, P., Bennett, N. (1992) 'Interaction between cGMP-phosphodiesterase and transducin alpha-subunit in retinal rods. A cross-linking study', *Journal of Biological Chemistry*, Vol . 267, No. 28, Issue of October 5, pp. 19948-19953.

Coco-Martin, R. M. *et al.* (2020) 'PRPH2-Related Retinal Diseases: Broadening the Clinical Spectrum and Describing a New Mutation', *Genes*, 11(7). doi: 10.3390/genes11070773.

Cornelis, S. S. *et al.* (2017) 'In Silico Functional Meta-Analysis of 5,962 ABCA4 Variants in 3,928 Retinal Dystrophy Cases', *Human Mutation*, 38(4), pp. 400–408. doi: 10.1002/humu.23165.

Cremers, F. P. M. *et al.* (1998) 'Autosomal recessive retinitis pigmentosa and cone-rod dystrophy caused by splice site mutations in the Stargardt's disease gene ABCR', *Human Molecular Genetics*, 7(3), pp. 355–362. doi: 10.1093/hmg/7.3.355.

Cremers, F. P. M. *et al.* (2018) 'Author Response: Penetrance of the ABCA4 p.Asn1868Ile Allele in Stargardt Disease', *Investigative ophthalmology & visual science*, 559, pp. 5566–5568.

Cremers, F. P. M. *et al.* (2020) 'Clinical spectrum, genetic complexity and therapeutic approaches for retinal disease caused by ABCA4 mutations', *Progress in Retinal and Eye Research*, p. 100861. doi: 10.1016/j.preteyeres.2020.100861.

Cubizolle, A. *et al.* (2020) 'Isopropyl-phloroglucinol-DHA protects outer retinal cells against lethal dose

of all-trans-retinal', *Journal of Cellular and Molecular Medicine*, 24(9), pp. 5057–5069. doi: 10.1111/jcmm.15135.

Cuchel, M. *et al.* (2010) 'Pathways by which reconstituted high-density lipoprotein mobilizes free cholesterol from whole body and from macrophages', *Arteriosclerosis, Thrombosis, and Vascular Biology*, 30(3), pp. 526–532. doi: 10.1161/ATVBAHA.109.196105.

Davidson, A. L. *et al.* (2008) 'Structure, Function, and Evolution of Bacterial ATP-Binding Cassette Systems', *Microbiology and Molecular Biology Reviews*, 72(2), pp. 317–364. doi: 10.1128/mmbr.00031-07.

Davis, W. and Tew, K. D. (2018) 'ATP-binding cassette transporter-2 (ABCA2) as a therapeutic target', *Biochemical Pharmacology*, 151, pp. 188–200. doi: 10.1016/j.bcp.2017.11.018.

Dawson, R. J. P., Hollenstein, K. and Locher, K. P. (2007) 'Uptake or extrusion: Crystal structures of full ABC transporters suggest a common mechanism', *Molecular Microbiology*, 65(2), pp. 250–257. doi: 10.1111/j.1365-2958.2007.05792.x.

Dawson, R. J. P. and Locher, K. P. (2006) 'Structure of a bacterial multidrug ABC transporter', *Nature*, 443(7108), pp. 180–185. doi: 10.1038/nature05155.

D'Amours, M. R. and Cote, R. H. (1999) 'Regulation of photoreceptor phosphodiesterase catalysis by its non-catalytic cGMP-binding sites', *Journal of Biological Chemistry*, Jun 15; 340(Pt 3): 863–869.

Dean, M. (2002) 'The Human ATP-Binding Cassette (ABC) Transporter Superfamily Introduction to ABC Protein and Gene Organization', (Figure 1), pp. 1–50.

Dean, M. and Allikmets, R. (1995) 'Evolution of ATP-binding cassette transporter genes', *Current Opinion in Genetics and Development*, 5(6), pp. 779–785. doi: 10.1016/0959-437X(95)80011-S.

DeStefano, G. M. *et al.* (2014) 'Mutations in the Cholesterol Transporter Gene ABCA5 Are Associated with Excessive Hair Overgrowth', *PLoS Genetics*, 10(5). doi: 10.1371/journal.pgen.1004333.

Deutman, A. F. (1972) 'The Hereditary Dystrophies of the Posterior Pole of the Eye', *American Journal of Ophthalmology*, 73(5), p. 797. doi: 10.1016/0002-9394(72)90402-3.

Downes, S. M., *et al.* (2012) 'Detection Rate of Pathogenic Mutations in ABCA4 Using Direct Sequencing: Clinical and Research Applications', 130(11), pp. 1486–1490.

Drolet, D. W. *et al.* (2016) 'Fit for the Eye: Aptamers in Ocular Disorders', *Nucleic Acid Therapeutics*, 26(3), pp. 127–146. doi: 10.1089/nat.2015.0573.

Duester, G. (2000) 'Families of retinoid dehydrogenases regulating vitamin A function. Production of visual pigment and retinoic acid', *European Journal of Biochemistry*, 267(14), pp. 4315–4324. doi: 10.1046/j.1432-1327.2000.01497.x.

Duncker, T. *et al.* (2015) 'Quantitative fundus autofluorescence and optical coherence tomography in ABCA4 carriers', *Investigative Ophthalmology and Visual Science*, 56(12), pp. 7274–7285. doi: 10.1167/iovs.15-17371.

- Duno, M. *et al.* (2012) 'Phenotypic and genetic spectrum of Danish patients with ABCA4-related retinopathy', *Ophthalmic Genetics*, 33(4), pp. 225–231. doi: 10.3109/13816810.2011.643441.
- Dyka, F. M. *et al.* (2019) 'Dual ABCA4-AAV Vector Treatment Reduces Pathogenic Retinal A2E Accumulation in a Mouse Model of Autosomal Recessive Stargardt Disease.', *Human gene therapy*, 30(11), pp. 1361–1370. doi: 10.1089/hum.2019.132.
- Emeis, D. H., *et al.* (1982) 'Complex formation between metarhodopsin II and GTP-binding protein in bovine protoreceptor membranes leads to a shift of the photoproduct equilibrium', *FEBS Letter*, Volume 143, Issue 1, 21 June 1982, Pages 29-34. [https://doi.org/10.1016/0014-5793\(82\)80266-4](https://doi.org/10.1016/0014-5793(82)80266-4).
- Ernest, P. J. G. *et al.* (2009) 'Outcome of ABCA4 microarray screening in routine clinical practice.', *Molecular vision*, 15(December), pp. 2841–2847.
- Ferrari, S. *et al.* (2011) 'Retinitis Pigmentosa: Genes and Disease Mechanisms', *Current Genomics*, 12(4), pp. 238–249. doi: 10.2174/138920211795860107.
- Fishman, G. A. (1976) 'Fundus flavimaculatus. A clinical classification', *JAMA Ophthalmology*, 94, pp. 2061–2067. doi: 10.1097/00029330-200601010-00015.
- Fishman, G. A. *et al.* (1987) 'Visual acuity loss in patients with Stargardt's macular dystrophy.', *Ophthalmology*, 94(7), pp. 809–814. doi: 10.1016/s0161-6420(87)33533-x.
- Fishman, G. A. *et al.* (1999) 'Variation of clinical expression in patients with Stargardt dystrophy and sequence variations in the ABCR gene', *Archives of Ophthalmology*, 117(4), pp. 504–510. doi: 10.1001/archophth.117.4.504.
- Fishman, G. A. *et al.* (2003) 'ABCA4 gene sequence variations in patients with autosomal recessive cone-rod dystrophy', *Archives of Ophthalmology*, 121(6), pp. 851–855. doi: 10.1001/archophth.121.6.851.
- Fishman, G. A., Farbman, J. S. and Alexander, K. R. (1991) 'Delayed rod dark adaptation in patients with Stargardt's disease.', *Ophthalmology*, 98(6), pp. 957–962. doi: 10.1016/s0161-6420(91)32196-1.
- Fitzgerald, M. L. *et al.* (2004) 'ATP-binding cassette transporter A1 contains a novel C-terminal VFNFA motif that is required for its cholesterol efflux and ApoA-I binding activities', *Journal of Biological Chemistry*, 279(46), pp. 48477–48485. doi: 10.1074/jbc.M409848200.
- Flores-Sánchez, B. C. and Tatham, A. J. (2019) 'Acute angle closure glaucoma', *British Journal of Hospital Medicine*, 80(12), pp. C174–C179. doi: 10.12968/hmed.2019.80.12.c174.
- Fong, D. S. *et al.* (2004) 'Retinopathy in Diabetes', *Diabetes Care*, 27(SUPPL. 1). doi: 10.2337/diacare.27.2007.s84.
- Ford, R. C. and Beis, K. (2019) 'Learning the ABCs one at a time: Structure and mechanism of ABC transporters', *Biochemical Society Transactions*, 47(1), pp. 23–36. doi: 10.1042/BST20180147.
- Fotiadis, D., Liang, Y., Filipek, S., Saperstein, D. A., Engel, A. and Palczewski, K. (2003) 'Atomic-force microscopy: rhodopsin dimers in native disc membranes', *Nature* 421, 127-128.

- Franceschetti, A. (1965) 'A special form of tapetoretinal degeneration: fundus flavimaculatus.', *Transactions - American Academy of Ophthalmology and Otolaryngology. American Academy of Ophthalmology and Otolaryngology*, 69(6), pp. 1048–1053.
- François, P. *et al.* (1975) '[Stargardt's disease and fundus flavimaculatus].', *Archives d'ophtalmologie et revue generale d'ophtalmologie*, 35(11), pp. 817–846.
- Fritsche, L. G. *et al.* (2014) 'Age-related macular degeneration: Genetics and biology coming together', *Annual Review of Genomics and Human Genetics*, 15, pp. 151–171. doi: 10.1146/annurev-genom-090413-025610.
- Fujinami, K., Lois, N., *et al.* (2013) 'A longitudinal study of Stargardt disease: Clinical and electrophysiologic assessment, progression, and genotype correlations', *American Journal of Ophthalmology*, 155(6). doi: 10.1016/j.ajo.2013.01.018.
- Fujinami, K., Sergouniotis, P. I., *et al.* (2013) 'Clinical and molecular analysis of stargardt disease with preserved foveal structure and function', *American Journal of Ophthalmology*, 156(3), pp. 487–502. doi: 10.1016/j.ajo.2013.05.003.
- Fujinami, K. *et al.* (2015) 'Clinical and molecular characteristics of childhood-onset stargardt disease', *Ophthalmology*, 122(2), pp. 326–334. doi: 10.1016/j.ophtha.2014.08.012.
- Fumagalli, A. *et al.* (2001) 'Mutational scanning of the ABCR gene with double-gradient denaturing-gradient gel electrophoresis (DG-DGGE) in Italian Stargardt disease patients', *Human Genetics*, 109(3), pp. 326–338. doi: 10.1007/s004390100583.
- Fung, B.K., Stryer, L. (1980) 'Photolyzed rhodopsin catalyzes the exchange of GTP for bound GDP in retinal rod outer segments' *Proc. Natl. Acad. Sci.* 77,2500-2504.
- Fung, B.K., Hurley, J. B., Stryer, L. (1981) 'Flow of information in the light-triggered cyclic nucleotide cascade of vision', *Proc. Natl. Acad. Sci.* Jan; 78(1): 152–156.
- Garces, F. *et al.* (2018) 'Correlating the expression and functional activity of ABCA4 disease variants with the phenotype of patients with stargardt disease', *Investigative Ophthalmology and Visual Science*, 59(6), pp. 2305–2315. doi: 10.1167/iovs.17-23364.
- Garces, F. A., Jessica, F., Molday, R. S. (2021) 'Functional Characterization of ABCA4 Missense Variants Linked to Stargardt Macular Degeneration', *International Journal of Molecular Sciences*, 2021, 22,185. <https://dx.doi.org/10.3390/ijms22010185>.
- Garwin, G. G. and Saari, J. C. (2000) 'High-performance liquid chromatography analysis of visual cycle retinoids', *Methods in Enzymology*, 316(1980), pp. 313–324. doi: 10.1016/s0076-6879(00)16731-x.
- Gelissen, O. and De Laey, J. J. (1985) 'A clinical review of Stargardt's disease and/or Fundus Flavimaculatus with follow-up', *International Ophthalmology*, 8(4), pp. 225–235. doi: 10.1007/BF00137651.
- Genead, M. A. *et al.* (2009) 'The natural history of stargardt disease with specific sequence mutation in

the ABCA4 gene', *Investigative Ophthalmology and Visual Science*, 50(12), pp. 5867–5871. doi: 10.1167/iovs.09-3611.

Gerber, S. *et al.* (2008) 'Structural basis of trans-inhibition in a molybdate/tungstate ABC transporter', *Science*, 321(5886), pp. 246–250. doi: 10.1126/science.1156213.

Gilliam, J. C., Chang, J. T., Sandoval, I. M., Zhang, Y., Li, T., Pittler, S. J., Chiu, W. and Wensel, T. G. (2012) 'Three-dimensional architecture of the rod sensory cilium and its disruption in retinal neurodegeneration', *Cell* 151, 1029-1041.

Gunkel, M., Schöneberg, J., Alkhalidi, W., Irsen, S., Noé, F., Kaupp, U. B. and Al-Amoudi, A. (2015) 'Higher-order architecture of rhodopsin in intact photoreceptors and its implication for phototransduction kinetics', *Structure* 23, 628-638.

Haller, J. F. *et al.* (2014) 'Endogenous β -glucocerebrosidase activity in Abca12^{-/-} epidermis elevates ceramide levels after topical lipid application but does not restore barrier function', *Journal of Lipid Research*, 55(3), pp. 493–503. doi: 10.1194/jlr.M044941.

Han, F. and Xu, G. (2020) 'Stem Cell Transplantation Therapy for Retinal Degenerative Diseases' *Adv. Exp. Med. Biol.* 1266:127-139.

Hartong, D. T., Berson, E. L. and Dryja, T. P. (2006) 'Retinitis pigmentosa.', *The Lancet*, 368, pp. 1795–809.

Heesterbeek, T. J. *et al.* (2020) 'Risk factors for progression of age-related macular degeneration', *Ophthalmic and Physiological Optics*, 40(2), pp. 140–170. doi: 10.1111/opo.12675.

Higgins, C. F. and Linton, K. J. (2004) 'The ATP switch model for ABC transporters', *Nature Structural and Molecular Biology*, 11(10), pp. 918–926. doi: 10.1038/nsmb836.

Hodges, R.S., Heaton, R.J., Parker, J.M., Molday, L., Molday, R. S. (1988) 'Antigen-antibody interaction. Synthetic peptides define linear antigenic determinants recognized by monoclonal antibodies directed to the cytoplasmic carboxyl terminus of rhodopsin', *J. Biol. Chem.* 263:11768–11775. [PubMed: 2457026]

Hollenstein, K., Frei, D. C. and Locher, K. P. (2007) 'Structure of an ABC transporter in complex with its binding protein', *Nature*, 446(7132), pp. 213–216. doi: 10.1038/nature05626.

Hu, F. Y. *et al.* (2019) 'ABCA4 gene screening in a Chinese cohort with Stargardt disease: Identification of 37 novel variants', *Frontiers in Genetics*, 10(JUL), pp. 1–8. doi: 10.3389/fgene.2019.00773.

Huang, L. *et al.* (2013) 'Exome Sequencing of 47 Chinese Families with Cone-Rod Dystrophy: Mutations in 25 Known Causative Genes', *PLoS ONE*, 8(6). doi: 10.1371/journal.pone.0065546.

Hui Sun and Jeremy Nathans (1997) 'Stargardt's ABCR is localized to the disc membrane of retinal rod outer segments', *Nature Genetics*, 15, pp. 57–61.

Husada, F. *et al.* (2018) 'Conformational dynamics of the ABC transporter McjD seen by single-molecule FRET', *The EMBO Journal*, 37(21), pp. 1–13. doi: 10.15252/embj.2018100056.

- Hwang, J. C. *et al.* (2009) 'Peripapillary atrophy in stargardt disease', *Retina*, 29(2), pp. 181–186. doi: 10.1097/IAE.0b013e31818a2c01.
- Ile, K. E. *et al.* (2004) 'Identification of a novel first exon of the human ABCA2 transporter gene encoding a unique N-terminus', *Biochimica et Biophysica Acta - Gene Structure and Expression*, 1678(1), pp. 22–32. doi: 10.1016/j.bbaexp.2004.01.007.
- Illing, M., Molday, L. L. and Molday, R. S. (1997) 'The 220-kDa rim protein of retinal rod outer segments is a member of the ABC transporter superfamily', *Journal of Biological Chemistry*, 272(15), pp. 10303–10310. doi: 10.1074/jbc.272.15.10303.
- Ishiguro, S. I. *et al.* (1991) 'Purification of retinol dehydrogenase from bovine retinal rod outer segments', *Journal of Biological Chemistry*, 266(23), pp. 15520–15524.
- Jaakson, K. *et al.* (2003) 'Genotyping Microarray (Gene Chip) for the ABCR (ABCA4) Gene', *Human Mutation*, 22(5), pp. 395–403. doi: 10.1002/humu.10263.
- Jia, Y. *et al.* (2020) 'Alteration in the function and expression of SLC and ABC transporters in the neurovascular unit in alzheimer's disease and the clinical significance', *Aging and Disease*, 11(2), pp. 390–404. doi: 10.14336/AD.2019.0519.
- Jiang, F. *et al.* (2016) 'Screening of ABCA4 gene in a chinese cohort with stargardt disease or cone-rod dystrophy with a report on 85 novel mutations', *Investigative Ophthalmology and Visual Science*, 57(1), pp. 145–152. doi: 10.1167/iovs.15-18190.
- Jin, M. *et al.* (2005) 'Rpe65 is the retinoid isomerase in bovine retinal pigment epithelium', *Cell*, 122(3), pp. 449–459. doi: 10.1016/j.cell.2005.06.042.
- Jin, H., White, S. R., Shida, T., Schulz, S., Aguiar, M., Gygi, S. P., Bazan, J. F. and Nachury, M. V. (2010) 'The conserved Bardet-Biedl syndrome proteins assemble a coat that traffics membrane proteins to cilia', *Cell* 141, 1208-1219.
- Jurgensmeier, C., Bhosale, P. and Bernstein, P. S. (2007) 'Evaluation of 4-methylpyrazole as a potential therapeutic dark adaptation inhibitor', *Current Eye Research*, 32(10), pp. 911–915. doi: 10.1080/02713680701616156.
- Kadaba, N. S. *et al.* (2008) 'The high-affinity E. coli methionine ABC transporter: Structure and allosteric regulation', *Science*, 321(5886), pp. 250–253. doi: 10.1126/science.1157987.
- Kang-Derwent, J. J. *et al.* (2004) 'Dark adaptation of rod photoreceptors in normal subjects, and in patients with Stargardt disease and an ABCA4 mutation', *Investigative Ophthalmology and Visual Science*, 45(7), pp. 2447–2456. doi: 10.1167/iovs.03-1178.
- Kang, J. *et al.* (2011) 'Plant ABC Transporters', *The Arabidopsis Book*, 9, p. e0153. doi: 10.1199/tab.0153.
- Kevany, B. M. and Palczewski, K. (2010) 'Phagocytosis of retinal rod and cone photoreceptors.' *Physiology* 25, 8-15.

- Khalili, S. *et al.* (2018) 'Induction of rod versus cone photoreceptor-specific progenitors from retinal precursor cells', *Stem Cell Research*, 33, December 2018, Pages 215-227. <https://doi.org/10.1016/j.scr.2018.11.005>.
- Khan, M. *et al.* (2020) 'Resolving the dark matter of ABCA4 for 1054 Stargardt disease probands through integrated genomics and transcriptomics', *Genetics in Medicine*, 0(0). doi: 10.1038/s41436-020-0787-4.
- Khare, D. *et al.* (2009) 'Alternating Access in Maltose Transporter Mediated by Rigid-Body Rotations', *Molecular Cell*, 33(4), pp. 528–536. doi: 10.1016/j.molcel.2009.01.035.
- Killer, H. E. and Pircher, A. (2018) 'Normal tension glaucoma: Review of current understanding and mechanisms of the pathogenesis /692/699/3161/3169/3170 /692/699/3161 review-article', *Eye (Basingstoke)*, 32(5), pp. 924–930. doi: 10.1038/s41433-018-0042-2.
- Kim, J. M. *et al.* (2017) 'Identification of the PROM1 Mutation p.R373C in a Korean Patient With Autosomal Dominant Stargardt-like Macular Dystrophy.', *Annals of laboratory medicine*, 37(6), pp. 536–539. doi: 10.3343/alm.2017.37.6.536.
- Kim, L. S. and Fishman, G. A. (2006) 'Comparison of visual acuity loss in patients with different stages of Stargardt's disease.', *Ophthalmology*, 113(10), pp. 1748–1751. doi: 10.1016/j.ophtha.2006.04.027.
- Kim, W. S. *et al.* (2005) 'Abca7 null mice retain normal macrophage phosphatidylcholine and cholesterol efflux activity despite alterations in adipose mass and serum cholesterol levels', *Journal of Biological Chemistry*, 280(5), pp. 3989–3995. doi: 10.1074/jbc.M412602200.
- Kinting, S. *et al.* (2019) 'Potentiation of ABCA3 lipid transport function by ivacaftor and genistein', *Journal of Cellular and Molecular Medicine*, 23(8), pp. 5225–5234. doi: 10.1111/jcmm.14397.
- Klevering, B. J. *et al.* (2002) 'Phenotypic spectrum of autosomal recessive cone-rod dystrophies caused by mutations in the ABCA4 (ABCR) gene', *Investigative Ophthalmology and Visual Science*, 43(6), pp. 1980–1985.
- Kniazeva, M. *et al.* (1999) 'A new locus for autosomal dominant Stargardt-like disease maps to chromosome 4', *American Journal of Human Genetics*, 64(5), pp. 1394–1399. doi: 10.1086/302377.
- Korkhov, V. M., Mireku, S. A. and Locher, K. P. (2012) 'Structure of AMP-PNP-bound vitamin B 12 transporter BtuCD-F', *Nature*, 490(7420), pp. 367–372. doi: 10.1038/nature11442.
- Kozlov, G. and Gehring, K. (2020) 'Calnexin cycle – structural features of the ER chaperone system', *The FEBS Journal*, 287 (2020) 4322–4340. doi:10.1111/febs.15330.
- Krämer, F. *et al.* (2003) 'Ten novel mutations in VMD2 associated with Best macular dystrophy (BMD).', *Human mutation*, 22(5), p. 418. doi: 10.1002/humu.9189.
- Krieg, U.C., Walter, P., Johnson, A. E., (1986) 'Photocrosslinking of the signal sequence of nascent preprolactin to the 54-kilodalton polypeptide of the signal recognition particle', *Proc. Natl. Acad. Sci.*, 83, pp. 8604-8608
- Kubota, R. *et al.* (2014) 'Phase 1, dose-ranging study of emixustat hydrochloride (ACU-4429), a novel

visual cycle modulator, in healthy volunteers.’, *Retina (Philadelphia, Pa.)*, 34(3), pp. 603–609. doi: 10.1097/01.iae.0000434565.80060.f8.

Kukura, P., McCamant, D.W., Yoon, S., Wandschneider, D. B., Mathies R. A. (2005) ‘Structural observation of the primary isomerization in vision with femtosecond-stimulated Raman’, *Science*, Nov 11;310(5750):1006-9. doi: 10.1126/science.1118379.

Kurzchalia, T. V., Wiedmann, M., Girshovich, A. S., Bochkareva, E. S., Bielka, H., Rapoport, T. A. (1986) ‘The signal sequence of nascent prolactin interacts with the 54K polypeptide of signal recognition particle’ *Nature*, 320 (1986), pp. 634-636.

Lamb, T. D. and Pugh, E. N. (2006) ‘Phototransduction, dark adaptation, and rhodopsin regeneration: The proctor lecture’, *Investigative Ophthalmology and Visual Science*, 47(12), pp. 5138–5152. doi: 10.1167/iovs.06-0849.

Lambertus, S. *et al.* (2015) ‘Early-onset stargardt disease: Phenotypic and genotypic characteristics’, *Ophthalmology*, 122(2), pp. 335–344. doi: 10.1016/j.ophtha.2014.08.032.

Lambertus, S. *et al.* (2016) ‘Progression of late-onset stargardt disease’, *Investigative Ophthalmology and Visual Science*, 57(13), pp. 5186–5191. doi: 10.1167/iovs.16-19833.

Lane, T. S. *et al.* (2016) ‘Diversity of ABC transporter genes across the plant kingdom and their potential utility in biotechnology’, *BMC Biotechnology*, 16(1). doi: 10.1186/s12896-016-0277-6.

Leach, M. R. and Williams, D. B. (2013) ‘Calnexin and Calreticulin, Molecular Chaperones of the Endoplasmic Reticulum’ *Landes Bioscience*; 2000-2013.

Lee, R., Wong, T. Y. and Sabanayagam, C. (2015) ‘Epidemiology of diabetic retinopathy, diabetic macular edema and related vision loss’, *Eye and Vision*, 2(1), pp. 1–25. doi: 10.1186/s40662-015-0026-2.

Lee, W. *et al.* (2017) ‘Genotypic spectrum and phenotype correlations of ABCA4-associated disease in patients of south Asian descent’, *European Journal of Human Genetics*, 25(6), pp. 735–743. doi: 10.1038/ejhg.2017.13.

Lenis, T. L. *et al.* (2018) ‘Expression of ABCA4 in the retinal pigment epithelium and its implications for Stargardt macular degeneration’, *Proceedings of the National Academy of Sciences of the United States of America*, 115(47), pp. E11120–E11127. doi: 10.1073/pnas.1802519115.

Lewis, R. A. *et al.* (1999) ‘Genotype/phenotype analysis of a photoreceptor-specific ATP-binding cassette transporter gene, ABCR, in Stargardt disease’, *American Journal of Human Genetics*, 64(2), pp. 422–434. doi: 10.1086/302251.

Li, J. *et al.* (2015) ‘Involvement of endoplasmic reticulum stress in all-trans-retinal-induced retinal pigment epithelium degeneration’, *Toxicological sciences : an official journal of the Society of Toxicology*, 143(1), pp. 196–208. doi: 10.1093/toxsci/kfu223.

Li, Y. *et al.* (2019) ‘Metabolic labelling of choline phospholipids probes ABCA3 transport in lamellar bodies’, *Biochimica et Biophysica Acta - Molecular and Cell Biology of Lipids*, 1864(12), p. 158516. doi: 10.1016/j.bbalip.2019.158516.

- Liebman, P. A. and Entine, G. (1974) 'Lateral diffusion of visual pigment in photoreceptor disk membranes', *Science* 185, 457-459.
- Linton, K. J. (2007) 'Structure and Function of ABC Transporters ABC Transporters are Ubiquitous', *Physiology*, 22(27), pp. 122–130.
- Liu, J. *et al.* (2000) 'The biosynthesis of A2E, a fluorophore of aging retina, involves the formation of the precursor, A2-PE, in the photoreceptor outer segment membrane', *Journal of Biological Chemistry*, 275(38), pp. 29354–29360. doi: 10.1074/jbc.M910191199.
- Liu, Q. *et al.* (2019) 'The CFTR corrector, VX-809 (Lumacaftor), rescues ABCA4 trafficking mutants: A potential treatment for stargardt disease', *Cellular Physiology and Biochemistry*, 53(2), pp. 400–412. doi: 10.33594/000000146.
- Loo, T. W., Bartlett, M. C. and Clarke, D. M. (2003) 'Simultaneous binding of two different drugs in the binding pocket of the human multidrug resistance P-glycoprotein', *Journal of Biological Chemistry*, 278(41), pp. 39706–39710. doi: 10.1074/jbc.M308559200.
- MacDonald, I. M. and Sieving, P. A. (2018) 'Investigation of the effect of dietary docosahexaenoic acid (DHA) supplementation on macular function in subjects with autosomal recessive Stargardt macular dystrophy', *Ophthalmic Genetics*, 39(4), pp. 477–486. doi: 10.1080/13816810.2018.1484931.
- Macé, S. *et al.* (2005) 'ABCA2 is a strong genetic risk factor for early-onset Alzheimer's disease', *Neurobiology of Disease*, 18(1), pp. 119–125. doi: 10.1016/j.nbd.2004.09.011.
- Maeda, A., Maeda, T., *et al.* (2009) 'Involvement of all-trans-retinal in acute light-induced retinopathy of mice', *Journal of Biological Chemistry*, 284(22), pp. 15173–15183. doi: 10.1074/jbc.M900322200.
- Maeda, A., Golczak, M., *et al.* (2009) 'Limited roles of Rdh8, Rdh12, and Abca4 in all-trans-retinal clearance in mouse retina', *Investigative Ophthalmology and Visual Science*, 50(11), pp. 5435–5443. doi: 10.1167/iovs.09-3944.
- Maia-Lopes, S. *et al.* (2009) 'ABCA4 mutations in Portuguese Stargardt patients: Identification of new mutations and their phenotypic analysis', *Molecular Vision*, 15(March), pp. 584–591.
- Mackenzie, D., Arendt, A., Hargrave, P., McDowell, J. H., Molday, R.S. (1984) 'Localization of binding sites for carboxyl terminal specific anti-rhodopsin monoclonal antibodies using synthetic peptides', *Biochemistry*, 23:6544–6549. [PubMed: 6529569]
- Mäntyjärvi, M. and Tuppurainen, K. (1992) 'Color vision in Stargardt's disease', *International Ophthalmology*, 16(6), pp. 423–428. doi: 10.1007/BF00918432.
- Martinez-Mir, A. *et al.* (1998) 'Retinitis pigmentosa caused by a homozygous mutation in the Stargardt disease gene ABCR', *Nature*, 18, pp. 11–12.
- Mary, C., Scherrer, A., Huck, L., Lakkaraju, A. K., Thomas, Y., Johnson, A. E., Strub, K., (2010) 'Residues in SRP9/14 essential for elongation arrest activity of the signal recognition particle define a positively charged functional domain on one side of the protein' *RNA*, 16, pp. 969-979.

- Masutomi, K. *et al.* (2012) ‘All-Trans Retinal Mediates Light-Induced Oxidation in Single Living Rod Photoreceptors’, *Photochemistry and photobiology*, (25), pp. 1356–1361. doi: 10.1111/j.1751-1097.2012.01129.x.
- Mata, N. L., Weng, J. and Travis, G. H. (2000) ‘Biosynthesis of a major lipofuscin fluorophore in mice and humans with ABCR-mediated retinal and macular degeneration’, *Proceedings of the National Academy of Sciences of the United States of America*, 97(13), pp. 7154–7159. doi: 10.1073/pnas.130110497.
- Maugeri, A. *et al.* (1999) ‘The 2588G→C mutation in the ABCR gene is a mild frequent founder mutation in the western European population and allows the classification of ABCR mutations in patients with Stargardt disease’, *American Journal of Human Genetics*, 64(4), pp. 1024–1035. doi: 10.1086/302323.
- Maugeri, A. *et al.* (2002) ‘The ABCA4 2588G > Stargardt mutation: Single origin and increasing frequency from South-West to North-East Europe’, *European Journal of Human Genetics*, 10(3), pp. 197–203. doi: 10.1038/sj.ejhg.5200784.
- Maugeri, A. *et al.* (2004) ‘A Novel Mutation in the ELOVL4 Gene Causes Autosomal Dominant Stargardt-like Macular Dystrophy’, pp. 4263–4267. doi: 10.1167/iovs.04-0078.
- McBee, J. K. *et al.* (2001) ‘Confronting complexity: The interlink of phototransduction and retinoid metabolism in the vertebrate retina’, *Progress in Retinal and Eye Research*, 20(4), pp. 469–529. doi: 10.1016/S1350-9462(01)00002-7.
- McClements, M. E. *et al.* (2019) ‘An AAV Dual Vector Strategy Ameliorates the Stargardt Phenotype in Adult *Abca4*^{-/-} Mice’, *Human Gene Therapy*, 30(5), pp. 590–600. doi: 10.1089/hum.2018.156.
- McNeish, J. *et al.* (2000) ‘High density lipoprotein deficiency and foam cell accumulation in mice with targeted disruption of ATP-binding cassette transporter-1’, *Proceedings of the National Academy of Sciences of the United States of America*, 97(8), pp. 4245–4250. doi: 10.1073/pnas.97.8.4245.
- Megaw, R. and Hurd, T. W. (2018) ‘Photoreceptor actin dysregulation in syndromic and non-syndromic retinitis pigmentosa’, *Biochemical Society Transactions*, 46(6), pp. 1463–1473. doi: 10.1042/BST20180138.
- Mehat, M. S. *et al.* (2018) ‘Transplantation of Human Embryonic Stem Cell-Derived Retinal Pigment Epithelial Cells in Macular Degeneration’, *Ophthalmology*, 125(11), pp. 1765–1775. doi: 10.1016/j.ophtha.2018.04.037.
- Michaelides, M. *et al.* (2007) ‘ABCA4 mutations and discordant ABCA4 alleles in patients and siblings with bull’s-eye maculopathy’, *British Journal of Ophthalmology*, 91(12), pp. 1650–1655. doi: 10.1136/bjo.2007.118356.
- Molday, R.S., MacKenzie, D. (1983) ‘Monoclonal antibodies to rhodopsin: Characterization, cross-reactivity, and application as structural probes’, *Biochemistry* 1983, 22, 653–660.
- Molday, L. ., Rabin, A. . and Molday, R. . (2000) ‘ABCR expression in foveal cone photoreceptors and

its role in Stargardt macular dystrophy', *American Journal of Ophthalmology*, 130(5), p. 689. doi: 10.1016/s0002-9394(00)00756-x.

Molday, R. S., Zhong, M. and Quazi, F. (2009) 'The role of the photoreceptor ABC transporter ABCA4 in lipid transport and Stargardt macular degeneration', *Biochimica et Biophysica Acta - Molecular and Cell Biology of Lipids*, 1791(7), pp. 573–583. doi: 10.1016/j.bbalip.2009.02.004.

Molday, L. L. and Molday, R. S. (2014) '1D4 – A Versatile Epitope Tag for the Purification and Characterization of Expressed Membrane and Soluble Proteins', *Methods Mol. Biol.* 1177: 1–15. doi:10.1007/978-1-4939-1034-2_1.

Molday, R. S. (2015) 'Insights into the Molecular Properties of ABCA4 and Its Role in the Visual Cycle and Stargardt Disease', 1st edn, *Progress in Molecular Biology and Translational Science*. 1st edn. Elsevier Inc. doi: 10.1016/bs.pmbts.2015.06.008.

Molday, R. S. and Moritz, O. L. (2015) 'Photoreceptors at a glance', *Journal of Cell Science*, 128(22), pp. 4039–4045. doi: 10.1242/jcs.175687.

Molday, L. L. *et al.* (2018) 'Localization and functional characterization of the p.Asn965Ser (N965S) ABCA4 variant in mice reveal pathogenic mechanisms underlying Stargardt macular degeneration', *Human Molecular Genetics*, 27(2), pp. 295–306. doi: 10.1093/hmg/ddx400.

Montanari, F. and Ecker, G. F. (2015) 'Prediction of drug-ABC-transporter interaction - Recent advances and future challenges', *Advanced Drug Delivery Reviews*, 86, pp. 17–26. doi: 10.1016/j.addr.2015.03.001.

Morizur, L. *et al.* (2020) 'Human pluripotent stem cells: A toolbox to understand and treat retinal degeneration', *Molecular and Cellular Neuroscience*, 107(January), p. 103523. doi: 10.1016/j.mcn.2020.103523.

Mou, H. *et al.* (1999) 'cGMP binding to noncatalytic sites on mammalian rod photoreceptor phosphodiesterase is regulated by binding of its gamma and delta subunits' *J. Biol. Chem.* 1999 Jun 25;274(26):18813-20. doi: 10.1074/jbc.274.26.18813.

Nachury, M. V., Loktev, A. V., Zhang, Q., Westlake, C. J., Peränen, J., Merdes, A., Slusarski, D. C., Scheller, R. H., Bazan, J. F., Sheffield, V. C. *et al.* (2007) 'A core complex of BBS proteins cooperates with the GTPase Rab8 to promote ciliary membrane biogenesis', *Cell* 129, 1201-1213.

Nakao, T. *et al.* (2012) 'Foveal sparing in patients with Japanese Stargardt's disease and good visual acuity', *Japanese Journal of Ophthalmology*, 56(6), pp. 584–588. doi: 10.1007/s10384-012-0172-1.

Nassisi, M. *et al.* (2018) 'Expanding the mutation spectrum in ABCA4: Sixty novel disease causing variants and their associated phenotype in a large french stargardt cohort', *International Journal of Molecular Sciences*, 19(8). doi: 10.3390/ijms19082196.

Nilsson, I., von Heijne, G. (1993) 'Determination of the distance between oligosaccharyltransferase active site and the endoplasmic reticulum membrane', *J. Biol. Chem.* 268:5798–5801.

Nõupuu, K. *et al.* (2014) 'Structural and genetic assessment of the ABCA4-associated optical gap phenotype', *Investigative ophthalmology & visual science*, 55(11), pp. 7217–7226. doi: 10.1167/iovs.14-

14674.

Nyathi, Y., Wilkinson, B. M., Pool, M. R. (2013) 'Co-translational targeting and translocation of proteins to the endoplasmic reticulum' *BBA – Mol. Cell. Res.*, Pages 2392-2402.

Oldani, M. *et al.* (2012) 'Clinical and molecular genetic study of 12 Italian families with autosomal recessive Stargardt disease.', *Genetics and molecular research : GMR*, 11(4), pp. 4342–4350. doi: 10.4238/2012.October.9.3.

Oldham, M. L. *et al.* (2007) 'Crystal structure of a catalytic intermediate of the maltose transporter', *Nature*, 450(7169), pp. 515–521. doi: 10.1038/nature06264.

Oldham, M. L., Davidson, A. L. and Chen, J. (2008) 'Structural insights into ABC transporter mechanism', *Current Opinion in Structural Biology*, 18(6), pp. 726–733. doi: 10.1016/j.sbi.2008.09.007.

Oltvai, Z. N. *et al.* (2020) 'Neonatal respiratory failure due to novel compound heterozygous mutations in the ABCA3 lipid transporter', *Cold Spring Harbor molecular case studies*, 6(3), pp. 1–12. doi: 10.1101/mcs.a005074.

Oner, A. *et al.* (2019) 'Six-month results of suprachoroidal adipose tissue-derived mesenchymal stem cell implantation in patients with optic atrophy: a phase 1/2 study', *International Ophthalmology*, 39(12), pp. 2913–2922. doi: 10.1007/s10792-019-01141-5.

Oram, J. F. and Lawn, R. M. (2001) 'ABCA1: The gatekeeper for eliminating excess tissue cholesterol', *Journal of Lipid Research*, 42(8), pp. 1173–1179.

Orelle, C. *et al.* (2010) 'Dynamics of α -helical subdomain rotation in the intact maltose ATP-binding cassette transporter', *Proceedings of the National Academy of Sciences of the United States of America*, 107(47), pp. 20293–20298. doi: 10.1073/pnas.1006544107.

Orsó, E. *et al.* (2000) 'Transport of lipids from Golgi to plasma membrane is defective in tangier disease patients and Abc1-deficient mice', *Nature Genetics*, 24(2), pp. 192–196. doi: 10.1038/72869.

Paloma, E. *et al.* (2001) 'Spectrum of ABCA4 (ABCR) gene mutations in Spanish patients with autosomal recessive macular dystrophies', *Human Mutation*, 17(6), pp. 504–510. doi: 10.1002/humu.1133.

Papaoiouannou, M. *et al.* (2000) 'An analysis of ABCR mutations in British patients with recessive retinal dystrophies', *Investigative Ophthalmology and Visual Science*, 41(1), pp. 16–19.

Papermaster, D. S. *et al.* (1979) 'Immunohistochemical Localization of a Large Intrinsic Membrane Protein to the Incisures and Margins of Frog Rod Outer Segment Disks', *The Journal of Cell Biology*, 78, pp. 415–425.

Papermaster, D. S., Reilly, P. and Schneider, B. G. (1982) 'Cone lamellae and red and green rod outer segment disks contain a large intrinsic membrane protein on their margins: an ultrastructural immunocytochemical study of frog retinas.', *Vision research*, 22(12), pp. 1417–1428. doi: 10.1016/0042-6989(82)90204-8.

- Parker, M. A. *et al.* (2016) ‘Test-retest variability of functional and structural parameters in patients with stargardt disease participating in the SAR422459 gene therapy trial’, *Translational Vision Science and Technology*, 5(5). doi: 10.1167/tvst.5.5.10.
- Passerini, I. *et al.* (2010) ‘Novel mutations in of the ABCR gene in italian patients with Stargardt disease’, *Eye*, 24(1), pp. 158–164. doi: 10.1038/eye.2009.35.
- Piccardi, M. *et al.* (2019) ‘Antioxidant saffron and central retinal function in ABCA4-related stargardt macular dystrophy’, *Nutrients*, 11(10), pp. 1–16. doi: 10.3390/nu11102461.
- Qian, H. *et al.* (2017) ‘Structure of the Human Lipid Exporter ABCA1’, *Cell*, 169(7), pp. 1228-1239.e10. doi: 10.1016/j.cell.2017.05.020.
- Quazi, F., Lenevich, S. and Molday, R. S. (2012) ‘ABCA4 is an N-retinylidene-phosphatidylethanolamine and phosphatidylethanolamine importer’, *Nature Communications*, 3(May), pp. 925–929. doi: 10.1038/ncomms1927.
- Quazi, F. and Molday, R. S. (2013) ‘Differential phospholipid substrates and directional transport by ATP-binding cassette proteins ABCA1, ABCA7, and ABCA4 and disease-causing mutants’, *Journal of Biological Chemistry*, 288(48), pp. 34414–34426. doi: 10.1074/jbc.M113.508812.
- Quazi, F. and Molday, R. S. (2014) ‘ATP-binding cassette transporter ABCA4 and chemical isomerization protect photoreceptor cells from the toxic accumulation of excess 11-cis-retinal’, *Proceedings of the National Academy of Sciences of the United States of America*, 111(13), pp. 5024–5029. doi: 10.1073/pnas.1400780111.
- Radu, R. A. *et al.* (2014) ‘Bisretinoid-mediated complement activation on retinal pigment epithelial cells is dependent on complement factor H haplotype’, *Journal of Biological Chemistry*, 289(13), pp. 9113–9120. doi: 10.1074/jbc.M114.548669.
- Raskin, N. H., Sligar, K. P. and Steinberg, R. H. (1976) ‘A pathophysiologic role for alcohol dehydrogenase: is retinol its “natural” substrate?’, *Annals of the New York Academy of Sciences*, 273, pp. 317–327. doi: 10.1111/j.1749-6632.1976.tb52894.x.
- Rees, D. C., Johnson, E. and Lewinson, O. (2009) ‘ABC transporters: The power to change’, *Nature Reviews Molecular Cell Biology*, 10(3), pp. 218–227. doi: 10.1038/nrm2646.
- Riveiro-Alvarez, R. *et al.* (2013) ‘Outcome of ABCA4 disease-associated alleles in autosomal recessive retinal dystrophies: Retrospective analysis in 420 Spanish families’, *Ophthalmology*, 120(11), pp. 2332–2337. doi: 10.1016/j.ophtha.2013.04.002.
- Rivera, A. *et al.* (2000) ‘A comprehensive survey of sequence variation in the ABCA4 (ABCR) gene in Stargardt disease and age-related macular degeneration’, *American Journal of Human Genetics*, 67(4), pp. 800–813. doi: 10.1086/303090.
- De Roeck, A., Van Broeckhoven, C. and Sleegers, K. (2019) ‘The role of ABCA7 in Alzheimer’s disease: evidence from genomics, transcriptomics and methylomics’, *Acta Neuropathologica*, 138(2), pp. 201–220. doi: 10.1007/s00401-019-01994-1.

- Rosenberg, T. *et al.* (2007) 'N965S is a common ABCA4 variant in Stargardt-related retinopathies in the Danish population', *Molecular Vision*, 13(October), pp. 1962–1969.
- Rotenstreich, Y., Fishman, G. A. and Anderson, R. J. (2003) 'Visual acuity loss and clinical observations in a large series of patients with Stargardt disease', *Ophthalmology*, 110(6), pp. 1151–1158. doi: 10.1016/S0161-6420(03)00333-6.
- Rozet, J. M. *et al.* (1999) 'Mutations of the retinal specific ATP binding transporter gene (ABCR) in a single family segregating both autosomal recessive retinitis pigmentosa RP19 and Stargardt disease: Evidence of clinical heterogeneity at this locus', *Journal of Medical Genetics*, 36(6), pp. 447–451. doi: 10.1136/jmg.36.6.447.
- Ruiz, A. and Bok, D. (2010) 'Focus on Molecules: Lecithin retinol acyltransferase', *Experimental Eye Research*, 90(2), pp. 186–187. doi: 10.1016/j.exer.2009.07.002.
- Runhart, E. H. *et al.* (2018) 'The common ABCA4 variant p.Asn1868ile shows nonpenetrance and variable expression of stargardt disease when present in trans with severe variants', *Investigative Ophthalmology and Visual Science*, 59(8), pp. 3220–3231. doi: 10.1167/iovs.18-23881.
- Runhart, E. H. *et al.* (2019) 'Late-onset Stargardt disease due to mild, deep-intronic ABCA4 alleles', *Investigative Ophthalmology and Visual Science*, 60(13), pp. 4249–4256. doi: 10.1167/iovs.19-27524.
- Rust, S. *et al.* (1999) 'Tangier disease is caused by mutations in the gene encoding ATP-binding cassette transporter 1', *Nature Genetics*, 22(4), pp. 352–355. doi: 10.1038/11921.
- Saari, J. C. *et al.* (1985) 'Properties of an interphotoreceptor retinoid-binding protein from bovine retina', *Journal of Biological Chemistry*, 260(1), pp. 195–201.
- Saari, J. C. (2012) 'Vitamin A metabolism in rod and cone visual cycles', *Annual Review of Nutrition*, 32, pp. 125–145. doi: 10.1146/annurev-nutr-071811-150748.
- Sabirzhanova, I. *et al.* (2015) 'Rescuing trafficking mutants of the ATP-binding cassette protein, ABCA4, with small molecule correctors as a treatment for Stargardt eye disease', *Journal of Biological Chemistry*, 290(32), pp. 19743–19755. doi: 10.1074/jbc.M115.647685.
- Salles, M. V. *et al.* (2017) 'Novel complex ABCA4 alleles in Brazilian patients with stargardt disease: Genotype-Phenotype Correlation', *Investigative Ophthalmology and Visual Science*, 58(13), pp. 5723–5730. doi: 10.1167/iovs.17-22398.
- Salles, M. V. *et al.* (2018) 'Variants in the ABCA4 gene in a Brazilian population with stargardt disease', *Molecular Vision*, 24(August), pp. 546–559.
- Sangermano, R. *et al.* (2016) 'Photoreceptor Progenitor mRNA Analysis Reveals Exon Skipping Resulting from the ABCA4 c.5461-10T→C Mutation in Stargardt Disease.', *Ophthalmology*, 123(6), pp. 1375–1385. doi: 10.1016/j.ophtha.2016.01.053.
- Sangermano, R. *et al.* (2018) 'ABCA4 midgenes reveal the full splice spectrum of all reported noncanonical splice site variants in Stargardt disease', *Genome Research*, 28(1), pp. 100–110. doi: 10.1101/gr.226621.117.

- Sarkar, H. and Moosajee, M. (2019) 'Retinol dehydrogenase 12 (RDH12): Role in vision, retinal disease and future perspectives', *Experimental Eye Research*, 188(May), p. 107793. doi: 10.1016/j.exer.2019.107793.
- Saraogi, I. Shan, S.O. (2011) 'Molecular mechanism of co-translational protein targeting by the signal recognition particle', *Traffic*, 12 (2011), pp. 535-542.
- Sauna, Z. E. *et al.* (2007) 'Catalytic cycle of ATP hydrolysis by P-glycoprotein: Evidence for formation of the E·S reaction intermediate with ATP- γ -S, a nonhydrolyzable analogue of ATP', *Biochemistry*, 46(48), pp. 13787–13799. doi: 10.1021/bi701385t.
- Sawada, O. *et al.* (2014) 'All-trans-retinal induces Bax activation via DNA damage to mediate retinal cell apoptosis', *Experimental Eye Research*, 123, pp. 27–36. doi: 10.1016/j.exer.2014.04.003.
- Scholl, H. P. N. *et al.* (2002) 'Alterations of slow and fast Rod ERG signals in patients with molecularly confirmed Stargardt disease type 1', *Investigative Ophthalmology and Visual Science*, 43(4), pp. 1248–1256.
- Schulz, H. L. *et al.* (2017) 'Mutation spectrum of the ABCA4 gene in 335 stargardt disease patients from a multicenter German cohort—impact of selected deep intronic variants and common SNPs', *Investigative Ophthalmology and Visual Science*, 58(1), pp. 394–403. doi: 10.1167/iovs.16-19936.
- Schwartz, S. D. *et al.* (2012) 'Embryonic stem cell trials for macular degeneration: A preliminary report', *The Lancet*, 379(9817), pp. 713–720. doi: 10.1016/S0140-6736(12)60028-2.
- Schwartz, S. D. *et al.* (2015) 'Human embryonic stem cell-derived retinal pigment epithelium in patients with age-related macular degeneration and Stargardt's macular dystrophy: Follow-up of two open-label phase 1/2 studies', *The Lancet*, 385(9967), pp. 509–516. doi: 10.1016/S0140-6736(14)61376-3.
- Ścieżyńska, A. *et al.* (2016) 'Next-generation sequencing of ABCA4: High frequency of complex alleles and novel mutations in patients with retinal dystrophies from Central Europe', *Experimental Eye Research*, 145, pp. 93–99. doi: 10.1016/j.exer.2015.11.011.
- Senior, A. E., Al-Shawi, M. K. and Urbatsch, I. L. (1995) 'The catalytic cycle of P-glycoprotein', *FEBS Letters*, 377(3), pp. 285–289. doi: 10.1016/0014-5793(95)01345-8.
- Shapiro, A. B. and Ling, V. (1994) 'ATPase activity of purified and reconstituted P-glycoprotein from Chinese hamster ovary cells', *Journal of Biological Chemistry*, 269(5), pp. 3745–3754.
- Sharon, D. *et al.* (2019a) 'A nationwide genetic analysis of inherited retinal diseases in Israel as assessed by the Israeli inherited retinal disease consortium (IIRDC)', *Human Mutation*, 41(1), pp. 140–149. doi: 10.1002/humu.23903.
- Sharon, D. *et al.* (2019b) 'A nationwide genetic analysis of inherited retinal diseases in Israel as assessed by the Israeli inherited retinal disease consortium (IIRDC)', *Human Mutation*, 41(1), pp. 140–149. doi: 10.1002/humu.23903.
- Sheth, J. J. *et al.* (2018) 'Harlequin ichthyosis due to novel splice site mutation in the ABCA12 gene:

postnatal to prenatal diagnosis', *International Journal of Dermatology*, 57(4), pp. 428–433. doi: 10.1111/ijd.13923.

Shroyer, N. F. (2001) 'Cosegregation and functional analysis of mutant ABCR (ABCA4) alleles in families that manifest both Stargardt disease and age-related macular degeneration', *Human Molecular Genetics*, 10(23), pp. 2671–2678. doi: 10.1093/hmg/10.23.2671.

Shroyer, N. F. *et al.* (2001) 'Null missense ABCR (ABCA4) mutations in a family with stargardt disease and retinitis pigmentosa', *Investigative Ophthalmology and Visual Science*, 42(12), pp. 2757–2761.

Siarheyeva, A., Liu, R. and Sharom, F. J. (2010) 'Characterization of an asymmetric occluded state of P-glycoprotein with two bound nucleotides: Implications for catalysis', *Journal of Biological Chemistry*, 285(10), pp. 7575–7586. doi: 10.1074/jbc.M109.047290.

Simon, W. A. *et al.* (2007) 'Soraprazan: Setting new standards in inhibition of gastric acid secretion', *Journal of Pharmacology and Experimental Therapeutics*, 321(3), pp. 866–874. doi: 10.1124/jpet.107.120428.

Simonelli, F. *et al.* (2000) 'New ABCR mutations and clinical phenotype in Italian patients with Stargardt disease', *Investigative Ophthalmology and Visual Science*, 41(3), pp. 892–897.

Simonelli, F. *et al.* (2005) 'Genotype-phenotype correlation in Italian families with Stargardt disease', *Ophthalmic Research*, 37(3), pp. 159–167. doi: 10.1159/000086073.

Sohma, Y., Yu, Y.-C. and Hwang, T.-C. (2013) 'Curcumin and Genistein: the Combined Effects on Disease-associated CFTR Mutants and their Clinical Implications', *Current Pharmaceutical Design*, 19(19), pp. 3521–3528. doi: 10.2174/13816128113199990320.

Song, W. K. *et al.* (2015) 'Treatment of macular degeneration using embryonic stem cell-derived retinal pigment epithelium: Preliminary results in Asian patients', *Stem Cell Reports*, 4(5), pp. 860–872. doi: 10.1016/j.stemcr.2015.04.005.

Sparrow, J. R. and Boulton, M. (2005) 'RPE lipofuscin and its role in retinal pathobiology', *Experimental Eye Research*, 80(5), pp. 595–606. doi: 10.1016/j.exer.2005.01.007.

Stahl, A. (2020) 'The Diagnosis and Treatment of Age-Related Macular Degeneration', *Dtsch. Arztebl. Int.* 117: 513–20. DOI: 10.3238/arztebl.2020.0513.

Stargardt, K. (1909) 'progressive degeneration in der maculagegend des auges', *Albrecht von Graefes Arch Klin Ophthalmology*, 71, pp. 534–550.

Stenirri, S. *et al.* (2008) 'Are microarrays useful in the screening of ABCA4 mutations in Italian patients affected by macular degenerations?', *Clinical Chemistry and Laboratory Medicine*, 46(9), pp. 1250–1255. doi: 10.1515/CCLM.2008.248.

Stone, E. M. *et al.* (1994) 'Clinical features of a Stargardt-like dominant progressive macular dystrophy with genetic linkage to chromosome 6q', *JAMA Ophthalmology*, 112, pp. 765–772.

Stone, E. M. *et al.* (1998) 'Allelic variation in ABCR associated with Stargardt disease but not age-

- related macular degeneration [3]', *Nature Genetics*, 20(4), pp. 328–329. doi: 10.1038/3798.
- Sun, D. *et al.* (2019) 'Non-viral Gene Therapy for Stargardt Disease with ECO/pRHO-ABCA4 Self-Assembled Nanoparticles', *Molecular Therapy*, 28(1), pp. 1–11. doi: 10.1016/j.ymthe.2019.09.010.
- Sun, H., Molday, R. S. and Nathans, J. (1999) 'Retinal stimulates ATP hydrolysis by purified and reconstituted ABCR, the photoreceptor-specific ATP-binding cassette transporter responsible for Stargardt disease', *Journal of Biological Chemistry*, 274(12), pp. 8269–8281. doi: 10.1074/jbc.274.12.8269.
- Sun, H., Smallwood, P. M. and Nathans, J. (2000) 'Biochemical defects in ABCR protein variants associated with human retinopathies', *Nature Genetics*, 26(2), pp. 242–246. doi: 10.1038/79994.
- Tanaka, A. R. *et al.* (2003) 'Effects of mutations of ABCA1 in the first extracellular domain on subcellular trafficking and ATP binding/hydrolysis', *Journal of Biological Chemistry*, 278(10), pp. 8815–8819. doi: 10.1074/jbc.M206885200.
- Tanaka, K. *et al.* (2018) 'The Rapid-Onset Chorioretinopathy Phenotype of ABCA4 Disease', *Ophthalmology*, 125(1), pp. 89–99. doi: 10.1016/j.ophtha.2017.07.019.
- Tanaka, N. *et al.* (2011) 'Roles of ATP-binding cassette transporter A7 in cholesterol homeostasis and host defense system.', *Journal of atherosclerosis and thrombosis*, 18(4), pp. 274–281. doi: 10.5551/jat.6726.
- Tanna, P. *et al.* (2017) 'Stargardt disease: Clinical features, molecular genetics, animal models and therapeutic options', *British Journal of Ophthalmology*, 101(1), pp. 25–30. doi: 10.1136/bjophthalmol-2016-308823.
- Tarling, E. J., Vallim, T. Q. d. A. and Edwards, P. A. (2013) 'Role of ABC transporters in lipid transport and human disease', *Trends in Endocrinology and Metabolism*, 24(7), pp. 342–350. doi: 10.1016/j.tem.2013.01.006.
- Tracewska, A. M. *et al.* (2019) 'Genetic spectrum of ABCA4-associated retinal degeneration in Poland', *Genes*, 10(12), pp. 1–12. doi: 10.3390/genes10120959.
- Tsang, S. H. and Sharma, T. (2018) 'Retinitis Pigmentosa (Non-syndromic)', in Tsang, S. H. and Sharma, T. (eds) *Atlas of Inherited Retinal Diseases*. Cham: Springer International Publishing, pp. 125–130. doi: 10.1007/978-3-319-95046-4_25.
- Tsybovsky, Y. *et al.* (2011) 'Posttranslational Modifications of the Photoreceptor-Specific ABC Transporter ABCA4'.
- Tsybovsky, Y. *et al.* (2013) 'Molecular organization and ATP-induced conformational changes of ABCA4, the photoreceptor-specific ABC Transporter', *Structure*, 21(5), pp. 854–860. doi: 10.1016/j.str.2013.03.001.
- Ueda, K. *et al.* (2016) 'Photodegradation of retinal bisretinoids in mouse models and implications for macular degeneration', *Proceedings of the National Academy of Sciences of the United States of America*, 113(25), pp. 6904–6909. doi: 10.1073/pnas.1524774113.

- Utz, V. M. *et al.* (2014) ‘Predictors of visual acuity and genotype-phenotype correlates in a cohort of patients with Stargardt disease’, *British Journal of Ophthalmology*, 98(4), pp. 513–518. doi: 10.1136/bjophthalmol-2013-304270.
- Valkenburg, D. *et al.* (2019) ‘Highly Variable Disease Courses in Siblings with Stargardt Disease’, *Ophthalmology*, 126(12), pp. 1712–1721. doi: 10.1016/j.ophtha.2019.07.010.
- Valverde, D. *et al.* (2006) ‘Microarray-based mutation analysis of the ABCA4 gene in Spanish patients with Stargardt disease: Evidence of a prevalent mutated allele’, *Molecular Vision*, 12(September 2005), pp. 902–908.
- Valverde, D. *et al.* (2007) ‘Spectrum of the ABCA4 gene mutations implicated in severe retinopathies in Spanish patients’, *Investigative Ophthalmology and Visual Science*, 48(3), pp. 985–990. doi: 10.1167/iovs.06-0307.
- Vasiliou, V., Vasiliou, K. and Nebert, D. W. (2009) ‘Human ATP-binding cassette (ABC) transporter family’, *Human Genomics*, 3(3), pp. 281–290.
- Verhalen, B. and Wilkens, S. (2011) ‘P-glycoprotein retains drug-stimulated ATPase activity upon covalent linkage of the two nucleotide binding domains at their C-terminal ends’, *Journal of Biological Chemistry*, 286(12), pp. 10476–10482. doi: 10.1074/jbc.M110.193151.
- Vijayasarathy, C., Ziccardi, L. and Sieving, P. A. (2012) ‘Biology of Retinoschisin’, in LaVail, M. M. *et al.* (eds) *Retinal Degenerative Diseases*. Boston, MA: Springer US, pp. 513–518.
- Wainwright, C. E. *et al.* (2015) ‘Lumacaftor-ivacaftor in patients with cystic fibrosis homozygous for phe508del CFTR’, *New England Journal of Medicine*, 373(3), pp. 220–231. doi: 10.1056/NEJMoal409547.
- Waldner, D.M., Bech-Hansen, N.T., Stell, W.K. (2018) ‘Channeling Vision: Ca_v1.4 – A Critical Link in Retinal Signal Transmission’, *BioMed Research Internationl*, vol. 2018, Article ID 7272630, 14 pages, 2018. <https://doi.org/10.1155/2018/7272630>
- Wang, N. *et al.* (2003) ‘ATP-binding Cassette Transporter A7 (ABCA7) Binds Apolipoprotein A-I and Mediates Cellular Phospholipid but Not Cholesterol Efflux’, *Journal of Biological Chemistry*, 278(44), pp. 42906–42912. doi: 10.1074/jbc.M307831200.
- Wang, J. and Deretic, D. (2015) ‘The Arf and Rab11 effector FIP3 acts synergistically with ASAP1 to direct Rabin8 in ciliary receptor targeting’, *J. Cell Sci.* 128, 1375-1385.
- Ward, A. *et al.* (2007) ‘Flexibility in the ABC transporter MsbA: Alternating access with a twist’, *Proceedings of the National Academy of Sciences of the United States of America*, 104(48), pp. 19005–19010. doi: 10.1073/pnas.0709388104.
- Webster, A. R. *et al.* (2001) ‘An analysis of allelic variation in the ABCA4 gene’, *Investigative Ophthalmology and Visual Science*, 42(6), pp. 1179–1189.
- Weinreb, R. N. *et al.* (2016) ‘Primary open-angle glaucoma’, *Nature Reviews Disease Primers*, 2. doi:

10.1038/nrdp.2016.67.

Weleber, R. G. (1994) 'Stargardt's Macular Dystrophy', *Archives of Ophthalmology*, 112, pp. 752–754.

Wen, P. C. and Tajkhorshid, E. (2011) 'Conformational coupling of the nucleotide-binding and the transmembrane domains in ABC transporters', *Biophysical Journal*, 101(3), pp. 680–690. doi: 10.1016/j.bpj.2011.06.031.

Weng, J. *et al.* (1999) 'Insights into the function of rim protein in photoreceptors and etiology of Stargardt's disease from the phenotype in abcr knockout mice', *Cell*, 98(1), pp. 13–23. doi: 10.1016/S0092-8674(00)80602-9.

Whelan, L. *et al.* (2020) 'Findings from a genotyping study of over 1000 people with inherited retinal disorders in Ireland', *Genes*, 11(1), pp. 1–23. doi: 10.3390/genes11010105.

Wilkens, S. (2015) 'Structure and mechanism of ABC transporters', *F1000Prime Reports*, 7(February), pp. 1–9. doi: 10.12703/P7-14.

Wiszniewski, W. *et al.* (2005) 'ABCA4 mutations causing mislocalization are found frequently in patients with severe retinal dystrophies', *Human Molecular Genetics*, 14(19), pp. 2769–2778. doi: 10.1093/hmg/ddi310.

Yatsenko, A. N. *et al.* (2001) 'Late-onset Stargardt disease is associated with missense mutations that map outside known functional regions of ABCR (ABCA4)', *Human Genetics*, 108(4), pp. 346–355. doi: 10.1007/s004390100493.

Young, R.W. and Droz, B. (1968) 'The renewal of protein in retinal rods and cones', *J. Cell Biol.* 39, 169-184.

Zernant, J. *et al.* (2011) 'Analysis of the ABCA4 gene by next-generation sequencing', *Investigative Ophthalmology and Visual Science*, 52(11), pp. 8479–8487. doi: 10.1167/iovs.11-8182.

Zernant, J. *et al.* (2014) 'Genetic and Clinical Analysis of ABCA4-Associated Disease in African American Patients', *Human Mutation*, 35(10), pp. 1187–1194. doi: 10.1002/humu.22626.

Zernant, J. *et al.* (2017) 'Frequent hypomorphic alleles account for a significant fraction of ABCA4 disease and distinguish it from age-related macular degeneration', *Journal of Medical Genetics*, 54(6), pp. 404–412. doi: 10.1136/jmedgenet-2017-104540.

Zernant, J. *et al.* (2018) 'Extremely hypomorphic and severe deep intronic variants in the ABCA4 locus result in varying Stargardt disease phenotypes', *Cold Spring Harbor molecular case studies*, 4(4), pp. 1–12. doi: 10.1101/mcs.a002733.

Zhang, N. *et al.* (2014) 'Protein misfolding and the pathogenesis of ABCA4-associated retinal degenerations', *Human Molecular Genetics*, 24(11), pp. 3220–3237. doi: 10.1093/hmg/ddv073.

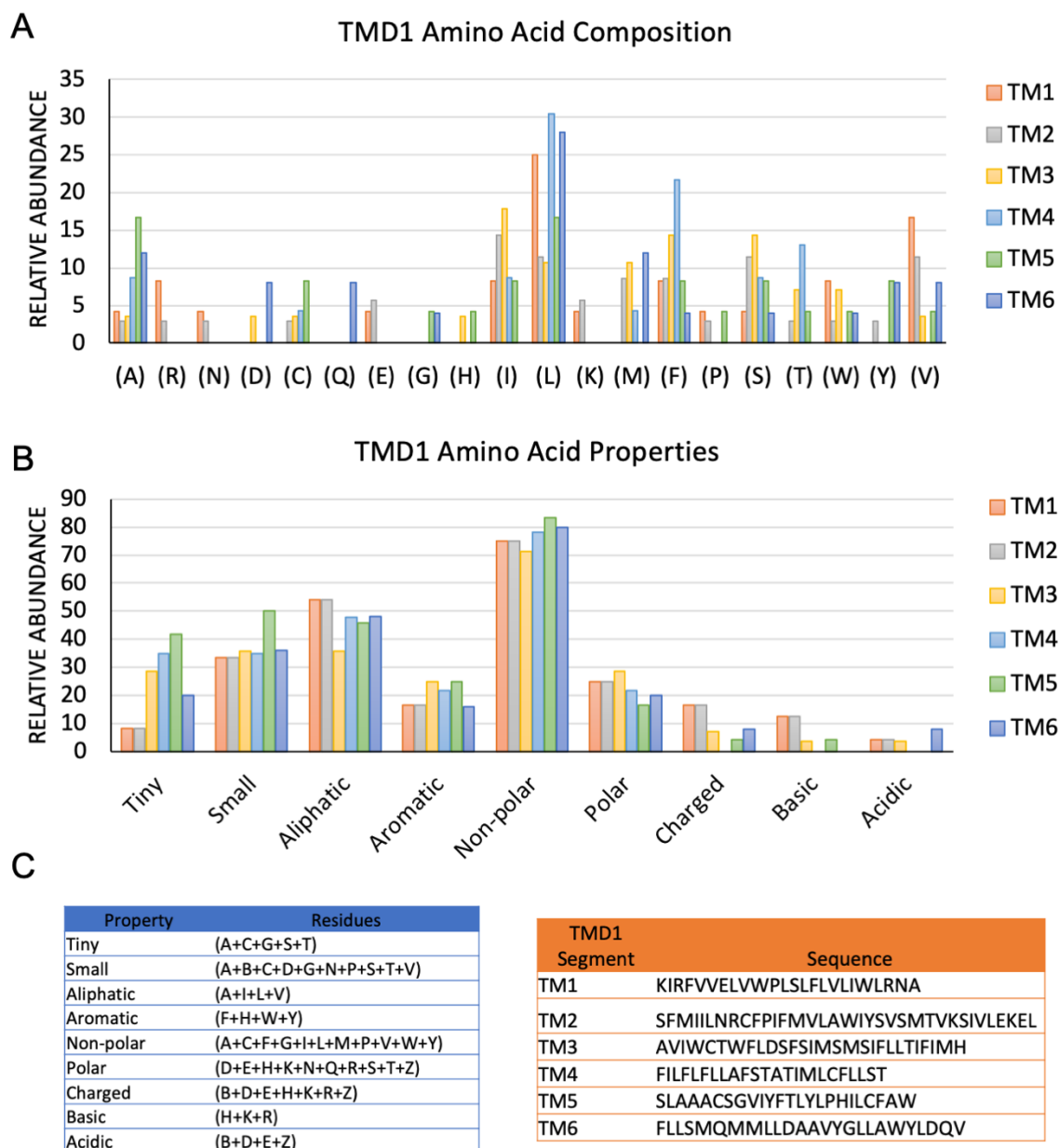
Zhong, M., Molday, L. L. and Molday, R. S. (2009) 'Role of the C terminus of the photoreceptor ABCA4 transporter in protein folding, function, and retinal degenerative diseases', *Journal of Biological Chemistry*, 284(6), pp. 3640–3649. doi: 10.1074/jbc.M806580200.

Zhong, M. and Molday, R. S. (2010) 'Binding of Retinoids to ABCA4, the Photoreceptor ABC Transporter Associated with Stargardt Macular Degeneration', in Sun, H. and Travis, G. H. (eds) *Retinoids: Methods and Protocols*. Totowa, NJ: Humana Press, pp. 163–176. doi: 10.1007/978-1-60327-325-1_9.

Zhu, X. *et al.* (2016) 'Induction of oxidative and nitrosative stresses in human retinal pigment epithelial cells by all-trans-retinal', *Experimental Cell Research*, 348(1), pp. 87–94. doi: 10.1016/j.yexcr.2016.09.002.

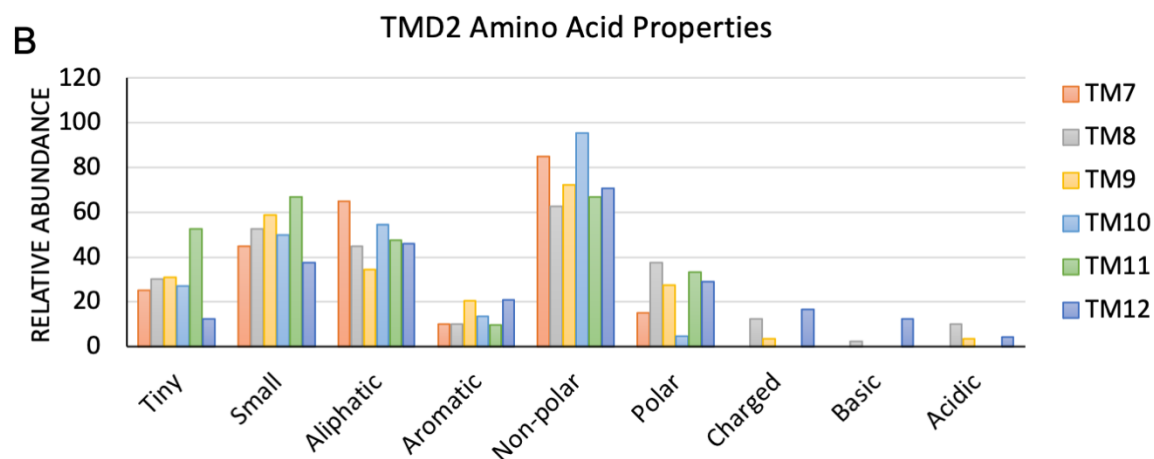
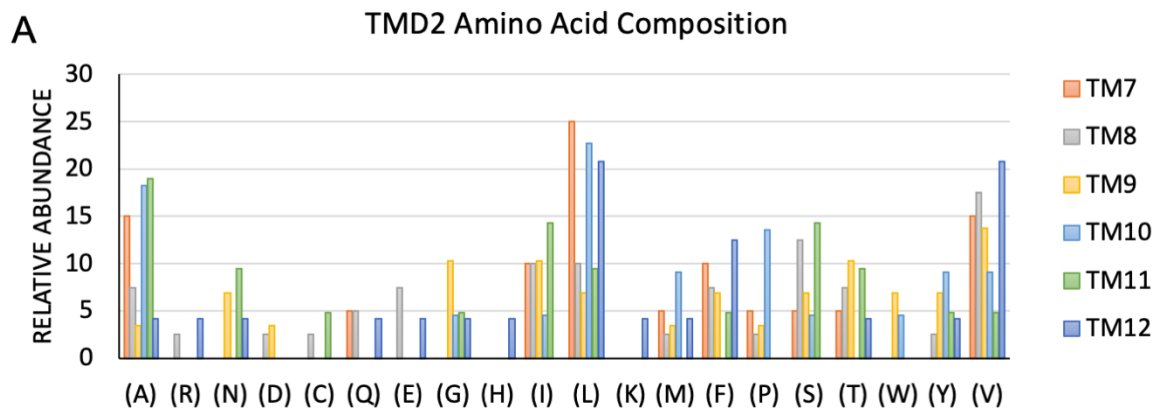
Appendices

A1. TMD1 amino acid composition



A. Amino acid composition of each TM segment B. Amino acid properties of each TM segment C. Amino acid residues grouped by biophysical properties (Blue table) and amino acid sequence of TM segments (orange table).

A2. TMD2 amino acid composition



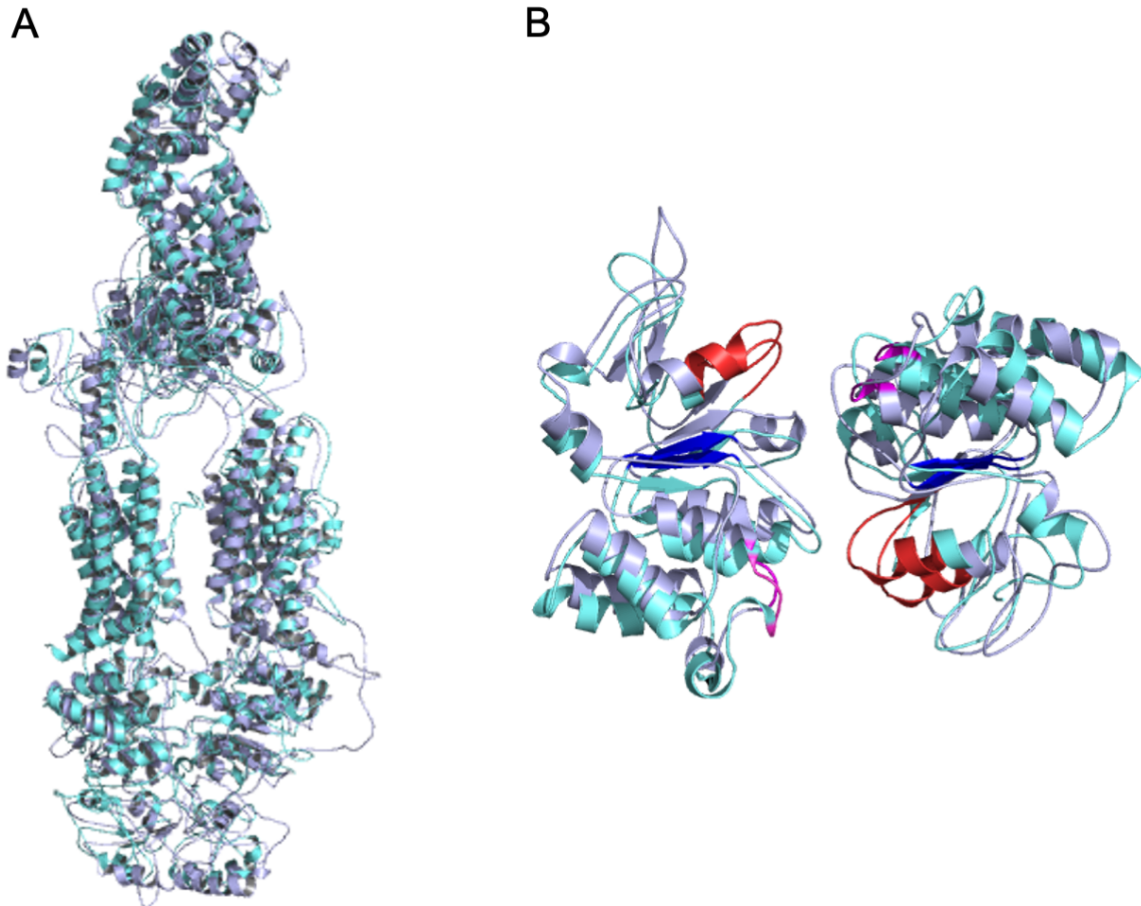
C

Property	Residues
Tiny	(A+C+G+S+T)
Small	(A+B+C+D+G+N+P+S+T+V)
Aliphatic	(A+I+L+V)
Aromatic	(F+H+W+Y)
Non-polar	(A+C+F+G+I+L+M+P+V+W+Y)
Polar	(D+E+H+K+N+Q+R+S+T+Z)
Charged	(B+D+E+H+K+R+Z)
Basic	(H+K+R)
Acidic	(B+D+E+Z)

TMD2 Segment	Sequence
TM7	LAQIVLPATFVFLALMLSIV
TM8	EQLSEITVLTTSVDAVVAICVIFSMSFVPASFVLYLIQER
TM9	PTTYWVTNFWLWIDIMNYSVSAGLVVGIFIG
TM10	PALVALLLYGWAVIPMMYPAS
TM11	TAYVALSCANLFIGINSSAIT
TM12	KNLFAMVVEGVVYFLLTLLVQRHF

A. Amino acid composition of each TM segment B. Amino acid properties of each TM segment C. Amino acid residues grouped by biophysical properties (Blue table) and amino acid sequence of TM segments (orange table).

A3. Alignments of ABCA4 homology models using I-TASSER and SWISS-MODEL



A. Global comparison of ABCA4-Homology models using SWISS-MODEL (grey) and I-TASSER (cyan)
B. Comparison of NBDs ABCA4-Homology models using SWISS-MODEL (grey) and I-TASSER (cyan).
Red = Walker-A motif, Blue = Walker-B motif, Pink = LSGGQ signature motif.

A4. TMD1 variants statistical analysis of protein expression levels after solubilization with CHAPS or SDS

Sample	Expression (CHAPS) (% WT)	Standard Deviation	Significance* (p-value)	Expression (SDS) (% WT)	Standard Deviation	Significance# (p-value)
WT	100	0		100	0	
R653C	102	9	0.561916	106	11	0.23
R653H	115	14	0.120687	119	16	0.10
L661R	20	11	0.000692	110	12	0.28
L686S	27	8	<0.000001	98	15	0.76
G690V	33	12	0.000006	80	15	0.02
T716M	98	16	0.708062	109	11	0.10
C764Y	100	12	0.926500	107	17	0.37
S765N	30	9	0.000007	104	11	0.41
S765R	29	11	0.000016	103	17	0.71
V767D	24	11	0.000100	101	11	0.91
L797P	25	5	<0.000001	101	14	0.85
G818E	51	13	0.000225	93	11	0.23
W821R	51	6	<0.000001	90	8	0.03
I824T	41	17	0.000316	108	4	0.03
M840R	26	4	<0.000001	94	5	0.12
D846H	30	9	0.000006	79	17	0.09
V849A	88	20	0.166351	90	19	0.37
G851D	27	11	0.000003	78	19	0.10
A854T	82	6	0.000946	108	13	0.23

*Statistical significance of expression levels of TMD1 variants relative to WT after CHAPS solubilization. P-value calculated using unpaired t test.

#Statistical significance of expression levels of TMD1 variants relative to WT after SDS solubilization. P-value calculated using unpaired t test.

A5. TMD2 variants statistical analysis of protein expression levels after solubilization with CHAPS or SDS

Sample	Expression (CHAPS) (% WT)	Standard Deviation	Significance* (p-value)	Expression (SDS) (% WT)	Standard Deviation	Significance# (p-value)
WT	100	0		100	0	
P1380L	53	12	0.00006	98	10	0.61
E1399K	102	15	0.78207	95	20	0.63
S1696N	96	17	0.61272	100	9	0.90
Q1703E	89	13	0.09770	101	17	0.93
Q1703K	52	11	0.00070	100	16	0.98
R1705L	40	13	0.00009	123	8	0.01
A1773E	21	4	0.00003	92	13	0.29
A1773V	36	19	0.00682	94	20	0.59
A1794D	76	4	0.00797	110	6	0.11
A1794P	55	15	0.00075	100	14	0.96
N1805D	82	19	0.14974	113	14	0.18
H1838D	56	16	0.00098	87	19	0.27
H1838N	107	14	0.30731	96	4	0.19
H1838R	27	6	0.00243	95	26	0.75
H1838Y	48	11	0.00222	105	12	0.49
R1843W	99	8	0.74538	92	11	0.25
N1868I	111	25	0.44002	108	17	0.43
R1898C	84	11	0.06250	94	16	0.49
R1898H	102	28	0.89250	104	3	0.02

*Statistical significance of expression levels of TMD2 variants relative to WT after CHAPS solubilization. P-value calculated using unpaired t test.

#Statistical significance of expression levels of TMD2 variants relative to WT after SDS solubilization. P-value calculated using unpaired t test.

A6. TMD1 variants statistical analysis of ATPase activity assays

Sample	ATPase Activity 0uM Retinal (% WT Basal)	Standard deviation	ATPase Activity 40uM Retinal (% WT Basal)	Standard deviation	Significance* (p-value)	Significance# (p-value)
WT	100	0	224	22	<0.000001	
R653C	113	21	134	17	0.243928	0.386947
R653H	130	15	239	39	0.000491	0.004591
L661R	13	4	16	3	0.265704	0.000713
L686S	18	9	30	16	0.338467	0.003596
G690V	41	12	59	14	0.10034	0.00227
T716M	94	4	228	13	0.000005	0.034056
C764Y	133	5	270	39	0.001343	0.000099
S765N	21	9	45	7	0.024741	0.004298
S765R	18	6	29	4	0.058089	0.001782
V767D	40	14	63	17	0.157529	0.018334
L797P	31	5	37	2	0.157214	0.001885
G818E	63	5	111	8	0.001649	0.005492
W821R	58	7	125	7	0.000305	0.008508
I824T	64	3	145	6	0.000137	0.003072
M840R	37	12	47	14	0.386336	0.010986
D846H	42	22	50	18	0.604148	0.013034
V849A	86	5	216	13	0.000065	0.010053
G851D	31	11	46	12	0.180036	0.008092
A854T	70	10	148	26	0.024106	0.0335

*Statistical significance of ATPase assays of TMD1 variants: 0uM vs. 40uM retinal values. P-value calculated using unpaired t test.

Statistical significance of ATPase assays of TMD1 variants: WT basal (0uM) ATPase activity vs. Variant basal ATPase activity. P-value calculated using unpaired t test.

A7. TMD2 variants statistical analysis of ATPase activity assays

Sample	ATPase Activity 0uM Retinal (% WT Basal)	Standard deviation	ATPase Activity 40uM Retinal (% WT Basal)	Standard deviation	Significance* (p-value)	Significance# (p-value)
WT	100	0	222	16	<0.000001	
P1380L	61	19	144	31	0.02489	0.069051
E1399K	94	11	202	34	0.001273	0.261136
S1696N	120	8	255	7	0.000024	0.046027
Q1703E	36	9	20	9	0.080213	0.005896
Q1703K	17	2	12	1	0.023037	0.000145
R1705L	76	5	113	9	0.007305	0.013423
A1773E	38	9	43	1	0.411169	0.006821
A1773V	25	4	46	9	0.037247	0.000769
A1794D	46	13	57	14	0.27731	0.003832
A1794P	74	11	137	27	0.013915	0.018259
N1805D	74	15	154	19	0.005201	0.092409
H1838D	48	13	96	40	0.158079	0.020909
H1838N	60	6	132	13	0.004454	0.00762
H1838R	23	8	28	11	0.502617	0.003346
H1838Y	48	18	75	20	0.09594	0.010763
R1843W	68	3	131	14	0.01439	0.002013
N1868I	134	14	259	29	0.007502	0.053176
R1898C	114	8	238	13	0.000015	0.044169
R1898H	112	17	270	36	0.000946	0.254775

*Statistical significance of ATPase assays of TMD2 variants: 0uM vs. 40uM retinal values. P-value calculated using unpaired t test.

Statistical significance of ATPase assays of TMD2 variants: WT basal (0uM) ATPase activity vs. Variant basal ATPase activity. P-value calculated using unpaired t test.

A8. TMD1 variants statistical analysis of N-ret-PE binding assays

Sample	Relative binding (0uM ATP)	Standard deviation	Relative binding (200uM ATP)	Standard deviation	Significance* (p-value)	Significance# (p-value)
WT	100	0	15	7	<0.000001	
R653C	17	12	15	10	0.80501	0.006871
R653H	31	12	9	3	0.029977	0.001539
L661R	36	6	18	2	0.10291	0.039737
L686S	16	8	11	7	0.404939	0.003049
G690V	21	9	11	7	0.183005	0.004035
T716M	59	7	9	8	0.001153	0.010384
C764Y	68	6	16	7	0.000026	0.001525
S765N	19	5	16	5	0.55428	0.001324
S765R	13	4	18	3	0.131251	0.000572
V767D	21	1	20	2	0.811313	0.000018
L797P	11	5	12	5	0.681421	0.000932
G818E	25	3	12	3	0.000181	<0.000001
W821R	19	8	17	6	0.675939	0.000254
I824T	33	2	13	4	0.004468	0.000223
M840R	12	2	14	2	0.399224	0.000231
D846H	13	12	14	7	0.936458	0.005822
V849A	51	12	12	9	0.002235	0.00346
G851D	13	8	12	10	0.966764	0.002886
A854T	60	15	21	9	0.024796	0.04457

*Statistical significance of TMD1 N-ret-PE binding assays: 0uM ATP Vs. 200uM ATP. P-value calculated using unpaired t test.

Statistical significance of TMD1 N-ret-PE binding assays: 0uM ATP WT vs. 0uM ATP variants. P-value calculated using unpaired t test.

A9. TMD2 variants statistical analysis of N-ret-PE binding assays

Sample	Relative binding (0uM ATP)	Standard deviation	Relative binding (200uM ATP)	Standard deviation	Significance* (p-value)	Significance# (p-value)
WT	100	0	16	7	<0.000001	
P1380L	55	20	21	11	0.199643	0.192017
E1399K	117	13	31	14	0.000112	0.078071
S1696N	116	16	27	13	0.000002	0.059116
Q1703E	42	16	36	10	0.510198	0.001199
Q1703K	37	6	35	20	0.921491	0.003088
R1705L	54	12	21	9	0.019884	0.020519
A1773E	39	9	31	16	0.499691	0.007217
A1773V	37	8	27	23	0.644882	0.060448
A1794D	49	16	16	9	0.162044	0.139863
A1794P	30	13	10	6	0.049274	0.001785
N1805D	44	11	18	3	0.047437	0.012405
H1838D	52	1	28	23	0.38325	0.006563
H1838N	48	2	33	10	0.275265	0.018184
H1838R	53	6	27	14	0.199537	0.05405
H1838Y	34	8	16	3	0.039588	0.004315
R1843W	84	11	27	14	0.052387	0.271599
N1868I	101	9	21	6	0.016477	0.951125
R1898C	67	20	20	13	0.034209	0.103512
R1898H	121	14	24	10	0.001131	0.124239

*Statistical significance of TMD2 N-ret-PE binding assays: 0uM ATP Vs. 200uM ATP. P-value calculated using unpaired t test.

Statistical significance of TMD2 N-ret-PE binding assays: 0uM ATP WT vs. 0uM ATP variants. P-value calculated using unpaired t test.

A10. N965 and N1974 variants statistical analysis of protein expression levels after solubilization with CHAPS or SDS

Sample	Expression (CHAPS)	Standard Deviation	Significance* (p-value)	Expression (SDS)	Standard Deviation	Significance# (p-value)
WT	100	0		100	0	
N965D	96	7	0.3704	101	11	0.838
N965K	90	11	0.1811	109	9	0.145
N965S	86	5	0.0038	100	4	0.906
N965Y	78	4	0.0004	107	7	0.095
N965A	78	6	0.0209	101	9	0.863
N965Q	87	26	0.3380	103	8	0.426
N1974D	90	19	0.4639	113	5	0.046
N1974K	100	26	0.9845	110	8	0.148
N1974S	86	15	0.0657	103	6	0.280
N1974Y	106	13	0.4323	100	15	0.975
N1974A	91	10	0.1223	96	5	0.211
N1974Q	95	5	0.0713	102	6	0.454

*Statistical significance of expression levels of N965 and N1974 variants relative to WT after CHAPS solubilization. P-value calculated using unpaired t test.

#Statistical significance of expression levels of N965 and N1974 variants relative to WT after SDS solubilization. P-value calculated using unpaired t test.

A11. N965 and N1974 variants statistical analysis of ATPase activity assays

Sample	ATPase Activity 0uM Retinal (% WT Basal)	Standard deviation	ATPase Activity 40uM Retinal (% WT Basal)	Standard deviation	Significance* (p-value)	Significance# (p-value)
WT	100	0	226	23	<0.000001	
N965D	24	5	6	4	0.00026	0.000004
N965K	11	4	4	3	0.01477	<0.000001
N965S	96	23	151	11	0.00978	0.718877
N965Y	14	6	7	7	0.13382	0.000005
N965A	103	8	163	12	0.00383	0.612399
N965Q	60	9	50	11	0.08685	0.000021
N1974D	36	10	18	9	0.01901	0.000147
N1974K	45	15	11	2	0.05782	0.025052
N1974S	110	14	173	14	0.00012	0.203895
N1974Y	71	6	41	7	0.00012	0.000491
N1974A	94	15	160	9	0.00010	0.403210
N1974Q	85	6	120	9	0.00619	0.053906

*Statistical significance of ATPase assays of N965 and N1974 variants: 0uM vs. 40uM retinal values. P-value calculated using unpaired t test.

Statistical significance of ATPase assays of N965 and N1974 variants: WT basal (0uM) ATPase activity vs. Variant basal ATPase activity. P-value calculated using unpaired t test.

A12. N965 and N1974 variants statistical analysis of N-ret-PE binding assays

Sample	Relative binding (0uM ATP)	Standard deviation	Relative binding (200uM ATP)	Standard deviation	Significance* (p-value)	Significance# (p-value)
WT	100	0	12	7	<0.000001	
N965D	55	12	36	23	0.44197	0.1176
N965K	50	7	19	1	0.01476	0.0066
N965S	77	6	20	10	0.00002	0.0009
N965Y	82	1	27	4	0.01313	0.0353
N965A	83	18	13	4	0.10271	0.4156
N965Q	88	12	34	23	0.13957	0.3802
N1974D	22	7	11	5	0.21484	0.0408
N1974K	58	16	25	9	0.16204	0.1682
N1974S	74	7	10	1	0.04693	0.1210
N1974Y	77	10	16	3	0.05564	0.1881
N1974A	84	17	6	2	0.09232	0.4097
N1974Q	63	3	4	1	0.01493	0.0344
MM	58	10	47	3	0.18744	0.0176

*Statistical significance of N965 and N1974 variants N-ret-PE binding assays: 0uM ATP Vs. 200uM ATP. P-value calculated using unpaired t test.

Statistical significance of N965 and N1974 variants N-ret-PE binding assays: 0uM ATP WT vs. 0uM ATP variants. P-value calculated using unpaired t test.

A13. Variants of B.C. cohort Stargardt patients statistical analysis of protein expression levels after solubilization with CHAPS or SDS

Sample	Expression (CHAPS)	Standard Deviation	Significance* (p-value)	Expression (SDS)	Standard Deviation	Significance# (p-value)
WT	100	0		100	0	
G72R	89	13	0.1892	92	5	0.049
M448K	89	1	0.0002	98	15	0.807
L541P	93	10	0.2560	95	11	0.430
V552I	96	11	0.5197	104	4	0.139
A1038V	71	18	0.0485	100	11	>0.999999
G1091E	84	10	0.0493	114	7	0.028
A1357T	56	10	0.0031	107	14	0.391
A1794P	47	11	0.0024	96	9	0.440
G1961E	97	8	0.5077	97	15	0.716
L2027F	45	14	0.0043	103	3	0.139
R2077W	52	9	0.0018	104	10	0.482

*Statistical significance of expression levels of variants relative to WT after CHAPS solubilization. P-value calculated using unpaired t test.

#Statistical significance of expression levels of variants relative to WT after SDS solubilization. P-value calculated using unpaired t test.

A14. Variants of B.C. cohort Stargardt patients statistical analysis of ATPase activity assays

Sample	ATPase Activity 0uM Retinal (% WT Basal)	Standard deviation	ATPase Activity 40uM Retinal (% WT Basal)	Standard deviation	Significance* (p-value)	Significance# (p-value)
WT	100	0	208	43	0.000001	
G72R	42	19	50	14	0.591266	0.034
M448K	46	1	62	5	0.025738	0.008
L541P	59	23	61	18	0.895795	0.038
V552I	85	19	174	56	0.009849	0.111
A1038V	65	8	108	14	0.003574	0.003
G1091E	41	20	58	25	0.412102	0.036
A1357T	39	9	127	36	0.044455	0.007
A1794P	76	10	125	15	0.012869	0.053
G1961E	12	10	13	10	0.90843	0.004
L2027F	54	19	108	22	0.01029	0.017
R2077W	31	7	34	9	0.673579	0.003

*Statistical significance of ATPase assays of variants: 0uM vs. 40uM retinal values. P-value calculated using unpaired t test.

Statistical significance of ATPase assays of variants: WT basal (0uM) ATPase activity vs. Variant basal ATPase activity. P-value calculated using unpaired t test.

A15. Variants of B.C. cohort Stargardt patients statistical analysis of N-ret-PE binding assays

Sample	Relative binding (0uM ATP)	Standard deviation	Relative binding (200uM ATP)	Standard deviation	Significance* (p-value)	Significance# (p-value)
WT	100	0	6	5	<0.000001	
G72R	6	7	8	11	0.8058	0.0018
M448K	33	18	14	12	0.2131	0.0232
L541P	7	7	5	4	0.6949	0.0019
V552I	102	26	4	4	0.1113	0.9310
A1038V	33	15	7	4	0.0866	0.0163
G1091E	86	6	23	4	0.0003	0.0561
A1357T	108	11	14	6	0.0008	0.3349
A1794P	29	13	9	6	0.0462	0.0016
G1961E	36	19	38	22	0.9110	0.0281
L2027F	26	4	11	3	0.0080	0.0010
R2077W	22	7	18	5	0.4702	0.0027

*Statistical significance of N-ret-PE binding assays: 0uM ATP Vs. 200uM ATP. P-value calculated using unpaired t test.

Statistical significance of N-ret-PE binding assays: 0uM ATP WT vs. 0uM ATP variants. P-value calculated using unpaired t test.